SELECTED ION FLOW TUBE STUDIES OF SOME GASEOUS ION-MOLECULE REACTIONS

A thesis

submitted in partial fulfilment

of the requirements for the degree

of

Doctor of Philosophy in Chemistry

in the

University of Canterbury

by

J. S. Knight

University of Canterbury

1986

TO MY PARENTS

CONTENTS.

LIST OF PUBLICATIONS

The following papers relating to the research described in this thesis are to be published.

1. "Selected Ion Flow Tube Studies of HC_3N", J.S. Knight, C.G. Freeman, M.J. McEwan, N.G. Adams and D. Smith, Int. J. Mass Spectrum. Ion Phys., 67, 317 (1985).

2. "Ion-molecule Chemistry of Cyanoacetylene", J.S. Knight, C.G. Freeman, S.C. Smith, M.J. McEwan, N.G. Adams and D. Smith, Mon. Not. Royal Astrom. Soc., in press.

3. "Isomers of $C_2H_4N^+$ and the Proton Affinities of CH_3CN and CH_3NC", J.S. Knight, C.G. Freeman and M.J. McEwan, J. Am. Chem. Soc., in press.

4. "Association Reactions of Hydrocarbon Ions with C_2H_2", J.S. Knight, C.G. Freeman, M.J. McEwan, V.G. Anicich and W.T. Huntress, Jnr., J. Phys. Chem., to be submitted.

5. "Selected Ion Flow Tube Study of Association Reactions of Hydrocarbon Ions with HCN", J.S. Knight, C.G. Freeman and M.J. McEwan, J. Phys. Chem., to be submitted.

6. "The Ion-Molecule Chemistry and Proton Affinity of C_4H_2", J.S. Knight, C.G. Freeman and M.J. McEwan, Int. J. Mass Spectrum. Ion Phys., to be submitted.

7. "A SIFT Study of the Structural Isomers CNC^+ and CCN^+", J.S. Knight, C.G. Freeman and M.J. McEwan, Int. J. Mass Spectrum. Ion Phys., to be submitted.

ABSTRACT.

The Selected Ion Flow Tube technique requires a mass spectrometer to select the mass of the ion studied in a flow tube measurement. The performance of the SIFT developed and used in this study is discussed and the rate coefficients and product distributions for a number of positive ion-molecule reactions have been measured.

The relative proton affinity of cyanoacetylene (HC_3N) has been determined to be 751±2 kJ mol^{-1}. A number of reactions of HC_3N with ions of importance to interstellar chemistry as well as the reactions of HC_3N^+ and C_3N^+ with H_2 have also been investigated. The relevance of the results obtained are discussed with respect to the chemistry of HC_3N in interstellar clouds.

The relative proton affinities of acetonitrile (CH_3CN) and methyl isocyanide (CH_3NC) have been determined to be 788±2 and 844±2 kJ mol^{-1} respectively. Two distinct species were observed for the adduct ion $C_2H_4N^+$ produced in the reaction of CH_3^+ and HCN, CH_3CNH^+ (85±8%) and CH_3NCH^+ (15±8%). The former species was confirmed to have the same structure as protonated acetonitrile and the latter a protonated methyl isocyanide structure. The two $C_2H_4N^+$ isomers were distingushed in the flow tube by their different reactivity. A lower limit to the internal energy required to convert CH_3NCH^+ to CH_3CNH^+ was measured as 132 kJ mol^{-1}.

Two stable isomeric forms of the C_2N^+ ion were identified in the flow tube on the basis of their markedly different reactivity with CH_4. HC_2N^+ appeared to have one stable

structure only at flow tube pressures.

The relative proton affinity of diacetylene (C_4H_2) was estimated to be 738±3 kJ mol^{-1}. Rate coefficients and product distributions were determined for reactions of the neutrals C_2H_2, HCN, C_6H_6 and H_2 with a number of hydrocarbon ions. Some evidence for isomeric forms of the ions $C_4H_4^+$, $C_6H_4^+$ and $C_6H_5^+$ is also presented.

CHAPTER ONE

INTRODUCTION

1.1 A BRIEF REVIEW OF THE ROLE OF FLOW TUBES IN THE STUDY OF GASEOUS ION-MOLECULE CHEMISTRY.

At the present time a large proportion of the thermal ion-molecule data that has appeared in the literature has been measured using flow techniques. These flow techniques date from the development in 1963 of the flowing afterglow experiment by Ferguson et al[1,2]. The development of this experiment was in response to a requirement for information on near-thermal energy (<0.1eV) ion-molecule reactions which were thought to occur in ionospheric chemistry. Prior to the development of the flowing afterglow some ion-molecule measurements, obtained using the time-resolved afterglow technique, had been reported in the literature by Sayers and coworkers[3,4].

In the time-resolved (or stationary) afterglow, at pressures ($>10^{-4}$ Torr) where a collision dominated plasma will exist, the rate coefficient, k, for any particular ion-molecule reaction can be determined under controlled temperature conditions. A short pulse of high energy electrons or an rf electric field in a suitable gas is used initially to generate the afterglow plasma. The time decay of the ions of this plasma versus the neutral reactant pressure is then analysed to obtain a rate coefficient. However, the stationary afterglow presents difficulties for the accurate measurement

of thermal ion-molecule reaction rate coefficients because both the reactant and neutral gases are exposed to the ionising radiation. Further, it is also possible to produce vibrationally and electronically excited states of the primary ion in the ionizing process and this internal excitation may influence the rate coefficient.

For the study of thermal (<0.1ev) energy ion-molecule reactions, the ion beam and ion cyclotron resonance techniques present the same problems as the stationary afterglow experiment. Namely that the internal and kinetic energies of the reactant ions and neutrals under study in these techniques are not in thermal equilibrium. However, the ion beam experiment has been used to provide data on ion-molecule reactions over a wide range of interaction energies above 0.1 eV[5,6]. ICR experiments have also been used in a wide variety of applications pertaining to ion-molecule reactions (see for example the review of McIver[7] and the recent reports on ICR spectroscopy edited by Hartmann and Wanczek[8,9]).

The problem of neutral excitation in the flowing afterglow technique is avoided by the spatial separation of the ion discharge and reaction regions in the flow tube. The flowing afterglow technique as applied to the measurements of rate coefficients and product distributions for ion-molecule reactions will only be briefly described here. A number of reviews[2,10,11,12,13,14] in the literature provide detailed descriptions of both the technique itself and some of the data obtained since 1963 using the flowing afterglow.

A schematic outline of a typical flowing afterglow is shown in figure 1.0.

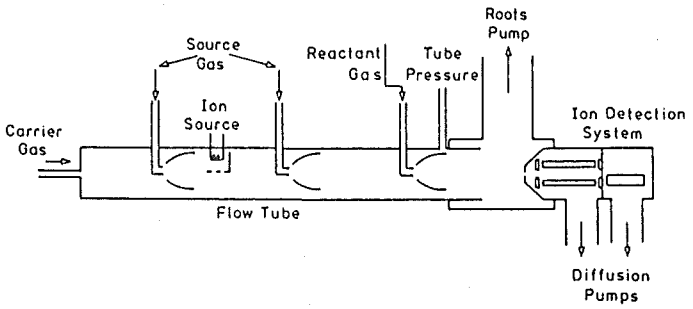

Fig. 1.0: Schematic diagram of a typical FA apparatus. (reproduced from Smith and Adams[14]).

A carrier gas is introduced into the flow tube at pressures typically between 0.1-1.0 Torr and at flow velocities of 10^4 cm s^{-1}. Ions are created at the flow tube entrance, usually by electron impact on either the carrier gas or a suitable source gas as well as the carrier. The resulting mixture of positive ions, electrons and neutrals as well as negative ions and metastable neutrals which may also be produced is described as an ion plasma[14]. As the afterglow plasma moves away from the ionisation region the individual constituents undergo collisional thermalisation down the length of the flow tube. A variety of reactant ions can also be created at a point downstream from the ion source by chemical reaction of a suitable gas with the afterglow plasma. The plasma is then sampled for positive or negative ions on axis at a point at the end of the flow tube, mass analysed and counted.

To measure a rate coefficient for an ion-molecule reaction in the FA technique, the decrease in the ion signal of interest with added neutral reagent is measured. The main advantage of the flowing afterglow technique over the stationary afterglow and ion cyclotron resonance techniques is that the neutral reactant is not subjected to the extreme

conditions of the ionising region but rather to the thermalised afterglow plasma. Internal excitation of the neutral species is therefore less likely.

Another important development of the flowing aferglow technique, especially for the study of the effects of ion energy on an ion-molecule reaction, was the flow-drift technique (FDT). First developed by MacFarland et al[15,16,17] in 1973, the technique has since allowed the study of ion-molecule reactions over a range of interaction energies from thermal energies to a few electron volts. A number of reviews of the FDT experiment and data obtained have appeared in the literature in recent years[14,18,19].

The most restrictive feature of the flowing afterglow and flow-drift techniques, as described above, is that the ions to be studied are generated in the flow tube. For example, the ion CH^+ may be generated in the flowing afterglow by electron impact on CH_4. Upon addition of a suitable neutral, reaction occurs not only with the ion of interest, CH^+, but also with the other ions formed in the ionisation process such as, C^+, CH_2^+, CH_3^+ and CH_4^+. In addition because the neutral source gas (in this case methane) is also present in the flowing afterglow plasma, reactions of this gas with the plasma ions will also occur. For example, the ion $C_2H_5^+$ formed from the reaction of CH_3^+ with CH_4 may be the largest ion signal observed in a plasma with CH_4 as the source gas. The product ions formed in these reactions can also react further with the neutral species present in the flow tube, with the end result that product analysis for each individual ion-molecule reaction becomes impossible.

Determination of rate coefficients for some ion-molecule reactions can also be complicated in a flowing afterglow plasma such as that created by electron impact on methane in a He carrier. If the primary ion under study, or a separate ion at the same mass-to-charge ratio (m/e), is also formed as the result of a side reaction of an adjacent ion, a curved decay for the primary ion may result upon the addition of the neutral of interest. This curved decay will result in an erroneous rate coefficient for the ion under study.

The presence in the afterglow plasma of electrons, metastable species and photons produced from the ion source can lead to additional problems in data analysis. Ion loss due to dissociative recombination (the addition of an electron to a positive ion species) competing with ion loss due to the ion-molecule reaction under study can result in erroneously high rate coefficients being measured[14]. Metastable species of ions and neutrals can react with the gases present in the plasma producing ions which will complicate product analysis[14,20]. Energetic photons may also ionise gases in the reactant zone further complicating analysis of ion-molecule rate coefficients[14].

The problems mentioned above with the flowing afterglow technique have been avoided to a large extent in the Selected Ion Flow Tube (SIFT) technique, developed in 1976 by Smith and Adams[14]. With the SIFT a range of ions of interest are initially produced in a remote ion source before a single m/e type is injected into the flow tube. That this supposedly "simple" advance in technique over the established flowing afterglow had not occurred previously was due to the

requirement of injecting a low density of ions from a quadrupole mass filter chamber against a pressure gradient and into the flow tube. Smith and Adams utilised the aspirator effect (reference 14 and section 2.5), where the carrier gas is injected into the flow tube around the mass filter chamber entrance creating a region of low pressure in the flow tube. This allows a significant number of mass selected low energy ions to pass from the low pressure chamber ($\sim 10^{-5}$ Torr) and into the flow tube (~ 0.3 Torr).

The advantages of being able to inject mass-selected ions into the flow tube are obvious. Instead of having, as in the flowing afterglow, a plasma of electrons with positive and negative ions coexisting in the flow tube, only a single ion mass removed from the source neutral gas is present. Smith and Adams[14] have described the resultant low density (typically $\sim 10^{3}$ ions cm^{-3}) collection of positive, or negative, ions formed in the SIFT as a "swarm" of ions.

Because a swarm of ions of a single m/e can be formed with a SIFT, accurate product distributions can be measured if the mass discrimination can be determined. Smith and Adams demonstrated that the SIFT instrument can be calibrated for mass discrimination over a wide range of masses by simply measuring the ion current on the nose cone versus the total ion count at the detector for the relevant ion (detailed in reference 14 and section 2.6). Accurate product analysis for ion-molecule reactions is essential to the development of chemical models used to describe the chemistry of plasmas such as those thought to exist in dense interstellar clouds, where a number of exotic compounds have been identified (reference 14

and section 3.5).

All of the ion-molecule reactions detailed in Chapters Three to Six have been investigated using the SIFT technique. Chapter Two describes the development and characteristics of the particular SIFT used in this study as well as its application to the measurement of ion-molecule rate coefficients and product distributions.

Since 1976 the SIFT technique has been used to study a wide range of ion-molecule reactions of importance to the understanding of chemical processes occurring in interstellar clouds, planetary atmospheres and hydrocarbon flames. The technique has also assisted our understanding of the fundamental processes of ion-neutral dynamics. One example of the successful application of the SIFT technique was the measurement of rate data for reactions of individual ions of the series CH_n^+ (n= 0-4) with the neutrals H_2, N_2, O_2, CO, CO_2, COS, H_2O, H_2S, NH_3, CH_4, H_2CO, CH_3OH and CH_3NH_2[14]. These reactions could not be satisfactorily studied with the FA technique alone.

Much of the data obtained using the SIFT technique at or near room temperature and the interstellar and atmospheric significance of these measurements has been comprehensively reviewed by Smith and Adams [14,21,22,23]. The emphasis of these reviews has mainly concerned the ion-molecule chemistry of positive ions. However, recently Paulson and coworkers have applied the SIFT technique to measure the rate coefficients and product ion distributions for the reactions of several negative ions known to atmospheric chemistry[24,35]. The reactions studied included the reactions of the cluster ions

$OH^-.(H_2O)_n$ with NO_2 and H_2[24,35]. DePuy, Bierbaum and coworkers using both the FA and SIFT techniques have also conducted a series of studies into the mechanisms involved in the reactions of a variety of negative organic ions with various neutrals[25,26].

Prior to these experiments Fehsenfeld and coworkers had utilised the FA technique to study many classes of negative ion-molecule reactions[27,28], especially those thought to be involved in the chemistry of the earth's lower atmosphere. These include negative ion exchange reactions, eg.

$$CO_3^- + NO \rightarrow NO_2^- + CO_2 \qquad (1.00)$$

electron transfer reactions, eg.

$$N_2^- + O_2 \rightarrow O_2^- + N_2 \qquad (1.01)$$

and associative detachment reactions, eg.

$$O^- + H_2 \rightarrow H_2O + e \qquad (1.02)$$

The SIFT technique has also been applied to the study of ion-molecule reactions at different temperatures[14,29,30,31]. By either cooling or heating a jacket surrounding the flow tube as well as precooling or heating the incoming carrier gas, reactions have been investigated over the temperature range of 80-550 K. Adams and Smith have discussed data obtained for a wide variety of reaction types using the variable temperature SIFT (VT-SIFT) experiment in two recent

reviews[30,31]. The temperature dependences of a number of exothermic binary positive[31,32] and negative ion-molecule[34,35] reactions have also been investigated. Measurements of equilibrium constants for near-thermoneutral ion-molecule reactions of the type shown in reaction (1.03)

$$XH^+ + Y \underset{k_r}{\overset{k_f}{\rightleftharpoons}} X + YH^+ \qquad (1.03)$$

have also been made at different temperatures using the VT-SIFT. In contrast to earlier work on similar near-thermoneutral reactions using other techniques such as the flowing afterglow and ICR cell, the forward and reverse rate coefficients, k_f and k_r, can be accurately measured as a function of temperature. From the variation of the equilibrium constant with temperature, both the relative enthalpies and entropies for the two species involved in the reaction can then be determined from the equation $\Delta G^\circ = -RT\ln K = \Delta H^\circ - T\Delta S^\circ$[30,31].

This approach has been applied to the study of the thermodynamics of isotope exchange reactions. For example a detailed study of the reactions of CH_3^+, CH_2D^+, CHD_2^+ and CD_3^+ with H_2, HD and D_2 over a range of temperatures has been made by Smith et al[100,32]. They were able to measure the temperature variation of k_f and k_r for several of these isotope exchange reactions and therefore determine ΔH° and ΔS° in each case. From these data the relative difference in bond strengths for the C-H and C-D bonds in CH_3^+ -type ions was then determined. SIFT isotope exchange studies have thus provided fundamental data on the kinetics of ion-molecule reactions. A further

outcome of the isotopic exchange studies has been information on the lifetime of the intermediate complexes involved. For example, isotopic scrambling was shown to occur[33] in the slightly exothermic reaction:

$$CH_4^+ + CH_4 \rightarrow CH_5^+ + CH_3 \qquad (1.04)$$

Prior to the study of Smith and Adams[33], it was assumed that this reaction (reaction (1.04)) occurred either by direct proton transfer or by hydrogen abstraction (or both). By studying the products of both this reaction and those of the allied reactions, CD_4^+ with CH_4 and CH_4^+ with CD_4 (reaction (1.05)) it was shown that the reaction actually occurs via a long lived intermediate, $(C_2H_8)^*$, to give a number of products (the longer lived the intermediate the more scrambling that occurs).

$$CH_4^+ + CD_4 \rightarrow$$
$$CH_4D^+(10\%),\ CH_3D_2^+(22\%),\ CH_2D_3^+(43\%),\ CHD_4^+(25\%) \qquad (1.05)$$

Another very successful application of the VT-SIFT technique has been the investigation of ternary association reactions whose efficiency is closely related to the complex lifetime. Ternary association reactions have been investigated by several techniques[14,29,31,32]. Results from these association studies have been used to estimate the rates of binary radiative association reactions which are thought to be important processes in interstellar chemistry[32,36].

The VT-SIFT experiment has been utilised to study the

association reactions of CH_3^+ with several neutrals at different temperatures[37]. For example, the ternary reaction:

$$CH_3^+ + H_2 + He \rightarrow CH_5^+ + He \qquad (1.06a)$$

was noted to proceed rapidly ($k = 1.5 \times 10^{-27}$ cm^6 s^{-1} at 80 K) with a temperature dependence of $\sim T^{-2.5}$. From the observed temperature dependence of the ternary rate coefficient, the rate coefficient for the equivalent binary radiative association reaction (1.06b) was estimated to be $\sim 10^{-13}$ cm^3 s^{-1}.

$$CH_3^+ + H_2 \rightarrow CH_5^+ + h\nu \qquad (1.06b)$$

Recently this binary reaction has been studied by Barlow et al[38] in a low temperature ion trap experiment (discussed on page 12) and the rate coefficient measured for the reaction was 1.1×10^{-13} cm^3 s^{-1} at 13 K. This result provides experimental confirmation of the technique used to obtain radiative association data on reactions of interstellar interest from the VT-SIFT experiment.

The data obtained using the VT-SIFT technique has also contributed to the development of realistic chemical models of the Earth's atmosphere[22,39] and of interstellar clouds[40,41,42], as well as providing insights into the actual kinetics involved in ion-molecule reactions. Although temperatures below 70 K have not been achieved in SIFT flow tubes, the measurements made above this temperature when combined with other very low temperature techniques have provided a valuable

contribution to the overall picture.

Recently measurements made on a number of ion-molecule reactions at temperatures approaching those of dense molecular clouds (10-50 K) have been appearing in the literature. In particular an ion trap experiment of Dunn and coworkers[38,43] has been used to measure a rate coefficient for the reaction of CH_3^+ and H_2 at 13 K[38]. In addition, Rowe and coworkers have developed a supersonic jet experiment[44,45,46] whereby reactions of ion plasmas with selected neutrals have been investigated at temperatures as low as 8 K[47]. The particular advantage of this technique, abbreviated to CRESU by the authors, is that reactions of ions with neutral species which have significant dipole moments such as H_2O and NH_3 can be studied at temperatures below 50 K where their vapour pressure is very small (CRESU stands for "Cinétique de Réaction en Ecoulement Supersonic Uniforme", which means "Reaction Kinetics in Uniform Supersonic Flow"). In essence the CRESU technique involves the creation of a uniform supersonic flow through isentropic expansion of a cooled buffer gas through a supersonic nozzle[46]. The supersonic expansion of the buffer gas then ensures that no condensation of the gas occurs on the vessel walls.

The reaction of O_2^+ and CH_4 (reaction (1.07)) has been studied at 20 K by Rowe et al[44] in a combined CRESU-SIFT experiment during which the total temperature range covered was 20-560 K.

$$O_2^+ + CH_4 \rightarrow CH_3O_2^+ + H \qquad (1.07)$$

In the CRESU experiment O_2^+ ions were initially created by electron impact on a cooled O_2 buffer gas. CH_4 was then added to the nozzle reservoir while the decay of the O_2^+ ion signal was monitored downstream of the nozzle by a quadrupole mass filter. Using this method a rate coefficient of 4.7×10^{-10} cm^3 s^{-1} was measured for the reaction at 20 K. With the SIFT technique the rate coefficient for the reaction was measured as 5.4×10^{-12} cm^3 s^{-1} at 290 K. The large temperature dependence observed for reaction (1.07) at low temperatures (figure 1.2a, p.18) has been interpreted by the authors in terms of a long-lived intermediate complex, $(CH_4O_2)^+$, for the longer the complex lifetime at lower temperatures the greater is the probability of reaction to form the products $CH_3O_2^+$ and H.

The low temperature data when combined with the VT-SIFT experiment thus provide a test of current theories on the temperature dependence of various types of ion-molecule reactions and current chemical models of interstellar molecular cloud plasmas. Differences in rates for reactions over a range of temperatures can also point to changes in mechanism, while clues to the actual mechanisms involved can be provided by detailed analysis of product distribution changes over the temperature range[30].

The Venturi buffer gas inlet has also been used successfully to inject selected ions into flow-drift tubes resulting in much the same advantages as with the SIFT technique. A selected ion flow drift tube (SIFDT), developed at the NOAA laboratory in Boulder USA by Fehsenfeld and coworkers[48], has been used to investigate individual ion-molecule reactions as a function of KE_{CM}, the centre of mass

energy of the reaction. As with the flow-drift tube technique, a fast flowing carrier gas is firstly established in the flow tube. Ions of a single m/e value are then selected with a quadrupole mass filter and injected through the venturi inlet to create a swarm of ions in the flow tube. These ions are then swept by the carrier gas flow into the drift region of the flow tube. After the addition of a suitable neutral, the effect of varying the reactant ion energy can then be studied by observing changes in the rate of reaction and product distribution.

A number of reactions of ions in both their ground and excited states (vibrational and electronic) have been studied using the SIFDT technique. For example, the reaction between N^+ and O_2:

$$N^+ + O_2 \rightarrow O_2^+ + N \quad (1.08a)$$
$$\rightarrow NO^+ + O \quad (1.08b)$$
$$\rightarrow O^+ + NO \quad (1.08c)$$

has been extensively investigated at room temperature[49,50,51] and a product distribution of about 0.50/0.43/0.7 measured for the product channels a/b/c. However, in a SIFDT study of this reaction, Howorka et al[48] measured a 0.79/0.19/0.02 product distribution at a KE_{CM} of 2eV. The changed product distribution was explained by the authors as resulting from the shorter time for charge transfer to produce O_2^+ as compared with the time required for atom rearrangement to form NO^+. Therefore, at higher collision energies the charge transfer product will predominate as observed.

The reactions of a number of metastable ions (both electronically and vibrationally excited), and of multiply-

charged ions have also been investigated at thermal energies using both the SIFT and SIFDT techniques. Studies of reactions involving these species have recently been reviewed by Lindinger and Smith[19]. One example of an investigation of a metastable reaction was the reaction of the metastable ions O^+ ($^2D, ^2P$) with N_2[52,83,84] (reaction (1.09)),

$$O^+ (^2D, ^2P) + N_2 \rightarrow N_2^+ + O \quad (90\%) \qquad (1.09)$$
$$\rightarrow NO^+ + N \quad (10\%)$$

and that of ground state $O^+(^4S)$ with N_2[84] (reaction (1.10)).

$$O^+ (^4S) + N_2 \rightarrow NO^+ + N \qquad (1.10)$$

Ground state $O^+(^4S)$ reacts only very slowly with N_2 ($k \sim 10^{-3}$ $k_{Collision}$ (k_C)) to give a single product NO^+. However metastable $O^+(^2D, ^2P)$ reacts rapidly ($k \sim k_C$) to produce a dominant N_2^+ product ion as well as NO^+. A common trait observed in reactions of metastable and doubly charged ions so far studied, is that there is an increase in rate coefficient for these ion types over the corresponding ground state ions as well as the appearance of extra reaction channels[19,54].

The logical extension to both the VT-SIFT and SIFDT experiments is the development of an experiment where both the effects of kinetic and internal energy excitation on a selected ion-molecule reaction can be studied at the same time. Smith and Adams have recently developed a flow tube experiment designed to be able to study ion-molecule reactions over the temperature range 80-600 K and with an interaction energy range from thermal energies to a few electron volts.

This experiment, which they have called the variable-temperature selected ion flow drift tube (VT-SIFDT), and its potential applications has been described in a recent review[14]. A schematic of the actual experiment used by Smith and Adams is shown in figure 1.1.

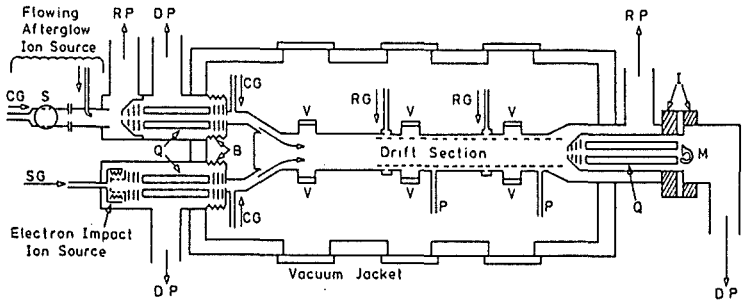

Fig. 1.1: Schematic diagram of the VT-SIFDT apparatus. V- optical viewports; I -electrical insulators; B -stainless steel bellows; CG -carrier gas; SG -source gas; S -microwave discharge source; RP -roots blower; DP -diffusion pump; Q -quadrupole mass filter; RG -reactant gas; P -pressure port; M -particle multiplier (reproduced from Smith and Adams[14]).

Swarms of ions of a particular m/e value are created in a carrier gas in the flow tube by the use of a quadrupole mass filter and Venturi inlet. As for the VT-SIFT, ion-molecule reaction data can then be obtained by studying the decay of the reactant ion with an added neutral reactant. The tube walls as well as the incoming carrier gas can then be either heated or cooled to study the effect of temperature variation on the reaction.

The inclusion of the drift section allows the effect of a variation in ion energy on the rate coefficient and product distribution for a particular reaction to be studied over a range of carrier flow temperatures. Note also the provision of two separate ion sources positioned at the entrance to the

flow tube, one of which is a flowing afterglow, in the equipment of Smith and Adams[14]. Two ion sources will enable both negative and positive ion species to be injected simultaneously, while the flowing afterglow source will allow the formation, stablisation and injection into the flow tube of weakly bound species such as ion clusters and protonated molecules.

As an example of the potential that the VT-SIFDT technique has for the study of ion-molecule reactions in general consider the following reaction:

$$O_2^+ + CH_4 \rightarrow CH_3O_2^+ + H \qquad (1.07)$$

Previous investigations of this reaction include a combined VT-SIFT and CRESU study[44] over the temperature range 20-560 K (detailed on p.12), and two FDT studies over a KE_{CM} range of 1.4eV at a gas temperature of 300 K[55,56]. As noted, the SIFT-CRESU study observed a minimum for the rate coefficient, k, for the reaction at 290 K, with $k_{1.07}$ increasing at both lower and higher temperatures (figure 1.2a).

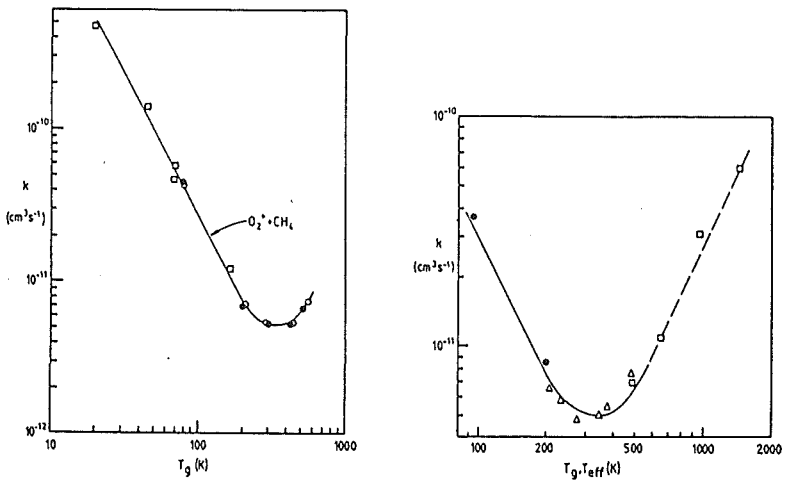

FIG. 1.2: Rate coefficients for the reaction $O_2^+ + CH_4 \rightarrow CH_3O_2^+ + H$.
(a) Vs. true temperature T_g.
(b) Rate coefficients measured at fixed T_g values of (●) 80 K, (Δ) 200 K and (□) 400 K and at various KE_{cm} values which are plotted vs. an effective temperature, T_{eff}, defined as $T_{eff} = T_g + \Delta KE_{cm}/nk$ where n= 8 (reproduced from Adams et al[57]).

This result was interpreted to imply that the reaction proceeded through a long lived intermediate, $(CH_3^+.HO_2)^*$, to form the product ion $CH_3O_2^+$ after the elimination of a hydrogen atom.

In the FDT studies Fehsenfeld and coworkers[55,56] observed the appearance of two previously endothermic reaction channels to form the product ions CH_3^+ and CH_4^+ at centre of mass energies of >0.5eV. The rate coefficient was noted to increase from 5.4×10^{-12} cm^3 s^{-1} at thermal energies (298 K) to 3×10^{-10} cm^3 s^{-1} at 1.4eV.

Using the VT-SIFDT experiment, Adams et al[31,57] have studied the reaction over a range of KE_{CM} values at three separate temperatures, 80 K, 200 K and 420 K. The kinetic energy range required to produce a certain change in rate coefficient for this reaction was found to be qualitatively equivalent to a similar range of temperatures. Figure 1.2b

shows the measured rate coefficients as a function of both the thermal temperature, T_g, and the effective temperature, T_{eff}. The authors defined T_{eff} as equal to T_g plus $\Delta KE_{CM}/nk$. When a value of 8 was chosen for n, the dependence of k on T_{eff} showed the same trend as the equivalent thermal energy temperature change shown in figure 1.2a. Adams et al[31,57] have shown that the value of n for the $(O_2^+-CH_4)^*$ intermediate is dependent upon the number of effective vibrational and rotational degrees of freedom of the intermediate involved in energy storage. The more effectively a particular degree of freedom could store the kinetic energy supplied by the drift field, the smaller the value of n would be and therefore the shorter the complex lifetime. Therefore, for the reaction of O_2^+ and CH_4, the VT-SIFDT technique has provided information on both the number and type of degrees of freedom participating in the $O_2^+-CH_4$ ion-molecule complex.

1.2 THERMAL ENERGY ION-MOLECULE REACTION COLLISION RATE THEORIES : A BRIEF OVERVIEW.

Thousands of rate coefficients have been measured for ion-molecule reactions at room temperature as well as a number over limited temperature ranges. The ionic and neutral species involved vary from monatomic ions to complex clusters of ions and from single atoms to large polyatomic neutrals. A number of theories have been developed in attempts to predict the rate coefficients of ion-molecule reactions in general (for a detailed discussion of the relative merits of published ion-molecule collision limit theories up to 1979, see

the review of Su and Bowers[58]. These models have all assumed that the interaction between an ion and a molecule results initially from the long range attractive forces occurring between the two species. Consequently the two accelerate together to form an orbiting complex. The resulting internal energy of the complex is then generally enough to overcome most activation energy barriers, therefore allowing reaction to occur.

Collision limit rate coefficients were first formulated on the basis of the polarisability, α, of the neutral molecule. Gioumousis and Stevenson[59] developed the following Langevin expression for a rate coefficient in the collision limit,

$$k_L = 2\pi q\left(\frac{\alpha}{u_r}\right)^{1/2} \qquad \text{Eqn. (1.0)}$$

where u_r equals the reduced mass of the ion-molecule pair and q equals the ionic charge.

The Langevin expression has been proven to successfully predict rate coefficient magnitudes for many ion-molecule reactions where the neutral species has no dipole moment[58,60]. It does not predict a temperature dependence for a rate coefficient, and indeed for many exothermic ion-molecule reactions the measured rate coefficient is independent of temperature[60]. However, for ion-molecule interactions where the molecule involved possesses a permanent dipole moment, u_d, the Langevin rate coefficient, k_L, has been shown to under estimate the observed rate coefficient by up to 40%[61].

Su and Bowers in 1973 proposed a theory to account for the effect of the ion-permanent dipole attractive potential on the

collision limit rate coefficient for an ion-molecule reaction where the neutral possessed a permanent dipole. Their Average Dipole Orientation theory (ADO)[62,63] assumed that the dipole was only partially locked to the ion attractive potential rather than an earlier theory[64] where a "locked dipole" was assumed. The parameterised form of the ADO theory is shown in equation (1.1),

$$k_{ADO} = \frac{2\pi q}{u_r^{1/2}} \left(\alpha^{1/2} + C u_d \left(\frac{2}{\pi kT}\right)^{1/2}\right) \qquad \text{Eqn. (1.1)}$$

where k stands for the Boltzmann constant, u_d is the dipole moment of the polar molecule and C is a dipole locking expression.

The ADO theory was later modified to account for the net conservation of angular momentum between the rotating molecule and the motion of the ion-molecule orbital[65]. The modified theory, labelled the AADO theory by its authors Su et al[65], is shown in parameterised form in equation (1.2),

$$k_{AADO} = \frac{2\pi q}{u_r^{1/2}} \left(\alpha^{1/2} + C u_d \left(\frac{2}{\pi kT}\right)^{1/2} + \frac{Z u_d I^{1/2}}{u_r^{1/4}}\right) \qquad \text{Eqn. (1.2)}$$

where Z is a temperature dependent parameter and I is the moment of inertia of the molecule.

Typically the AADO theory predicts a larger capture rate coefficient for a particular reaction than does the ADO theory, especially for those reactions involving molecules with large permanent dipole moments[58,65]. The predicted capture rate coefficients of the two theories have been found in general to

broadly agree with observed rate coefficients for the majority of exothermic ion-molecule reactions at room temperature[58,65,66].

Available experimental data show that the temperature dependence of most fast ion-molecule reactions, where the neutral has little or no dipole moment, is small[30,46]. Until recently therefore it was assumed that the temperature dependence of ion-molecule reactions involving molecules with larger dipole moments would also be small. This assumption was made simply because no experimental data were available for reactions of these neutrals at low temperatures where they readily condense.

Recently however, a theory has been developed by Clary[67] which predicts a much greater inverse temperature dependence for the rate coefficient of an ion-permanent dipole reaction than does the ADO theory.

The theory, termed the Adiabatic Capture Centrifugal Sudden Approximation theory (abbreviated ACCSA or k_{AC} when used in reference to rate coefficients calculated using the theory), predicts that the individual rotational state rate coefficient, k_J, will increase as the rotational quantum number, J, decreases. At dense interstellar cloud temperatures (5-50 K), where the majority of molecules are in J= 0 rotational states, the theory predicts that $k_{AC}(J=0)$ can be up to an order of magnitude greater than k_{ADO} at 300 K[69].

Two recent studies[68,70], detailed below, of the reactions of neutrals with large dipole moments at low temperatures provide support for the predicted temperature dependence of the ACCSA theory when applied to these ion-molecule reactions.

Clary et al[68] found excellent agreement between theory and experiment in a variable temperature SIFT study of the proton transfer reactions of H_3^+ with HCN and HCl, and HCO^+ with HCN over the temperature range 205-540 K. Rowe and coworkers[70] have studied the reactions of H_2O and NH_3 with He^+, C^+ and N^+ at 27 K using their CRESU (or supersonic jet) apparatus. They observed rate coefficients at this temperature which were much greater than those measured at 300 K and which were consistent with the predicted ACCSA theory collision limit values[68].

The activated complex theory suggests therefore that current models of chemical processes in interstellar clouds will need to revise upwards estimated collision rate coefficients for the reactions of neutrals with large dipole moments[69].

1.3 INTRODUCTION TO THE PRESENT WORK.

In this work the rate coefficients and product distributions for a large number of thermal energy positive ion-molecule reactions at 302±5 K and, unless stated otherwise, at pressures of 0.3 Torr have been determined using the SIFT technique.

For the purposes of this study radical cations and diradical cations (or carbene ions) have not been distingushed from simple cations (except where specifically mentioned). For example the radical cation $CH_3CN^{+\cdot}$ has been described in this study as simply CH_3CN^+. This convention has been adopted because with the SIFT technique radical cation, diradical cation and cation species can not be separately

identified.

The development of the particular SIFT used in this work and its operation is described in Chapter Two. Chapters Three to Six detail the results of measurements and discuss their significance while the final section contains suggestions for further research.

The measurements presented in Chapter Three were made in the course of obtaining the proton affinity of HC_3N. Also in Chapter Three the results obtained for a number of reactions of the HC_3N neutral with ions of interstellar significance are discussed as well as the reactions of ions derived from HC_3N with molecules known to exist in dense interstellar clouds.

Chapter Four presents measurements made to determine the proton affinities of CH_3CN and CH_3NC as well as the reactions of the ion $C_2H_4N^+$, derived from the reaction of the CH_3^+ ion with HCN. The ion $C_2H_4N^+$ is shown to exist in two stable isomeric forms in the flow tube and an estimate to the magnitude of the isomerisation barrier between the two isomers CH_3CNH^+ and CH_3NCH^+ is made.

Chapter Five discusses a programme of measurements made on the reactions of the ions C_2N^+ and HC_2N^+ with various neutrals. This series of measurements was initiated in an attempt to provide experimental evidence for the separate existence of isomers of C_2N^+ and HC_2N^+.

Chapter Six lists the results of a study of the reactions of a number of series of hydrocarbon ions (for example $C_4H_n^+$ (n= 0-6)) with the neutrals C_2H_2, HCN, C_6H_6 and H_2. Measurements made to determine the proton affinity of C_4H_2 are also presented.

For the majority of ion-molecule reactions documented in this thesis the overall reaction enthalpies (ΔH° at 298 K) are also tabulated. These ΔH° values have been estimated by the summing of the heats of formation (ΔH_f° at 298 K) of the participating ion and neutral species in each reaction. When evaluating the heats of formation of protonated species from neutrals for which the proton affinity was determined in this thesis, ΔH_f° (at 298 K) for a proton was taken as 1536.3 kJ mol^{-1} [167]. Heats of formation for neutrals were obtained from the evaluated data compilations of Lias et al[92], Stull and Prophet[167], and of Chase and coworkers[168,169]. Values of heats of formation for ions were taken from the following sources; Lias et al[92], Rosenstock et al[93], Harland et al[94,95] and Anicich et al[147].

The rate coefficients measured are also compared with the relevant theoretical collision limit rate coefficient (where the appropriate k_C is either k_L, k_{ADO}, k_{AADO} or k_{AC} depending upon the neutral reactant involved). The programmes used for the calculations of these collision limit rate coefficents are listed in Appendix 2.

Appendix 1 lists the programmes used for data sampling with the SIFT along with the programme used to obtain experimental rate coefficients from the raw experimental data.

Wherever appropriate, SI units are used in this thesis. However, non-SI units conventionally used in the literature are retained here to assist in direct data comparision with other tabulated values. A table defining all non-SI units used is given in Appendix 3.

CHAPTER 2

EXPERIMENTAL

2.1 GENERAL DESCRIPTION.

In order to measure a rate coefficient for a reaction by means of the selected ion flow tube (SIFT) a flow of a suitable carrier gas must first be established in the flow tube (fig. 2.0).

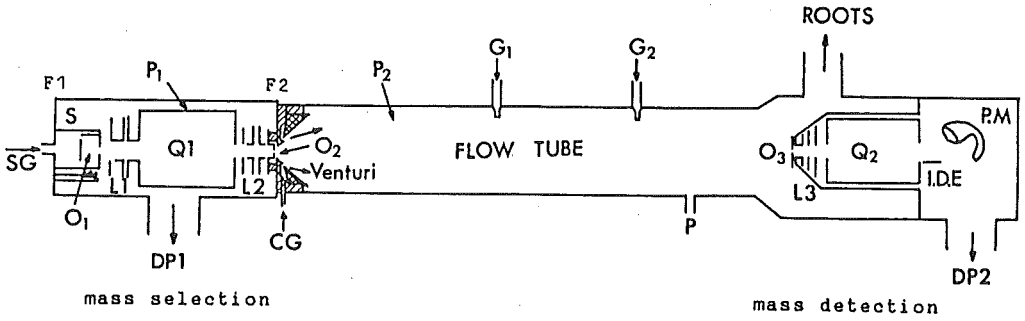

Fig. 2.0: Schematic diagram of the SIFT apparatus. SG- ion source gas; S- electron impact ion source; L1, L2, L3- electrostatic Einzel lens; Q1, Q2- quadrupole mass filters; O_1, O_2, O_3- orifices; DP1, DP2- diffusion pumps; CG- carrier gas; F1, F2- flanges; G1, G2- reactant gas inlets; PM- particle multiplier; IDE- ion deflection electrode.

In this study helium was the main carrier gas used, but hydrogen and argon were also used in minor roles. Helium volume flows between 40 STP cm^3 s^{-1} and 250 STP cm^3 s^{-1} at pressures between 0.15 Torr and 0.5 Torr were achieved using a Roots-type blower backed by a mechanical pump.

Primary ions were generated by electron impact upon a suitable source gas in the ion source. These ions were then

focused into the upstream quadrupole mass filter (Q1) where only ions of the required mass-to-charge ratio were transmitted. After injection into the Venturi inlet (Venturi, fig. 2.0) the ions flowed down the tube at an average velocity of $\sim 10^{+4}$ cm s^{-1}. The positive ion swarm thus generated was then perturbed by the addition of a known flow of a selected neutral reactant at either of the two inlet jets (G1, G2) shown in figure 2.0.

The product ions of the subsequent reaction and remaining primary ions were then sampled on axis through a small orifice (O_3) in the differentially pumped nose cone. Ions sampled by the nose cone orifice were focused into the entrance aperture of the downstream quadrupole mass filter (Q2), mass analysed, and then counted by a particle multiplier-pulse counter combination.

The rate coefficient for any particular reaction was determined by monitoring the primary ion count as a function of the neutral reactant flow rate. Where there was more than one product for a reaction, the ratios of the various product ions were established by monitoring the count rate of each product ion as a function of the neutral flow rate. Each product ion count was expressed as a fraction of the total product ion count and plotted as a function of the neutral gas flow. These product functions were then extrapolated to zero pressure of the neutral gas to find the ratio of primary product ions[14,49].

2.2 THE FLOW SYSTEM.

The flow tube used in this study was a stainless steel tube of 123cm length and 7.3cm i.d.. A carrier gas was introduced into the flow tube through the Venturi inlet nozzle at typical flow rates for helium between 40 STP cm^3 s^{-1} and 250 STP cm^3 s^{-1}, resulting in tube pressures of 0.15 Torr to 0.5 Torr. Ions were injected into the flow tube from the ion source chamber. This chamber was evacuated to a pressure typically less than 10^{-4} Torr during operation by a 10cm oil diffusion pump (Varian model VHS-4) backed by a mechanical pump (Jigtool model SE 200). A water cooled baffle was positioned between the diffusion pump and the ion source chamber to eliminate possible oil contamination. The pumping speed of the combined diffusion pump-baffle combination was ~0.5 m^3 s^{-1} for helium over the pressure range 10^{-3} to 10^{-6} Torr.

The carrier gas after flowing down the reaction tube, was exhausted through a 15cm diameter high-vacuum gate valve to a Roots-type blower backed by a mechanical pump via a 20cm diameter aluminium pipe. The Roots blower (Japan Vacuum Engineering model PMB-020) has a maximum pumping speed of 0.57 m^3 s^{-1} at 0.1 Torr. The backing pump (Japan Vacuum Engineering model PKS-030) has a pumping speed of 0.05 m^3 s^{-1}.

The downstream quadrupole chamber was maintained at a pressure of ~6 x 10^{-6} Torr during a helium carrier flow of 150 STP cm^3 s^{-1} by a 10cm oil diffusion pump (Varian model VHS-4). A liquid nitrogen cooled trap was positioned between the quadrupole chamber and the diffusion pump. The trap, in

combination with the diffusion pump, resulted in a pumping speed of ~0.45 $m^3 s^{-1}$ for pressures ranging from 10^{-3} to 10^{-6} Torr with helium.

Neutral reactants could be added into the flow tube at either of two inlet jets. These jets were located at 44.7cm and 84.7cm from the nose cone orifice and consisted of 1cm lengths of 16mm i.d. stainless steel tubing. Each inlet jet terminated 2.6cm from the flow tube axis in a 1.6mm diameter hole facing upstream at the end.

Observation ports were fitted immediately downstream from each of the neutral inlet jets. These ports consisted of a sapphire window mounted in the tube wall and positioned 2.5cm downstream from the respective reaction inlet jet. All the system joints were sealed with either Viton-A O-rings, Buna-N O-rings or aluminium cajon seals.

2.3 CONTROL AND MEASUREMENT OF FLOW AND PRESSURE.

For the accurate measurement of rate coefficients and product ion ratios with the SIFT system, the carrier gas flow and the neutral reactant flow must be able to be measured and controlled precisely. The same need for accuracy applies to the flow tube pressure and the ion source pressure.

The flow tube pressure was measured by a 10 Torr absolute capacitance manometer (MKS Baratron type 221). The sampling port (P, fig. 2.0) for this manometer was situated halfway between the downstream neutral reactant inlet jet and the nose cone orifice. The pressure of the incoming carrier gas upstream of the Venturi inlet was measured using one port of a

1000 Torr differential capacitance manometer (MKS Baratron type 221A). The other port of the manometer was pumped by a single stage glass oil diffusion pump backed by a mechanical pump to a base pressure of 1×10^{-5} Torr.

The carrier gas inlet line is shown schematically in figure 2.1. The carrier gas volume flow rate was measured using a mass flowcontroller (Tylan model FC-261). In this study the mass flow-meter was initially calibrated by placing a dry-test meter (George Wilson Ltd) in series with the mass flow-meter in the carrier gas handling line. The time taken for the passage of a given gas volume was then measured under steady flow conditions at a pressure of near one atmosphere. At helium flow rates less than 130 STP cm^3 s^{-1}, the measured flow rate of the dry test correlated linearly with the mass flow-meter readout. However the mass flow meter calibration could not be confirmed at volume flow rates greater than 130 STP cm^3 s^{-1} because the pressures used in the carrier gas line to sustain high flows were outside the operating range of the dry flow meter.

A second method of carrier flow calibration[14] was therefore used. Firstly the volume of a large cylinder was accurately measured by expansion of gas from a large glass bulb of known volume. The cylinder was then filled with helium to a pressure significantly greater than one atmosphere. The cylinder pressure was measured by one port of the 1000 Torr differential capacitance manometer. The reference port of this manometer was maintained at the prevailing atmospheric pressure, which meant helium pressures of up to 1000 Torr above atmosphere could be accurately monitored. The helium

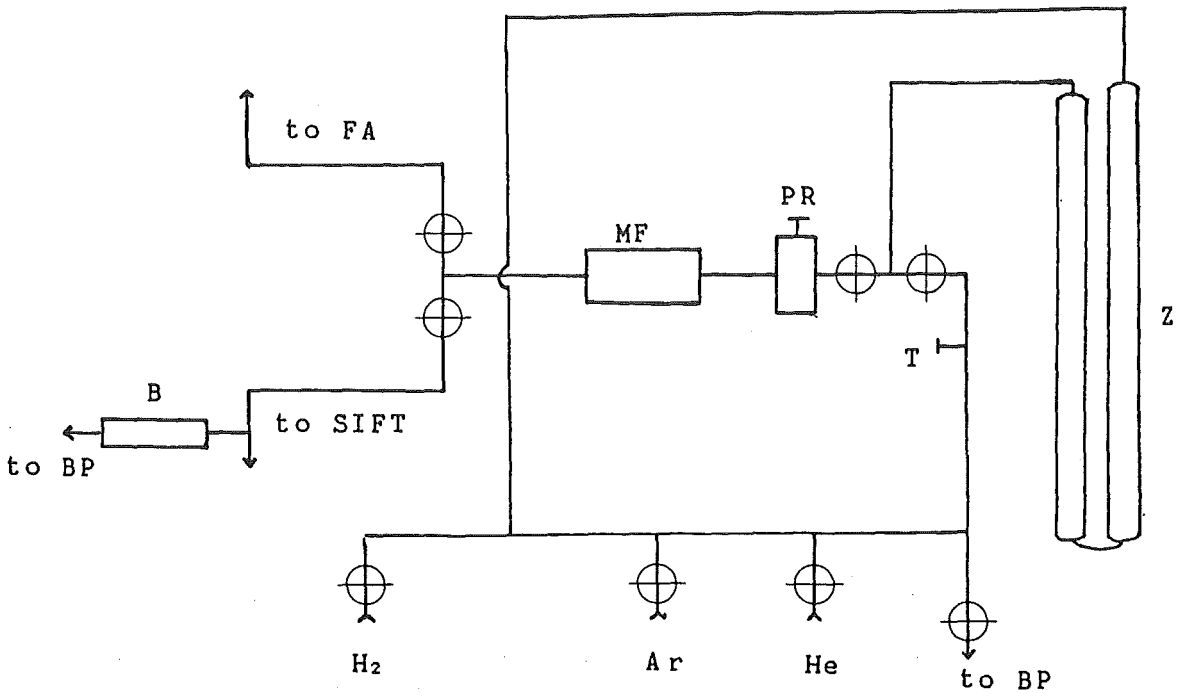

Fig. 2.1: Schematic diagram of the carrier gas inlet line. Z- zeolite trap; PR- pressure regulator; MF- mass flow controller; T- thermocouple; ⊕ - stopcock; BP- vacuum pump; B- 1000 Torr differential capacitance manometer.

from the known volume was then expanded through the mass flow-meter for a measured time interval. From the difference in pressures in the known volume over a measured time interval the carrier gas flow volume for the relevant mass flow-meter setting could then be calculated. A linear relationship was found between the carrier gas flow rate and the mass flow-meter output up to volume flow rates of 180 STP cm^3 s^{-1}. Unfortunately the pressures needed to sustain flows higher than than this value exceeded the range of the 1000 Torr Baratron. It was assumed that this relationship held up to the highest volume flow rates used in this study of 280 STP cm^3 s^{-1}. Verification of this assumption came from the observation of invariant rate coefficients for bimolecular reactions at different carrier gas flow rates.

The neutral reactant was added through either the first or second inlet jet from a glass line shown schematically in figure 2.2. This line was evacuated to a pressure of 1×10^{-5} Torr by a single stage oil glass diffusion pump backed by a two-stage mechanical pump (Alcatel model 370-C55). Each inlet jet had available four separate calibrated volumes, depending upon the neutral flow rate needed. The flow rate of the neutral gas was measured by sampling the pressure drop of a calibrated volume over a specified time interval.

To control the magnitude of the neutral flow for inlet jet no. 1 a Whitey-type (LB 1B) needle valve was used. For inlet jet no. 2 a variable leak valve (Varian model 951-5100) allowed for very fine gradations in the neutral flow. In most of the rate coefficients measured in this study, inlet jet no. 2 was used for neutral reactant addition. The pressure drop in the

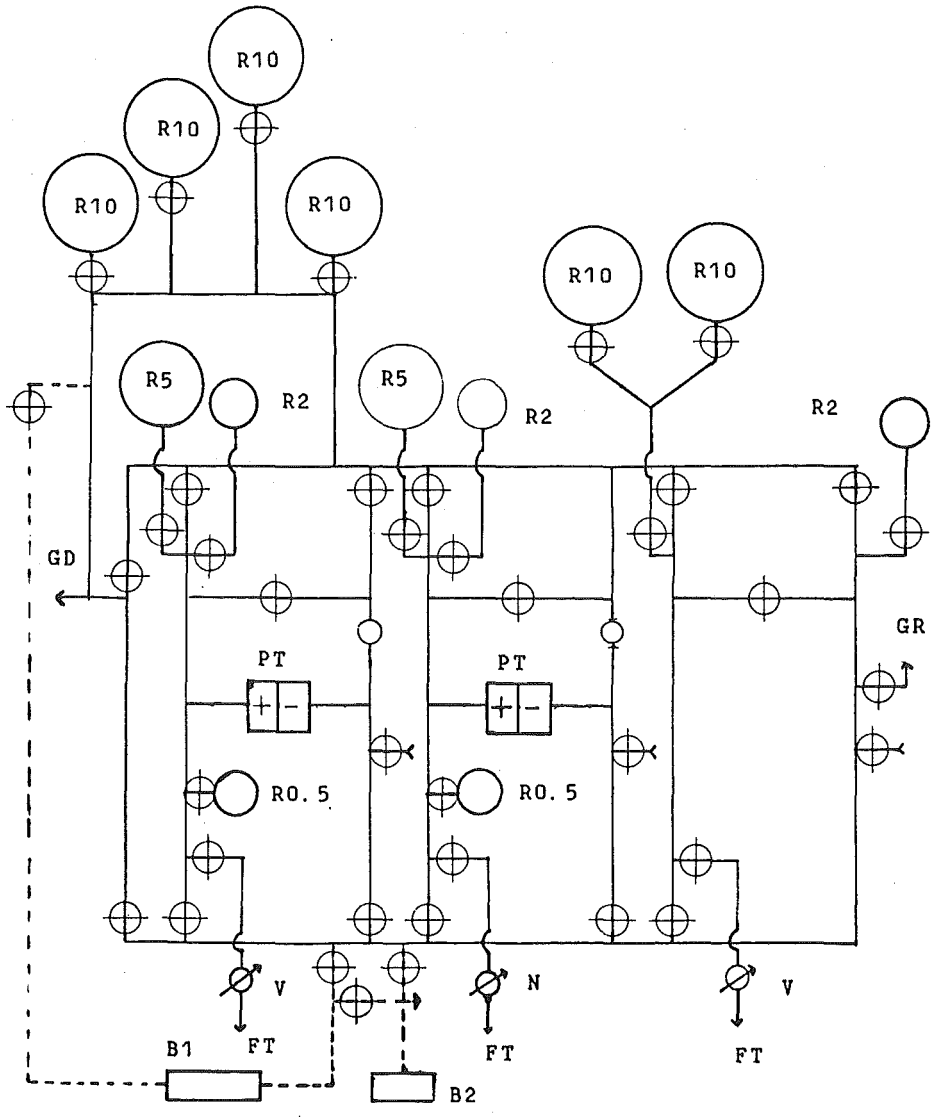

Fig 2.2: Schematic diagram of the neutral reactant gas handling line. PT- pressure transducer; FT- to the flow tube; N- needle valve; V- variable leak valve; GD- to glass diffusion pump and two-stage backing pump; GR- to gas regulators; B1- 1000 Torr differential capacitance manometer; B2- 10 Torr absolute capacitance manometer; RO.5- 0.5l bulb; R2- 2l bulb; R5- 5l bulb; R10- 10l bulb; ⊕ - stopcock.

chosen volume was monitored using a differential transducer (Validyne model DP15-20, 7 Torr diaphragm). The change in pressure on one side of the differential transducer resulted in a change in capacitance on the transducer diaphragm. This capacitance change in turn produced a voltage response which was scaled by an amplifier (Validyne control unit model MC1-10C) to a desired voltage output. In this study an output of 0.7 volts from the control unit was set to correspond to a pressure differential of 7 Torr.

This voltage was periodically sampled by an analogue-to-digital interface and instrumentation amplifier unit (ADALAB Interface (tm), Interactive Microware, Inc.) controlled by an assembly language programme running on an Apple 2e micro-computer (this program listing is shown in Appendix 1). The corresponding pressure drop per second in the relevant calibrated volume was then calculated using a basic language programme (TEMPWAND, Appendix 1) and printed out for later analysis. Another basic programme (MR BIG, Appendix 1) could display the voltage output of the Validyne transducer corresponding to a particular neutral gas flow rate. The computer sampled the transducer output at predetermined time intervals and then permitted one appropriate value to be recorded along with the primary ion count at that flow rate. A real time plot of the log of the ion count versus neutral reactant flow was then displayed.

2.4 ION SOURCE.

The ion source is schematically outlined in figure 2.3.

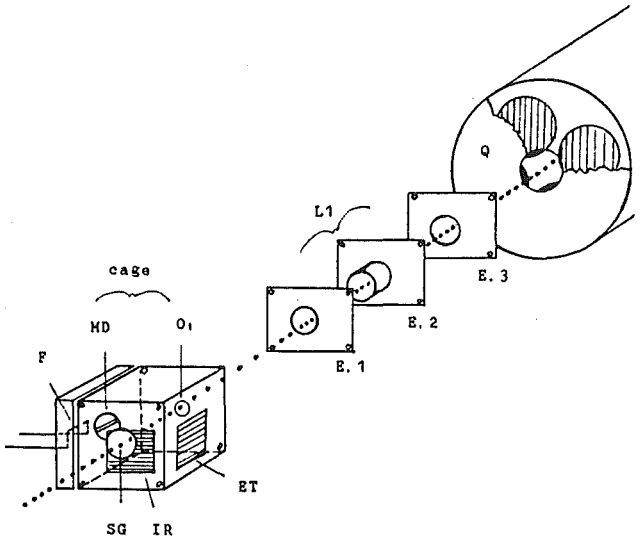

Fig. 2.3: Schematic diagram of the SIFT electron impact ion source. F- filament; MD- molybdenum disc; ET- electron trap; IR- ion repeller; SG- source gas entrance; O_1- orifice 1; E.1, E.2, E.3- Einzel lens combination; Q- quadrupole case.

Ions were generated by electron impact on a neutral gas inside a stainless steel box, designated as the ion source "cage" (fig. 2.3). This cage was mounted, with its centre on-axis, to the inlet aperture of the upstream mass filter chamber. The gas to be ionised was passed by a variable leak valve (Varian model 951-5100) from the ion source gas handling line (shown in fig. 2.2) and into the base of the cage. The electrons were generated from a heated 1cm length of rhenium ribbon 2mm in width and 0.5mm thick. This filament ribbon (F) was mounted on two molybdenum rods located outside the ion source cage. These rods, 3mm in diameter and approximately 2cm long, were insulated by a ceramic block from the source cage. Other materials were also tried as electron emitters and included iridium wire, platinum- 13% rhodium wire coated with barium zirconate, and tungsten wire. However the rhenium strip was

found to perform best for the ion source pressures (less than or equal to 2 x 10^{-4} Torr) and gas mixtures used in this study. For some hydrocarbon compounds, especially acetylene and diacetylene, rhenium ribbon was the only material able to be used as an electron emitter for any length of time.

All the potentials described with respect to the ion source were referenced to ground. The filament was maintained at a negative potential of typically 25 V to force electrons generated towards the cage. An emission control unit was used to supply emission current in the range of 0.2 to 2.0 mA. This control unit, built in the department, was capable of stable current output from 0.1 to 10.0 mA at a potential of 10 to 100 volts. The cage itself was maintained at a positive potential (~5 V) to draw the electrons to a 5mm by 0.9mm entrance slit in a molybdenum disc (MD) pressed into the cage side.

A stainless steel electrode, the "electron trap" (ET), was mounted on the cage wall opposite to the electron entrance. This trap was maintained at typically +20 V to draw the electrons from the entrance slit through the neutral gas in the ion source. The "ion repeller" (IR), another electrode of stainless steel, was sited at the source gas entrance (SG). A positive voltage (typically 25 V) on the repeller forced ions formed through electron impact towards a 3mm diameter orifice (O_1) in the cage top. A negative potential field generated by a three element Einzel lens combination (L1) then focused ions ejected from the cage into the entrance aperture of the upstream quadrupole mass filter (Q1). Typical voltages on each Einzel lens element were -230 V on E.1, -5 V on E.2, and -230 V on E.3..

2.5 SIFT MASS SELECTION REGION.

The mass filter and Venturi inlet used in this study are shown in detail in figure 2.4.

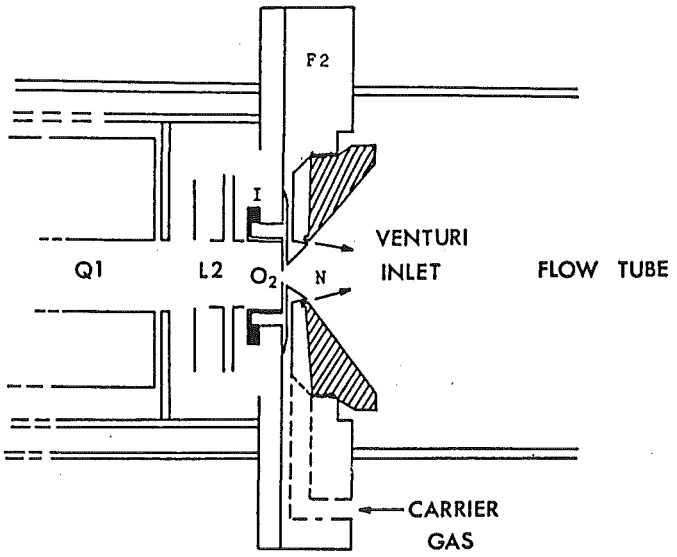

Fig. 2.4: Schematic diagram of the SIFT Venturi inlet. I- electrical insulators; N- nozzle; all other symbols as in Fig. 2.0.

The stainless steel quadrupole mass filter (made by Precision Engineering, Boulder, Colorado) had rods 16cm in length with an overall field radius of 1.49cm. The power supply was a commercial radio frequency voltage scanning instrument (made by Extranuclear Laboratories Inc.). The high Q head used (Extranuclear model 13) limited the mass range of ions able to be injected to 0-200 amu. Near unit mass resolution could be achieved over the whole of this mass range. For example, the isotopes of the bromoform ion ($C_2H_2Br_2^+$) at 184, 186 and 188 amu respectively, were able to be selected individually by the upstream mass filter (Q1) and separately injected into the flow tube. Figure 2.5 shows a series of graphs illustrating the selectivity of the upstream mass filter at high masses.

The ions, once focused into the vicinity of the mass filter

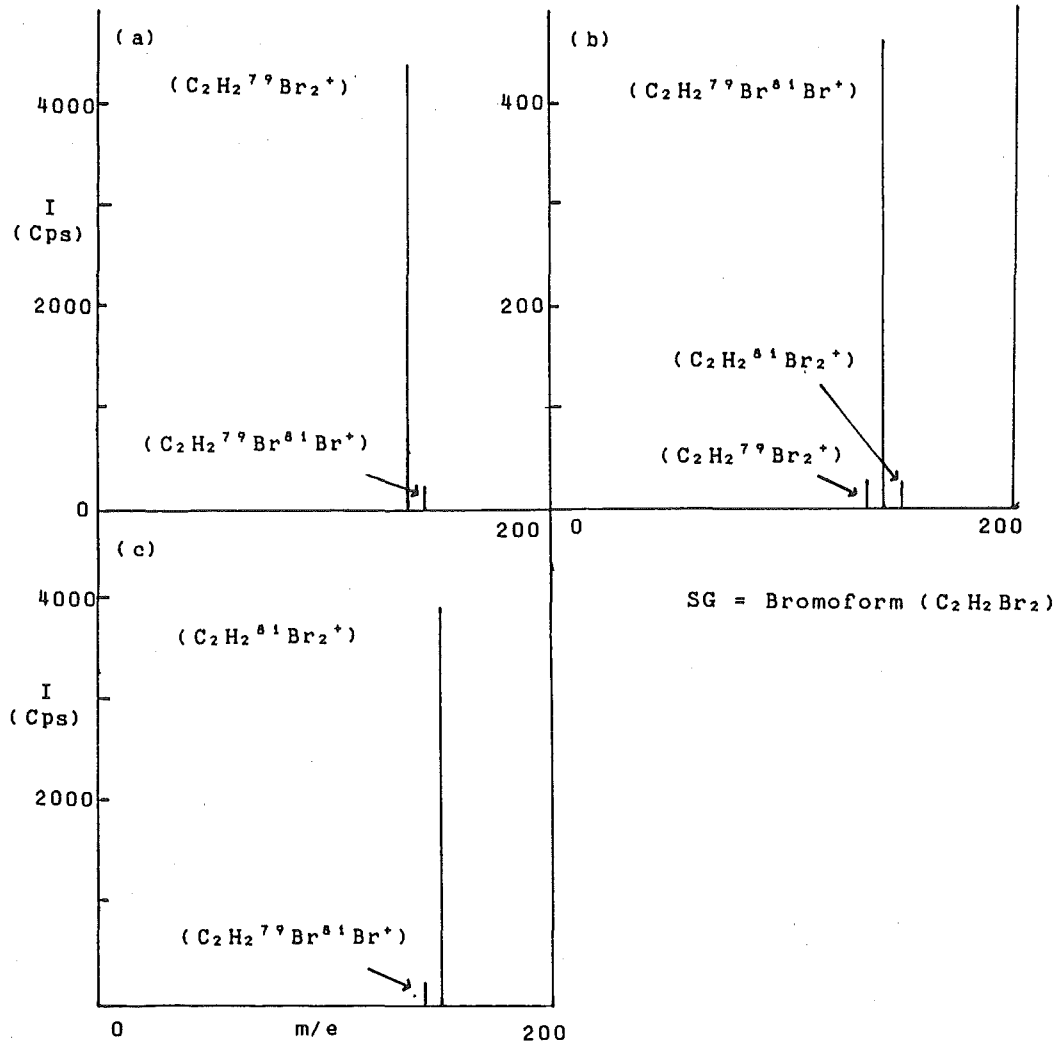

Fig 2.5: The upstream quadrupole mass filter selectivity at high mass-to-charge ratios. The three graphs show the resulting ion peaks after selection and injection into the flow tube of the following m/e's- (a) 184 ($C_2H_2{}^{79}Br_2^+$)
(b) 186 ($C_2H_2{}^{79}Br^{81}Br^+$)
(c) 188 ($C_2H_2{}^{81}Br_2^+$)

case aperture, passed through this 1cm orifice under the influence of a 5 V negative potential on the case itself. The quadrupole mass filter rods were also biased at typically -15 V to assist in ion transmission. After passing through the mass filter, the ions were then focused by a second three element Einzel lens configuration (L2) into the Venturi inlet exit orifice (O_2, fig. 2.4). The orifice, a 1.5mm diameter hole in a 10mm o.d. molybdenum disc, was positioned on axis by a stainless steel ring. This ring or "exit" element, of 10mm inside diameter, was positioned 1cm above the exit orifice (O_2). Together the exit element and exit orifice were biased at ~4-6 V to provide a final attractive potential field which, in concert with the Venturi inlet, "drifted" the ions through to the flow tube.

Typical operating pressures in the flow tube were 0.1-0.4 Torr whilst pressures in the source region ranged from 3×10^{-5} Torr to 2×10^{-4} Torr. The resultant pressure gradient through which an ion must pass to be injected into the flow tube was overcome by the use of a Venturi inlet[14]. In the Venturi inlet used in this study, the carrier gas entered around the outside of the nozzle (N) through a 6.4mm diameter channel in the flow tube flange (F1). The carrier gas (typical upstream pressure was 1100 Torr) was forced through a narrow 0.03mm annular gap in the nozzle base. The effect of the carrier gas being forced forward into the flow tube was to prevent scattering of ions as they drifted from the low pressure ion source region into the higher pressure flow tube.

The success of the Venturi inlet used in this study in reducing backstreaming from the flow tube is illustrated by

the following test[71]. When the diffusion pump (DP1, fig. 2.0) was isolated from the ion source chamber, backstreaming from the flow tube at pressure P2 resulted in an equilibrium pressure, P1, within the source chamber. Under the above conditions with a helium carrier gas, the ratio of P2 to P1 was 13 in the flow range 90-250 STP cm^3 s^{-1}. With the diffusion pump open to the source chamber, at a helium carrier flow of 178 STP cm^3 s^{-1} the pressure P1 was 2.6×10^{-5} Torr. These diagnostics compare favourably with the performances of Venturi inlets in other SIFT systems[71].

The possibility also exists that in forcing the carrier gas through the Venturi nozzle, the laminar flow region in the flow tube might not be established until after the point of neutral reactant addition. To establish whether turbulent flow was a problem in our flow tube, the reaction of the ion C^+ with the neutral O_2 was studied over the flow tube pressure range 0.25-0.40 Torr with both helium and hydrogen as carrier gases. In contrast to Mackay et al[72], the rate coefficients measured for the reaction remained constant over the total pressure range for both inlet jets, and both carrier gases.

The central requirement in the use of the SIFT technique is the ability to select and inject ions of only one particular mass-to-charge ratio. The extent to which the ideal of a positive ion swarm, containing ions of a single amu type, was achieved depended upon a number of factors. The three most important of these variables were the ion source gas type, the ion energy during injection into the flow tube and the ion source region pressure. For example when CH_3^+ was generated by electron impact on CH_4, the optimum ratio of CH_3^+ in the

mixture of ions at m/e 13, 14, 15 and 16 injected into the flow tube was 2/5/100/1. This ratio was achieved with an ion energy of 15 V and an ion source pressure of 8 x 10^{-5} Torr. At this source pressure a peak at a m/e of 29 ($C_2H_5^+$) resulting from CH_4 leaking into the flow tube was also present. If the source pressure was then increased to 2 x 10^{-4} torr the ratio of 15 to 29 amu decreased from ~100/1 to ~100/30. If the ion energy was increased to 25 V the resultant m/e ratios for the ions 13, 14, 15 and 16 were only 30/30/100/50. However if CH_3^+ was generated by electron impact on CH_3I at a source pressure of 4 x 10^{-5} Torr and an ion energy of 15 V, then ions of solely 15 amu could be injected (table 2.0 lists the neutrals used to generate specific ions in this study, along with the percentage impurities for each ion).

Table 2.0: Neutrals used to generate specific ion types.

ion	neutral	% impurities[a,b]			
C^+	CH_4	13 (8%)	14 (5%)	15 (2%)	
	CO	16 (5%)			
	CCl_4	$(C^+)^*$ [c]			
	CO_2	$(C^+)^*$ [c]			
CH^+	CH_4	12 (10%)	14 (10%)	15 (5%)	
	$CHCl_3$	12 (5%)			
CH_2^+	CH_4	12 (5%)	13 (10%)	15 (8%)	
	CH_2Br_2	13 (2%)			
CH_3^+	CH_4	13 (2%)	14 (5%)	16 (1%)	29 (1%)
	CH_3Br	-			
	CH_3I	-			
C_2^+	C_2H_2	25 (5%)			
	C_2Cl_4	-			
	C_2HCl_3	25 (5%)			
C_2H^+	C_2H_2	24 (35%)	26 (40%)		
	C_2HCl_3	24 (1.8%)	26 (1.6%)		
	$C_2H_2Br_2$	24 (30%)			

Table 2.0 continued.

$C_2H_2^+$	C_2H_2	25 (5%)	27 (7%)
	$C_2H_2Br_2$	25 (1.4%)	27 (1.4%)

(a) Represents the optimum ratio of the required ion to other ions.
(b) The m/e values shown represent the impurity ions present in the relevant primary ion swarm, while the numbers in parenthesis are the magnitudes of these impurities with respect to the primary ion concentration. eg. 15 (2%) represents a 2% impurity at m/e= 15.
(c) A large fraction of the observed ions were metastable. See section 5.3 p.163.

It was also possible, at low ion energies, to inject cluster ions such as $(CH_3CN)_2H^+$ and $(HC_3N)_2H^+$ without breakup into the flow tube. A typical mass spectrum of the $(CH_3CN)_2H^+$ ion peak versus breakup ions is shown in figure 2.6a, while figure 2.6b shows a spectrum of the same cluster ion injected at a higher ion energy.

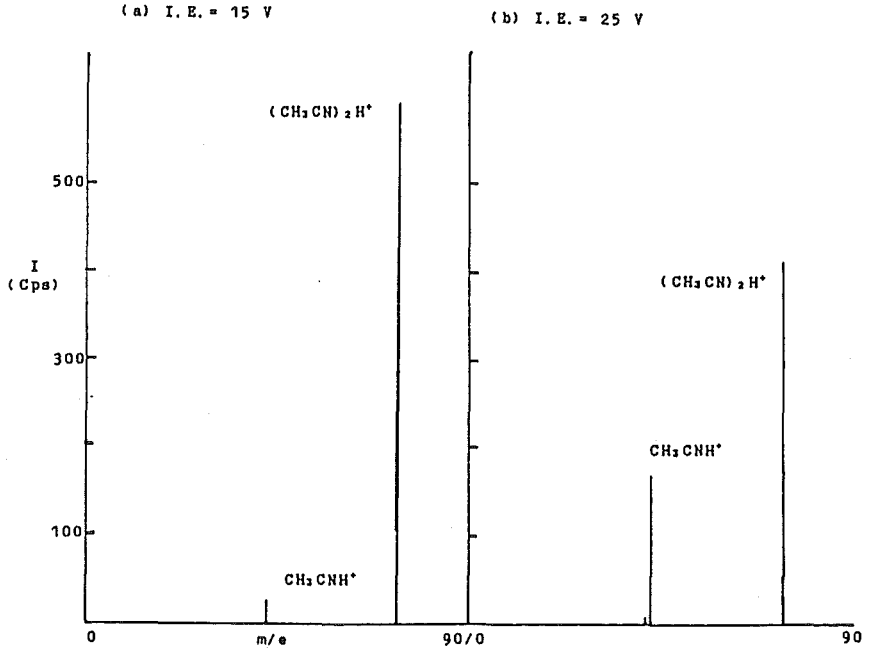

Fig. 2.6: Mass spectra of the ion $(CH_3CN)_2H^+$ at injection energies of (a) 15 V and (b) 25 V.

2.6 SIFT MASS ANALYSIS REGION.

A diagram of the downstream ion detection system is shown in figure 2.7.

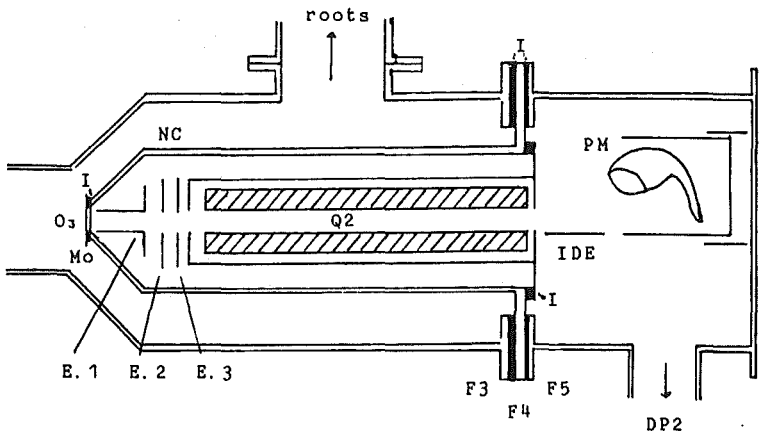

Fig. 2.7: A schematic diagram of the downstream ion detection system. NC- nose cone; Mo- molybdenum disc; I- electrical insulators; E.1, E.2, E.3- Einzel lens combination; F3, F4, F5- flanges. All other symbols as in Fig. 2.0.

A small percentage of the positive ion swarm flowing down the tube was sampled on axis by a small hole in the nose cone (O_3). After being focused into the downstream quadrupole mass filter (Q2) the sampled ions were detected by a particle multiplier.

The stainless steel nose cone had the shape of a cylinder topped with a truncated cone. The cylindrical part of the nose cone was 20.4cm in length and 8.9cm in diameter. The final truncated cone was 3.6cm in length and tapered at a 45° angle from the base to the apex. In the present study an insulated 2.5cm diameter molybdenum disc with a 0.46mm orifice was positioned at the nose cone apex. The nose cone flange (F4) was sealed between the flow tube flange (F3) and the downstream mass filter flange (F5) by two Viton-A O-rings. Teflon washers were used to insulate the nose cone from these flanges. The

nose cone was biased at approximately -7 V and the molybdenum disc at -5 V to improve the overall nose cone sampling efficiency of ions.

The first element of the nose cone Einzel lens combination (L3) was positioned inside the nose cone, 1mm below the molybdenum disc. The other two elements were positioned 1.5cm and 3cm respectively from the molybdenum disc. Typical potentials of -19 V on E.1, -50 V on E.2 and -60 V on E.3 were used to focus ions sampled through the nose cone into the mass filter (Q2) entrance. The transmission of positive ions from the flow tube through to the mass filter and particle multiplier depended critically on the nose cone potentials and Einzel lens potentials of the downstream lens assembly. For example, a change in potential of 0.3 V on element 1 of the nose cone Einzel lens caused a complete defocusing of the ion beam, as seen in the ion transmission falling to zero.

The downstream quadrupole mass filter and case were of the same material and dimensions as the quadrupole and case used for ion selection. An Extranuclear power supply was also used to drive the downstream filter, however a different high-Q head (Extranuclear model 15) enabled mass detection over the range 0-400 amu. The mass filter axis and housing were floated at the nose cone potential. A magnetic ceramic insert ("ceramag", patented by Extranuclear Laboratories, Inc.), positioned at the downstream quadrupole entrance, made little difference to the quadrupole performance.

The ions, having passed through the mass filter, were then deflected by an "ion deflection" electrode (IDE) at a positive potential of typically 1200 V towards the entrance aperture of

a continuous dynode particle multiplier (Galileo Electro-optics model 4816). The particle multiplier (PM) was firmly mounted off axis, on teflon supports, to prevent photons from the ion source registering as ions. The surface coating at the entrance region of the particle multiplier was biased at -2800 V to draw ions towards, and into the multiplier. The circuit used to apply this potential to the multiplier base and that used to monitor ion events are shown in figure 2.8.

Each pulse of electrons, corresponding to one ion event in the particle multiplier, was converted to a voltage pulse by a preamplifier. The voltage pulse was then compared to a standard adjustable voltage level from a comparator (the preamplifier-comparator circuit used in this study is equivalent to the circuit used in Extranuclear model 032-3). The resulting low-going TTL pulse was then counted by an A-D pulse counting circuit built into a ratemeter (circuit equivalent to Extranuclear model 275-K2). TTL pulses collected in this manner could then be displayed as an ion count over a 1, 10 or 100 second interval. The ratemeter also developed a 0-10 V analog signal which was directly proportional to the preamplifier count rate. This analog signal was used to drive an oscilloscope display (Kikisui Digitial Storage oscilloscope model DSS (65210)).

Several of the ion-molecule reactions investigated in this study produced products that were widely different in mass. For example the reaction of $C_2H_5IH^+$ with C_4H_2, which was one of the reactions investigated (section 6.2), produced product ions at m/e= 51 ($C_4H_3^+$) and at m/e= 207 ($C_2H_5IH^+.C_4H_2$). As the m/e value of the ion increases, the transmission

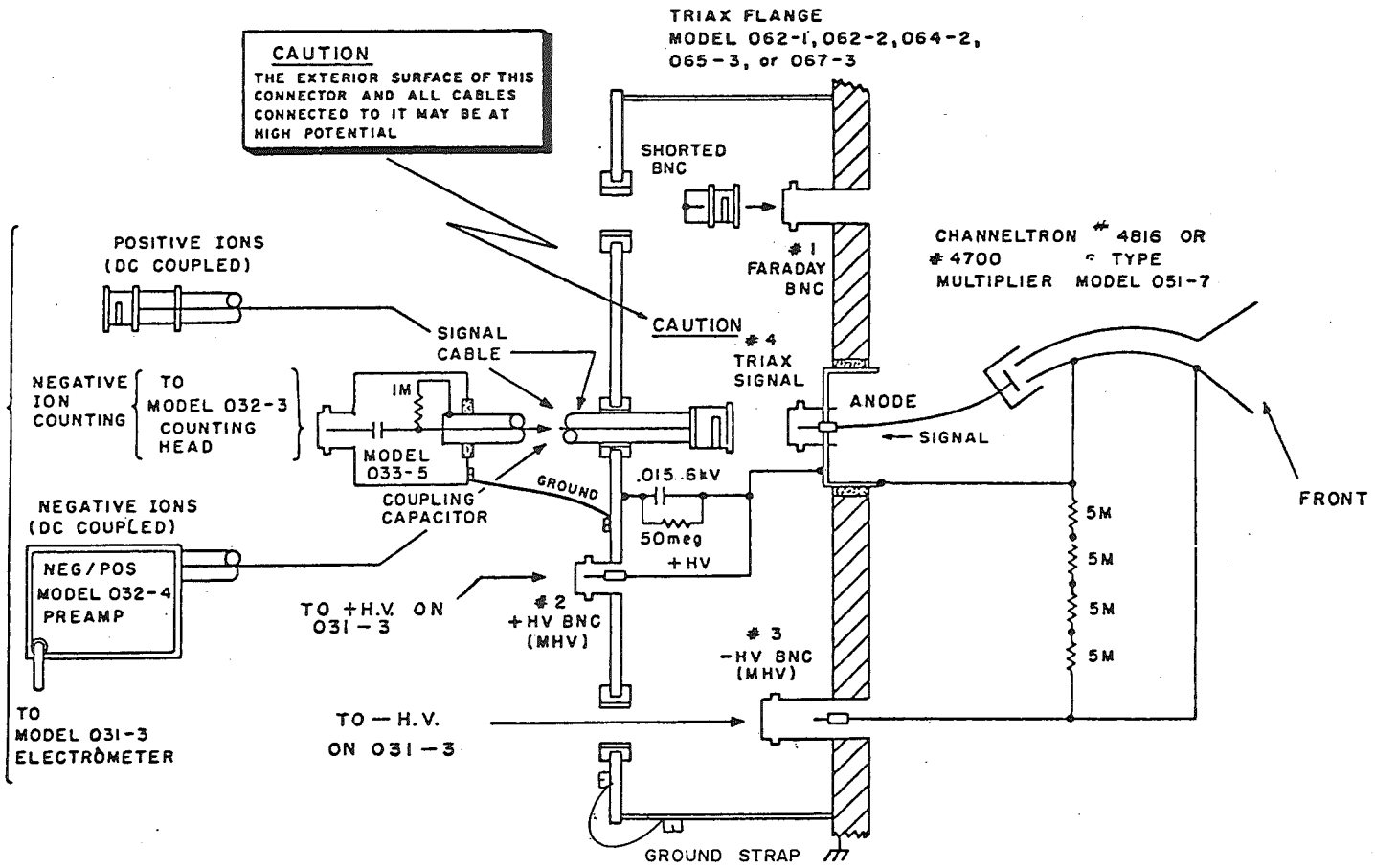

FIG. 2.8: Particule multiplier output circuitry (reproduced from Extranuclear Laboratories, Inc., Triax flange manual).

efficiency of a quadrupole mass filter decreases[73]. It is therefore expected that in a reaction resulting in product ions of widely differing mass-to-charge ratios, the higher mass product ions will be discriminated against by the sampling system.

The method used in this study to determine the mass discrimination of the downstream mass filter was first described by Smith and Adams[14]. This method involved injecting ions of a single mass into the flow tube and measuring the resultant current on the nose cone molybdenum disc. The number of ions passed by the mass filter at this particular m/e ratio, over a certain time interval, was then measured. If the quadrupole mass control unit was set at a specified resolution then the relationship between the molybdenum disc current and the number of ions counted could be studied over a range of m/e ratios at this resolution. A compilation of mass discrimination factors for three separate resolution settings, at a number of m/e values, is shown in table 2.1.

Table 2.1: Downstream quadrupole mass filter mass discrimination performance. The mass discrimination for each ion at each arbitrary setting is referenced to the CH_3^+ ion.

ion type	m/e	arbitary resolution setting		
		5.5	6.0	6.3
CH_3^+	15	1.0	1.0	1.0
Ar^+	40	1.0	1.0	1.3
$CH_3NO_2H^+$	62	1.0	1.01	1.6
THP^+	86	1.0	1.05	3.03
$^{81}BrCN^+$	107	1.1	1.2	5.6
$^{131}Xe^+$	131	1.2	1.3	~15

Table 2.1 continued.

$C_2{}^{35}Cl_4{}^+$	164	1.25	1.4	~23
$CH_2{}^{81}Br_2{}^+$	174	1.3	1.5	~30

It can be seen that at a resolution setting of 6.0 the mass discrimination in the downstream sampling system, over a wide range of m/e values, is less than 1.5. The setting of 6.0 was used in the majority of product ratios measured in this study. This setting represented a compromise between adequate adjacent peak separation and an acceptable mass discrimination.

There were also two possible complications that could influence the sensitivity of the SIFT ion detection system. These were the particle multiplier gain and the breakup of weakly bound ionic species such as cluster ions in the sampling process. No evidence was obtained for the breakup of ionic species upon sampling over a wide range of helium carrier flow rates. A number of cluster ions, such as $(CH_3CN)_2.H^+$ and $CH_3NO_2H^+$, were sampled over a 1-5 V range of potentials on the molybdenum nose cone disc. No breakup ions resulting from nose cone sampling were observed.

The second possible detection complication, the particle multiplier gain, was of concern if the actual multiplier gain was significantly less than manufacturer specifications. A loss of multiplier gain could occur for reasons such as diffusion pump oil contamination, coronal discharges through use at high pressures breaking down the multiplier surface coating or simply through prolonged use at pressures in the region of 1×10^{-5} Torr.

To test the multiplier two methods were used. The first method compared the actual number of pulses counted over a period of time with the maximum number of ions, calculated from the molybdenum disc current, able to be transmitted to the particle multiplier. The two values were always within a factor of two.

In the second method the analogue current output of the multiplier, at a known high voltage, was compared with the actual pulse count number per time interval. Both methods showed that the multiplier gain, at the entrance region potential of -2800 V used in this study, was approximately equal to the theoretical multiplier gain under SIFT operating conditions.

2.7 SYSTEM DESIGN PROBLEMS.

During the continuing development of the Selected Ion Flow Tube used in this study many problems have been encountered. For example, the ion source has evolved from one used in the department in a different application to the present configuration shown in figure 2.3.

Initially the ion source electron trap was placed outside the ion source cage and, instead of a repeller electrode, a circular disc placed above the cage top was used to extract ions. The cage top orifice was originally 1.5cm in diameter which resulted in ion cage pressures similar to those in the ion source chamber during operation. The lower operating pressure of the ion cage combined with a smaller electron flux and ineffective potential field for ion extraction resulted in

an inefficient ion source. Consequently, to achieve sufficient ion densities downstream, high voltages were needed in the ion source resulting in the production of high energy ions.

Various combinations of the lens elements used to focus ions from the ion source into the upstream mass filter were tried. All the elements were initially made of aluminium but this material unfortunately quickly oxidised under standard operating conditions. The resulting insulating layer of aluminium oxide, of variable depth on the Einzel lens electrodes (L1) meant inefficient focusing of ions which were already at high energies.

The injection of high energy ions into the upstream mass filter signicantly lowered the resolution capabilities of this filter. For example, when a 20/1 mixture of H_2 and CH_3OH was subjected to electron impact in an attempt to produce the $CH_3OH_2^+$ ion, high energy ions at adjacent masses were also passed by the mass filter in significant numbers. The injection of the ion $CH_3OH_2^+$ through the Venturi inlet at high energy also resulted in the appearance of large amounts of the breakup ions CH_3O^+ and CH_3^+. The effect of high energy ions was a reduction in the ion selection capabilities of the SIFT.

By replacing all the aluminium lens elements with stainless steel ones, introducing a repeller element into the ion cage, and closing up the various cage exit holes, ions could be injected in appreciable quantities into the flow tube. For example, typical ion currents measured on the 2.5cm nose cone disc for Ar^+ and $BrCNH^+$ ions were 3.6 and 5.8 x 10^{-12} A respectively. A laser was also used to align the source exit orifice with the Venturi inlet orifice and the

nose cone orifice. The quadrupole rods were also biased negative to further improve ion transmission. The best resolution of the ion injection mass filter was obtained when the ion injection energy was less than 15 eV.

In the initial SIFT design used in this study, the ratio of ions detected and counted by the downstream injection system to the number of ions injected was very poor. The whole nose cone including the molybdenum disc, was biased at ~-10 volts. Furthermore, the first element of the nose cone Einzel lens combination was positioned 3.5cm downstream from the disc orifice.

In an attempt to improve the ion sampling efficiency of the nose cone, the molybdenum disc was increased in diameter from 1cm to 2.5cm and insulated from the nose cone. To improve the focusing of ions through to the mass filter (Q2) the first Einzel lens element was moved to within 1mm of the orifice O_3. Many lens elements of varying dimensions were then tried in an attempt to improve the overall transmission of ions from the disc orifice to the mass filter (Q2). The present three lens elements, as sketched in figure 2.7, represent the best combination of those tried. Typically ~90% of all the ions sampled by the present downstream ion detection apparatus are detected by the particle multiplier. For example a current of 3.6×10^{-12} A of Ar^+ ions on the nose cone disc resulted in ~8000 cs^{-1} of ions at 40 amu (100% transmission efficiency ~9000 cs^{-1} with a geometric factor of 4×10^{-4}).

Initially the particle multiplier was mounted parallel to, but off the flow tube axis inside a grounded aluminium box. An orifice of 2cm in diameter in the top of this box was

positioned 3cm downstream from the mass filter exit. Initial high background counts from the multiplier were partially overcome by completely shielding the multiplier signal leads with copper sheet, thus reducing "pick-up" from the quadrupole RF leads.

Another contributing noise factor was the presence of earth loops in the power supplies used to provide the lens voltages. To eliminate these loops all circuit earths were referenced directly to a single chassis earth point. To reduce possible noise pickup from mechanical vibrations the multiplier was firmly mounted on blocks of teflon. Conductor leads inside the mass detection chamber were shortened and grouped together and coaxial electrode cables outside the chamber were taped in position. The net result of the above measures, when the RF quadrupole power supply was on, was to reduce the background count level to the manufacturers specifications (0.2 c.p.s.). To further improve the transmission of ions from the mass filter exit to the particle multiplier the box cover was removed. The multiplier itself was moved to within 1cm of the mass filter exit. A deflecting electrode was inserted near the tube axis to bend the ion beam into the multiplier entrance. These measures together reduced the average scatter in a successive number of counts to approximately that expected from count statistics.

There proved to be two main factors in improving the ion transmission of the SIFT system as initially designed. The first was reducing the distance between the ion source and the quadrupole mass filter Q1 by ~5cm. The second factor was the improvement in alignment of orifices O_1, O_2 and O_3 so that

they all centred on the flow tube axis. In the SIFT apparatus used to determine the data presented in this study, it was possible to roughly optimise the quadrupole and lens assemblies in the absence of any carrier gas in the flow tube. Sufficient ions could be transmitted from the source region along the flow tube to be easily detected by the multiplier and counting system. Typical count rates for an injected ion, C^+ at m/e= 12, in the absence of a carrier gas were ~200 c.p.s..

2.8 IMPURITIES.

Impurities, which can give misleading results arose from three main sources: the carrier gas, the neutral reactant and from the ion source chamber.

Carrier gas impurities were mainly water vapour and nitrogen and were not a great problem in this work. If the carrier gas used met the supplier's stated purity limits then a liquid nitrogen cooled zeolite trap in the carrier gas line usually reduced the mass peaks from water and nitrogen to less than 1% levels of the major ion under study. This trap had a total length of 200cm and a diameter of 3.5cm and was filled with Union Carbide type 5A molecular sieve. It was periodically baked to 80°C while being pumped with a mechanical pump to purify the molecular sieve. About 20% of the bottles of helium received from the suppliers had an impurity level that was too high for the trap to cope with. These bottles were returned to the suppliers.

The largest source of impurity ions originated in the ion source chamber. Upon injection of ions of a particular m/e

ratio into the tube, ions adjacent in mass to the ion of interest were transmitted on occasions by the quadrupole mass filter, Q1. Furthermore, unwanted ions were produced by fragmentation of the parent ion during the injection process and also by reaction of the primary ion with trace levels of source gas which entered the flow tube by leaking through the Venturi orifice. However, by carefully selecting the neutral from which the ion of interest was formed, operating the ion source at low pressures and injecting the ion at a low energy, these impurity ions could be eliminated or reduced to a minimum. Also an advantage of the SIFT technique is that these impurities themselves could be injected individually and subsequently reacted with the neutral of interest to establish products and rates.

Neutral reactant impurities were potentially a serious problem, particularly in a slow reaction where small traces of a reactive impurity in the neutral source gas could account for all the reaction observed. In the present work when contamination of the reactant gas was suspected it was always tested by reaction with helium ions. The product ions were then checked for ion peaks not common to the neutral of interest. For example, the final step in the preparation of HC_3N required that propiolamide be dehydrated in a xylene solvent. Xylene boils at 142°C whilst HC_3N boils at 42°C, so therefore HC_3N should easily be separated from xylene by vacuum distillation. The two principal ions formed in the reaction of xylene and He^+ occur at a m/e ratio of 106 and 96 respectively. To detect whether a sample of HC_3N was contaminated with xylene, the products of the reaction between

He^+ and HC_3N were examined for ions at m/e= 96 and 106.

Also during the course of any particular reaction a mass scan over the relevant mass range were undertaken. All ion peaks observed were checked with a view to possible formation from a neutral contaminant.

2.9 MATERIALS.

2.9.1 Carrier Gases

Helium was the main carrier gas used during the course of this work. All the rate coefficients presented in this thesis were measured in a helium carrier unless stated otherwise. Hydrogen was used mainly for calibration purposes.

Helium: industrial grade, supplied by New Zealand Industrial Gases Ltd (NZIG) and purified by passage through a zeolite trap cooled with liquid nitrogen.

Hydrogen: industrial grade, supplied by NZIG and purified by passage through a zeolite trap cooled with liquid nitrogen.

2.9.2 Neutral reactant and ion source gases

Acetaldehyde (CH_3CHO): analytical reagent (AR) grade, supplied by British Drug Houses Chemicals Ltd England (BDH), and further purified by a number of freeze-pump-thaw cycles and trap-to-trap distillation.

Acetylene: industrial grade, supplied by NZIG, and further purified by passage through a dry ice-acetone cooled

zeolite trap.

Cyanoacetylene (HC_3N): prepared by ammonolysis of methyl propiolate followed by dehydration[74]. After trapping the sample under vacuum, further purification was achieved by trap-to-trap distillation.

Diacetylene (C_4H_2): a crude sample was prepared by refluxing a mixture of 1,4 dichlorobut-2-yne, potassium hydroxide, water and dioxane[75]. The diacetylene sample was then collected by passage over a trap at -25 °C and finally purified by trap-to-trap distillation.

Vinylacetylene (C_4H_4): synthesised using the standard method described in reference 76 and further prepared by trap-to-trap distillation.

Ammonia: commercial purity (CP) grade, supplied by Christchurch gases Ltd., 99% pure. It was further purified by a number of freeze-pump-thaw cycles.

Argon: welding grade, supplied by NZIG. Purified by repeated freeze-pump-thaw cycles.

Benzene: AR grade, supplied by BDH, and purified by a number of freeze-pump-thaw cycles followed by trap-to-trap distillation.

Carbon monoxide: CP grade, supplied by the Matheson company, 99.5% pure. When used as a neutral reactant, it was purified by passage through a zeolite trap cooled by liquid nitrogen.

Carbon dioxide: industrial grade, supplied by NZIG, and purified by repeated freeze-pump-thaw cycles.

Carbon tetrachloride: AR grade, supplied by BDH. Purified as for benzene.

Carbon tetrabromide: lab. grade, supplied by BDH. Purified as for benzene.

Dicyanogen (C_2N_2): supplied by the Matheson Company, 98.5% pure. It was purified through repeated freeze-pump-thaw cycles.

Hydrogen Cyanide: prepared by the action of either phosphoric acid or sulphuric acid on sodium cyanide. HCN was dried over phosphorus pentoxide and further purified by trap-to-trap distillation.

Cyanogen bromide (BrCN): prepared by reacting bromine with excess mercuric cyanide under vacuum. The crude cyanogen bromide was collected in a trap cooled to -78°C, and then purified by sublimation.

Diethyl ether ($C_2H_5OC_2H_5$): lab. grade, supplied by May and Baker Ltd. England (MB), and further purified as for benzene.

Ethylene (C_2H_4): CP grade, supplied by the Matheson Company. Further purified by a number of freeze-pump-thaw cycles.

Dibromoethylene ($C_2H_2Br_2$): lab. grade, supplied by Aldrich Chem. Co. Inc. USA., and purified as for benzene.

Trichloroethylene (C_2HCl_3): AR grade, supplied by May and Baker Pty. Ltd. Australia, and further purified as for benzene.

Tetrachloroethylene (C_2Cl_4): technical grade, supplied by BDH, and further purified as for benzene.

Iodoethane (C_2H_5I): lab. grade, supplied by BDH, and purified as for benzene.

1,3-Butadiene (C_4H_6): purity> 99%, supplied by Tokyo Kasei Kogyo Co Ltd Japan. It was further purified by a number of freeze-pump-thaw cycles.

Formic acid (HCOOH): AR grade, supplied by Hopkins and Williams, England, and further purified as for Benzene.

Hydrogen: industrial grade, supplied by NZIG. Purified by passage through a liquid nitrogen cooled sieve.

Methane: ultra high purity grade (min. purity 99.97%), supplied by the Matheson Company, and further purified by passage through a liquid nitrogen cooled zeolite trap.

Methyl bromide: lab. grade, supplied by BDH and further purified as for benzene.

Dichloromethane: lab. grade, supplied by BDH and further purified as for benzene.

Methyl iodide: lab. grade, supplied by MB, and further purified as for benzene.

Methyl formate (CH_3O_2CH): lab. grade, supplied by BDH, and purified as for benzene.

Methyl cyanide (CH_3CN): analytical grade, supplied by Riedel-de Haen, West Germany. It was purified through a number of freeze-pump-thaw cycles and trap-to-trap distillation.

Methyl nitrate (CH_3NO_2): lab. grade, supplied by BDH, and purified by repeated freeze-pump-thaw cycles followed by trap-to-trap distillation.

Methanol: AR grade, supplied by J. T. Baker Chemical Co., USA Purified as for methyl nitrate.

Methyl isocyanide (CH_3NC): prepared by reacting N-methyl

formamide with toluene-p-sulfonyl chloride and freshly distilled quinoline[77]. It was purified by repeated trap-to-trap distillation.

Nitrogen: diving grade, supplied by NZIG, and further purified by passage through a zeolite trap cooled with liquid nitrogen.

Oxygen: ultra-high purity grade, 99.95% minimum purity, supplied by the Matheson company and used without further purification.

Hydrogen sulphide (H_2S): prepared by the addition of phosphoric acid to solid sodium sulphate. It was then dried over phosphorus pentoxide and purified by trap-to-trap distillation.

Nitrous oxide: medical grade, supplied by NZIG, and further purified by trap-to-trap distillation.

Tetrahydrofuran (cyclo-C_4H_8O): solvent grade, supplied by BDH, and further purified by a number of freeze-pump-thaw cycles and trap-to-trap distillation.

Tetrahydropyran (cyclo-$C_5H_{10}O$): solvent grade, supplied by BDH Chemicals Ltd, England, and purified in the same manner as for tetrahydrofuran.

Water: prepared through a number of freeze-pump-thaw cycles on distilled water.

2.10 REACTION ANALYSIS.

The general reaction of the ion A^+ with the neutral B leading to the product ion C^+ and neutral D is represented by reaction (2.00).

$$A^+ + B \rightarrow C^+ + D \qquad (2.00)$$

For this reaction the following rate equation describes the rate of loss of the A^+ ion with added neutral B over a period of time t,

$$-\frac{d[A^+]}{dt} = k\,[A^+]\,[B] \qquad \text{Eqn. (2.1)}$$

where k equals the bimolecular rate coefficient for the reaction.

Typical conditions within the flow tube during the course of analysis of a reaction similar to (2.00) are; ion density= 10^3 ions cm^{-3}; neutral reactant density= 10^{15} molecules cm^{-3}. Under these conditions, where the neutral reactant concentration is in vast excess of the primary ion concentration, the rate of loss of A^+ with added B can be described as

$$-\frac{d[A^+]}{dt} = k'\,[A] \qquad \text{Eqn. (2.2)}$$

where $k' = k[B]$ and is the pseudo first order rate coefficient for the reaction.

The rate coefficient is obtained from the observed decrease

of the reactant ion count [A^+] with an added neutral [B] in reaction (2.00). It is assumed that the velocity of these ions in the flow tube equals that of the carrier gas. If the axis of the flow tube is designated the z axis and if the carrier gas flow velocity v_0 is constant and directed along the z axis, then equation (2.1) can be rewritten as follows:

$$v_0 \frac{\partial [A^+]}{\partial z} = -k [A^+] [B] \qquad \text{Eqn. (2.3)}$$

A rate coefficient can then be obtained from equation (2.3) by monitoring the reactant ion decay against the rate of neutral addition over a set reaction distance, z, if the carrier gas velocity is known.

To test the validity of the assumption that the ion and carrier gas velocities are equivalent, the well tested results from fluid dynamics can be applied to the flow dynamics of the carrier gas and ion swarm in the flow tube. At the typical carrier gas throughputs (Q) and flow tube pressures (p) used in this study, the carrier gas flow is almost laminar with a non-zero (though close to zero) gas velocity at the tube walls[78]. The radial velocity ($v_g(r)$) of such a carrier gas flow is given in equation (2.4)[2,78,79],

$$v_g(r) = \frac{2v_0(1-(r^2/a^2)+(2s/a))}{1+(4s/a)} \qquad \text{Eqn. (2.4)}$$

where a is the tube radius, v_0 the carrier gas bulk velocity (equal to $Q/\pi a^2 p$) and $s = s'/p$, where s' is the pressure-independent slip coefficient.

From equation (2.4) the carrier gas throughput, Q, can be

expressed as

$$Q = \frac{\pi a^4}{8\eta}\left(\frac{p + 4s'}{a}\right)\Delta p \qquad \text{Eqn. (2.5),}$$

where η is the carrier gas viscosity, Δp is the pressure drop per unit length of the flow tube and p is the average pressure. Ferguson et al[2] have shown that the equation (2.4) correctly predicts the true form of the velocity profile through Pitot-tube experiments in a flowing afterglow apparatus. Under the conditions of near laminar flow described above, and assuming as above that the instantaneous ion-velocity profile in the flow tube equals that of the carrier gas[14], the variation in primary ion profile $[A^+]$ over the reaction length (z) of interest can be described as follows:

$$v_g(r)\frac{\partial[A^+]}{\partial z} = \underbrace{\frac{D_e}{r}\left(\frac{\partial}{\partial r}\left(r\frac{\partial[A^+]}{\partial r}\right)\right)}_{(A)} - \underbrace{D_e\frac{\partial^2[A^+]}{\partial z^2}}_{(B)} - \underbrace{k[B][A^+]}_{(C)} \qquad \text{Eqn. (2.6)}$$

The terms A, B and C represent the respective radial diffusive, axial diffusive and reactive contributions to the SIFT flow tube instantaneous ion-velocity profile. D_e represents the effective free ion diffusion coefficient, while k is the reaction rate coefficient and r and z are the radial and axial coordinates respectively in the cylindrical coordinate system (r, θ, z) used to describe the ion-velocity profile in equation (2.6).

The numerical solution[78,79] to this equation is

$$[A^+]_z \quad [A^+]_0 \exp-\left(\frac{\Delta D_e}{a^2} + \Gamma k [B]\right) \frac{z(1-\varepsilon)}{v_0} \qquad \text{Eqn. (2.7),}$$

where $[A^+]_0$ and $[A^+]_z$ are the ion densities at the relevant neutral gas inlet jet and at the nose cone apex respectively. Γ and Δ stand for pressure dependent factors which are related to s', the slip coefficient in equation (2.4) and ε equals $(\lambda^2/v_0)D_e^2$ (λ is a separation constant used in describing the axial diffusion of the ion A^+).

Smith et al[80] have monitored the ion density at different positions along the flow tube in a pure helium flowing afterglow (FA) where the only ion loss process was ambipolar diffusion. They deduced a value for the ambipolar diffusion coefficient within a few percent of the accepted value. Plasma flow velocity measurements[2,78] using Langmuir probes have also confirmed the validity of the analysis as applied to the FA technique. In the SIFT, only ions of a single charge type are present whereas a flowing afterglow plasma consists of both ions and electrons. The solution to the rate equation for a SIFT is therefore identical to the solution for the FA except that the ambipolar diffusion coefficient used in the FA analysis is replaced in the SIFT analysis by the free diffusion coefficient, De, for a given ion.

Smith and Adams, in an extensive review of their SIFT technique[14], have stated that the analysis of rate coefficients from SIFT data is identical to that of FA data, apart from the minor modifications stated above. Therefore the programme used in this study to calculate rate coefficients (listed in Appendix 1) is based upon equation (2.7). The

actual expression used to calculate k for a particular reaction, equation (2.8), is obtained by differentiating equation (2.7) with respect to the neutral reactant throughput, Q_n (where Q_n equals $\pi a^2 v_o [B]$).

$$k = - \frac{\pi a^2 v_o^2}{\Gamma z (1-\varepsilon)} \left(\frac{d \log_e [A^+]}{dQ_n} \right) \qquad \text{Eqn. (2.8)}$$

The solution to the axial diffusion correction factor (B) in equation (2.6) is included in the programme analysis, though in practice, at 0.3 Torr, it makes only a small difference (~2%) to the final value for the rate coefficient k. Free diffusion coefficients (D_e) are calculated from the relevant ion mobility (U_o) values[81,82,83] using equation (2.9)[81],

$$D_e = U_o \frac{760}{p} \frac{T}{273.16} \frac{kT}{e} \qquad \text{Eqn. (2.9),}$$

where k is the Boltzmann constant, T the tube temperature and e the charge on the electron. The final rate coefficient for most ion-molecule reactions, in a helium carrier at typical SIFT pressures, is also insensitive to the actual D_e value. For example, most of the ions investigated in this study such as CH_3^+, CH_3CNH^+ and $H_2C_3N^+$, exhibited only a ~2% increase in k for a 100% increase in D_e at 0.3 Torr.

In calculating the rate coefficient for a reaction, allowance must also be made for the assumption in the above analysis that the neutral reactant is introduced into the flow tube uniformly along the plane z= 0. In practice a correction to the reaction length (z) is required to allow for the distance needed for uniform mixing of the neutral species after addition from a point source.

The magnitude of this "end correction" in the present SIFT design should be small because the neutral reactant inlet jets have 1.6mm exit holes and face upstream in the flow tube. The end correction was calculated empirically by measuring the rate coefficients for well documented reactions of C^+ with O_2 and O^+ with O_2 at both inlet jets 1 and 2. For each reaction the rate coefficients obtained at each inlet jet were then fitted to the literature values of $k= 7.4 \times 10^{-10}$ cm^3 s^{-1} for C^+ and O_2 and $k= 2.3 \times 10^{-11}$ cm^3 s^{-1} for O^+ and O_2 (refs. 52 and 84 respectively) by adding a constant correction to each reaction length. This procedure was repeated a number of times within the pressure range of 0.29-0.38 Torr to obtain a value of 2±3cm for the end correction with the inlet jets used in this study. This value results in a 5% increase in the magnitude of a rate coefficient, for a neutral added at portal 2, at 0.29 Torr.

The end correction will be expected to depend to some extent on the diffusion coefficient of the neutral reactant in the carrier gas. It has been assumed that the actual end correction value is fairly insensitive to the diffusion coefficient of any particular neutral gas used in this study. This assumption is supported by Bohme et al[86] who have shown that the diffusion coefficients of a number of atmospheric gases in helium are similar (in the range of 0.59-0.79 cm^2 s^{-1}). Any pressure dependence of the end correction over the pressure range accessed in this study (0.15-0.5 Torr) has also been ignored, because differences in the end correction with pressure are less than the measured uncertainty in the end correction.

The rate coefficients reported in this study are within

±25% unless otherwise noted. This uncertainty is made up from:

(1) A potential calibration error in the carrier gas flow velocity (v_o) of up to ±5% which is derived from the calibration error of the Tylan flow controller (detailed in section 2.3). As the expression used in this work for the rate coefficient, k, (Eqn. (2.9)) depends on $(v_o)^2$ the resultant error in k increases to ±10%.

(2) From an uncertainty in the least squares value of the slope dlog $[A^+]/dQ$, which is typically ±3%.

(3) From systematic errors introduced in the approximations made in the flow analysis. Adams et al[78] have estimated that these errors arising from uncertainties in the neutral gas and plasma velocities result in a further ±7% error in the final rate coefficient. The method of flow analysis used by these authors to calculate the velocities for a FA system was the same as that outlined earlier in this section. As the end correction discussed above also introduces an error of typically ±5%, the overall absolute accuracy for a rate coefficient measured in this work is estimated to be ±25%. Generally however, the reproducibility of a series of successive measurements on a rate coefficient for a particular reaction is better than ±15%.

Periodically during the course of this study the rate coefficients for the three calibration reactions, C^+ with CO_2, C^+ with O_2 and O^+ with O_2, were measured as a check on the overall SIFT calibration. Agreement between the experimentally measured rate coefficients and the literature values[52,84] for these reactions was at all times within an error of 15%. The only exception was during the initial

stages of this study when a correction factor of 1.30 was applied to the rate coefficient to allow for an error in the calibration of the carrier flow (section 2.3).

The major source of error involved in measuring a product distribution is in estimating the quadrupole mass filter discrimination between individual product ions. In any particular reaction the difference in amu of the products may be large or small. Consequently the product distribution error varies due to the determination of the mass discrimination. However, the average error for the majority of product distributions measured in this study is estimated to be $\pm$10%. This error value represents an upper limit to the average uncertainty with which the mass discrimination between a number of ions of various different m/e values (table 2.1) has been determined.

CHAPTER THREE

REACTIONS OF HC_3N

3.1 INTRODUCTION.

In this chapter results of measurements undertaken with the neutral molecule cyanoacetylene (HC_3N) and a wide range of positive ions are reported. The proton affinity of HC_3N has also been determined and the reactions of a number of fragment ions of HC_3N that are of relevance to interstellar chemistry have been investigated.

The ion chemistry of HC_3N has been studied in some detail using the Flowing Afterglow (FA) technique in an earlier study in this department[87]. Unfortunately, subsequent to that study the ion sampling system used in the FA apparatus was discovered to discriminate severely against ions of higher mass. Consequently many of the possible exothermic product channels available to the reactions investigated may have been missed in the FA study.

HC_3N and the similar higher chain cyanopoly-ynes HC_5N, HC_7N and HC_9N have been detected in the Taurus dust cloud complex[88,89] and other clouds[90,91]. Various reaction schemes[40,41,42] have been postulated in the literature to explain the observed abundances of the HC_nN(n=1,3,5,7,9) molecules, particularly with regard to accounting for the Taurus TMC-1 observations.

The reactions detailed in this chapter were undertaken with a view to investigating the product distributions of

reactions known to be in doubt from the earlier FA study, and also to investigate other reactions of possible relevance to the interstellar chemistry of HC_3N.

3.2 REACTIONS OF THE HC_3N NEUTRAL.

After initial preparation (detailed in section 2.9), to avoid polymerization the HC_3N samples used in the following reactions were stored in the dark at liquid nitrogen temperatures until required. Before use the samples of HC_3N were added to a swarm of He^+ ions to test for potential impurities (section 2.8).

Table 3.0 lists the observed rate coefficients and product distributions for reactions of the neutral HC_3N with a number of selected ions. The relevant exothermicity of each reaction channel, where available, is also shown. Exothermicities have been estimated from standard sources of enthalpies[92,93] and from references 94 and 95 (these references detail some recent electron impact experiments by Harland and MacIntosh on CH_3CN, CH_3NC and C_2N_2[94] and on HC_3N[95]). For the reactions in table 3.0 the observed experimental rate coefficients are compared with the collision limit [illegible] values obtained from two different theoretical models: the ADO model of Su and Bowers[58], shown as k_{ADO}, and the recent model of Clary[67], k_{AC}. These models are summarized briefly in section 1.2.

Details of specific reactions in table 3.0 are summarized in the following discussion.

Table 3.0 continued.

3.15	HCN^+	$HC_3N^+ + HCN$ $H_2C_3N^+ + CN$	0.52 0.48	4.6	2.5[b]	3.4	5.2	196 227
3.16	CH_3CNH^+ *	$CH_3CNH^+.HC_3N$	1.0	0.59	0.50[f]	3.0	4.6	?
3.17	CO^+	$HC_3N^+ + CO$	1.0	3.8	2.3[b] 3.1[c]	3.4	5.2	232
3.18	HCO^+ *	$H_2C_3N^+ + CO$	1.0	3.8	3.7[b] 4.0[f]	3.3	5.1	150
3.19	CH_3CHOH^+	$CH_3CHOH^+.HC_3N$	1.0	3.0[e]		2.9	4.5	?
3.20	$CH_3NO_2H^+$	$H_2C_3N^+ + CH_3NO_2$ $CH_3NO_2H^+.HC_3N$	0.90 0.10	1.95[e]	1.8[f]	2.7	4.1	1[h] ?
3.21	$HBrCN^+$	$H_2C_3N^+ + BrCN$ $HBrCN^+.HC_3N$	0.99 0.01	2.0		2.4	3.8	3[h] ?
3.22	HC_3N^+ *	$HC_3N^+.HC_3N$	major	1.0		2.9	4.4	?
3.23	$H_2C_3N^+$ *	$H_2C_3N^+.HC_3N$	major	0.1		2.8	4.4	?

* Indicates that the ion labelled reacts only slowly with H_2.

(a) Uncertainties in ΔH° are typically ± 20 kJ mol^{-1} except where otherwise indicated. A positive ΔH° value represents an exothermic reaction channel.
(b) reference 87.
(c) reference 97.
(d) The observation of this channel allows a value of 1768 kJ mol^{-1} to be set as an upper limit for ΔH_f° (HC_3N^+).
(e) Pseudo second order rate coefficient at helium pressures 0.29-0.39 Torr.
(f) reference 96.
(g) C_2N^+ represents an indeterminate mixture of the isomers CNC^+ and CCN^+.
(h) Obtained from this work. Estimated uncertainty ± 2 kJ mol^{-1}.
(i) ΔH° value shown represents formation of the higher energy ion involved.

Reaction (3.00) $He^+ + HC_3N$

Using the SIFT technique it was possible to create a swarm containing only He^+ and He_2^+ ions in the flow tube. The conversion of injected He^+ ions to He_2^+ ions occurred through ternary association with the He carrier. At pressures of 0.22 Torr however, the fraction of He_2^+ ions present was only 20% of He^+. Subsequent product analysis, upon the addition of HC_3N, showed four dissociative charge transfer channels for reaction (3.00), with the products as shown in table 3.0. An overall rate coefficient of 7.9×10^{-9} cm^3 s^{-1} was observed for the decay of the He^+ ion. All of these product channels are exothermic by at least 400 kJ mol^{-1}.

The rate coefficient for reaction of the dimer ion He_2^+ with HC_3N was 5.4×10^{-9} cm^3 s^{-1}. Product ion assignment for the He_2^+ ion reaction was ambiguous as the best obtainable ratio of He_2^+ to He^+ was only ~1/1 at a tube pressure of 0.42 Torr. Raksit and Bohme[96,97] in a recent SIFT study on some reactions of HC_3N observed a total of six dissociative charge transfer products for the combined reaction of He_2^+ and He^+ with HC_3N (at 0.3 Torr). In addition to the four products seen in this study they also observed the ions CN^+ and C_3^+. They did not report separate product distributions for reactions of the ions He^+ and He_2^+ with HC_3N.

Reaction (3.01) $C^+ + HC_3N$

The rate coefficient for the overall reaction of C^+ with HC_3N was 5.0×10^{-9} cm^3 s^{-1}. This value is significantly below

the two previous experimental determinations[87,96] of 8.7 and 6.1 x 10^{-9} cm^3 s^{-1} respectively, but is between the ADO and Clary model limits as shown in table 3.0. The C^+ ion, generated from CO, was able to be injected into the flow tube with only a 5% signal from O^+ impurity ions at m/e= 16. Formation of ground state $C^+(^2P)$ by electron impact on CO also resulted in the production of a small percentage of metastable $C^+(^4P)$ ions (an upper limit of 10% was able to be placed for $C^+(^4P)$ formation from studies of the C_2N^+ ion in Chapter Five).

Apart from the four exothermic product channels mentioned below, a small charge transfer channel (~5%) leading to the HC_3N^+ ion was also observed in this study of reaction (3.01). Production of the HC_3N^+ ion from the reaction of ground state $C^+(^2P)$ is endothermic by 36 kJ mol^{-1}. It is likely therefore that the charge transfer product ion results from the presence of O^+ ions and/or metastable $C^+(^4P)$ ions in the C^+ reactant ion swarm.

Figure 3.0 shows a typical set of data obtained for the reaction of C^+ with HC_3N. Four product channels were observed leading to the ions C_3H^+, C_3^+, C_2N^+ and C_4N^+. The major product ion C_3H^+, is likely have a carbene cation type structure as shown in structure (1).

$:C^+-C\equiv CH$ (1) $:C^+-C\equiv C-CN$ (2) $:C=C=C=N^+=C:$ (3)

The C_4N^+ ion can have two possible structural isomers, either (2) or (3), depending upon which end of the HC_3N molecule is attacked. The structures of the two minor products C_3^+ and

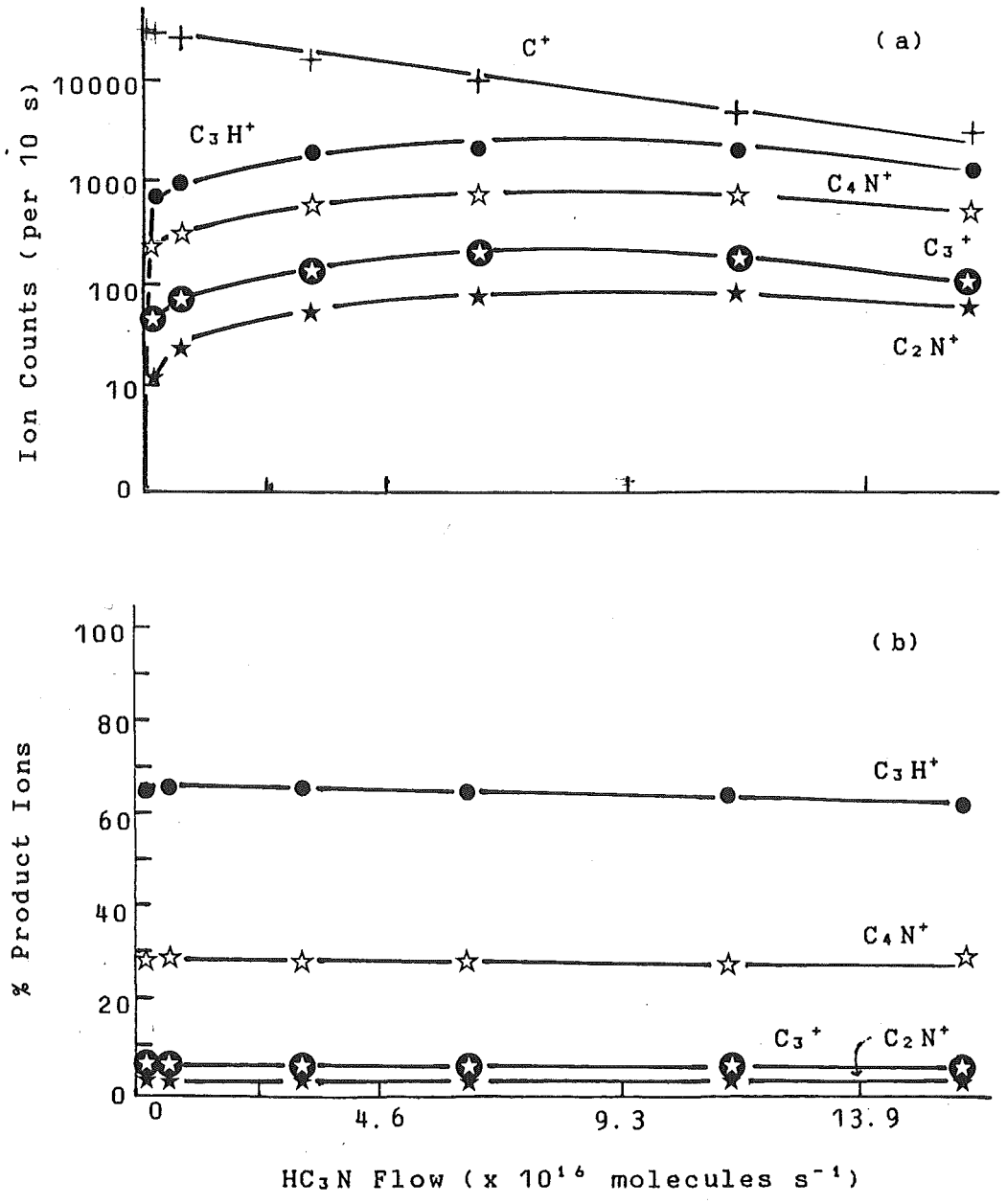

Fig. 3.0: Data for the reaction of C^+ with HC_3N.
(a) Ion count versus HC_3N flow for this reaction.
(b) Product ion percentage versus HC_3N flow.

C_2N^+, which were not observed by Raksit and Bohme[97], are most probably $:C=C=C.^+$ and $:C=N^+=C:$ or $:C=C=N:^+$ (for a discussion of the two isomers of the C_2N^+ ion see Chapter Five). All of these primary product ions were observed to react further with HC_3N. According to Bohme and Raksit[98], C_4N^+ associates to give the adduct $C_4N^+.HC_3N$ with a pseudo second order rate coefficient of 1.0×10^{-9} cm^3 s^{-1} at a helium pressure of 0.35 Torr. The reactions of the other product ions with HC_3N are detailed later in this section.

Reaction (3.02) $CH_3^+ + HC_3N$

The CH_3^+ ion was generated from electron impact on either CH_4, CH_3Br, or CH_3I. If CH_3Br was the ion source gas then ions of m/e= 15 only were able to be injected free of adjacent impurity ions.

Typical data obtained for reaction (3.02) is shown in figure 3.1. Two product channels were observed for this reaction leading to ions at m/e= 39 and m/e= 66. The first ion has the empirical structure $C_3H_3^+$. Formation of the other possible product ion at m/e= 39, HC_2N^+, can be discounted on energy grounds. Two isomeric structures are energetically possible for the $C_3H_3^+$ ion, the lower energy cyclopropenyl form (structure (4)) and the higher energy propargyl isomer (5).

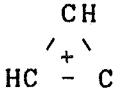

(4)

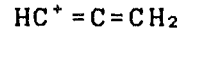

(5)

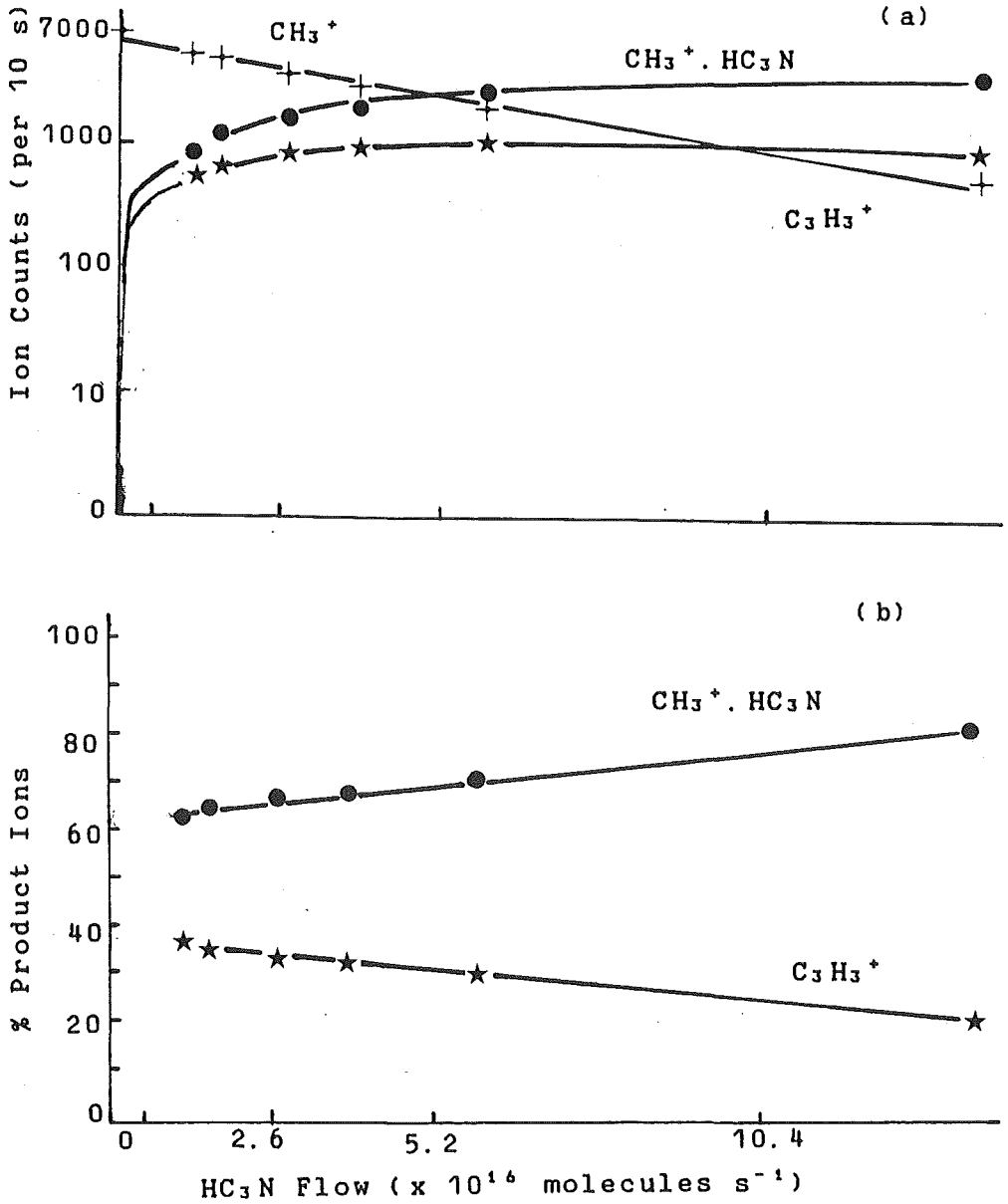

Fig. 3.1: Data for the reaction of CH_3^+ with HC_3N.
(a) Ion count versus HC_3N flow for this reaction.
(b) Product ion percentage versus HC_3N flow.

2 1

$HC\equiv C-C\equiv N:$ (6)

$H_2\overset{+}{C}-\underset{CN}{C}-CH_2$ (7)

The ion at m/e= 66 is the association product $CH_3^+.HC_3N$ and may have a structure similar to the cyanopropenylium ion, $CH_3-CH=C^+-CN$. Bohme and Raksit[98] have suggested that the two product channels observed may result from two separate positions of attack on the HC_3N neutral. Attack on the carbon labelled 1 in structure (6) may lead to the formation of the cyclopropenyl ion (4), while attack at the second carbon (C2) may result in formation of the cyanopropenylium adduct ion. The most stable structure however, is likely to be the 2-cyanoallyl ion (7).

At higher flows of HC_3N both products were observed to undergo further reaction. The adduct reacted slowly to give a peak at m/e= 117, $CH_3^+.(HC_3N)_2$, while $C_3H_3^+$ associated with HC_3N to form the ion $C_3H_3^+.HC_3N$ at m/e= 90.

The overall rate coefficient for reaction (3.02) was measured to be 4.4×10^{-9} cm^3 s^{-1} over the pressure range 0.30-0.38 Torr which is consistent with the reaction being in the high pressure limit and also with the previous SIFT result[97]. The earlier FA study however, reported the major product ion to be $C_3H_3^+$ rather than the association ion $CH_3^+.HC_3N$ as observed in this study.

Reaction (3.03) $C_2^+ + HC_3N$

The source gases used to generate the C_2^+ ion were C_2Cl_4 and C_2H_2. With the former gas a swarm of ions consisting

only of m/e= 24 could be created. The measured value for the rate coefficient and the observed product distribution for reaction (3.03) were both independent of the choice of source gas which suggests that no metastable $(C_2^+)^*$ ions were formed after electron impact on either C_2Cl_4 or C_2H_2. In a theoretical study of the electronic states of the C_2^+ ion Petrongolo et al[99] have shown that no low lying accessible metastable states of this ion exist.

A typical set of data for reaction (3.03) is shown in figure 3.2. From figure 3.2b it can be seen that upon the addition of HC_3N, five primary product channels were observed. Four of these channels resulted in the products C_4^+, C_5N^+, C_4H^+ and C_3H^+. A small amount of a fifth product, HC_3N^+, resulted from charge transfer. All of these product channels are exothermic, but the extent of exothermicity for the C_3H^+ channel is not known. Unfortunately there is no record of ΔH_f° in the literature for the dicarbene C_2N formed with this ion. Possible structures for these product ions are shown in diagrams (8) to (11) (the structure of C_3H^+ is given with the discussion on reaction (3.01)).

$C^+{\equiv}C-C{\equiv}CH$ (8)

$\cdot C{\equiv}C-C{\equiv}C-CN^+$ (9)

$\cdot C{\equiv}C-C{\equiv}C^+$ (10)

$HC{\equiv}C-CN^+$ (11)

Secondary reaction with HC_3N was observed for all the primary product ions. C_5N^+, C_3H^+ and HC_3N^+ were observed to associate with HC_3N. The measured rate coefficient for reaction (3.03) was 3.3×10^{-9} cm^3 s^{-1}.

Raksit and Bohme[97] observed 4 products for this reaction,

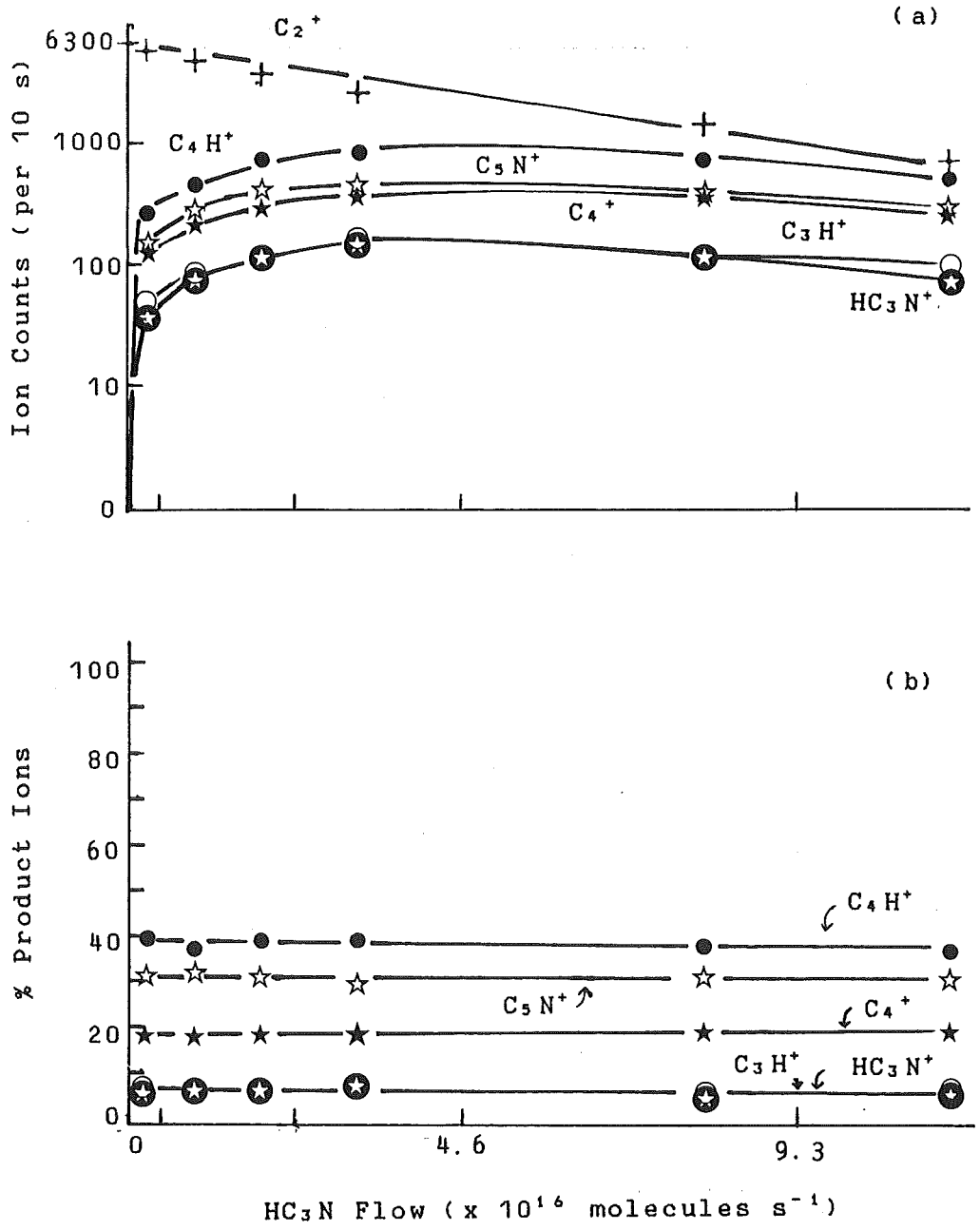

Fig. 3.2: Data for the reaction of C_2^+ with HC_3N.
(a) Ion count versus HC_3N flow for this reaction.
(b) Product ion percentage versus HC_3N flow.

$H-C\equiv C-C\equiv C-CN^+$ (12) $H_2C=C=C=N^+:$ (13)

$H-C\equiv C-C^+=C:$ (14) $H-C^+=C\cdot-C\equiv C-H$ (15)

There are two alternative empirical formulae possible for the fourth (and minor) channel observed at m/e= 50. Both $C_4H_2^+$ and C_3N^+ are candidates for m/e= 50. However the latter possibility is at least 90 kJ mol^{-1} endothermic, whereas the former channel is exothermic. The measured rate coefficient for reaction (3.04) was 4.4×10^{-9} cm^3 s^{-1}.

In this reaction all the product ions reacted further with HC_3N. For HC_5N^+, $H_2C_3N^+$, and $C_4H_2^+$ association products were observed. The reactions of $C_4H_2^+$ and $H_2C_3N^+$ are discussed in detail in reactions (3.11) and (3.23). Though not accurately measured, the rates of decay of the ions, HC_5N^+ and C_4H^+, with added HC_3N appeared to be approximately the same as that of the $C_4H_2^+$ ion.

Raksit and Bohme[97] observed the formation of the ion HC_3N^+ in reaction (3.04), but did not report C_4H^+. In this study an upper limit of 1% was able to be placed on the formation of the charge transfer product HC_3N^+ through the reaction of C_2H^+ with HC_3N. Raksit and Bohme also noted the major product channel as proton transfer, leading to $H_2C_3N^+$, in contrast to this work where the largest product ion was HC_5N^+. In their study of reaction (3.04) these authors formed C_2H^+ ions from electron impact on HC_3N with, in total, 9% of the impurity ions H_3O^+, $C_2H_2^+$ and $H_2C_2O^+$ also present in the flow tube. This no doubt considerably complicated their product analysis for the reaction of the C_2H^+ ions with HC_3N.

Reaction (3.05) $C_2H_2^+ + HC_3N$

The pseudo second order rate coefficient for this reaction was 3.7×10^{-9} cm^3 s^{-1} over the pressure range 0.30-0.40 Torr. This value is greater than the previously reported values of 1.9 and 3.2×10^{-9} cm^3 s^{-1} (refs. 87 and 97 respectively) but is in agreement with the ADO and AC limiting values of 3.4 and 5.3×10^{-9} cm^3 s^{-1}.

Product assignments were readily obtained as $C_2H_2^+$ was able to be generated from $C_2Br_2H_2$ with adjacent mass ions at less than 2% of the primary ion signal. Data obtained for reaction (3.05) are shown in figure 3.3. The major (66%) product observed was the association adduct $C_2H_2^+.HC_3N$ along with a 40% channel resulting in a peak at m/e= 50. As with the minor product channel of reaction (3.04), there exist two possible empirical formulae for the latter ion product. Again the only ion for which formation is exothermic is $C_4H_2^+$ (the C_3N^+ channel is endothermic by at least 448 kJ mol^{-1} in this case).

A possible structure for the association adduct is shown in diagram (16).

$H_2C=C-C^+=CH-C\equiv N:$ (16)

This adduct was not observed to associate with HC_3N at higher flows of the neutral reactant.

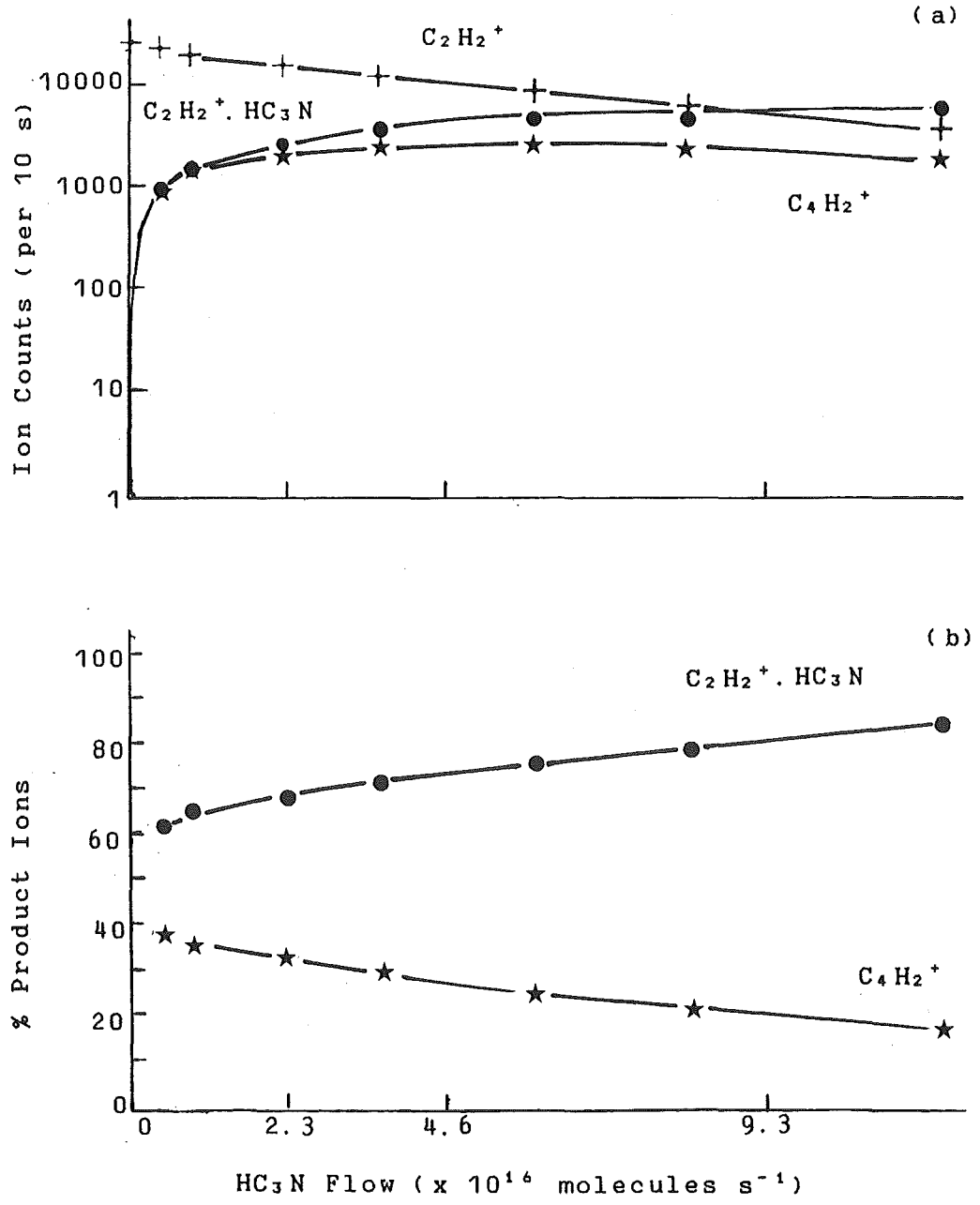

Fig. 3.3: Data for the reaction of $C_2H_2^+$ with HC_3N.
(a) Ion count versus HC_3N flow for this reaction.
(b) Product ion percentage versus HC_3N flow.

Reactions (3.06, 3.07) $C_2H_3^+$, $C_2H_5^+$ + HC_3N

Proton transfer was the only observed product channel with the ions $C_2H_3^+$ and $C_2H_5^+$. The measured rate coefficients for reactions of these ions with HC_3N were 3.8 and 3.3 x 10^{-9} cm^3 s^{-1} respectively, which compare favourably with the ADO and AC rates shown in table 3.0. Previously reported values for reaction of the former ion are 1.8 and 3.9 x 10^{-9} cm^3 s^{-1} (refs. 87 and 96 respectively).

Reaction (3.08) C_3^+ + HC_3N

The ion C_3^+ was generated from HC_3N in the ion source. One product channel only, giving the ion C_5H^+, was evident upon reaction with HC_3N. This ion, produced with a rate coefficient of 3.2 x 10^{-9} cm^3 s^{-1}, possibly has some carbene character as is shown in the following hypothetical structure (17):

$:C^+-C\equiv C-C\equiv CH$ (17)

C_5H^+, possibly because of its carbene type structure, also reacted rapidly with HC_3N to give the association adduct $C_5N^+.HC_3N$ (at ~10^{-9} cm^3 s^{-1}).

Reaction (3.09) C_2N^+ + HC_3N

C_2N^+ was generated by electron impact on either HC_3N or C_2N_2 in the ion source. With dicyanogen as the source gas C_2N^+

was produced with less than 1% of other ion types present in the flow tube.

The ion C_2N^+ represents a mixture of the structural isomers CCN^+ and CNC^+ (detailed further in Chapter Five). Plots of the logarithm of the primary ion signal versus added HC_3N reactant (shown in figure 3.4) were linear indicating that the reaction rate for these two isomers is similar. The only product ion observed was C_3H^+ and the rate coefficient was 3.5×10^{-9} cm^3 s^{-1}.

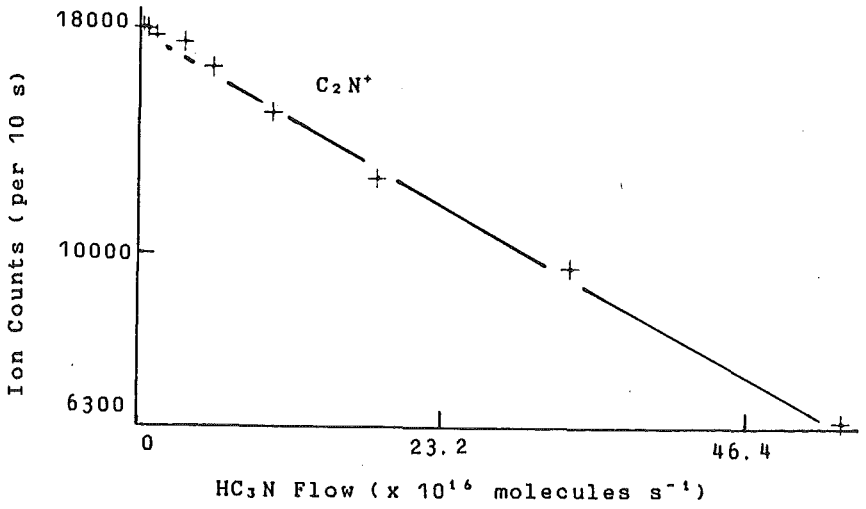

Fig. 3.4: A semilogarithmic plot of the C_2N^+ ion signal versus the flow of HC_3N.

Reaction (3.10) $C_3H^+ + HC_3N$

C_3H^+ was formed through electron impact on HC_3N. The adjacent ions C_3^+ and C_2N^+ were also present as impurity ions after injection of the primary ion into the flow tube. The best possible ratios of C_3H^+ to C_2N^+ and C_3H^+ to C_3^+ were

3.2/1 and 2.1/1 respectively. However, as these two impurity ions could be introduced into the reaction tube in isolation and their reactions with HC_3N studied, it was possible to deduce that only a single association channel occurred leading to the adduct (18).

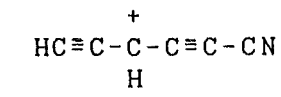

(18)

This adduct ion was not observed to react at the highest neutral flows used in the analysis of reaction (3.10).

Over the pressure range of 0.29-0.35 Torr the rate coefficient for reaction (3.10) was 1.2×10^{-9} cm^3 s^{-1}, after allowance was made for a contribution to the primary ion signal from C_2N^+ (C_2N^+ reacts with HC_3N to produce C_3H^+ (reaction (3.09)). The reaction therefore appears to obey pseudo second order kinetics at room temperature over this pressure range. Raksit and Bohme[97] are in close agreement with their reported value of 1.3×10^{-9} cm^3 s^{-1}, however the ADO and AC model values, at 3.1 and 4.7×10^{-9} cm^3 s^{-1}, are considerably higher.

Reaction (3.11) $C_4H_2^+ + HC_3N$

$C_4H_2^+$ was generated almost free of impurity ions from neutral C_4H_2 (table 6.1, Chapter Six details the relevant impurities). A rate coefficient of 1.7×10^{-9} cm^3 s^{-1} was measured for reaction (3.11) with the only product observed being the association adduct $C_4H_2^+.HC_3N$ (structure (19)).

$$HC{\equiv}C-C{\equiv}C-\overset{+}{\underset{H}{N}}=C^{\cdot}-C{\equiv}CH \qquad (19)$$

This adduct did not appear to react with HC_3N.

Reaction (3.12) $N^+ + HC_3N$

For this reaction two product channels were observed leading to the ions HC_3N^+ (50%) and C_3H^+ (50%), both of which reacted further with HC_3N (reactions (3.22) and (3.10)). The overall rate coefficient was 4.2×10^{-9} cm^3 s^{-1} compared to the values of 4.3 and 6.7×10^{-9} cm^3 s^{-1} for the ADO and AC models respectively. The production of C_3H^+ in reaction (3.12) is significant in that the formation of this ion requires the breaking of the carbon-nitrogen bond in HC_3N.

Reactions (3.13, 3.14) N_2^+, $N_2H^+ + HC_3N$

Both the above two ions reacted with HC_3N through a single channel. For N_2^+ charge transfer occurred with a rate coefficient of 2.9×10^{-9} cm^3 s^{-1}, whilst for N_2H^+ the rate coefficient for proton transfer was measured to be 4.3×10^{-9} cm^3 s^{-1}. Both of these rates were in accord with the calculated ADO and AC model collision limits and, for the N_2H^+ ion, with two previous studies[87,96].

Reaction (3.15) $HCN^+ + HC_3N$

The ion HCN^+ was generated from neutral HCN and injected into the flow tube free of impurities except for a small peak

at m/e= 28 (H_2CN^+ and $H^{13}CN^+$) which was 6% of the primary ion. Charge transfer and proton transfer, in approximately equal amounts, were the two product channels observed in reaction (3.15). The overall rate coefficient was 4.6×10^{-9} cm^3 s^{-1}.

Reaction (3.16) $CH_3CNH^+ + HC_3N$

An association adduct $CH_3CNH^+.HC_3N$ at m/e= 93 was the only primary product ion observed for this reaction. The observed rate coefficient of 5.9×10^{-10} cm^3 s^{-1} for the reaction at 0.30 Torr corresponds to a much smaller pseudo bimolecular rate than that predicted by the ADO and AC collision limit models. The result is in accord with the measurements of Raksit and Bohme[97] who measured a rate coefficient of 5.0×10^{-10} cm^3 s^{-1}. This reaction possibly warrants further examination to determine its pressure dependence as it may not be in the pressure saturated regime at 0.30 Torr.

Reactions (3.17, 3.18) CO^+, $HCO^+ + HC_3N$

The reaction of CO^+ with HC_3N resulted in the charge transfer product HC_3N^+ only. The rate coefficient for reaction (3.17) was measured to be 3.8×10^{-9} cm^3 s^{-1}. Proton transfer was the only product channel observed for the reaction of HCO^+ with HC_3N. The product ion $H_2C_3N^+$ was produced with a rate coefficient of 3.8×10^{-9} cm^3 s^{-1}.

Reaction (3.19) $CH_3CHOH^+ + HC_3N$

The rate coefficient for this reaction, where association to produce $CH_3CHOH^+.HC_3N$ (20) is the only product channel, was observed to be 3.0×10^{-9} cm^3 s^{-1} over the pressure range 0.29-0.38 Torr. The absence of a proton transfer channel indicates that the proton affinity (PA) of HC_3N is less than that of CH_3CHO (PA= 781 kJ mol^{-1}).

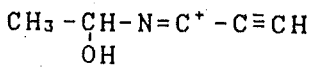

(20)

The absence of any pressure dependence for the rate coefficient suggests that the reaction is in the pressure saturation regime.

Reaction (3.20) $CH_3NO_2H^+ + HC_3N$

The overall rate coefficient for reaction (3.20) was measured to be 1.95×10^{-9} cm^3 s^{-1} which agrees, within experimental error, with the value of 1.8×10^{-9} cm^3 s^{-1} reported by Raksit and Bohme[97] in a hydrogen carrier. In a **helium** carrier gas two product channels were observed, 90% proton transfer giving $H_2C_3N^+$ and 10% association leading to $CH_3NO_2H^+.HC_3N$. Raksit and Bohme, with a hydrogen carrier, reported only proton transfer as well as a product at m/e= 66 which they suggested was the ion $H_4C_4N^+$. They did not report the association channel at m/e= 113.

For this reason the reaction in a **hydrogen** carrier was repeated in this study and resulted in a very different

product distribution to that observed with a helium carrier gas. The following channels were detected,

$CH_3NO_2H^+$ + HC_3N	→	$H_2C_3N^+$ + CH_3NO_2		(0.63)
	→	$H_4C_4N^+$ + HNO_2		(0.17)
	→	$CH_3NO_2H^+.HC_3N$		(0.19)
	→	$HC_3N_2O^+$ + CH_3OH		(0.01)

Reaction (3.20) was repeated at different nose cone disc potentials between 1 and 5 V. The product distribution shown above remained constant which supports the idea that the mass peaks observed at m/e= 66 (probably $H_4C_4N^+$) and m/e= 81 ($HC_3N_2O^+$) do not result from "break-up" of the association product upon nose cone sampling.

With hydrogen as the carrier gas, the ions NO_2^+ and NO^+ were found to be present in small amounts due to collisional breakup of $CH_3NO_2H^+$ upon injection into the flow tube. At the lowest ion injection energy used (about 15 V) NO^+ and NO_2^+ were 9% and 5% respectively of the primary ion signal. These two ions were reacted separately with HC_3N. For both ions the only observed channel was a slow clustering process, the product for NO^+ being $NO^+.HC_3N$ (m/e= 81) whilst that for NO_2^+ was $NO_2^+.HC_3N$ (m/e= 97). After correction, at low HC_3N flows, for the contribution to the mass peak at m/e= 81 resulting from reaction of NO^+ a 1% channel from reaction (3.20) remained. The difference in product distributions observed for reaction (3.20) between hydrogen and helium carrier gases suggests that molecular hydrogen may be involved in the reaction in some way other than simply as an inert buffer gas. The reaction clearly merits further work.

Reaction (3.21) $HBrCN^+ + HC_3N$

$HBrCN^+$ ions were generated from a mixture of BrCN (a solid at room temperature) and hydrogen. For this reaction, only ions containing the higher mass isotope of bromine (^{81}Br) at m/e= 108 were injected into the SIFT flow tube. The only impurity ion able to be detected in the resultant ion swarm was a peak at m/e= 109 at ~1.5% of the primary ion signal (the natural abundance of ^{13}C as a percentage of ^{12}C is 1.11%, therefore this ion signal is mostly $HBr^{13}CN^+$).

Upon reaction two products were observed to be formed, 99% of $H_2C_3N^+$ from proton transfer and 1% of the association ion $HBrCN^+.HC_3N$, with an overall rate coefficient of 2.0×10^{-9} $cm^3\ s^{-1}$. The ADO and AC rates for reaction (3.18) are 2.4 and 3.8×10^{-9} $cm^3\ s^{-1}$ respectively, indicating that the proton transfer reaction was fast and proceeded at close to every collision.

Reactions (3.22, 3.23) HC_3N^+, $H_2C_3N^+ + HC_3N$

The rate coefficients for the reactions of these two ions with HC_3N were measured from the rates of secondary reactions following those in which the ions were produced as primary products. In both cases the major product channel was observed to be association. The measured rate coefficients for reactions (3.22) (HC_3N^+) and (3.23) ($H_2C_3N^+$) were 1.0 and 0.1 $\times 10^{-9}$ $cm^3\ s^{-1}$ respectively at pressures of 0.3 Torr.

3.3 REACTIONS OF IONS DERIVED FROM HC_3N.

For reactions involving the protonated cyanoacetylene ion, $H_2C_3N^+$, the ion was generated from a 20/1 mixture of hydrogen and HC_3N. The only other ion present was HC_3N^+ (at 2% of $H_2C_3N^+$ count as shown in figure 3.5a).

For the reactions of the ions HC_3N^+ and C_3N^+ with H_2 the primary ions were produced using pure HC_3N in the ion source. It was possible to inject HC_3N^+ into the flow tube with only one other ion type present, $H_2C_3N^+$, at 6% of the primary ion (figure 3.5b). Under the optimum conditions of injection for the ion C_3N^+, the relative signals from the ions present, C_2N^+ (from "breakup" of C_3N^+ on injection), C_3N^+ and HC_3N^+ were in the ratio 0.1/1/0.7 (figure 3.5c). However, as C_2N^+ did not react with H_2 and HC_3N^+ reacted only very slowly, product analysis was straightforward.

Table 3.1 shows the results of this study for ions derived from HC_3N with some selected neutral reagents. The measured rate coefficients are compared with the relevant collision limits calculated from ADO theory[58] (k_{ADO}), or from simple Langevin theory (k_L), together with estimates of the exothermicity of each channel where known.

Table 3.1: Rate coefficients and product distributions for reactions of selected ions derived from HC_3N with the neutrals shown. Rate coefficients, k, have units of 10^{-9} cm^3 s^{-1} whilst the overall reaction enthalpies listed are in units of kJ mol^{-1}.

no.	ion	neutral	products	B.R.	k	k_{ADO} or k_L	$-\Delta H^\circ$
3.24	$H_2C_3N^+$	HCO_2CH_3	$H_2CO_2CH_3^+ + HC_3N$	1.0	1.8	1.6	45
3.25	$H_2C_3N^+$	CH_3OH	$CH_3OH_2^+ + HC_3N$	1.0	1.9	1.7	10
3.26	$H_2C_3N^+$	CH_3CHO	$CH_3CHOH^+ + HC_3N$	1.0	2.4	2.2	36

Table 3.1 continued.

3.27	$H_2C_3N^+$	CH_3NO_2	$CH_3NO_2H^+ + HC_3N$	0.61	2.1[b]	2.7	-1
			$H_2C_3N^+.CH_3NO_2$	0.39			?
3.28	$H_2C_3N^+$	BrCN	$HBrCN^+ + HC_3N$	0.50	0.83	2.0	-3
			$H_2C_4N_2^+ + Br$	0.30			?
			$H_2C_3N^+.BrCN$	0.20			?
3.29	HC_3N^+	H_2	$H_2C_3N^+ + H$	0.76	0.007	1.5	113
			$C_2H_2^+ + HCN$	0.24			7
3.30	C_3N^+	H_2	$HC_3N^+ + H$	0.90	0.91	1.5	162[a]
			$H_2C_3N^+$	0.10			711[a]

(a) ΔH° values calculated for reaction of the lowest energy C_3N^+ ion (table 3.3).
(b) Pseudo second order rate coefficient at helium pressures of 0.295-0.35 Torr.

The first five reactions listed were performed as part of a determination of the proton affinity of HC_3N (to be discussed fully in section 3.4).

Reactions (3.24, 3.25 and 3.26)

HCO_2CH_3, CH_3OH and $CH_3CHO + H_2C_3N^+$

The reactions of $H_2C_3N^+$ with HCO_2CH_3 (methyl formate) (3.24), CH_3OH (3.25), and CH_3CHO (3.26) all proceeded by a proton transfer pathway with rate coefficients of 1.8, 1.9 and 2.4 x 10^{-9} cm^3 s^{-1} respectively. A small association peak (less than 1% of the product total) was observed for CH_3OH.

Reactions (3.27, 3.28) CH_3NO_2, BrCN + $H_2C_3N^+$

With CH_3NO_2 a significant association channel was observed in addition to proton transfer. The relative yields for association and proton transfer were 39% and 61%. The overall

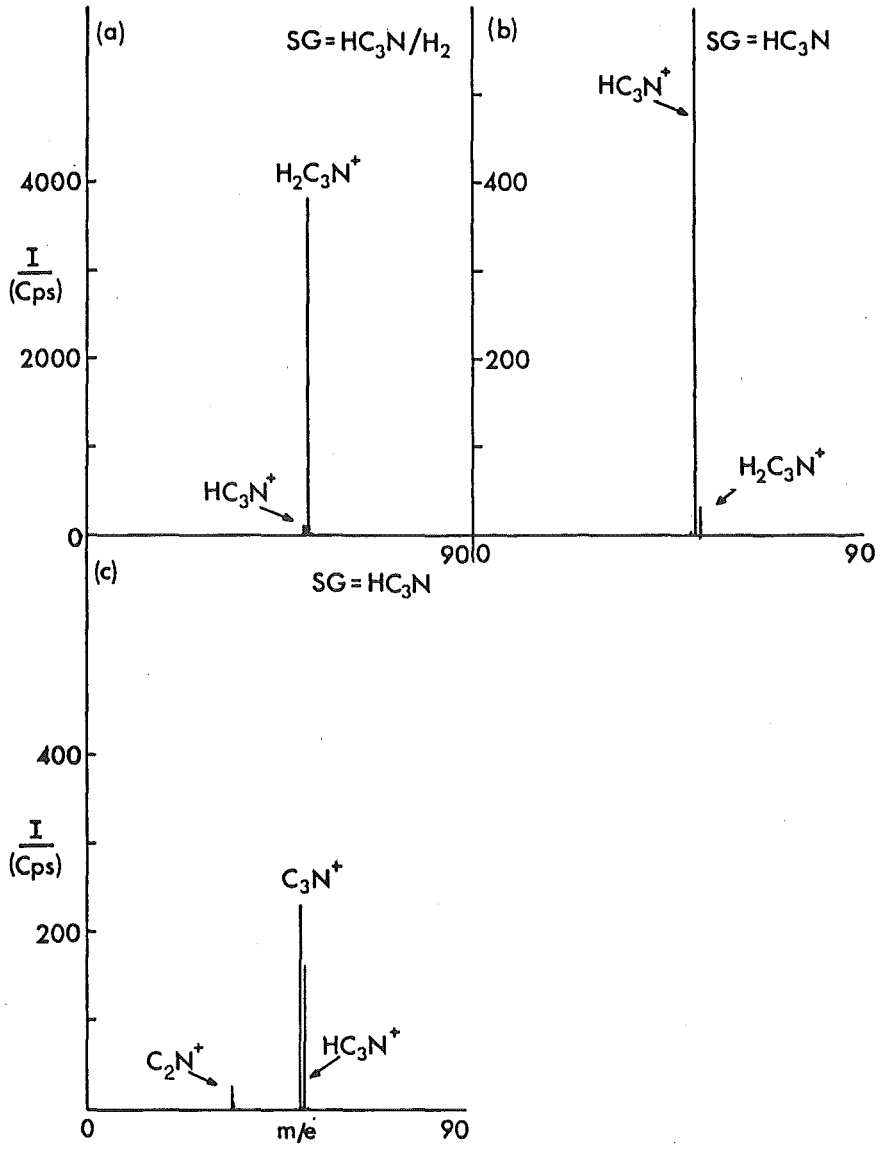

Fig. 3.5: Mass spectra of the following primary ions:
(a) $H_2C_3N^+$
(b) HC_3N^+
(c) C_3N^+

rate coefficient for reaction (3.27) was 2.1 x 10^{-9} cm^3 s^{-1} over the pressure range 0.295-0.35 Torr.

The reaction of $H_2C_3N^+$ with BrCN produced not only a proton transfer product, $HBrCN^+$ (50%) and an association adduct $H_2C_3N^+.BrCN$ (20%), but also the ion $H_2C_4N_2^+$ (30%). In making the product analysis for this reaction due allowance was made for the presence of two isotopes of Br. The overall rate coefficient for reaction (3.28) at 0.30 Torr was measured to be 8.3 x 10^{-10} cm^3 s^{-1}.

Reaction (3.29) $HC_3N^+ + H_2$

The overall rate coefficient (at 0.295 Torr) for reaction of HC_3N^+ with H_2 was measured as 7 x 10^{-12} cm^3 s^{-1}. Two reaction channels were observed, one leading to the major product ion $H_2C_3N^+$ through hydrogen abstraction, and the other forming the ion $C_2H_2^+$ (m/e= 26). Another empirical possibility at m/e= 26 is CN^+. However, as the channel leading to this ion is endothermic by ~604 kJ mol^{-1}, formation of this ion is most unlikely.

Reaction (3.30) $C_3N^+ + H_2$

Upon reaction with H_2 the ion C_3N^+ produced two products, HC_3N^+ by hydrogen abstraction and a smaller association peak $H_2C_3N^+$, with an overall rate coefficient of 9.1 x 10^{-10} cm^3 s^{-1}. The decay of the C_3N^+ ion with added H_2 included two distinct exponential slope regimes (figure 3.6). Confirmation of this observation was provided by the reaction of CH_4 with C_3N^+ where two separate exponential components of the C_3N^+ decay were also noted.

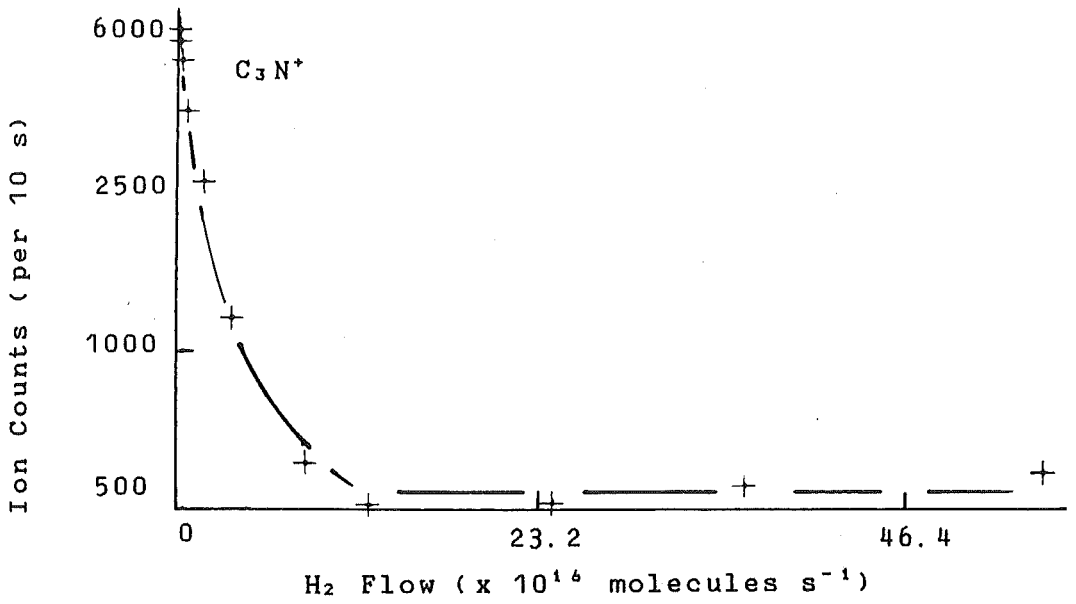

Fig. 3.6: A semilogarithmic plot of the C_3N^+ ion signal versus the flow of H_2.

This phenomenon is probably due to the presence of two stable structural isomers, $CCCN^+$ (21) and $CCNC^+$ (22) of C_3N^+ in the flow tube.

$:C{=}C{=}C{=}N^+:$ (21) $:C{=}C{=}N^+{=}C:$ (22)

Harland[95] in a study of the C_3N^+ ion formed by electron impact on HC_3N also observed evidence for the presence of two forms of C_3N^+. The ionisation efficiency curve for the C_3N^+ ion showed a sharp ionisation threshold followed by a break ~0.9eV above the initial appearance energy of the C_3N^+ ion. The author attributed this to the presence of either a second stable isomer or a metastable electronic state of the ion. Studies of similar structural isomers; CH_3CN^+ and CH_3NC^+; and CNC^+ and CCN^+ are detailed in Chapters Four and Five respectively. Further study of the C_3N^+ ion with a number of

neutral reactants and over a range of pressures is intended in this laboratory.

In summary, of the ions derived from cyanoacetylene only C_3N^+ displayed clear evidence of being produced in two isomeric forms. For reactions involving the ions HC_3N^+ and $H_2C_3N^+$ only single exponential decays were observed, indicating that these ions probably existed in one stable structure in the flow tube.

3.4 THE PROTON AFFINITY OF HC_3N.

Two earlier values have been reported in the literature for the proton affinity (PA) of HC_3N. The value obtained from an earlier FA study[87] of HC_3N in this laboratory is now considered to be in error for reasons discussed in section 3.1. The second study[96], using a SIFT apparatus, reported a value of 770 ± 17 kJ mol^{-1} for the PA of HC_3N by bracketing HC_3N between the PA values of CH_3NO_2 and CH_3CN.

In the present study the reaction of CH_3CNH^+ (protonated acetonitrile) and HC_3N was investigated initially with association being the only channel observed as discussed in section 3.2. In the course of experimental work carried out on a series of analogous reactions (determination of the PA of CH_3CN and CH_3NC, Chapter Four) it became apparent that, if the neutral had a permanent dipole moment, association competed with proton transfer only when the PA's of the two species involved were within ~10 kJ mol^{-1}. If the overall proton transfer reaction enthalpy was greater than a few kJ mol^{-1}

exothermic, only a proton transfer channel was observed for the reaction. If proton transfer was endothermic by more than a few kJ mol^{-1}, only association was noted. When the overall reaction enthalpy was within these two extremes both proton transfer and association occurred. Smith et al[100] have previously noted competition between association and proton transfer occurring under the same conditions in a study of the reactions of CH_3^+, CH_2D^+, CHD_2^+ and CD_3^+ with H_2, HD and D_2. The observation of association as the sole product in the reaction of CH_3CNH^+ and HC_3N therefore indicates that the PA of HC_3N is significantly below the reported value of 788 kJ mol^{-1} for the PA of CH_3CN[92].

The reactions of the ion $H_2C_3N^+$ were then studied with HCO_2CH_3 (methyl formate, PA= 790 [92]), CH_3CHO (PA= 772 [92]) and CH_3OH (PA= 761 [92]) with proton transfer being the only product channel observed in each case, as noted earlier in this chapter. These results therefore confined the PA of HC_3N to a value at least 10 kJ mol^{-1} below that of CH_3OH. Consequently, CH_3NO_2 and BrCN, with previously measured PA's of 750 and 746 kJ mol^{-1} respectively[92], were chosen for investigation with the ion $H_2C_3N^+$. Proton transfer was observed to occur with these neutrals as well as association. As noted in section 3.2 proton transfer also competed with association in the reverse reactions involving the neutral HC_3N with the ions $CH_3NO_2H^+$ and $BrCNH^+$. The observation of proton transfer in both directions indicates that the PA of HC_3N is likely to be within 10 kJ mol^{-1} of the PA values for CH_3NO_2 and BrCN. To obtain a more precise value for the PA of HC_3N, equilibrium constants were then determined for each of the following three

systems:

$$CH_3NO_2H^+ + HC_3N \rightleftharpoons H_2C_3N^+ + CH_3NO_2 \qquad K_1$$

$$HBrCN^+ + HC_3N \rightleftharpoons H_2C_3N^+ + BrCN \qquad K_2$$

$$HBrCN^+ + CH_3NO_2 \rightleftharpoons CH_3NO_2H^+ + BrCN \qquad K_3$$

For the third system K_3 was calculated from the following observed experimental data:

$$HBrCN^+ + CH_3NO_2 \rightarrow CH_3NO_2H^+ + BrCN \quad (0.96) \qquad (3.31)$$
$$\rightarrow HBrCN^+.CH_3NO_2 \quad (0.04)$$

$$CH_3NO_2H^+ + BrCN \rightarrow HBrCN^+ + CH_3NO_2 \quad (0.72) \qquad (3.32)$$
$$\rightarrow CH_3NO_2H^+.BrCN \quad (0.28)$$

The rate coefficients for reactions (3.31) and (3.32) were determined to be 1.7 and 0.81 x 10^{-9} cm^3 s^{-1} respectively (the values given represent the overall bimolecular rate coefficient for each reaction at a pressure of 0.30 Torr and at room temperature). As with the earlier reaction involving the ion $HBrCN^+$, only ions containing the higher bromine isotope (m/e= 81) were injected into the flow tube.

Consider now the general case of reaction of AH^+ with B (reaction 3.33) below), when association may occur in competition with proton transfer.

$$AH^+ + B \rightleftharpoons [AH^+.B]^* \underset{k_r}{\overset{k_f}{\rightleftharpoons}} BH^+ + A \qquad (3.33)$$

$$+ m \rightarrow AH^+.B + M$$

In order to determine the rate coefficient for the proton transfer channel above it is necessary to measure the product distribution for that reaction accurately. k_f, the rate coefficient for the proton transfer channel in the "forward" direction (usually taken arbitrarily as the preferred direction of proton transfer) can then be calculated by multiplying the overall observed rate coefficient for the forward direction by the observed channel efficiency for proton transfer. k_r, the rate coefficient for the reverse process of proton transfer from BH^+ to A, is then determined in the same manner. The equilibrium constant, K, for the proton transfer equilibrium between the two species A and B is then simply given by the ratio of k_f (the rate coefficient for proton transfer from AH^+ to B) to k_r (the rate coefficient for proton transfer from BH^+ to A).

The difference in gas phase basicities of A and B is equal to the negative of the free energy change associated with this reaction ($(GB_B - GB_A) = -\Delta G^\circ$), whilst the difference in proton affinities is simply the negative of the corresponding enthalpy change ($(PA_B - PA_A) = -\Delta H^\circ$). If the equilibrium constants are substituted into the expression for the free energy change of a reaction, $\Delta G^\circ = -RT\ln K$, the difference in gas phase basicities (ΔGB) for each species can be derived.

The difference in proton affinities (ΔPA) of A and B is then determined by adding an entropy contribution (ΔS°) to the difference in GB in accordance with the equation $\Delta H^\circ = \Delta G^\circ + T\Delta S^\circ$. For this study the entropy changes for each reaction, were taken from established values listed in Lias et al[92]. These ΔS°'s were determined in a variety of ways,

1: By calculating exact partition functions for the reactants and products[101].

2: By taking standard entropy data from the literature for the relevant neutral and assuming that the standard entropy for an ion will be the same as the corresponding isoelectronic molecule.

3: By taking the ratio of the rotational symmetry numbers of the reactant neutral and product ion as follows[92], $\Delta S^{o}_{=}$ $R\ln[(\sigma M)/(\sigma MH^{+})]$, where (σM) and (σMH^{+}) are the rotational symmetry numbers of M and MH^{+}. (The last two methods are approximate only).

Values of $K_1 = 1.38$, $K_2 = 4.77$ and $K_3 = 2.81$ were determined, as described above, for the three equilibrium systems given on page 98. ΔGB measurements of 0.8 (ΔGB_1), 3.9 (ΔGB_2) and 2.6 (ΔGB_3) kJ mol^{-1} were then determined for the three equilibrium systems as described above. The GB of CH_3NO_2 has been determined by several groups[102,103,104] and for this reason the derived GBs' of HC_3N and BrCN, shown in table 3.2, have been referenced to GB(CH_3NO_2). In a recent evaluation of gas phase basicities Lias et al[92] suggest a value of 718 kJ mol^{-1} for the absolute GB of CH_3NO_2.

Table 3.2: Relative gas phase basicities and proton affinities of HC_3N, CH_3NO_2 and BrCN referenced to the gas phase basicity of CH_3NO_2 at 718 kJ mol^{-1} [92].

compound	GB[a]	PA[b]	literature values
HC_3N	719	751	770[96]
CH_3NO_2	718	750	750[92]
BrCN	715	748	746[92]

(a) Estimated uncertainty in relative measurements is ±1 kJ mol^{-1}.

(b) Estimated uncertainty in relative measurements is ±2 kJ mol^{-1}.

Though each equilibrium constant was determined separately the three values are linked by the expression $K_2 = K_1 K_3$, and hence the three GB measurements by the expression $\Delta GB_2 = \Delta GB_1 + \Delta GB_3$. The internal consistency of these ΔGB measurements can therefore be tested. From K_1 and K_3 $\Delta GB(1) + \Delta GB(3)$ equals 3.4 kJ mol^{-1}, while for the second equilibrium system this value equals 3.9 kJ mol^{-1}. The relative gas phase basicity shown in table 3.2 for $GB(HC_3N)$ reflects the average of these values. The average error in each of the relative measurements is ± 1 kJ mol^{-1}. This error reflects the overall uncertainty resulting from the rate coefficients and product distributions used in the determination of each equilibrium constant.

The measured value for the PA of HC_3N from this study is 751 ± 2 kJ mol^{-1} (the error limit of ± 2 kJ mol^{-1} allows for uncertainty in ΔS°[92]). This value is lower than the figure of 770 ± 17 kJ mol^{-1} suggested by Raksit and Bohme[96] which they estimated by bracketing the PA of HC_3N between CH_3CN and CH_3NO_2. Our reactions were all carried out in a helium carrier, whereas Raksit and Bohme studied the reaction of $CH_3NO_2H^+$ and HC_3N in a hydrogen carrier gas and did not report any association product (as noted earlier). Our measured value of PA $(HC_3N) = 751$ kJ mol^{-1} along with the recently determined value for $\Delta H_f^{\circ}(HC_3N)$ of 354 kJ mol^{-1} given by Harland[95] leads to $\Delta H_f^{\circ}(H_2C_3N^+) = 1139 \pm 10$ kJ mol^{-1}.

Table 3.3 shows some ΔH_f° measurements for a number of ions involved in reactions detailed in this chapter, along with some previously unmeasured values determined in this study.

Table 3.3: Heats of formation of selected ions and neutrals (in kJ mol^{-1}).

species	ΔH_f° [a]	reference
$H_2C_3N^+$ [b]	1139	this work (Chapter 3)
HC_3N^+	1470	95
$C_3N^+(1)$	1850	95
$C_3N^+(2)$	1935	95
HC_3N	354	95
C_4N^+	~1880	105
HC_5N^+	<1768	this work (Chapter 3)
C_5N^+	<2060	105
CNC^+	1620	94
CCN^+	1726	94
$HCNC^+$	1554	94
$HCCN^+$	1622	94
CH_3CNH^+ [b]	822	this work (Chapter 4)
CH_3NCH^+ [b]	865	"
$C_4H_3^+$ [b]	1271	this work (Chapter 6)

(a) Estimated uncertainties are ±10 kJ mol^{-1} except where indicated otherwise.
(b) ΔH_f° values for these ions have been determined using H^+ (ΔH_f°) = 1536.3 kJ mol^{-1} [167].

In the range of flow tube pressures of 0.30-0.38 Torr at which this study of the PA of HC_3N was conducted, the process of association is efficient, occurring through stablisation of the association complex by collision with a third body. In all of the reactions used to determine the PA of HC_3N, association competed with proton transfer. From studies on the PA of CH_3CN (detailed in Chapter 4), it appears that this competition does not influence the equilibrium constants obtained for proton transfer.

3.5 INTERSTELLAR IMPLICATIONS.

The detection of HC_3N and its related higher analogues HC_5N, HC_7N and HC_9N in several interstellar sources[88,89,90,91] has led to attempts by several groups[40,41,42] to account for the presence of these molecules at their observed abundances.

Most of the models have assumed an interlinking chemistry for the cyanopoly-yne series with the larger molecules being synthesised from HC_3N.

The measurements detailed in this chapter confirm an earlier conclusion of Bohme and Raksit[98] that for reactions of HC_3N with many hydrocarbon ions such as CH_3^+, C_2^+, C_2H^+, $C_2H_2^+$, C_3^+, C_3H^+, $C_4H_2^+$, HC_3N^+ and HCN^+, association is a major product channel. In these association reactions the reaction intermediate is stabilised by collision in the flow tube (k_2 in the example below). However under typical conditions in an interstellar cloud where [m] is negligible, the stabilisation of the collision complex must occur by photon emission (k_r). Consider as a typical example, the reaction of CH_3^+ with HC_3N (3.02).

$$CH_3^+ + HC_3N \underset{\tau^{-1}}{\overset{k_1}{\rightleftharpoons}} (CH_3^+.HC_3N)^* + m \quad \begin{matrix} \overset{k_2}{\rightarrow} CH_3^+.HC_3N + m & (3.02i) \\ \overset{k_r}{\rightarrow} CH_3^+.HC_3N + h\nu & (3.02ii) \end{matrix}$$

The efficiencies of these two alternative stablisation processes are both dependent upon the lifetime of the intermediate (τ). The assumption can therefore be made that if collisional stabilisation for a reaction is measured to be efficient in the flow tube, then stabilisation by radiative association may also be efficient at the low pressures and temperatures of an interstellar cloud. Support for this assumption has been provided in the agreement achieved between the calculated and observed fractional abundances of a number of neutrals (and radicals) when the models used to derive the calculated abundances have assumed efficient radiative association. For example Herbst et al[106] have recently shown

that the observed fractional abundance of the radical C_3O in the dense interstellar gas cloud TMC-1 can be accounted for via a series of ion-molecule reactions including processes involving radiative association. In a separate study[107] Herbst has modelled the fractional abundances of a number of hydrocarbon and cyanoacetylene molecules using revised radiative association rates to achieve improved agreement with the observed abundances. It therefore appears reasonable to assume that if a three body collisional association reaction is fast at pressures of ~0.30 Torr then the equivalent ion-molecule radiative association reaction will also proceed at a significant fraction of the collisional association rate at interstellar temperatures.

The majority of the ion-molecule reactions involving HC_3N which were examined in this study proceeded with rate coefficients close to their respective collision limiting values at 300 K ($k \sim 10^{-9}$ cm^3 s^{-1}). A recent theoretical model developed by Clary[67] (section 1.2) to estimate ion-molecule reaction collision limits predicts an increase in k at lower temperatures for molecules with large permanent dipoles such as HC_3N. This theory has been shown to give a good fit to experimentally measured rate coefficients for reactions of HCN and HCl over a range of temperatures[68,69]. Clary et al[69] have predicted that where reactions of HC_3N are observed to proceed at rates close to their respective collision limits at room temperature, these reactions will also occur at collision limiting rates ($\sim 10^{-7}$ cm^3 s^{-1}) at interstellar cloud temperatures.

As hydrogen is the dominant interstellar cloud species,

for the ion-molecule reactions considered in this study only those primary ions that do not react rapidly with H_2 will be available as precursor ions to react with HC_3N in interstellar clouds. Of the reactions detailed in table 3.0 (reactant ions that react slowly with H_2 are marked with an *) the reactions of C^+, CH_3^+, $C_2H_2^+$, $C_4H_2^+$ and CH_4CN^+ with HC_3N all resulted in the production of longer chain length ions (as detailed in section 3.2). Association adducts were observed for the ions CH_3^+, $C_2H_2^+$, $C_4H_2^+$ and CH_4CN^+. Under the conditions existing in interstellar clouds, these adduct ions will be stablised by radiative asssociation, as discussed above.

Those adduct ions which are formed through the association of ions with HC_3N appear to be covalently bound ions with new structural identities rather than weak electrostatically bound clusters of the original species (section 3.2 details a number of possible adduct ion structures formed after ion-molecule reactions with HC_3N as the neutral). Presumably these adducts are formed through an intermediate complex whose lifetime is sufficiently long to allow the complex time to find a suitably deep potential well on its potential surface corresponding to a covalently bound structure.

Subsequent neutralisation of the product ions observed for the reactions of HC_3N in interstellar clouds, may occur through a variety of reaction types some of which are: charge transfer, reaction (3.34); proton transfer from the product ion to a suitable neutral, reaction (3.35); condensation involving the product ion followed by elimination of the relevant neutral, for example reaction (3.36); and

dissociative recombination through an electron (or a negative ion), as for example reactions (3.37) and 3.38).

$CH_3^+.HC_3N + A \rightarrow H_4C_4N^{\cdot} + A^+$ ($H_3C-CH=C^{\cdot}-C\equiv N:$) (3.34)

$CH_3^+.HC_3N + A \rightarrow H_3C_4N + AH^+$ ($H_3C-C\equiv C-C\equiv N:$) (3.35)

$C_2H_2^+.HC_3N + H_2 \rightarrow H_4C_5 + HN^+$ ($H_3C-C\equiv C-C\equiv C-H$) (3.36)

$C_2H_2^+.HC_3N + e \rightarrow HC_5N + H_2$ ($HC\equiv C-C\equiv C-C\equiv N:$) (3.37)

$C_4H_2^+.HC_3N + e \rightarrow HC_7N + H_2$ ($HC\equiv C-C\equiv C-C\equiv C-C\equiv N:$) (3.38)

The association adducts formed in the reactions of the ions $C_2H_2^+$ and $C_4H_2^+$ with HC_3N may undergo dissociative recombination in interstellar clouds[108] to form HC_5N and HC_7N (reactions (3.37) and (3.38) respectively). However other possible neutralisation routes exist for these ions, for example reaction of the adduct $C_2H_2^+.HC_3N$ with H_2 may result in the formation of the neutral hydrocarbon CH_3C_4H as well as HN^+ (reaction (3.36)). The molecule CH_3C_2H and its analogue CH_3C_4H have both been detected in the interstellar cloud TMC-1[109,110] along with molecules of the cyanopoly-yne series.

If the adduct ion formed from association between CH_3^+ and HC_3N has a cyanopropenylium ion structure, $CH_3-CH=C^+-CN$ (p. 76, section 3.2), then neutralisation either by proton transfer to a suitable neutral, as shown in reaction (3.35), or alternatively through dissociative recombination, may yield methylcyanoacetylene[98]. This molecule has also recently been observed in the interstellar medium[111]. However, as mentioned in section 3.2 the most stable form of this adduct ion is probably the 2-cyanoallyl structure (page 76, section 3.2) for which the dissociative recombination products are uncertain.

The association reactions of HC_3N discussed above may therefore provide a variety of routes to the synthesis of many of the longer chain molecules observed in interstellar clouds. These may include both the cyanopoly-yne and the methylcyanopoly-yne series as well as a number of types of hydrocarbons. For a more detailed understanding of the ion-molecule mechanisms involved in the synthesis of these larger molecules the actual structures of the adducts need to be known as well as the products of dissociative recombination. Clearly there is a need for more extensive experimental investigation of dissociative recombination reactions of these types as well as determination of the neutral products of these reactions.

It should also be pointed out that other non-polar hydrocarbon molecules which cannot be observed by radiowave spectroscopy are almost certainly present in interstellar clouds and at appreciable concentrations. These will also participate in ion-molecule reaction schemes to provide a complex interwoven fabric of chemical linkages between the observed poly-ynes, alkenes, cyanopoly-ynes, etc.

A favoured scheme[40,41,42] for production of interstellar HC_3N itself involves reaction (3.39) followed by the hydrogen

$$C_3H_2^+ + N \rightarrow HC_3N^+ + H \qquad (3.39)$$

$$HC_3N^+ + H_2 \rightarrow H_2C_3N^+ + H \qquad (3.29)$$

$$H_2C_3N^+ + e \rightarrow HC_3N + H \qquad (3.40)$$

abstraction reaction (3.29) and finally dissociative

recombination to form HC_3N through reaction (3.40). This scheme assumes the rate of reaction (3.29) to be fast ($k \sim 10^{-9}$ cm^3 s^{-1}), however the overall rate coefficient measured in this study was 7×10^{-12} cm^3 s^{-1} at 305 K for the production of <u>two</u> product ions: $H_2C_3N^+$ (76%) and $C_2H_2^+$ (24%). Ion-molecule reactions of this type which proceed at only a very small fraction of the collision rate at room temperature usually become still less efficient at interstellar cloud temperatures. A fall-off in efficiency at lower temperatures for reaction (3.29), usually assumed to be due to the presence of an activation energy barrier on the reactive potential energy surface, would obviously inhibit the eventual production of HC_3N through the scheme (3.39), (3.29) and (3.40).

Recently the analogous reaction of NH_3^+ with H_2 was studied over the temperature range (85-510 K) in a temperature variable SIFT[112] (in conjunction with ion trap measurements of the reaction at 10 K by Dunn and Barlow[113]). At room temperature NH_4^+ was produced by very slow hydrogen atom abstraction. However at temperatures below 80 K the reaction rate coefficient was noted to increase sharply[113,114]. Adams and Smith suggested that the increasing reaction rate at low temperatures was due to a change in the reaction mechanism. Unless a similar mechanism change occurs for the reaction of HC_3N^+ with H_2 it is unlikely that the suggested reaction scheme ((3.39), (3.29) and (3.40)) can explain the observed abundances of HC_3N in interstellar clouds.

As an alternative source for the ion $H_2C_3N^+$ the reaction between C_3N^+ and H_2 was studied. This process (reaction (3.30)), detailed in section 3.3, produced $H_2C_3N^+$ (10%)

through an association channel and HC_3N^+ (90%) by exothermic hydrogen atom abstraction. The rate of reaction was fast ($k = 9.1 \times 10^{-10}$ cm^3 s^{-1}) and therefore the reaction appears to provide a possible source of $H_2C_3N^+$ and hence HC_3N. However Bates[115] has stated that for reactions where an exothermic channel competes with radiative stablisation, the exothermic channel may severely suppress the radiative channel.

In a very recent experimental study Lindinger[116] has measured a rate coefficient of $\sim 1 \times 10^{-10}$ cm^3 s^{-1} at 300 K for the reaction between atomic nitrogen and the ion $C_3H_3^+$ (reaction 3.41).

$$C_3H_3^+ + N \rightarrow H_2C_3N^+ + H \qquad (3.41)$$

The magnitude of this rate coefficient supports the suggestion of Herbst et al[42] that if this reaction is fast then, in concert with reaction (3.40) above (the dissociative recombination of $H_2C_3N^+$), it could be the major route to the formation of HC_3N in interstellar clouds.

In summary, HC_3N has been shown to associate with a wide range of ions indicating that the molecule could be active in the formation of many of the larger neutrals and radicals observed in interstellar clouds.

3.6 CONCLUSION.

The behaviour of HC_3N in reactions (3.00)-(3.30) has shown several broad trends. The most immediate of these is the

propensity of the neutral cyanoacetylene to associate with a wide variety of ions.

Generally highly exothermic ion-molecule reactions such as proton transfer, atom abstraction, charge transfer, and dissociative charge transfer were observed to occur at rates close to the respective collision limits. When proton transfer was near thermo-neutral ($\Delta H^{\circ} < \pm 10$ kJ mol^{-1}), as for example with reactions (3.20) and (3.21), it occurred in competition with association. When proton transfer to HC_3N was more than 10 kJ mol^{-1} endothermic, for example with the ions CH_3CHOH^+, CH_3CNH^+ and $C_4H_2^+$ association still occurred at a significant fraction of the collision rate.

These adduct ions, formed through association channels, may be of two possible structural types. Either a strongly bound covalent ion with a distinct chemical identity, or a weakly bound cluster ion complex held together only by electrostatic interaction. Examples of both types of adducts are seen in the reactions of CH_3^+ with O_2, H_2, and N_2. Adams and Smith[37] have confirmed that the association of CH_3^+ with H_2 produces the stable ion CH_5^+, while O_2 and N_2 produce the weak cluster ions $CH_3^+.O_2$ and $CH_3^+.N_2$. In the similar association reaction between CH_3^+ and HCN, the product ion signal at m/e= 42 has been confirmed to be of the former type (section 4.4). The product ion, $C_2H_4N^+$, was observed to consist of a 6:1 mixture of the ions CH_3CNH^+ and CH_3NCH^+. The fast rate of association for this reaction, which exhibits a pseudo bimolecular rate close to the collision limit, suggests that almost every collision between CH_3^+ and HCN is subsequently stabilised by a third body collision at the

pressures used (~0.3 Torr).

HC_3N also associated at rates near to the collision limit for many of the reactions discussed in this chapter and by analogy with the association products of CH_3^+ and HCN, it is assumed that the HC_3N association adducts are also covalently bound.

CHAPTER FOUR

A STUDY OF CH_3CN, CH_3NC, AND THE ION $C_2H_4N^+$

4.1 INTRODUCTION.

The ion $C_2H_4N^+$ is formed from the association reaction of CH_3^+ with HCN (reaction (4.00)).

$$CH_3^+ + HCN\ (+M) \rightarrow C_2H_4N^+\ (+M) \qquad (4.00)$$

This reaction has been studied using low pressure ICR mass spectrometry (discussed in the introductory chapter) by McEwan et al[117] who suggested that at low pressures the reaction may be radiatively stabilised. At least two possible structural isomers may be written for the association adduct formed in reaction (4.00). The two most likely isomers, CH_3CNH^+ (1) and CH_3NCH^+ (2), may also be formed by proton transfer to acetonitrile (CH_3CN) and methyl isocyanide (CH_3NC) respectively.

$CH_3-C^+=NH$ (1) $\qquad$ $CH_3-N^+\equiv CH$ (2)

The proton affinity (PA) of CH_3CN has been established by several groups including flowing afterglow experiments[118] and pulsed ICR cell experiments[119,120]. The value chosen by Lias et al in their reference tabulation of PA and gas phase basicity (GB) values[92] is 788±8 kJ mol^{-1}. The only reported value for the PA of CH_3NC is 828 kJ mol^{-1} from Illies et al[121]

who state the exothermicity of proton transfer from $CH_3OH_2^+$ to CH_3NC and quote a proton affinity determination of Aue et al[122].

Using the known heats of formation[123] of CH_3CN and CH_3NC, and the quoted PA's, the heats of formation of the ions CH_3CNH^+ and CH_3NCH^+ are calculated to be 822 kJ mol^{-1} and 881 kJ mol^{-1} respectively. These values are sufficiently different to suggest that two stable isomers may exist in the gas phase for the product ion $C_2H_4N^+$ derived from reaction (4.00).

In this chapter the results of a study undertaken to confirm the structural identity of the $C_2H_4N^+$ ion are detailed. The proton affinities of CH_3CN and CH_3NC are measured and thus the heats of formation of the two isomers CH_3CNH^+ and CH_3NCH^+ are established. Finally an attempt is made to measure an upper limit for the barrier (E_a) to isomerisation.

4.2 PROTON AFFINITY OF CH_3CN.

In this section the PA of CH_3CN was found by observing the rate and direction of proton transfer between CH_3CN and CH_3CHO (acetaldehyde, reaction (4.01), and HCO_2CH_3 (methyl formate, reaction (4.02)).

$$CH_3CNH^+ + CH_3CHO \underset{k_r}{\overset{k_f}{=}} CH_3CHOH^+ + CH_3CN \qquad (4.01) \qquad K_1$$

$$CH_3CNH^+ + HCO_2CH_3 \underset{k_r}{\overset{k_f}{=}} H_2CO_2CH_3^+ + CH_3CN \qquad (4.02) \qquad K_2$$

The ion CH_3CNH^+ was generated by two methods. The first involved electron impact on a 20/1 mixture of hydrogen and CH_3CN. If the ion source pressure was kept below 1 x 10^{-4} Torr the ion at m/e= 42 could be injected free of impurities into the flow tube. When the ion source pressure was increased beyond 1 x 10^{-4} Torr a mass peak at m/e= 83, corresponding to the proton bound dimer ion $(CH_3CN)_2H^+$, also appeared in the flow tube from the clustering reaction between CH_3CNH^+ and small amounts of CH_3CN leaking through the SIFT source orifice.

In the second method the ion HCO^+ was generated from electron impact on a H_2/CO mixture and injected into the flow tube. CH_3CN was added from portal 1 and the ensuing reaction produced CH_3CNH^+ through proton transfer from HCO^+. At neutral flows sufficient to convert the swarm of HCO^+ ions completely to CH_3CNH^+, significant amounts of the dimer ion $(CH_3CN)_2H^+$ were formed as well. Although the presence of this dimer ion considerably complicated product analysis in subsequent reactions, the method was utilised to form the CH_3CNH^+ ion with as little excess internal energy as possible (and therefore with only a small chance of any isomerisation to CH_3NCH^+). The neutrals of interest were then introduced through the second flow tube port (portal 2) and the ensuing proton transfer reaction studied in the usual way.

No differences were noticed between the product distributions or the rate coefficients for the neutrals investigated when the reactant ion was produced by either of the two different methods. The first method of generation, where a swarm of only CH_3CNH^+ ions was able to be created in

the flow tube, was therefore preferred for reactions involving this ion.

The two other primary ions used in the determination of the PA of CH_3CN, viz., CH_3CHOH^+ and $H_2CO_2CH_3^+$, were generated from ionisation of mixtures of approximately equal pressures of H_2 and CH_3CHO or HCO_2CH_3. No significant impurity ion peaks were noted upon injection of the respective ions into the flow tube (CH_3CHO^+ and $HCO_2CH_3^+$ were present at less than 1% of the primary ion concentration in each case).

The measured rate coefficients and product distributions for each of the half reactions in the equilibrium systems (4.01) and (4.02) are listed in table 4.0. The measured rate coefficients are compared in each case with k_{ADO} (or k_{AADO}), the theoretical collision limit (detailed in section 1.3).

Table 4.0 Ion-molecule reactions used to establish the PA of CH_3CN. Rate coefficients, k, are expressed in units of 10^{-9} cm^3 s^{-1}. The flow tube pressure, P, is in units of Torr. The abbreviation "B.R." stands for reaction branching ratio.

ion	neutral	products	B.R.	k	k_c[a]	P
CH_3CNH^+	CH_3CHO	$CH_3CHOH^+ + CH_3CN$	0.17	0.91	2.4	0.38
		$CH_3CNH^+.CH_3CHO$	0.83			
CH_3CNH^+	HCO_2CH_3	$H_2CO_2CH_3^+ + CH_3CN$	0.72	1.7	1.8	0.30
		$CH_3CNH^+.HCO_2CH_3$	0.28			
$H_2CO_2CH_3^+$	CH_3CN	$CH_3CNH^+ + HCO_2CH_3$	0.50	1.7	3.9	0.30
		$H_2CO_2CH_3^+.CH_3CN$	0.50			
CH_3CHOH^+	CH_3CN	$CH_3CNH^+ + CH_3CHO$	0.95	3.4	4.1	0.30
		$CH_3CHOH^+.CH_3CN$	0.05			

(a) k_c represents theoretical collision limit rate coefficients calculated using either the ADO or AADO theories.

In all of the proton transfer reactions between protonated CH_3CN, HCO_2CH_3 and CH_3CHO, association occurred in conjunction conjunction with proton transfer as a product channel.

Therefore, as with the determination of the PA of HC_3N in Chapter Three, the product distribution for all of these reactions needed to be known accurately to determine the actual proton transfer rate coefficient for each reaction. After allowance was made for the contribution to the overall rate coefficient from association, the equilibrium constants K_1, for reaction (4.01), and K_2, for reaction (4.02), were determined to be 0.048 and 1.44 respectively. The relative gas phase basicities for the two equilibrium systems were then calculated from the expression $\Delta G^{\circ} = -RT\ln K$. Table 4.1 shows the relative GB values determined for each of CH_3CN, CH_3CHO, and HCO_2CH_3, along with literature values determined by three separate low pressure studies[124,119,120]. For purposes of comparison the GB of CH_3CN has been assigned a value of zero.

Table 4.1: Relative gas phase basicities (ΔGB) of CH_3CN, HCO_2CH_3 and CH_3CHO referenced to the established GB of CH_3CN (in kJ mol^{-1}).

neutral	ref. 124	ref. 119	ref. 120	this work[a]
CH_3CN	0.0	0.0	0.0	0.0
HCO_2CH_3	-2.1	2.9	3.3	0.9
CH_3CHO	-8.4	-8.4	-7.5	-7.6

(a) Estimated uncertainty in relative measurements is $\pm$1 kJ mol^{-1}.

The relative GB values for the three neutrals determined in this study at pressures of ~0.3 Torr agree well with the results from the earlier low pressure (~10^{-6} Torr) ICR mass spectroscopy studies[124,119,120]. Competition from association channels during ion-molecule reactions where proton transfer is involved does not therefore appear to noticeably influence the derived proton transfer rates. Davidson et al[125], in a

high pressure drift cell ICR study on the PA of a number of molecules, have also noted that association does not markedly interfere with proton transfer.

The relative PA values for CH_3CN, CH_3CHO, and HCO_2CH_3 are shown in table 4.2 and have been referenced to the established literature value of 788±8 kJ mol^{-1} for the PA of CH_3CN. These PA's were derived from the relative GB values shown in table 4.1 in the same manner as for the PA of HC_3N in Chapter Three.

Table 4.2: Proton affinities (in kJ mol^{-1}) estimated from ΔGB's of tables 4.1 and 4.4.

species	proton affinity[a]
NH_3[b]	835.5
CH_3NC[b]	844
EtOEt[b]	842
THP[b]	<834
THF[b]	<830
HCO_2CH_3[c]	789
CH_3CN[c]	788
CH_3CHO[c]	782

(a) Estimated uncertainties for these relative PA's are ±2 kJ mol^{-1}.
(b) These results are referenced to the value PA (NH_3) = 853.5 kJ mol^{-1} [92].
(c) These results are referenced to the value PA (CH_3CN) = 788 kJ mol^{-1} [92].

4.3 THE PROTON AFFINITY OF CH_3NC.

The PA of CH_3NC was established in a similar way to that for CH_3CN, by observing the rate and direction of proton transfer from CH_3NCH^+ to a number of neutral compounds of similar PA's. The equilibrium systems of CH_3NC with these compounds, viz., NH_3, EtOEt (diethylether), THF (cyclo-C_4H_8O, tetrahydrofuran) and THP (cyclo-$C_5H_{10}O$, tetrahydropyran), are

CH_3NCH^+	+	NH_3	⇌	NH_4^+	+	CH_3NC	(4.03) K_3
CH_3NCH^+	+	EtOEt	⇌	$EtOEtH^+$	+	CH_3NC	(4.04) K_4
CH_3NCH^+	+	THF	⇌	$THFH^+$	+	CH_3NC	(4.05) K_5
CH_3NCH^+	+	THP	⇌	$THPH^+$	+	CH_3NC	(4.06) K_6

Initially the ion CH_3NCH^+ was generated by electron impact on a 20/1 mixture of H_2 and CH_3NC in the ion source. When the ion source pressure was less than 1×10^{-4} Torr, the ion at m/e= 42 could be injected free of impurity ions into the flow tube. At a later stage in this study of the isomers of $C_2H_4N^+$ a second method of generation was tried. A swarm of CH_3^+ ions (from any of the species CH_3I, CH_3Br, or CH_4) was initially created in the reaction tube. Neutral CH_3NC was then added through portal 1 to produce a swarm of CH_3NCH^+ ions by proton transfer from CH_3^+.

A comparison of the two CH_3NCH^+ formation methods showed that producing CH_3NCH^+ by electron impact in the ion source resulted in some isomerisation to the more stable ion CH_3CNH^+. For example, if HCO_2CH_3 (MeF) was added to a swarm of CH_3NCH^+ ions created by electron impact on CH_3NC, a significant proton transfer channel corresponding to $H_2CO_2CH_3^+$ (16%) was also seen along with the dominant association channel (84%). If CH_3NCH^+ was produced by chemical reaction at portal 1 however, only the association product was observed. It is shown later (p. 131) that proton transfer to HCO_2CH_3 can occur only from CH_3CNH^+ and not from CH_3NCH^+. Therefore the latter method was preferred in the determination of the PA of CH_3NC.

Product analyses, for reactions where CH_3NCH^+ was formed

by proton transfer at portal 1, were slightly complicated by the presence of the dimer ion $(CH_3NC)_2H^+$ at higher flows of the neutral CH_3NC. However, as this dimer ion could be formed in isolation at portal 1 by the addition of high flows of CH_3NC to the primary ion CH_3^+, product distributions for the reactions of CH_3NCH^+ could be easily analysed by making appropriate corrections to the products observed from the $CH_3NCH^+/(CH_3NC)_2H^+$ mixture (the reactions of the dimer ion are detailed in reactions 4.07-4.11, p.122).

The ions $EtOEtH^+$, $THFH^+$, $THPH^+$, $H_2CO_2CH_3^+$ and NH_4^+ were each produced by electron impact upon a mixture of H_2 and the respective neutral. At low injection energies, $THPH^+$ was injected into the reaction tube free of impurities. Under the same conditions for the ion $THFH^+$ however, fragment peaks from dissociation of the parent ion were always present even at the lowest injection energies that were accessible. Therefore for product analysis in reactions involving the $THFH^+$ ion a hydrogen carrier was used. With H_2 as the buffer gas, a swarm containing only $THFH^+$ ions could be produced by injecting THF^+ ions into the flow tube where they underwent H atom abstraction with the carrier gas. For NH_4^+ and $EtOEtH^+$, the impurity ions NH_3^+ and $EtOH_2^+$ (m/e= 47) were present at 8% and 15% respectively. $EtOH_2^+$ was found to proton transfer rapidly only to CH_3NC, whilst NH_3^+ charge transferred to the CH_3NC neutral. Therefore the product distribution for the reaction of $EtOEtH^+$ with CH_3NC (detailed in table 4.3) was found by appropriately correcting the proton transfer channel for the contribution from $EtOH_2^+$.

The respective equilibrium constants K_3 (11.875), K_4

(0.124), K_5 (0.124) and K_6 (0.906) for proton transfer between CH_3NC and NH_3, EtOEt, THF and THP were determined from the measured rate coefficients and product distributions (listed in table 4.3) for each half reaction. Again, as with CH_3CN, association competed with proton transfer in the majority of the reactions investigated.

Table 4.3: Ion-molecule reactions used to establish the proton affinity of CH_3NC. Rate coefficients, k, are in units of 10^{-9} cm^3 s^{-1} while the flow tube pressure, P, is in units of Torr.

ion	neutral	products	B.R.	k	k_{ADO}	P
CH_3NCH^+	HCO_2CH_3	$CH_3NCH^+.HCO_2CH_3$	1.0	0.014 (0.042	1.8	0.29 0.38)
CH_3NCH^+	THP	$CH_3NCH^+.THP$	1.0	1.0	2.1	0.30
CH_3NCH^+	THF	$CH_3NCH^+.THF$	1.0	0.81	2.0	0.30
$THPH^+$	THF	$THFH^+$ + THP $THPH^+.THF$	0.07) 0.93)	1.3	1.7	0.30
$THFH^+$	THP	$THPH^+$ + THF $THFH^+.THP$	0.40) 0.60)	1.1	1.8	0.30
$THPH^+$	CH_3NC	CH_3NCH^+ + THP $THPH^+.CH_3NC$	0.46) 0.54)	2.4	2.7	0.34
$THFH^+$	CH_3NC	CH_3NCH^+ + THF $THFH^+.CH_3NC$	0.82) 0.18)	2.0	2.8	0.21
CH_3NCH^+	NH_3	NH_4^+ + CH_3NC	1.0[a]	1.9	1.9	0.29
CH_3NCH^+	EtOEt	$EtOEtH^+$ + CH_3NC $CH_3NCH^+.EtOEt$	0.10) 0.90)	1.3	3.3	0.30
NH_4^+	CH_3NC	CH_3NCH^+ + NH_3	1.0	0.16	4.0	0.30
$EtOEtH^+$	CH_3NC	CH_3NCH^+ + EtOEt $EtOEtH^+.CH_3NC$	0.50) 0.50)	2.1	2.8	0.30

(a) A small amount (1-2%) of $CH_3NCH^+.NH_3$ was also observed.

The relative gas phase basicities for each of CH_3NC, NH_3, EtOEt, THF and THP, determined from the equilibrium constants

K_3, K_4, K_5, and K_6, in the same manner as for the GB of CH_3CN in section 4.1, are shown in table 4.4. The GB of NH_3 has been assigned a value of zero for comparison purposes with the other reference data[124,119,120].

Table 4.4: Relative gas phase basicities (ΔGB) in kJ mol^{-1}. The ΔGB of NH_3 has been assigned a value of zero for comparison purposes.

compound	ref. 124	ref. 119	ref. 120	this work[a]
NH_3	0.0	0.0	0.0	0.0
CH_3NC	-	-	-	-6
EtOEt	-14	-15	-13	-11
THP	-13	-17	-	<-17[b]
THF	-17	-20	-17	<-21[c]

(a) The estimated uncertainty in these relative ΔGB's is $\pm$1 kJ mol-1.
(b) Limit is derived from the non-observation of proton transfer from CH_3NCH^+ to THP.
(c) Limit is derived from (b) and the relative GB(THP)-GB(THF).

Agreement is obtained, within experimental error and where comparison is possible, between the relative GB values obtained in this study, and those from low pressure pulsed ICR measurements[124,119,120].

The relative proton affinities of the five neutrals, calculated in the same manner as the PA of CH_3CN, are shown in table 4.2 and have been referenced to the PA value for NH_3 of 853.5 kJ mol^{-1} [92,125].

The value for the PA of CH_3NC obtained in this study is 844 ± 2 kJ mol^{-1}. This value is considerably higher than the result of Aue et al[122] quoted by Illies et al[121] of 828 kJ

mol^{-1}. However Aue et al chose a different PA reference scale to that used in this study for their CH_3NC PA determination[126].

The measured proton affinities determined in this study for CH_3CN and CH_3NC (table 4.2) lead to $\Delta H_f^\circ [CH_3CNH^+] = 822 \pm 10$ kJ mol^{-1} and $\Delta H_f^\circ [CH_3NCH^+] = 865 \pm 10$ kJ mol^{-1}.

Reactions (4.07-4.11)

NH_3, EtOEt, HCO_2CH_3, THP, THF with $(CH_3NC)_2H^+$

The reactions discussed in this section were studied to enable corrections to be made to the product distributions of the previous section for the presence of the dimer ion $(CH_3NC)_2H^+$ in the equivalent CH_3NCH^+ ion reactions.

The rate coefficients and product distributions for the reactions of the five neutrals NH_3, EtOEt, HCO_2CH_3, THP and THF with $(CH_3NC)_2H^+$ are shown in table 4.5.

Table 4.5: Reactions of the dimer ion $(CH_3NC)_2H^+$. Rate coefficients, k, are expressed as 10^{-9} cm^3 s^{-1}. The tube pressure, P, has units of Torr, while the abbreviation "no." stands for the reaction number.

no.	neutral	products	P.R.	k	P
4.07	NH_3	$CH_3NCH^+.NH_3 + CH_3NC$	0.66	0.19	0.30
		$(CH_3NC)_2H^+.NH_3$	0.33		
4.08	EtOEt	$CH_3NC.EtOEtH^+ + CH_3NC$	1.0	0.33	0.30
4.09	HCO_2CH_3	$(CH_3NC)_2H^+.HCO_2CH_3$	1.0	$\leq$ 0.1	0.30
4.10	THP	$(CH_3NC)_2H^+.THP$	1.0	0.06	0.30
4.11	THF	$(CH_3NC)_2H^+.THF$	1.0	0.13	0.30

Ammonia was observed to react with the dimer ion $(CH_3NC)_2H^+$

through two product channels, the major one producing the association switching product $CH_3NCH^+.NH_3$ along with a smaller association adduct. At 0.30 Torr the ratio of product ions was to 3 to 1 for $CH_3NCH^+.NH_3$ (m/e= 59) over $(CH_3NC)_2.NH_3^+$ with an overall reaction rate of 1.9×10^{-10} cm^3 s^{-1}. EtOEt reacted with the dimer ion $(CH_3NC)_2H^+$ to produce the association switching product $EtOEtH^+.CH_3NC$ (m/e= 116) with a rate coefficient of 3.3×10^{-10} cm^3 s^{-1}.

The neutrals HCO_2CH_3, THF, and THP were all observed to react with the dimer ion, yielding association products only, at pseudo second order rate coefficients of 1.3 and 0.6 x 10^{-10} cm^3 s^{-1} for THF and THP respectively at a flow tube pressure of 0.30 Torr. The rate of association of $(CH_3NC)_2H^+$ with HCO_2CH_3, although not measured, was also noted to be slow ($\lesssim 1 \times 10^{-10}$ cm^3 s^{-1}).

Reactions (4.12-4.14) CH_3^+ + HCN, CH_3CN, CH_3NC

Initially the CH_3^+ ion swarm for reactions (4.12-4.14) was generated by electron impact on CH_4 in the ion source. However the impurity ions CH^+, CH_2^+, CH_4^+ and the dimer ion $C_2H_5^+$, even through present at concentrations in total of less than 5% of the primary ion signal still resulted in a peak at m/e= $\overset{28}{=}$ (H_2CN^+) when HCN was added. Therefore, to accurately determine the product distribution for this reaction, CH_3I and CH_3Br were both used as a source of CH_3^+ in the ion source. With these neutral gases, and at low injection energies, a swarm of only CH_3^+ ions was produced in the flow tube, with a consequent straightforward product analysis for reactions

(4.12-4.14).

The product distributions and rate coefficients of reactions (4.12), (4.13) and (4.14) are shown in table 4.6. Of these three reactions, only in the case of CH_3^+ with CH_3NC is proton transfer exothermic and only for this reaction was it noted. The rate coefficient for proton transfer from CH_3^+ to CH_3NC was 1.1×10^{-9} cm^3 s^{-1}.

Table 4.6: Ion-molecule reactions of CH_3^+ with HCN, CH_3CN and CH_3NC. Rate coefficients, k, are in units of 10^{-9} cm^3 s^{-1}. The flow tube pressure, P, has units of Torr.

no.	neutral	products	B.R.	k	k_{AADO}	P	k(lit)
4.12	HCN	$C_2H_4N^+$	1.0	1.7[a] (~1.6	4.8	0.45 0.26)	0.2[b], 2.0[c]
4.13	CH_3CN	$CH_3^+.CH_3CN$	1.0	5.9[a] (~4.0	5.8	0.36 0.30)	
4.14	CH_3NC	$CH_3NCH^+ + CH_2$	1.0	1.1	5.7	0.30	

(a) Pseudo second order rate coefficient.
(b) Reference 85.
(c) reference 127, pseudo second order rate coefficient at 0.5 Torr.

For the other two species, HCN and CH_3CN, very rapid association with CH_3^+ was observed to occur. The measured pseudo second order rate coefficient for reaction (4.13) was 5.9×10^{-9} cm^3 s^{-1} at 0.36 Torr. The theoretical collision limit (k_{AADO}) for the association of CH_3^+ with CH_3CN is 5.7×10^{-9} cm^3 s^{-1}, which indicates that at 0.36 Torr the reaction efficiency is near unity. A lower limit to the ternary rate coefficient for this reaction of 5.1×10^{-25} cm^6 s^{-1} was estimated over the pressure range 0.30-0.36 Torr.

For the reaction with HCN (reaction (4.12)), a single

product, the association adduct $CH_3^+.HCN$ [$C_2H_4N^+$], was produced with a pseudo second order rate coefficient of 1.6 x 10^{-9} cm^3 s^{-1} at 0.29 Torr, and 1.7 x 10^{-9} cm^3 s^{-1} at 0.45 Torr. An apparent pressure dependence for the reaction at these pressures has been estimated by Adams and Smith[31] from SIFDT measurements as ~5 x 10^{-25} cm^6 s^{-1}. Schiff and Bohme[127] have also studied the reaction using the SIFT technique and, at 0.5 Torr, measured a pseudo second order rate coefficient for association between CH_3^+ and HCN of 2.0 x 10^{-9} cm^3 s^{-1}.

4.4 ISOMER STRUCTURES OF THE ION $C_2H_4N^+$.

The reaction of CH_3^+ with HCN appears to produce a mixture of two isomers, as indicated in the introduction to this chapter. Gilbert and McEwan[128], in a theoretical analysis of this reaction used a weak collision model for energy transfer in a helium bath gas. The authors concluded that the pressure dependence of the rate coefficient for reaction (4.12) strongly favoured the initial formation of the isomer CH_3NCH^+.

The initial formation of the CH_3NCH^+ ion from the reaction of CH_3^+ with HCN is also supported in the recent work of DeFrees et al[129]. They have shown theoretically that the minimum energy pathway for the reaction leads to the CH_3NCH^+ isomer. However, if the reaction is sufficiently exothermic, subsequent isomerisation to the more stable isomer CH_3CNH^+ may occur before the excess internal energy is dissipated through collision with a third body. It was proposed in this study to distinguish between these isomers on the basis of their different reactivities.

The reactions of the ion $C_2H_4N^+$, produced as a product of the reaction between CH_3^+ and HCN at portal 1, with NH_3, THP, THF and HCO_2CH_3 were studied to test for a possible change in reactivity over a range of flows for each neutral. The results of these reactions and the reactions of CH_3CNH^+ and CH_3NCH^+ with the same neutrals are shown in Table 4.7. A distinct change in the log plot of the $C_2H_4N^+$ ion concentration ($\log(I_{42})$) against varying neutral flow (f_n) was observed for THF and HCO_2CH_3 (see figures 4.0, and 4.1). It is likely that the curved decays are the result of two isomers of $C_2H_4N^+$, viz., CH_3CNH^+ and CH_3NCH^+ both being produced in the reaction. Thus a double exponential decay curve was fitted to the data to determine the individual rate coefficients and isomer ratios. The form of the double exponential decay equation is given in equation (4.0).

$$I_{42} = C1 \exp(-k_1 f_n) + C2 \exp(-k_2 f_n) \qquad \text{Eqn. (4.0)}$$

C1 and C2 are pre-exponential decay constants representing the initial concentrations of each isomer, and k_1 and k_2 are the respective decay constants for each slope. The actual programme ("Expon") used to calculate these values is detailed in Appendix 1. This programme fits the input data ($\log(I)$) as a function of the neutral reactant flow (f_n) to the initial input parameters provided (C1, C2 and k_1, k_2). It outputs corrected rate coefficients, k, and isomer concentrations, C, for each decay curve. The uncertainties associated with the rate coefficients and product distributions obtained through fitting data by the "Expon" programme have been estimated from

Table 4.7: Ion-molecule reactions of the ions $C_2H_4N^+$, CH_3CNH^+ and CH_3NCH^+ with THF, THP, HCO_2CH_3 (MeF) and NH_3. The rate coefficients, k, are in units of 10^{-9} cm^3 s^{-1}, whilst the tube pressure, P, has units of Torr.

no.	neutral	ion	products	B.R.	k	P	k_{ADO}
4.15	THF	$C_2H_4N^+$	$THFH^+ + C_2H_3N$ $C_2H_4N^+.THF$	0.90 0.10	1.7, 0.7[a]	0.30	2.0
4.16		CH_3CNH^+	$THFH^+ + CH_3CN$	1.0	1.6	0.30	2.0
4.17		CH_3NCH^+	$CH_3NCH^+.THF$	1.0	0.81	0.30	2.0
4.18	THP	$C_2H_4N^+$	$THPH^+ + C_2H_3N$ $C_2H_4N^+.THP$	0.80 0.20	1.4	0.33	2.1
4.19		CH_3CNH^+	$THPH^+ + CH_3CN$	1.0	1.3	0.30	2.1
4.20		CH_3NCH^+	$CH_3NCH^+.THP$	1.0	1.0	0.30	2.1
4.21	MeF	$C_2H_4N^+$	$MeFH^+ + C_2H_3N$ $C_2H_4N^+.MeF$	0.65 0.35	1.6, 0.01[a]	0.30	1.8
4.22		CH_3CNH^+	$MeFH^+ + CH_3CN$ $CH_3CNH^+.MeF$	0.72 0.28	1.7	0.30	1.8
4.23		CH_3NCH^+	$CH_3NCH^+.MeF$	1.0	0.014 (0.042	0.29 0.38)	1.8
4.24	NH_3	$C_2H_4N^+$	$NH_4^+ + C_2H_3N$ $C_2H_4N^+.NH_3$	0.97 0.03	1.8	0.25	1.9
4.25		CH_3CNH^+	$NH_4^+ + CH_3CN$	1.0	2.0	0.30	1.9
4.26		CH_3NCH^+	$NH_4^+ + CH_3NC$	1.0[b]	1.9	0.29	1.9

(a) These rate coefficients were obtained from a 2-exponential fit to the observed decay in the $C_2H_4N^+$ signal.

(b) A small amount (~1-2%) of $CH_3CNH^+.NH_3$ was also observed.

standard deviations of the functions over a number of runs.

The individual isomers were identified by comparing the two components of the decay from the $C_2H_4N^+$ ion with the rate coefficients and product distributions of pure CH_3CNH^+ and CH_3NCH^+ for the reagents THF and HCO_2CH_3. These reagents were chosen because of their very different reactivites with the two isomers CH_3CNH^+ and CH_3NCH^+. THP showed only a small change in the rate coefficient for reaction with each of the isomers, and NH_3 showed no detectable difference in reactivity with either isomer.

Reactions (4.15-4.17) $C_2H_4N^+$, CH_3CNH^+, CH_3NCH^+ with THF

Reaction (4.16), the reaction of CH_3CNH^+ with THF, formed only the proton transfer product $THFH^+$ with a rate coefficient of 1.6×10^{-9} cm^3 s^{-1}. Proton transfer was expected to be rapid as the PA (THF) is larger by 42 kJ mol^{-1} than the PA (CH_3CN) (see table 4.2).

In contrast the PA (CH_3NC) (from table 4.2) is at least 14 kJ mol^{-1} larger again than PA (THF) and only association was observed as expected. The adduct $CH_3NCH^+.THF$ was produced with a pseudo second order rate coefficient of 0.81×10^{-9} cm^3 s^{-1} at a tube pressure of 0.30 Torr.

When THF was added to $C_2H_4N^+$ formed at portal 1 from the reaction of CH_3^+ with HCN (reaction (4.12)), both association (10%) and proton transfer (90%) were observed as products of the reaction. Figure 4.0c shows the decay of the $C_2H_4N^+$ ion with added THF, while figures 4.0a and 4.0b show the separate decays of the isomers CH_3CNH^+ and CH_3NCH^+ respectively.

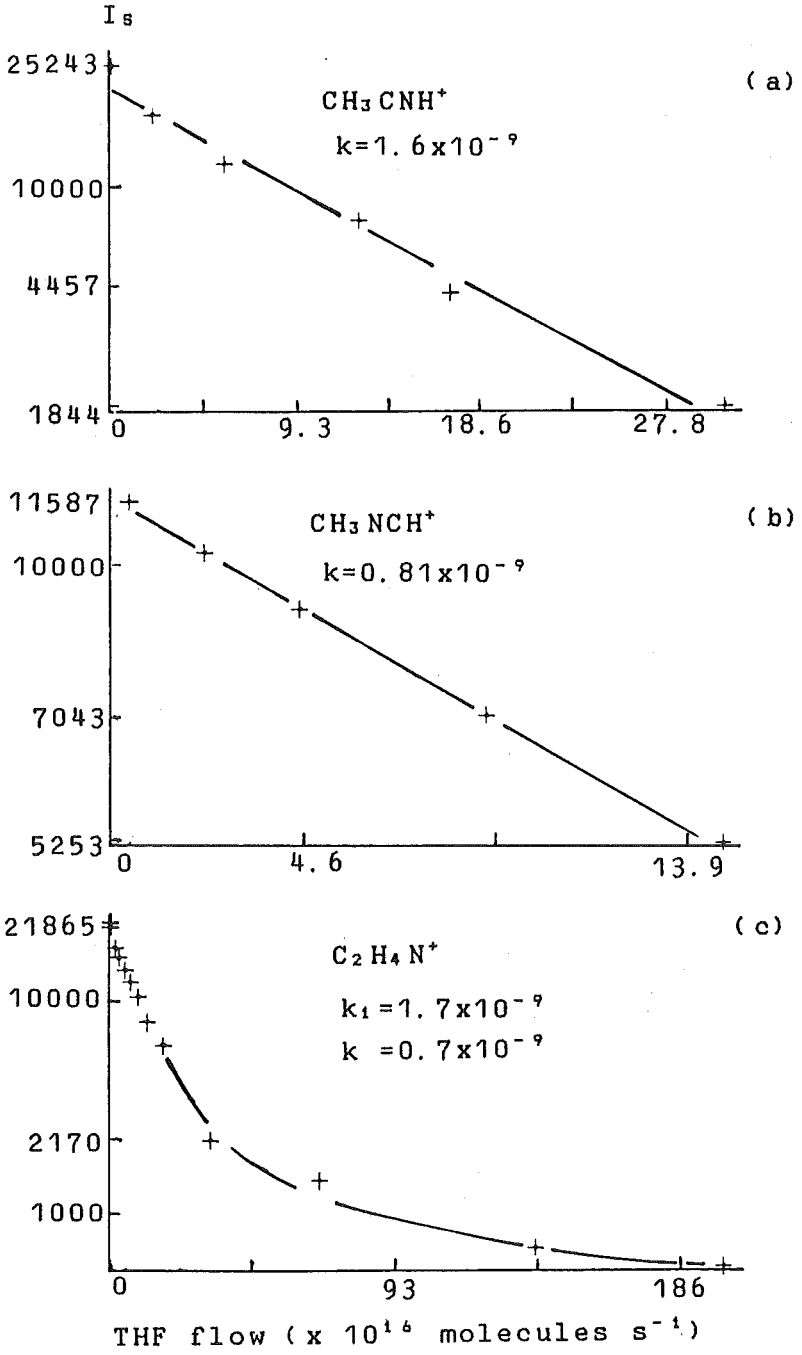

Fig. 4.0: Semilogarithmic plots of I_s, the ion signal at m/e = 42, versus the flow of THF for the following ions:
(a). CH_3CNH^+ formed by proton transfer from HCO^+ to CH_3CN.
(b). CH_3NCH^+ formed by proton transfer from CH_3^+ to CH_3NC.
(c). C_2H_4N formed from the reaction of CH_3^+ with HCN.

Therefore, by comparison with reactions (4.16) and (4.17) where CH_3CNH^+ produced only a proton transfer product and CH_3NCH^+ only an association adduct, the relative proportions of the two isomers formed from reaction (4.12) can be found. This ratio could then be confirmed by analysis of the two decay log plot of the 42 amu ion for reaction (4.15). From the best fit of "Expon" to the measured decay curve two rate coefficients and two pre-exponential decay constants were provided for each decay. If the two isomers present were CH_3CNH^+ and CH_3NCH^+ then the rates should correspond to the individually measured rates for reaction of these two species with THF. Also the ratio of the two pre-exponential decay constants [C1, C2] should correspond to the percentages of each isomer initially formed, as measured from the product distribution for reaction (4.15).

The "best fit" rate coefficient, calculated from the fastest of the two exponential decays, was 1.7×10^{-9} cm^3 s^{-1} (an average over a number of runs). The "best fit" value for the slower decay was 0.7×10^{-9} cm^3 s^{-1}. These results agree, within experimental error, to the rate coefficients obtained separately for the reaction of each isomer with THF; 1.6×10^{-9} cm^3 s^{-1} for CH_3CNH^+ (4.16); and 0.81×10^{-9} for CH_3NCH^+ (4.17).

From the fitted pre-exponential decay constants the ratio of CH_3CNH^+ to $CH_3\overset{NC}{\cdots}H^+$ was 85±8/15±8. This again agrees with the ratio obtained from the product distribution for reaction (4.15).

Reactions (4.18-4.20) $C_2H_4N^+$, CH_3CNH^+, CH_3NCH^+ with THP

The reactions of the ions CH_3CNH^+ and CH_3NCH^+ with THP followed the trends established with THF, as was expected from the difference in PA between the THP and THF neutrals which is only 4 kJ mol^{-1}. For reaction (4.19) the overall rate coefficient was 1.3 x 10^{-9} cm^3 s^{-1} with the only product channel observed being proton transfer. Association with a pseudo second order rate coefficient of 1.0 x 10^{-9} cm^3 s^{-1} was the only observed channel for reaction (4.20), as proton transfer from CH_3NCH^+ to THP is endothermic.

Only a small change in slope was noted for the decay of the ion $C_2H_4N^+$ with added THP (reaction 4.18) and therefore this reaction was not analysed through the "Expon" program. However the observed product channel distribution for reaction (4.18) was 80% for proton transfer versus 20% for assocation indicating that approximately 20% of the initial $C_2H_4N^+$ ion swarm present in the flow tube had the CH_3NCH^+ ion structure.

Reactions (4.21-4.23) $C_2H_4N^+$, CH_3CNH^+, CH_3NCH^+ with HCO_2CH_3

A marked difference in the reactivity of the CH_3CNH^+ and CH_3NCH^+ towards HCO_2CH_3 was observed in reactions (4.22) and (4.23). While CH_3CNH^+ underwent rapid proton transfer (72%) in conjunction with association (28%) at an overall rate coefficient of 1.7 x 10^{-9} cm^3 s^{-1}, CH_3NCH^+ associated only very slowly with HCO_2CH_3. At 0.29 Torr the pseudo second order rate coefficient for reaction (4.23) was 1.4 x 10^{-11} cm^3 s^{-1} increasing to 4.2 x 10^{-11} cm^3 s^{-1} at 0.38 Torr, leading

to a lower limit of 2.8 x 10^{-27} cm^6 s^{-1} for the rate coefficient of the three body reaction (4.23) at 0.38 Torr.

$$CH_3NCH^+ + HCO_2CH_3 \ (+M) \rightarrow CH_3NCH^+.HCO_2CH_3 \ (+M) \quad (4.23)$$

As a result of the very different behaviour of each of the structural isomers CH_3CNH^+ and CH_3NCH^+ with methyl formate, it was no surprise to note a curved decay plot (figure 4.1c) for $C_2H_4N^+$ with HCO_2CH_3. The faster decay rate coefficient, corresponding to the CH_3CNH^+ ion, was 1.6 x 10^{-9} cm^3 s^{-1}, which is in good agreement with the value measured separately in reaction (4.22). The fitted rate coefficient for the slower decay was 1.0 x 10^{-11} cm^3 s^{-1}, again in agreement with the value obtained from the separate reaction of the CH_3NCH^+ ion with HCO_2CH_3. Analysis of the product distribution in reaction (4.21) to obtain an isomer ratio for the reactant $C_2H_4N^+$ ions was slightly complicated by the observation of association products for each isomer in separate reaction with HCO_2CH_3. However the estimated ratio of ~6/1 for the isomers CH_3CNH^+ and CH_3NCH^+ agreed with the average ratio of the fitted pre-exponential decay constants from reaction (4.21).

Reactions (4.24-4.26) $C_2H_4N^+$, CH_3CNH^+, CH_3NCH^+ with NH_3

A single exponential decay was observed in the reaction of NH_3 with $C_2H_4N^+$ corresponding to a rate coefficient of 1.8 x 10^{-9} cm^3 s^{-1} (figure 4.2c). The single decay was expected as the measured rate coefficients for the separate reaction of the two isomers CH_3CNH^+ and CH_3NCH^+ with NH_3, at 2.0 and 1.9 x

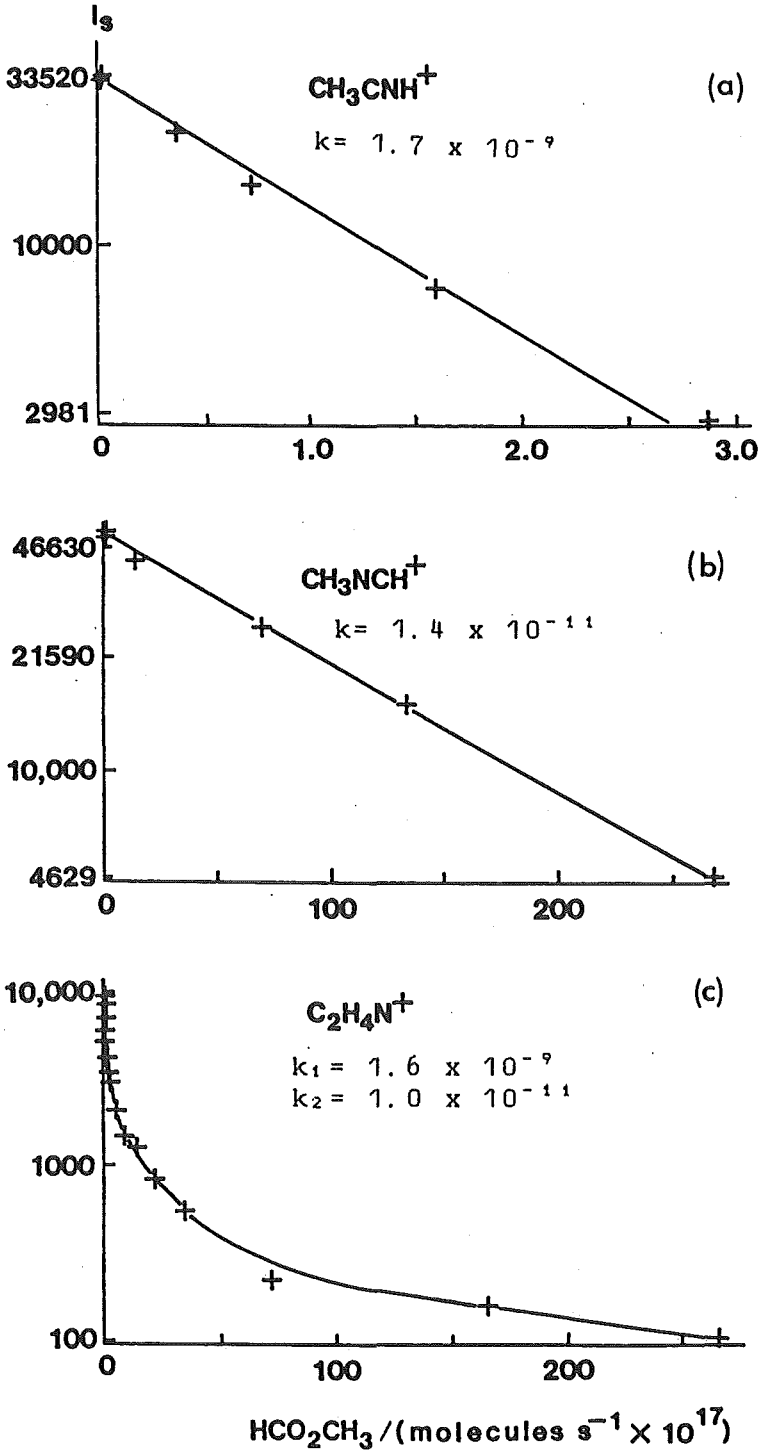

Fig. 4.1: Semilogarithmic plots of I_s, the ion signal at m/e = 42, versus the flow of HCO_2CH_3 for the following ions: (a). CH_3CNH^+ formed by proton transfer from HCO^+ to CH_3CN.
(b). CH_3NCH^+ formed by proton transfer from CH_3^+ to CH_3NC.
(c). C_2H_4N formed from the reaction of CH_3^+ with HCN.

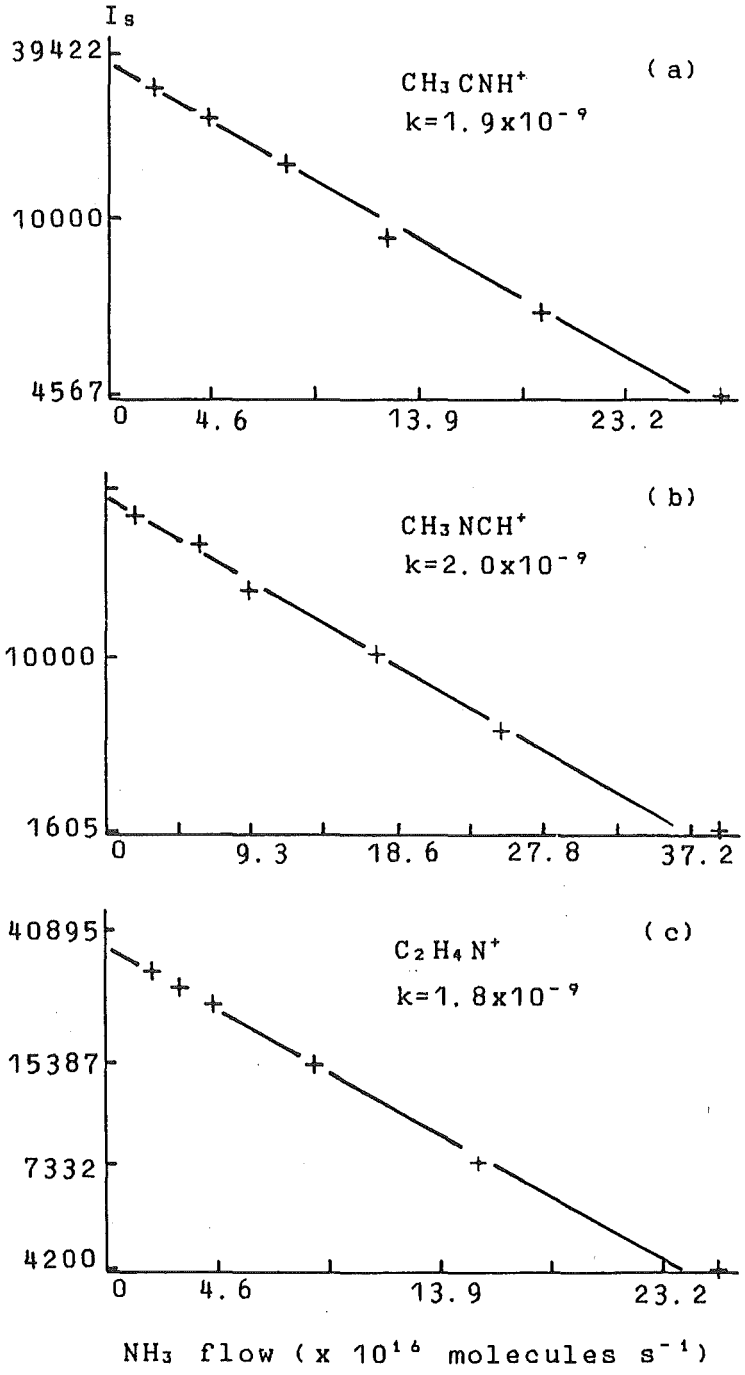

Fig. 4.2: Semilogarithmic plots of I_s, the ion signal at m/e = 42, versus the flow of NH_3 for the following ions:

(a). CH_3CNH^+ formed by proton transfer from HCO^+ to CH_3CN.

(b). CH_3NCH^+ formed by proton transfer from CH_3^+ to CH_3NC.

(c). $C_2H_4N^+$ formed from the reaction of CH_3^+ with HCN.

10^{-9} cm^3 s^{-1} respectively, were identical within experimental error. A single proton transfer product channel was observed for the CH_3CNH^+ ion reaction, while a very small association peak (<2%) along with the dominant proton transfer product ion, NH_4^+, was also noted for both CH_3NCH^+ and $C_2H_4N^+$ with NH_3. Such an outcome is expected as proton transfer to NH_3 is exothermic for both isomers and would therefore be expected to be fast, as was observed for both CH_3CNH^+ and CH_3NCH^+.

In summary, the results of the isomer ratio determination for the ion $C_2H_4N^+$ discussed in this chapter show that the association reaction between CH_3^+ and HCN leads to a distribution of 85±8% CH_3CNH^+ and 15%±8 CH_3NCH^+ in the $C_2H_4N^+$ product.

This isomeric distribution shows that the substantial internal energy provided to the CH_3NCH^+ ion (-362 kJ mol^{-1}) initially formed[128,129] in the highly exothermic reaction of CH_3^+ with HCN is sufficient to overcome the barrier to structural inter-conversion between CH_3CNH^+ and CH_3NCH^+. Subsequent third body collisions with the helium bath gas yield the observed ratio for the two isomers.

DeFrees et al[129] have calculated the relative energies of the two structures CH_3NCH^+ and CH_3NCH^+ (~42 kJ mol^{-1}) and the barrier to isomerisation (~272 kJ mol^{-1} for conversion from CH_3NCH^+ to CH_3CNH^+ and 314 kJ mol^{-1} for the reverse) between these two isomers. They estimated that, upon formation from the reaction of CH_3^+ with HCN under laboratory conditions, the complex $(C_2H_4N^+)^*$ would rapidly interchange between the two isomeric structures as it lost energy through collisional relaxation. When the relaxing molecules possessed

insufficient energy to surmount the isomerisation barrier the resultant equilibrium between the two isomers CH_3CNH^+ and CH_3NCH^+ would then be frozen in proportion to their relative density of states. They obtained a value for the equilibrium between the two isomers of 1/6 (CH_3NCH^+/CH_3CNH^+) with the difference in zero point energies and the isomerisation barrier height as above.

This calculated equilibrium value of 0.167 agrees exactly with the experimental ratio of isomers obtained here for the reaction between CH_3^+ and HCN. The experimental zero point energy difference in this study between the two ions CH_3CNH^+ and CH_3NCH^+ is 43 kJ mol^{-1}, which is also in agreement with the value of 42 kJ mol^{-1} calculated by DeFrees et al[129]. It can therefore be expected that the calculated isomerisation barrier height of ~272 kJ mol^{-1} obtained by DeFrees et al should be similar to the actual barrier between the two isomers under SIFT laboratory conditions. However the barrier height calculation is also dependent on the assumed transition state structure of DeFrees et al shown in structure (7).

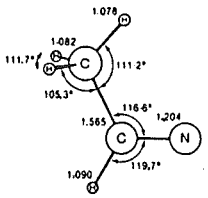

(3)

Experiments that were performed in this work to estimate the isomerisation barrier height between CH_3CNH^+ and CH_3NCH^+ are detailed in section 4.5.

A previous collision induced dissociation study (CID) by Illies et al[121] of the $C_2H_4N^+$ ion produced in reaction (4.12) reported only a single structure for the product ion; the lower energy CH_3CNH^+ isomer. In that study it was assumed

that when CH_3NC was added to protonated methanol, $CH_3OH_2^+$, only the isomer CH_3NCH^+ was formed. It is likely that the ion CH_3NCH^+, produced in this manner in a tandem mass spectrometer, may possibly have been contaminated with CH_3CNH^+. Consequently a CID study of any potential difference in the breakup patterns of the $C_2H_4N^+$ ion, generated by reaction between CH_3^+ and HCN, and those of the isomers CH_3NCH^+ and CH_3NCH^+ would be considerably complicated.

In the final part of this chapter results of measurements on the barrier to isomerisation between the CH_3CNH^+ and CH_3NCH^+ ions are presented.

4.5 THE ISOMERISATION BARRIER BETWEEN PROTONATED ACETONITRILE AND PROTONATED METHYL ISOCYANIDE IONS.

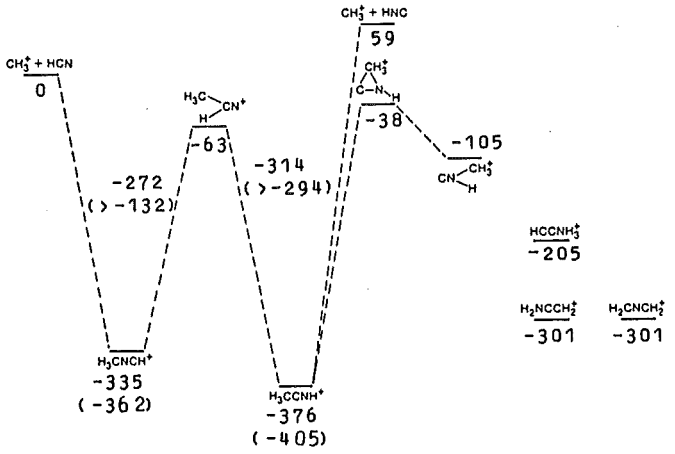

Fig. 4.3: Relative theoretical energies of the $C_2H_4N^+$ potential energy surface in kJ mol^{-1} (from DeFrees et al[129]. Relative experimentally determined values are shown in brackets).

A substantial barrier to interconversion between the two isomers CH_3CNH^+ and CH_3NCH^+ may be inferred from their separate identification in the flow tube. For example, the reaction of CH_3CNH^+ with added THP produced only the proton transfer product $THPH^+$, whereas CH_3NCH^+ associated with THP to give the adduct $CH_3NCH^+.THP$. Thus results were obtained by producing either CH_3CNH^+ and CH_3NCH^+ by proton transfer from HCO^+ (CH_3CN) or CH_3^+ (CH_3NC) to the respective neutral added at portal 1. Upon the addition of THP at portal 2, $THPH^+$ was the only product observed for added CH_3CN, while for added CH_3NC only $CH_3NCH^+.THP$ was observed. Therefore the two isomers were able to be formed separately in the flow tube and once formed did not isomerise.

If however the CH_3NCH^+ ion could be generated with sufficient internal energy from a reaction, such as the general proton transfer reaction (4.27), some isomerisation might occur to produce the CH_3CNH^+ isomer.

$$\begin{aligned} XH^+ + CH_3NC &\rightarrow CH_3NCH^+ + X \\ &\rightarrow CH_3CNH^+ + X \end{aligned} \qquad (4.27)$$

Any isomerisation that did occur could be easily detected by adding THP through portal 2. The evidence of isomerisation to CH_3CNH^+ would then be seen in the appearance of a protonated THP product ($THPH^+$). If however the association adduct $CH_3NCH^+.THP$ was the only product observed in reaction (4.27), it could be concluded that the internal energy of the reaction complex $(CH_3NCH^+.THP)^*$ was insufficient to overcome the barrier to isomerisation between CH_3CNH^+ and CH_3NCH^+.

By using a range of neutrals having different PA's, a

series of ions XH^+ were generated which, upon proton transfer to CH_3NC, provided different amounts of internal energy in the reaction complex formed in reaction (4.27). The difference in PA between the species X and CH_3NC that was required to broach the isomerisation barrier was thus able to be bracketed through either the observance, or non observance, of a $THPH^+$ product.

In a similar manner, the proton transfer reactions of the general species XH^+ with CH_3CN were investigated. The difference in PA's necessary before the barrier to isomerisation from CH_3CNH^+ to CH_3NCH^+ could be overcome was also bracketed for reaction (4.28).

$$\begin{array}{lcll} XH^+ + CH_3CN & \rightarrow & CH_3CNH^+ + X & (4.28) \\ & \rightarrow & CH_3NCH^+ + X & \end{array}$$

In this case the occurrence of interconversion from CH_3CNH^+ to CH_3NCH^+ was indicated by the observation of an association channel upon reaction of the CH_3NCH^+ ion with THP.

A direct comparison of the difference in proton affinities between XH^+ and CH_3NC (CH_3CN) required to overcome the barrier to isomerisation of the reactant complexes for reactions (4.27) and (4.28), and the height of the actual barrier to isomerisation (fig. 4.3) can not made. When a reactant complex fragments, the energy in excess of the thermodynamic heat of reaction may be distributed amongst the fragments as rotational, vibrational, translational, and electronic energy. Obviously, depending upon the size and structural makeup of the primary protonated ions XH^+ and the reaction products produced, the contributions to each particular mode will vary.

If the neutral X in the complex $(CH_3NC.XH^+)^*$ (or $(CH_3CN.XH^+)^*$) is a monatomic species then upon complex breakup the amount of energy tied up in translational energy of this atomic fragment compared to the total internal energy of the $(CH_3NCH^+)^*$ species will be small. In this case the actual internal energy remaining in the $(CH_3NCH^+)^*$ fragment after proton transfer will approach the total overall reaction exothermicity. However, for more complicated diatomic and polyatomic neutral products of the reaction a much larger proportion of the total internal energy of the proton transfer complex may be retained by the neutral species upon reaction completion. A possible reaction mechanism for the general proton transfer reaction (4.27) is therefore as follows,

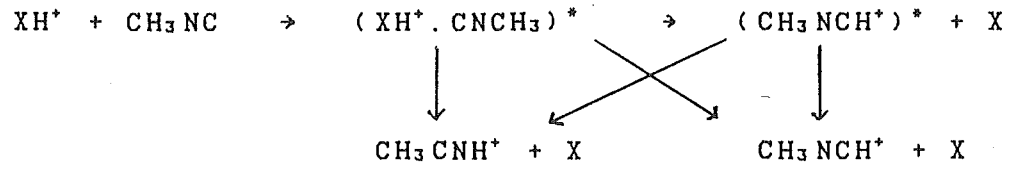

Prehaps the most important consideration is the perturbation that the presence of X in the complex has on the height of the isomerisation barrier. If isomerisation occurs within the proton transfer complex $(XH^+.CNCH_3)^*$ then the presence of X will almost certainly lower the barrier height from that between the two isomers. Under these circumstances the measurements described here can provide a lower limit only to the barrier height between CH_3NCH^+ and CH_3CNH^+. But if proton transfer occurs first with loss of X and the isomerisation process takes place after proton transfer as a

consequence of the internal energy remaining, these measurements should then provide some indication of the height of the barrier. As there is no simple way of determining in which step of the mechanism isomerism occurs, it is assumed that these measurements provide a lower limit only to the height of the barrier.

Both the reactions of CH_3NCH^+ and CH_3CNH^+ with the neutral THP occur at rates relatively close to their calculated collision limits and therefore the sensitivity of the technique enabled small concentrations of each isomer to be detected. However for the technique to be successful it was essential that swarms of the required primary ions were able to be created free from all impurities. For example, if small amounts of impurity ions such as H_3O^+ and N_2H^+ were present during the addition of THP to a swarm of CH_3NCH^+ ions, then the detection of the onset of isomerisation becomes very difficult as $THPH^+$ can be produced in two ways: by proton transfer from CH_3CNH^+ produced in the isomerisation reaction (4.27) and also by proton transfer from N_2H^+ and H_3O^+.

Further complications in reaction (4.28) concern the detection of isomerisation of CH_3CNH^+ to CH_3NCH^+, as the dimer ion of CH_3CNH^+, $(CH_3CN)_2H^+$, which was also present in the flow tube, reacted with THP to give $CH_3CNH^+.THP$ at m/e= 128. This peak obscured the association peak $CH_3NCH^+.THP$ which was used to identify the presence of CH_3NCH^+ and hence isomerisation of CH_3CNH^+ in reaction (4.28). The equivalent product at high flows of CH_3NC, viz., $(CH_3NC)_2H^+$ did not prove to be the same problem as the proton bound dimer only clustered with THP (section 4.3).

4.5.1 Limit of the CH_3NCH^+/ CH_3CNH^+ isomerisation barrier.

The $C_2H_4N^+$ ion was produced with various amounts of internal energy by proton transfer to CH_3NC at portal 1 from the ions, CH_3^+, $CH_3OH_2^+$, H_2CN^+, H_3S^+, H_3O^+, $C_2H_5^+$, COH^+, XeH^+, N_2H^+, OH^+ and ArH^+. These ions are listed in order of decreasing PA of the neutral and therefore increasing internal energy in the $(CH_3NC.HX^+)^*$ or $(CH_3NCH^+)^*$ complex.

The primary ions used in the generation of $C_2H_4N^+$, the difference in PA between the neutral species and CH_3NC, and the final derived isomer distributions after reaction with THP are all shown in table 4.8a.

A brief discussion follows on the individual reactions used to characterise the barrier to isomerisation. The neutral CH_3NC was added through portal 1 to a swarm of XH^+ ions to form an intermediate complex of the type $(XH^+.CH_3NC)^*$ (reaction (4.27)), from which X was subsequently eliminated to complete the proton transfer reaction.

Reaction (4.29) $CH_3^+ + CH_3NC \rightarrow C_2H_4N^+ + CH_2$

A swarm of CH_3^+ ions was produced in the flow tube, free of impurities, after electron impact on CH_3Br in the ion source. The addition of sufficient CH_3NC neutral at portal 1 to reduce the CH_3^+ concentration to zero resulted in the formation of a small percentage of the dimer ion $(CH_3NC)_2H^+$ as well as the principal ion CH_3NCH^+. The product distribution for the reaction of THP added at portal 2 with the product ion $C_2H_4N^+$ from reaction (4.29) placed an upper

Table 4.8a: Observed percentages of isomerisation for the product ion $C_2H_4N^+$ formed in the general reaction (4.27). The difference in proton affinity for the neutral species X and CH_3NC is also shown. Units of ΔPA are kJ mol^{-1}.

no.	X	ΔPA	%CH_3CNH^+
4.29	CH_2	8	<0.1
4.30	CH_3OH	83	<1.0
4.31	HCN	127	<0.1
4.32	H_2S	132	5.0
4.33	H_2O	147	5.0
	C_2H_4	164	2.0
	CO	250	3.0
	Xe	348	8.0
	N_2	349.5	2.5
	O	357	8.1
	Ar[a]	473	~8

(a) ArH^+ resulted in the breakup of the CH_3NC neutral (5% of the ion CH_3^+ was present).

Table 4.8b: Observed percentages of isomerisation for the product ion $C_2H_4N^+$ formed in the general reaction (4.28). The difference in proton affinity between the neutral species X and CH_3CN is also shown. Units of ΔPA are kJ mol^{-1}.

no.	X	ΔPA	%CH_3NCH^+
4.34	CO_2	240	<1
4.36	Xe	292	10-25
4.35	N_2	293.5	<1
4.37	Ar	417	10-25

limit on the formation of $THPH^+$ (and therefore CH_3CNH^+) of <0.1%.

Reaction (4.30) $CH_3OH_2^+ + CH_3NC \rightarrow C_2H_4N^+ + CH_3OH$

Protonated methanol was generated from a 5/1 mixture of H_2 and CH_3OH (saturated vapour pressure, 100 Torr at 21 °C). Unfortunately, even at low ion injection energies, a small amount of collisional breakup of $CH_3OH_2^+$ occurred to produce small amounts of the ions CH_3^+ and CH_2OH^+, at 8% and 1% of the primary ion concentration respectively. Furthermore, 1% of the adjacent mass CH_3OH^+ was also injected. After the addition of CH_3NC in sufficient quantities to reduce the initial peaks to zero, other peaks (m/e= 83 $(CH_3NC)_2H^+$ (30%)) and m/e= 70 ($H_3O^+.CH_3NC$) (3%)) apart from $C_2H_4N^+$ were also present. When THP was added at inlet portal 2 a small proton transfer channel was observed, probably from the impurity peaks present, along with the dominant association channel, the result being the observed product distribution of <1% $THPH^+$ and >99% $CH_3NCH^+.THP$.

Reaction (4.31) $H_2CN^+ + CH_3NC \rightarrow C_2H_4N^+ + HCN$

H_2CN^+ was generated by electron impact on a 20/1 mixture of H_2 and HCN and subsequently injected into the flow tube with the adjacent mass ion HCN^+ as the only impurity at 2% of H_2CN^+. After the addition of CH_3NC at inlet portal 1 and then THP at inlet portal 2, an upper limit of 0.1% of CH_3CNH^+ formation in reaction (4.31) was placed through the

nonobservance of a $THPH^+$ channel (<0.1%). Figure 4.4b shows a sample of data obtained for this reaction.

Reaction (4.32) $H_3S^+ + CH_3NC \rightarrow C_2H_4N^+ + H_2S$

H_3S^+ was generated from electron impact on H_2 and H_2S. The only impurity ion upon injection into the flow tube was the adjacent mass ion at m/e= 36 (probably the ions $H_3{}^{33}S^+$ and $H_2{}^{34}S^+$, at 3% of the primary ion concentration). After the addition of CH_3NC and then THP, the product analysis for the reaction between $C_2H_4N^+$ and THP confirmed a product distribution of 5% $THPH^+$ and 95% $CH_3CNH^+.THP$ (figure 4.4a). The 5% proton transfer channel indicates that some conversion from CH_3NCH^+ to CH_3CNH^+ has occurred during the formation of $C_2H_4N^+$ in reaction (4.32).

Reaction (4.33) $H_3O^+ + CH_3NC \rightarrow C_2H_4N^+ + H_2O$

H_3O^+ was formed by electron impact on a mixture of H_2 and H_2O. The only impurity ion observed was H_2O^+ which was present at <1% of the primary ion concentration. $C_2H_4N^+$ was then formed by by proton transfer from H_3O^+ to CH_3NC at portal 1 (reaction (4.33)). Upon reaction of the $C_2H_4N^+$ product with THP at portal 2, a 5% proton transfer channel was noted as well as the dominant association adduct $CH_3NCH^+.THP$ (95%). The observation of a proton transfer product indicated that, as for reaction (4.32), some isomerisation to form CH_3CNH^+ had occurred during the proton transfer reaction of H_3O^+ and CH_3NC.

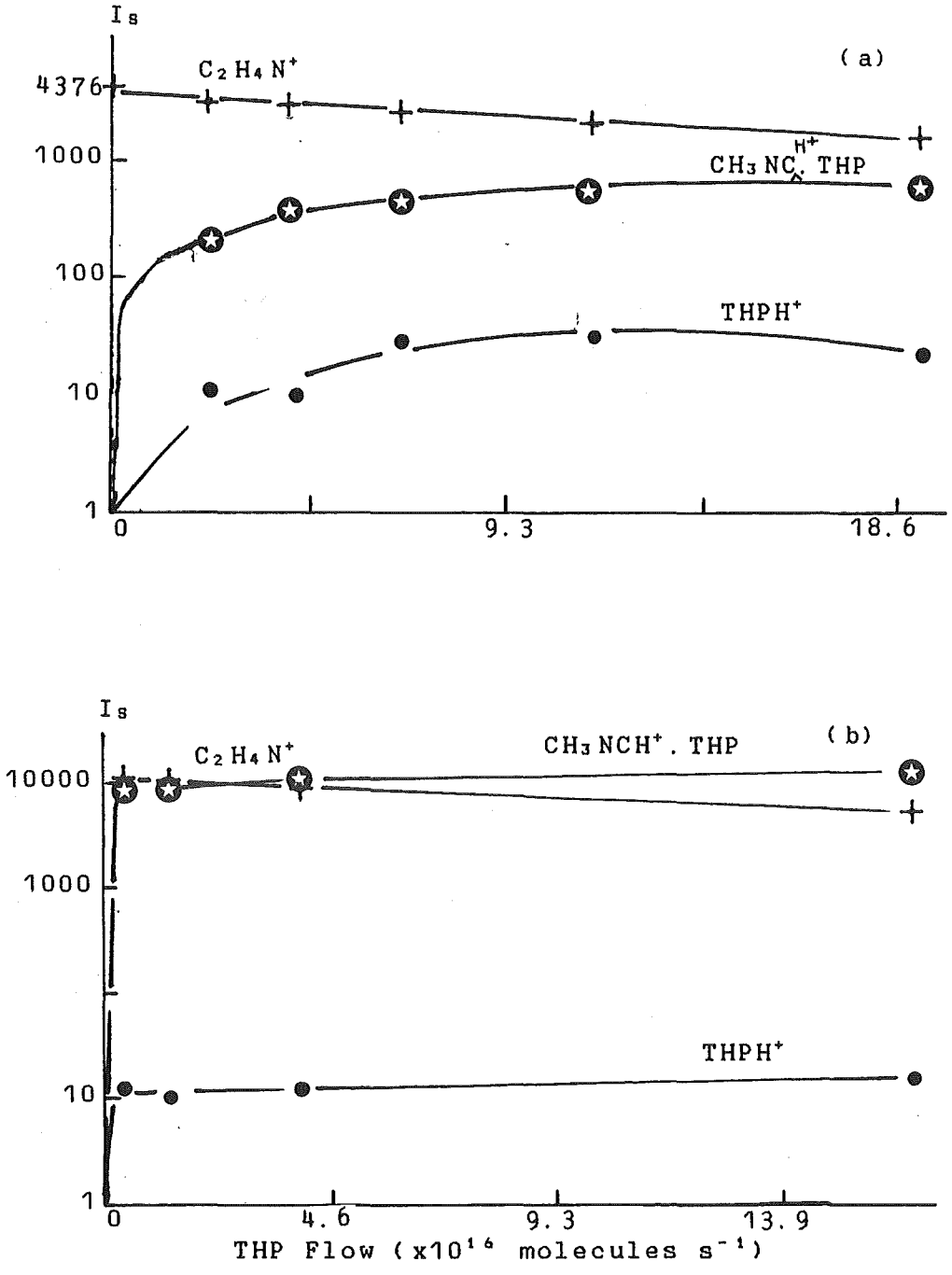

Fig 4.4: Semilogarithmic plots of I_s, the ion signal at m/e = 42, versus the flow of THP where the 42 amu ion is formed through (a). proton transfer from H_3S^+ to CH_3NC.
(b). proton transfer from H_2CN^+ to CH_3NC.

In common with reactions (4.32) and (4.33), proton transfer channels were also noted upon the reaction of THP with $C_2H_4N^+$ generated by proton transfer from the ions $C_2H_5^+$, XeH^+, N_2H^+, OH^+, and ArH^+ (the neutral species derived from these ions all have lower PA's than H_2O). Table 4.8a details the derived percentage of the isomer CH_3CNH^+ as found from the magnitude of $THPH^+$ for these reactions.

In summary, for the general reaction (4.27) involving proton transfer from the species XH^+ to neutral CH_3NC, when the general species X corresponds to HCN (or species of higher PA than HCN), the intermediate complex $(CH_3NC.HX^+)^*$ or $(CH_3NCH^+)^*$ has insufficient internal energy available to surmount the activation energy barrier between the two structural isomers. However, when H_2S is substituted for HCN in reaction (4.27), isomerisation from CH_3NCH^+ to CH_3CNH^+ is observed to occur.

A lower limit to the barrier between interconversion from the CH_3NCH^+ structure to the CH_3CNH^+ isomer can therefore be placed. As the overall reaction exothermicity for reaction (4.31) (A= HCN) is 127 kJ mol^{-1} whilst that for reaction (4.32) (A= H_2S) is 132 kJ mol^{-1}, at least 132 kJ mol^{-1} is needed before the complex skeletal structure, $(CH_3NCH^+)^*$ (or $(CH_3NC.XH^+)^*$), can change to $(CH_3CN.H^+)^*$ (or $(CH_3CN.XH^+)^*$).

4.5.2 Limit of the CH_3CNH^+/ CH_3NCH^+ isomerisation barrier.

As indicated in the introduction to this section, the observation of CH_3NCH^+ ions produced through rearrangement of the reaction complex fragment $(CH_3CN.HX^+)^*$ (or $(CH_3CNH^+)^*$),

formed after the general reaction (4.28), was complicated by the simultaneous presence of the proton bond dimer $(CH_3CN)_2H^+$.

$$XH^+ + CH_3CN \rightarrow C_2H_4N^+ + X \qquad (4.28)$$

When $C_2H_4N^+$ was produced at portal 1 in reaction (4.28), only a low flow ($\sim 10^{16}$ molecules s^{-1}) of CH_3CN could be added to ensure that that the dimer ion $(CH_3CN)_2H^+$ (which reacts with THP to give $CH_3CNH^+.THP$) was not produced. Unfortunately this requirement meant that the $C_2H_4N^+$ ion signal in the flow tube was also small. A consequence of a small $C_2H_4N^+$ signal is that any isomerisation that did occur in reaction (4.28) resulted in a very small signal of the adduct $CH_3NCH^+.THP$ (m/e= 128) which was used to detect isomerisation (section 4.3). If the largest $C_2H_4N^+$ peak magnitude able to be achieved was 100 cs^{-1} then, upon the addition of THP, even a 5% adduct peak would result in only 3-4 cs^{-1} (after allowing for mass discrimination). In practice a larger flow of CH_3CN was added in reaction (4.28) to produce a sizable $C_2H_4N^+$ peak as well as a small dimer product at m/e= 128. Upon the addition of THP, the change in magnitude of the m/e= 128 peak was then monitored.

The $C_2H_4N^+$ ion to be analysed was formed by proton transfer from the ions CO_2H^+, XeH^+, N_2H^+, ArH^+ and HeH^+ to CH_3CN. The resulting isomer ratios derived from the reactions of this $C_2H_4N^+$ ion with THP are outlined in table 4.8b. The difference in PAs of the participating species (the overall reaction enthalpy) for each reaction is also shown and a brief discussion of individual reactions follows.

Reactions (4.34, 4.35)

CO_2H^+, N_2H^+ + CH_3CN → $C_2H_4N^+$ + CO_2, N_2

The ion $C_2H_4N^+$ was unable to be generated in sufficient quantities for accurate analysis (as outlined in the introduction to this section) when formed through the reactions of the ions N_2H^+ and CO_2H^+ with CH_3CN. However the product distributions that were observed for both ions upon the addition of THP indicated that less than 1% of the isomer CH_3NCH^+ was formed.

Reaction (4.36) $XeH^+ + CH_3CN \rightarrow C_2H_4N^+ + Xe$

XeH^+ was formed in the ion source from electron impact on a 20/1 mixture of H_2 and Xe. The higher protonated xenon isotopes ($^{132}XeH^+$ (14%), $^{134}XeH^+$ (38%), $^{136}XeH^+$ (48%)) only were injected into the flow tube to ensure that no $^{128}Xe^+$ was present during the reaction (as the natural abundance of $^{128}Xe^+$ is 1.9%, this isotope if present could obscure a possible association peak $CH_3NCH^+.THP$ (m/e= 128)).

After $C_2H_4N^+$ was generated at portal 1, with low flows of CH_3CN added to XeH^+ to minimise formation of the dimer ion $(CH_3CN)_2.H^+$, an association adduct (10-25%) was observed for the reaction of $C_2H_4N^+$ with THP, as well as the major proton transfer product, the ion $THPH^+$. The presence of the association peak $CH_3NCH^+.THP$ indicates that some interconversion of the reaction complex configuration occurred during the course of reaction (4.36).

Reaction (4.37) $ArH^+ + CH_3CN \rightarrow C_2H_4N^+ + Ar$

A swarm of ArH^+ ions was formed in the flow tube free of impurity ions after electron impact on a 20/1 mixture of H_2 and Ar. After addition of a low flow of CH_3CN at portal 1, proton transfer took place and the $C_2H_4N^+$ species was formed. THP was then added through portal 2 to the $C_2H_4N^+$ ion swarm and 10-25% of the adduct $CH_3NCH^+.THP$ was produced from the reaction of THP with $C_2H_4N^+$. Therefore the internal energy of the complex formed in reaction (4.37) was again sufficient to result in some isomerisation of the CH_3CNH^+ ion.

In summary, an indication of the magnitude of the internal energy in the complex required to promote isomerisation could be found. For the general reaction of proton transfer from XH^+ to CH_3CN (reaction (4.28)), when the general species X corresponded to Xe, isomerisation from CH_3CNH^+ to CH_3NCH^+ was observed to occur. As the overall reaction exothermicity for reaction (4.37) (X= Xe) is 294 kJ mol^{-1}, at least 294 kJ mol^{-1} of internal energy is needed for structural interconversion of CH_3CNH^+ to CH_3NCH^+.

From figure 4.3 it can be seen that the difference in the heats of formation of CH_3CNH^+ and CH_3NCH^+ (ΔZPE) should equal the difference in internal energy required for each ion to surmount the activation energy barrier to isomerisation. From this study, at least 132 kJ mol^{-1} of internal energy must be provided to the intermediate complex formed in reaction (4.27) for isomerisation to occur. For the equivalent complex formed in reaction (4.28) at least 294 kJ mol^{-1} is needed.

The experimental difference in the heats of formation for the two ions (determined in section 4.3) is 43 kJ mol^{-1}. However the observed difference in internal energy required to promote isomerisation in reactions (4.27) and (4.28) is 162 kJ mol^{-1}. The marked difference in the above relative ΔZPE energy values suggests that, in some reactions at least, the isomerisation takes place within the $(CH_3NC.HX^+)^*$ complex.

As mentioned previously, DeFrees et al[129] obtained a value of 272 kJ mol^{-1} for the barrier to structural interconversion from CH_3NCH^+ to CH_3CNH^+ (and a value of 314 kJ mol^{-1} for the reverse). The measurements of this value indicate that the barrier height should be at least 132 kJ mol^{-1}, but as it was not possible to ascertain at what stage in the reaction mechanism isomerisation occurred the conclusions drawn can not be more specific.

It is interesting to note that a small percentage only of structural interconversion has been observed in this study (typically 5-20%, column 4, table 4.8), even when a large excess of internal energy is available to the intermediate complex concerned. DeFrees et al[129] have shown that the complex $(C_2H_4N^+)^*$ formed in the reaction of CH_3^+ with HCN will rapidly isomerise as it relaxes through third body collisions. The ultimate distribution of isomers formed was shown to equal the distribution of the isomers present after the internal energy of the relaxing molecules was insufficient to surmount the isomerisation barrier. Figure 4.5 shows a graph of the calculated equilbrium constant between CH_3NCH^+ and CH_3CNH^+ as a function of complex energy. A theoretical ZPE difference of 42 kJ mol^{-1} was used by DeFrees et al[129] for the calculations

required.

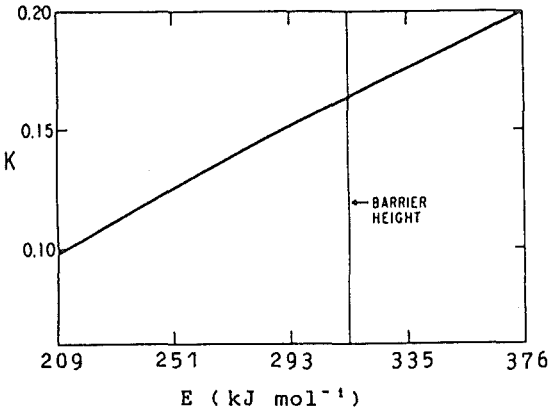

Fig. 4.5: Calculated equilibrium coefficient (K) between CH_3NCH^+ and CH_3CNH^+ as a function of energy above the zero-point level at the bottom of the CH_3CNH^+ potential energy well (figure reproduced from DeFrees et al[129]).

When isomerisation has been observed for the general proton transfer reaction (4.27) the observed equilibrium proportion of isomers has in each case been in the range of 2-8% CH_3CNH^+ versus 92-98% CH_3NCH^+. The variation in the equilibrium proportion for each individual reaction is almost certainly due to the varying effect of the neutral (X) on the amount of internal energy remaining in the ($CH_3NC.H^+$) complex after proton transfer.

For the general reaction (4.28) when isomerisation has occurred, the observation of 10-25% only of the CH_3NCH^+ isomer suggests that the reaction complex formed after proton transfer was in each case collisionally stabilised before an equilibrium proportion of isomers could be attained. ie. if the complex had possessed sufficient internal energy allowing rapid structural interchange to occur, the observed isomer proportion would have been in favour of the CH_3NCH^+ structure.

An alternative possibility for the observation of the

curved decay of the $C_2H_4N^+$ species (fig. 4.1c) with HCO_2CH_3 and other reactants is that the faster of the two exponential decays results from the presence in the flow tube of an internally excited $(CH_3CNH^+)^*$ species. Such a possibility is most unlikely and can be refuted on four counts.

(1). After formation of the $(CH_3^+.HCN)^*$ complex at portal 1 in the flow tube, and before the addition of a suitable neutral at portal 2 (40cm in distance from portal 1), this complex will undergo an average of ~4 x 10^4 collisions at 0.30 Torr of He. Assuming that each collision removes ~8 kJ mol^{-1} of energy[128] and that the total initial internal energy available to each complex is 405 kJ mol^{-1} (if CH_3CNH^+ is eventually formed) or 362 kJ mol^{-1} (if CH_3NCH^+ is formed) then, after only ~45 collisions for the CH_3NCH^+ complex and ~51 for the CH_3CNH^+ complex, both will be thermally stabilised.

(2). The reaction of the ion $C_2H_4N^+$, formed from CH_3^+ and HCN, with HCO_2CH_3 was studied over the pressure range 0.295 to 0.34 Torr. No difference in the ratio of the isomer ions was noted in this pressure range. A difference would be expected however if the faster decay observed was due to internally excited $(CH_3CNH^+)^*$, as the greater the pressure the higher the rate of relaxation of the internally excited CH_3CNH^+ ion.

(3). The rate coefficients for the proton transfer and association reactions of separately formed swarms of the CH_3CNH^+ and CH_3NCH^+ isomers with the neutrals THF, THP and HCO_2CH_3 agreed within experimental error to the two rate coefficients obtained from fitting the curved decay of $C_2H_4N^+$ with each reactant.

(4). The thermal distribution of the $C_2H_4N^+$ isomers

produced in the reaction of CH_3^+ with HCN, established experimentally in this study to be approximately 1/6 in favour of the CH_3CNH^+ isomer, is supported by the theoretical equilibrium distribution for the two isomers calculated by DeFrees et al[129].

4.6 CONCLUSION.

The protonated ions CH_3CNH^+ and CH_3NCH^+ have been shown to have different structures in the gas phase and to maintain their integrity through a substantial barrier to isomerisation. The relative proton affinities of CH_3NC and CH_3CN have been measured to be 844±2 kJ mol^{-1} and 788±2 kJ mol^{-1} respectively. The equilibrium concentration of the two isomers, CH_3CNH^+ and CH_3NCH^+, formed from the reaction of CH_3^+ with HCN has been estimated to be 85±8% in favour of the CH_3CNH^+ ion. Finally a lower limit (132 kJ mol^{-1}) has been placed upon the difference in proton affinity between a neutral species X and CH_3NC required to promote isomerisation of the complex formed in the general reaction (4.27). Therefore, a lower limit to the internal energy required for interconversion from the isomeric structure CH_3NCH^+ to CH_3CNH^+ can be set at 132 kJ mol^{-1}.

CHAPTER FIVE

REACTIONS OF THE IONS C_2N^+ AND HC_2N^+

5.1 INTRODUCTION.

Various reaction schemes[130,127,131] have attempted to model the abundances observed in interstellar clouds of the unsaturated carbon chain cyanopoly-yne series $HC_{2n+1}N$(n= 1, 2, 3, 4) and other nitrogen containing neutral species. Harquist and Dalgarno[130] have estimated that C_2N^+ is the most abundant interstellar ion other than HCO^+. Experimental evidence for this assumption was provided by Schiff and Bohme[127] who found the rate of formation of the C_2N^+ ion by reaction of C^+ with HCN to be fast, while the reaction of C_2N^+ with H_2, the most abundant interstellar neutral, was very slow. Recent theoretical studies[132,133] have indicated that two stable isomers may exist in the gas phase for the ion C_2N^+, viz., CNC^+ (1) and CCN^+ (2).

$:C{=}N^+{=}C:$ (1) $:C{=}C{=}N^+:$ (2)

Haese and Woods[132], using double zeta self consistent field (SCF) calculations, have estimated that the activation energy barrier to isomerisation is approximately 272 kJ mol^{-1} above the energy of the metastable CCN^+ ion. Harland and McIntosh[94], in a recent electron impact study on the isomers of C_2N^+, measured heats of formation of 1620 and 1726 kJ mol^{-1} for CNC^+ and CCN^+ respectively, in good agreement with

the theoretical values of Yoshimine and Kraemer[133] and Haese and Woods[132]. These experimental heats of formation, along with the calculated barrier to isomerisation between the two isomers, suggest that once formed the two isomers will retain separate chemical identities in the interstellar environment and in the flow tube. Haese and Woods suggested that the ions CCN^+ and CNC^+ could be formed separately through reactions (5.00) and (5.01) in dense interstellar clouds.

$$C^+ + HCN \rightarrow CNC^+ + H \qquad (5.00)$$

$$C^+ + HNC \rightarrow CCN^+ + H \qquad (5.01)$$

The structural isomers hydrogen cyanide, HCN, and hydrogen isocyanide, HNC, have both been detected in interstellar clouds[134].

Schiff and Bohme[127] have used the SIFT technique to study some reactions of the C_2N^+ ion. For this study reaction (5.00) was used to generate the C_2N^+ ion. McEwan et al[135] generated the ions CCN^+ and CNC^+ by electron impact on C_2N_2 and investigated a number of reactions of these ions in an ICR cell. Differences in the observed products of the reaction of C_2N^+ with NH_3 were tentatively attributed, in the later ICR study, to the presence of two isomers. However the overall conclusion drawn from the general agreement in rate coefficients between the two studies was that both isomers were of similar reactivity with the neutrals chosen.

In this chapter evidence is presented to confirm the predictions of Haese and Woods[132] that the reactivities of the two isomers of C_2N^+ may differ in some reactions.

$$C^+ + C_2N_2 \rightarrow C_2N^+ + CN \qquad (5.02)$$

Reaction (5.02) and reaction (5.00) as well as electron impact on the molecules CH_3CN, HC_3N, and C_2N_2 were used to generate CNC^+ and CCN^+ in this study. Reactions of a number of small neutrals with the CNC^+ and CCN^+ ions, formed from these sources, were then studied in an effort to distinguish between the two isomers.

Harland and McIntosh[94], using electron impact on CH_3CN and CH_3NC, also concluded that the two isomers $HCCN^+$ and $HCNC^+$ differed in their respective heats of formation by 68 kJ mol^{-1}. Some reactions of the ion HC_2N^+ were therefore also investigated in an attempt to observe evidence for the independent existence of the isomers $HCNC^+$ and $HCCN^+$ under typical flow tube conditions.

5.2 GENERATION OF CNC^+ AND CCN^+.

Unless otherwise indicated the term C_2N^+ refers to an unspecified mixture of both of the isomers CNC^+ and CCN^+. For the reactions detailed in this chapter C_2N^+ was variously formed through the addition of C^+ to HCN and C_2N_2 (reactions (5.00) and (5.02)) and by electron impact on CH_3CN, HC_3N, and C_2N_2 (reactions (5.03), (5.04), and (5.05)).

$$\begin{aligned} CH_3CN + e &\rightarrow CNC^+ + H_2 + H + 2e \\ &\rightarrow CCN^+ + H_2 + H + 2e \end{aligned} \qquad (5.03)$$

$$\begin{aligned} HC_3N + e &\rightarrow CNC^+ + CH + 2e \\ &\rightarrow CCN^+ + CH + 2e \end{aligned} \qquad (5.04)$$

$$C_2N_2 + e \rightarrow CNC^+ + CN + 2e \qquad (5.05)$$
$$\rightarrow CCN^+ + CN + 2e$$

The rate coefficients, product distributions and overall reaction enthalpies for reactions (5.00) and (5.02) are shown in Table 5.0. Although not studied, the enthalpies of reaction for the production of the isomers CNC^+ and CCN^+ from the addition of HNC to C^+ (reaction (5.01)) are also shown for comparison.

Table 5.0: Reactions of the C^+ ion with HCN, HNC and C_2N_2. The rate coefficients, k, shown have units of 10^{-9} cm^3 s^{-1}, whilst reaction enthalpies, $\Delta H°$, are in units of kJ mol^{-1}. The abbreviations "no." and "B.R." represent the reaction number and product distribution respectively.

no.	neutral	products	B.R.	k	k(lit.)	k_{ADO} or k_L	$-\Delta H°$ [a]
5.00	HCN	$CCN^+ + H$ } 1.0 $CNC^+ + H$ }		3.2	2.5[85], 3.5[127] 2.8[136], 3.2[137] 3.1[68]	3.8	-11 95
5.01	HNC	$CCN^+ + CN$ } - $CNC^+ + CN$ }		-		3.8	-169 -63
5.02	C_2N_2	$CCN^+ + CN$ } 1.0 $CNC^+ + CN$ }		1.8		1.6	-54 52

(a) A positive reaction enthalpy indicates an exothermic channel.

The measured rate coefficient for the generation of C_2N^+ from C^+ and HCN (reaction (5.00)) in this study was 3.2 x 10^{-9} cm^3 s^{-1}. The dominant isomer produced in this reaction should be the ion CNC^+, production of which is exothermic by 95 kJ mol^{-1}, as formation of the metastable CCN^+ is endothermic by 11 kJ mol^{-1}. However if C^+ ions are formed in an excited electronic state during electron impact in the ion source and retain their excitation until after injection into the flow tube, CCN^+ ions may also be produced in the

subsequent reaction with HCN.

These metastable $(C^+)^*$ ions, which have an electronic state designation of ^4P, are some 511 kJ mol^{-1} in energy above the ground state C^+ ions. In this study the C^+ ions were formed by electron impact on several different source gases including CO, CH_4, CO_2, and CCl_4. With the last two molecules significant amounts of electronically excited C^+ ions were in fact observed to be formed (the experimental evidence for this will be presented in section 5.3). Therefore when attempting to generate swarms of C_2N^+ ions containing only the CNC^+ isomer through reaction (5.00), the neutrals CO and CH_4 were used as only with these gases could CNC^+ be produced in the absence of CCN^+ from reaction (5.00). Unfortunately with these neutrals, upon injection of C^+ into the flow tube, impurity ion peaks were also present. These impurity peaks were present at m/e values of 16 amu (5% of the signal at 12 amu) for CO, and at 13 amu (8%) and 14 amu (5%) for CH_4.

The CNC^+ ion was also the dominant isomer formed from reaction (5.02), the reaction of C^+ with C_2N_2. Here the overall rate coefficient for production of C_2N^+ was measured to be 1.8×10^{-9} cm^3 s^{-1}. A small peak at m/e= 52 ($C_2N_2^+$ at ~3%) was also observed as a primary product in this reaction indicating that charge transfer is exothermic as a reaction channel for $(C^+)^*$ with C_2N_2 (the corresponding channel with ground state C^+ is endothermic by 207 kJ mol^{-1}).

Harland and McIntosh, in their investigation of the C_2N^+ ion through electron impact[94], observed a single threshold only for the appearance of C_2N^+ from CH_3CN which they attributed to the ion CCN^+. In this study, electron impact

on CH_3CN (reaction (5.03)) appeared to produce a mixture of both C_2N^+ isomers, as detailed in the discussion of the reaction of C_2N^+ with CH_4 (reaction (5.06), section 5.3). After electron impact on CH_3CN and the formation of a swarm of C_2N^+ ions (38 amu) in the flow tube, mass peaks at m/e values of 38/39/40/41 were present in a ratio of 1/2.8/1.1/0.4. This ratio represents the best possible compromise that could be achieved through tuning the upstream quadrupole below m/e= 38 to minimise the signal at m/e values of greater than 38 amu, while still retaining a usable signal at m/e= 38.

Similarly, electron impact on HC_3N (reaction (5.04)) in the ion source could not produce the C_2N^+ ion in the flow tube free of adjacent impurity ions, and ion peaks at m/e values of 36/37/38/39 were present in a ratio of 0.1/0.6/1/0.1. For electron impact on HC_3N, Harland[95] observed two appearance potentials corresponding to the isomers CNC^+ and CCN^+.

When dicyanogen, C_2N_2, was used as the source gas (reaction (5.05)) ions of m/e= 38 only were able to be injected, and as a consequence C_2N_2 was used as a "clean" source of C_2N^+ ions when measuring product distributions for the reactions of C_2N^+ detailed in this chapter. Earlier electron impact studies on C_2N_2[105,138] reported only a single appearance potential for the C_2N^+ ion fragment, however Harland and MacIntosh[94] were able to characterise the appearance potentials of both isomers of C_2N^+.

5.3 REACTIONS OF THE C_2N^+ ION.

Table 5.1 lists the rate coefficients and product distributions for each of the reactions involving the ion C_2N^+ detailed below. Previous measurements from the literature[127,135,139] are shown for comparison and, where known, reaction channel enthalpies are also included.

Reaction (5.06) $C_2N^+ + CH_4$

When C_2N^+ was generated through electron impact on each of CH_3CN, HC_3N, and C_2N_2, the decay curve of $\log(I(C_2N^+))$ versus CH_4 showed two distinct linear regions (as illustrated, for example, in figure 5.0c for the decay of C_2N^+ when generated by electron impact on C_2N_2). Analysis of the two exponential decays (using the "Expon" programme as detailed in section 4.4) yielded averaged rate coefficients for reaction (5.06) of 4.1×10^{-10} and 5×10^{-12} $cm^3\ s^{-1}$. The measured product distribution for the reaction, with C_2N_2 as a source of C_2N^+ ions, was 60% of $C_2H_3^+$ (production of the other possible ion product at 27 amu, HCN^+, is endothermic by 76 and 182 kJ mol^{-1} for CCN^+ and CNC^+ respectively), 30% for $H_2C_3N^+$ and 10% of an ion at m/e= 28. The reaction channels leading to the two possible ion structures for the 28 amu peak, H_2CN^+ and $C_2H_4^+$, are exothermic for both the CNC^+ and CCN^+ isomers.

For reaction (5.06), when C_2N^+ was generated from reactions (5.00) ($C^+ + HCN$) and (5.02) ($C^+ + C_2N_2$) and where the C^+ ion swarm formed for these reactions resulted from electron impact on CH_4, decays similar to that shown in figure

Table 5.1: Reactions of the C_2N^+ ion. Rate coefficients, k, have units of 10^{-9} cm^3 s^{-1}. The overall enthalpies of reactions involving the CNC^+ and CCN^+ ions are in units of kJ mol^{-1}.

no.	neutral	products	B.R.	k	k(lit.)	k_{ADO} or k_L	$-\Delta H°$ CCN^+	$-\Delta H°$ CNC^+
5.06	CH_4	$C_2H_3^+ + HCN$	0.60	~0.37[a]	<0.01[d],	1.1	399	293
		$H_2CN^+ + C_2H_2$	0.10	~0.005[b]	0.0044[e]		484	378
	or	$C_2H_4^+ + CN$	0.30				141	35
		$H_2C_3N^+ + H_2$					512	406
5.07	C_2H_2	$H_2CN^+ + C_3$	0.06	~1.6[a]	1.0[d],	1.1	176	70
		$C_3H^+ + HCN$	0.85	~0.88[b]	0.89[e]		198	92
		$HC_4N^+ + H$	0.09				?	?
5.08	N_2O	$NO^+ + C_2N_2$	0.22	~1.2[a]		0.96	516	410
		$N_2O^+ + C_2N$	0.05	~0.4[b]			?	?
		$CN_3^+ + CO$	0.73				84	-22
	or	$C_2NO^+ + N_2$					?	?
5.09	H_2O	$H_2CN^+ + CO$	0.08	0.17	0.34[d]	2.1	655	549
		$HCO^+ + HCN$	0.92				767	661
5.10	HCN	$C_2N^+.HCN$	1.0	0.42[c]	<0.03[d] 0.311[f]	2.8	?	?
5.11	NH_3	$N_2H^+ + C_2N$	<0.01	1.9	1.9[d]	2.0	?	?
		$H_2CN^+ + HCN$	>0.99		1.8[e]		651	545
	H_2	-	-	<0.0001		1.5		
	O_2	-	-	<0.00001		0.70		
	N_2	-	-	<0.00001		0.77		

(a) Represents the rate of decay of CNC^+. Fitted using the "Expon" program detailed in Appendix 1.
(b) Represents the rate of decay of CCN^+. Fitted using "Expon".
(c) Pseudo second order rate coefficient at 0.30 Torr.
(d) Reference 135.
(e) Reference 127
(f) Reference 139.

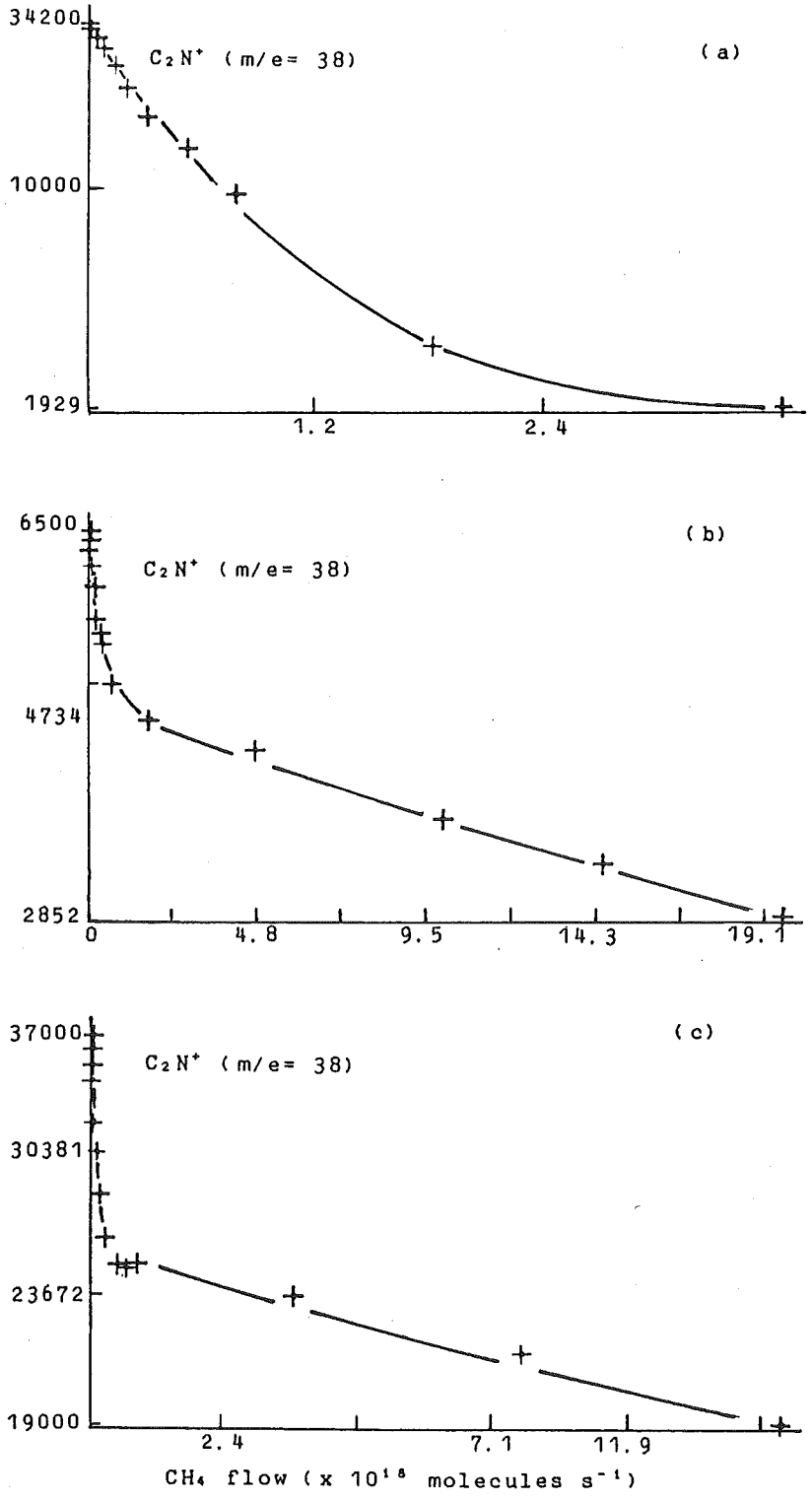

Fig. 5.0: Semilogarithmic plots of I_s, the ion signal at m/e= 38 against the flow of CH_4, where the mass peak at 38 amu is formed through the reaction of C^+ with C_2N^+ and where C^+ is generated from

(a) $CH_4 + e \rightarrow C^+ + 2H_2 + 2e$

(b) $CCl_4 + e \rightarrow C^+ + 2Cl_2 + 2e$

(c) $C_2N_2 + e \rightarrow C^+ + CN_2 + 2e$

5.0a were observed. The decay of the C_2N^+ ion shown in figure 5.0a includes two distinct exponential components, resulting from the different rates of reaction of the two isomers CNC^+ and CCN^+ with CH_4.

Analysis of the C_2N^+ decay curve with the "Expon" programme allowed evaluation of the pre-exponential constants (C1 and C2, section 4.4). A limit of 90±5% was indicated for the fraction of the species responsible for the rapid decay and 10±5% for that giving the slower decay. The rate coefficient for the rapid decay was 3.3×10^{-10} cm^3 s^{-1} (the value of 3.7×10^{-10} cm^3 s^{-1} shown in table 5.1 for the faster decay measured in reaction (5.06) represents an average of the rate coefficients obtained for the five separate methods of C_2N^+ formation shown in table 5.2). The observed products for the reaction of C_2N^+, when formed through reactions (5.00) and (5.02), with CH_4 were the same as for C_2N^+ formed from electron impact on C_2N_2, CH_3CN and HC_3N.

When the neutrals CO_2 and CCl_4 were used as the source for C^+ ions in reactions (5.00) and (5.02), once again two definite linear regimes were noted in the decay of the product ion C_2N^+ upon the addition of CH_4 (figure 5.0b). In this case the percentage of ions contributing to the slower portion of the C_2N^+ decay was determined to be 70±5% (table 5.2).

Theoretical studies[132,133] on reaction (5.00) (ground state $C^+(^2P)$ and HCN) have indicated that only the production of the lower energy isomer CNC^+ is energetically possible. From available thermodynamic data[93,94], reaction (5.02) ($C^+(^2P)$ and C_2N_2) will also produce only CNC^+. Therefore the

Table 5.2: Observed percentages of isomers and impurity ions for C_2N^+ and HC_2N^+.

ion	reaction		%CNC^+	%CCN^+	%impurities[a,b]
C_2N^+	5.00	$C^+ + HCN$			-
	where	$CH_4 + e \rightarrow C^+ + 2H_2 + 2e$	>90	<10	
	"	$CO + e \rightarrow C^+ + O + 2e$	>90	<10	
	"	$CO_2 + e \rightarrow C^+ + O_2 + 2e$	30	70	
	"	$CCl_4 + e \rightarrow C^+ + 2Cl_2 + 2e$	30	70	
	5.02	$C^+ + C_2N_2$			-
	where	$CO + e \rightarrow C^+ + O + 2e$	>90	<10	
	"	$CO_2 + e \rightarrow C^+ + O_2 + 2e$	30	70	
	"	$CCl_4 + e \rightarrow C^+ + 2Cl_2 + 2e$	45	65	52(3%)
	5.03	$CH_3CN + e \rightarrow C_2N^+ + H_2 + H + 2e$	20	80	39(280%) 40(110%) 41(40%)
	5.04	$HC_3N + e \rightarrow C_2N^+ + CH + 2e$	30	70	36(10%) 37(60%) 39(10%)
	5.05	$C_2N_2 + e \rightarrow C_2N^+ + N + 2e$	30	70	-
			%$HCCN^+$	%$HCNC^+$	
HC_2N^+		$CH_3CN + e \rightarrow HC_2N^+ + H_2 + 2e$	-	-	38(66%) 40(160%) 41(37%)
		$CH_3NC + e \rightarrow HC_2N^+ + H_2 + 2e$	-	-	"
		$HC_3N + e \rightarrow HC_2N^+ + C + 2e$	-	-	38(40%)
		$CH^+ + HCN$			c
		where $CH_4 + e \rightarrow CH^+ + H_2 + H + 2e$			12(10%) 14(10%) 15(3%)

(a) Represents the optimum percentage attained of the primary ion concerned.
(b) The m/e values shown represent the impurity ions present in the relevant primary ion swarm, while the numbers in parenthesis are the magnitude of these impurity ions with respect to that of the primary ion. eg. 52(3%) indicates that the peak at 52 amu is 0.03 times the C_2N^+ ion peak magnitude.
(c) The percentage of HC_2N^+ formation in this reaction is 10%[85].

initial rapid decay observed for the reaction of C_2N^+ with CH_4 (reaction (5.06)) must result from the CNC^+ isomer reacting with CH_4, while the isomer CCN^+ will result in the second slower decay. The endothermicity of the CCN^+ product ion channel for both reactions (5.00) and (5.02) also suggests that, when these reactions are used as the C_2N^+ source in reaction (5.06), the CCN^+ ions contributing to the second decay must result from metastable $C^+(^4P)$ ions. Table 5.2 summarizes the percentages observed of the two isomeric forms of C_2N^+ for each method of C_2N^+ formation as diagnosed using reaction (5.06).

Note that an upper limit to the proportion of metastable $(C^+)^*$ ions present in a C^+ ion swarm created from electron impact on either of CH_4 or CO can be set at 10±5%. Correspondingly, electron impact on CCl_4 or CO_2 results in the formation of an ion swarm at 12 amu consisting of 70±5% of $(C^+)^*$ ions.

The observation that CNC^+ appears to react significantly faster than the CCN^+ isomer in reaction (5.06) is in contradiction to the predictions of Haese and Woods[132]. They suggested that the more energetic CCN^+ isomer would show a greater reactivity than its counterpart CNC^+. However the most likely structural configuration of the CNC^+ ion (structure (1), p.155) has a higher degree of carbene character than the equivalent CCN^+ ion structure (structure (2), p.155). Therefore it could be expected that the CNC^+ isomer may show more reactivity[140] towards a neutral such as CH_4 (with a polarisability of 2.6×10^{-24} cm^3) than the CCN^+ isomer even though the heat of formation of the CNC^+ isomer is lower.

Schiff and Bohme[127] in a SIFT study on the reactions of the C_2N^+ ion investigated the reaction with methane (5.06). As mentioned in the introduction to this chapter, reaction (5.00) (C^+ + HCN) was used to generate C_2N^+ ions in their study, but no discussion was given on how the C^+ ions were produced. They reported a rate coefficient for the reaction of 4.4×10^{-12} cm^3 s^{-1} with product ions being reported at values of 27, 28 and 52 amu. These peaks were assigned to $C_2H_3^+$, H_2CN^+ and $H_2C_3N^+$.

McEwan et al[135] have also studied the reaction of C_2N^+ with CH_4 in an ICR cell. In that study C_2N^+ was generated by electron impact on C_2N_2, thereby creating a mixture of the two isomers, but they assumed that mainly ions of the type CNC^+ were present. No decay of the C_2N^+ ions was observed with added CH_4 up to the pressure limits of the ICR cell, which they noted corresponded to an upper limit for the rate coefficient of the reaction of 1×10^{-11} cm^3 s^{-1}.

Reaction (5.07) $C_2N^+ + C_2H_2$

The C_2N^+ ion swarm for this reaction was formed either through reactions (5.00) or (5.02), or from electron impact on HC_3N and C_2N_2. The C^+ ion swarm used for reactions (5.00) and (5.02) was formed through electron impact on CO_2 and CCl_4 respectively and therefore in each case ~70% of the swarm consisted of $(C^+)^*$ ions (table 5.2). Upon the addition of C_2H_2 two distinct exponential decay components were noted for all four methods of generation of the C_2N^+ ion. In each case the percentage of the slower decay as a fraction of the total

C_2N^+ ion signal was observed to be 70±5% (ie 70% of CCN^+ present, as shown in table 5.2). The faster decay due to reaction of CNC^+ corresponded to an average rate coefficient of 1.6×10^{-9} cm^3 s^{-1}, whilst the slower was 8.8×10^{-10} cm^3 s^{-1}.

The products of reaction (5.07) were found by injecting C_2N^+ cleanly into the flow tube after electron impact on C_2N_2. Upon the addition of C_2H_2 three product ions were observed. The major ion was C_3H^+ (85%) while the minor product species were HC_4N^+ and H_2CN^+, at 9% and 6% of the total product ion distribution respectively.

McEwan et al[135] reported 80% of C_3H^+ and 20% of HC_4N^+ with an overall rate coefficient of 1.0×10^{-9} cm^3 s^{-1} for reaction (5.07), while Schiff and Bohme[127] noted the production of C_3H^+ (90%) and H_2CN^+ (10%) with an overall rate coefficient of 8.9×10^{-10} cm^3 s^{-1}.

Reaction (5.08) $C_2N^+ + N_2O$

Reaction (5.08) was studied using two separate source reactions for C_2N^+; electron impact on C_2N_2 in the ion source, and reaction between C^+ and C_2N_2 (reaction (5.02)) at portal 1. In the latter case CCl_4 was used to generate the C^+ ions, and therefore in both source reactions mixtures of ~70% CCN^+ and ~30% CNC^+ were present (table 5.2).

Upon the addition of N_2O, two separate exponential decay components were noted with both sources (the percentage of the slower exponential decay, corresponding to CCN^+ ions, was 68±5% of the total C_2N^+ ion swarm in each case). The rate

coefficient for the faster decay was measured to be ~1.2 x 10^{-9} cm^3 s^{-1} while the slower was ~4.0 x 10^{-10} cm^3 s^{-1}. No differences in the product distribution for this reaction were noted when C_2N^+ was generated either by electron impact on C_2N_2 or by reaction (5.02).

The major product ion was observed to occur at m/e= 54. Two possible molecular configurations can be written for this peak, CN_3^+ and C_2NO^+. The CN_3^+ reaction channel is exothermic by 84 kJ mol^{-1} for the isomer CCN^+, but is endothermic by 22 kJ mol^{-1} for the other isomer CNC^+. Unfortunately no data on the enthalpy of formation of the ion C_2NO^+ is available, so it is possible that both of the possible product ions at 54 amu may be formed through reaction (5.08). If C_2NO^+ is actually formed, an upper limit to ΔH_f° (C_2NO^+) of 1702 kJ mol^{-1} can be set (ie. for the formation of C_2NO^+ to be exothermic in reaction (5.08) its heat of formation has to be <1702 kJ mol^{-1}). Apart from the major product ion at m/e= 54 (73%), two other minor product ions were also noted, NO^+ (22%) and N_2O^+ (5%). The route to the production of NO^+ from reaction (5.08) is exothermic for both CNC^+ and CCN^+, however the overall enthalpy changes for charge transfer from these ions to N_2O^+ were unable to be determined as ΔH_f° for the radical C_2N is unknown.

It would also be of interest, for both reactions (5.07) (C_2N^+ and C_2H_2) and (5.08) (C_2N^+ and N_2O), to study whether the observed product distribution shows a change when the isomeric composition of the C_2N^+ ion swarm is varied (as noted in table 5.2 both reactions (5.00) and (5.02), when

either CO or CH_4 are used as the source of C^+ ions, result in the formation of 90±5% of the isomer CNC^+).

The reactions of three other small molecules, H_2O, HCN and NH_3, with the ion C_2N^+ showed no significant change in either rate coefficients or product distributions when the isomeric composition of the C_2N^+ ion swarm was varied.

Reaction (5.09) $C_2N^+ + H_2O$

A single exponential decay with a rate coefficient of 1.7 x 10^{-10} cm^3 s^{-1} was observed for this reaction when C_2N^+ was generated from either electron impact on C_2N_2 and HC_3N, or through reactions (5.00) (C^+ and HCN) and (5.02) (C^+ and C_2N_2). When electron impact on C_2N_2 was used to create a swarm of C_2N^+ free of impurity ions two product ion peaks were observed for reaction (5.09). These peaks at m/e values 29 and 28 corresponded to HCO^+ (92%) and H_2CN^+ (8%) respectively (the formation of the other possible product ion at m/e= 28, CO^+, is endothermic for both isomers of C_2N^+).

After electron impact on C_2N_2 in a low pressure ICR cell, McEwan et al[135] observed HCO^+ as the major product for reaction (5.09), but noted only HC_2N^+ as a minor product. However, recent appearance potential measurements of Harland et al[94] for both the C_2N^+ and HC_2N^+ ions (shown in table 3.3) may be used to show that the formation of the isomers $HCCN^+$ and $HCNC^+$ from the reactions of either CCN^+ or CNC^+ with H_2O are endothermic (by at least 109 kJ mol^{-1} for CCN^+ and by at least 215 kJ mol^{-1} for CNC^+). Therefore the peak

at 39 amu observed by McEwan et al may have been the result of secondary reactions occurring in the ICR cell.

Reaction (5.10) $C_2N^+ + HCN$

The sole product channel observed for the reaction of C_2N^+ with HCN was association leading to the ion $C_2N^+.HCN$. The C_2N^+ decay was fitted by a single exponential leading to a pseudo second order rate coefficient of 4.2×10^{-10} cm^3 s^{-1} at 0.30 Torr. This value was observed for the reaction when C_2N^+ was generated both by electron impact on C_2N_2 and through reaction (5.02).

Reaction (5.11) $C_2N^+ + NH_3$

For reaction (5.11) a single exponential decay of the C_2N^+ ion was observed with added NH_3 giving an overall rate coefficient of 1.9×10^{-9} cm^3 s^{-1}. This value is in good agreement with the previously reported rates of Schiff and Bohme[127] and McEwan et al[135]. When C_2N^+ was produced cleanly in the flow tube by electron impact on C_2N_2, the only product ion observed was H_2CN^+. Schiff and Bohme also observed a single ion product only, H_2CN^+. McEwan et al on the other hand observed both N_2H^+ (10%) and H_2CN^+ (90%) product ions for reaction (5.11) using C_2N^+ generated from electron impact on C_2N_2. In this study however, at very low NH_3 flows ($\sim 4 \times 10^{-15}$ molecules s^{-1}) the ion peak at 29 amu was observed to be less than 1% of the H_2CN^+ product ion peak in magnitude.

Summary

In conclusion, two separate exponential decay components were observed for the reaction of C_2N^+ with CH_4 (5.06), when C_2N^+ was formed from electron impact on CH_3CN, HC_3N and C_2N_2, while one decay only was observed from CNC^+ formed through reactions (5.00) and (5.02). The observation of a single exponential decay provides experimental confirmation of the existence of a substantial barrier to isomerisation between CCN^+ and CNC^+. From these results and in combination with the available thermodynamic data[93,94] it can be inferred that CNC^+ is the only isomer formed in the gas phase from the reactions of ground state C^+ with HCN and C_2N_2, in agreement with the theoretical predictions of Haese and Woods[132].

However, for the reaction of C^+ with HNC (5.01) recent experimental thermodynamic data[94] indicates that formation of both the isomers CCN^+ and CNC^+ from reaction (5.01) is endothermic (by 169 and 62 kJ mol^{-1} respectively, table 5.0). In contrast Haese and Woods[132] suggested that production of a single CCN^+ isomer only would result from this reaction. The overall reaction enthalpies for each ion from reaction (5.01) however, are dependent upon ΔH_f° of HNC which has only been approximately measured to be 196±21 kJ mol^{-1} [141].

That the CNC^+ isomer appears to be more reactive with certain neutrals than does CCN^+ can possibly be explained by the additional carbene character of the most likely CNC^+ ion structure.

5.4 REACTIONS OF THE HC_2N^+ ION.

In a recent electron impact study on the appearance potentials of fragment ions derived from CH_3NC and CH_3CN, Harland and McIntosh[94] reported the heats of formation for two isomers of HC_2N^+, $HCCN^+$ (structure (3)) and $HCNC^+$ structure (4)), to be 1622 and 1554 kJ mol^{-1} respectively.

$$\underline{\underline{H}}-\underline{\underline{C}}=\overset{+}{\underline{\underline{C}}}=\underline{\underline{N}}: \qquad (3) \qquad\qquad \underline{\underline{H}}-\underline{\underline{C}}=\overset{+}{\underline{\underline{N}}}=\underline{\underline{C}}: \qquad (4)$$

They observed only a single appearance potential for HC_2N^+ formation after electron impact on each of CH_3CN (corresponding to $HCCN^+$) and CH_3NC (corresponding to $HCNC^+$). This suggests that, once the respective isomers are formed, the barrier to isomerisation is sufficient to allow each to exist as a separate entity in the gas phase.

In an attempt to investigate the reactions of the HC_2N^+ ion and possibly to observe evidence for the existence of separate isomers, the reactions of HC_2N^+ with the neutrals O_2, H_2, H_2O and N_2 were studied. The results of these reaction studies are shown in table 5.3.

Table 5.3: Reactions of the HC_2N^+ ion. Rate coefficients, k, are in units of 10^{-9} cm^3 s^{-1}. Overall reaction enthalpies for $HCCN^+$ and $HCNC^+$ are in kJ mol^{-1}.

no.	neutral	products	B.R.	k	k_{ADO} or k_L	$-\Delta H°$ $HCCN^+$	$-\Delta H°$ $HCNC^+$
5.12	O_2	$HCO^+ + CNO$	major	0.26	0.70	114	46
		$O_2^+ + HC_2N$	minor?			?	?
		$C_2NO^+ + OH$	medium			-119[a]	-187[a]
5.13	H_2	$CH_3^+ + CN$	-0.88	0.50	1.5	95	27
		$H_2CN^+ + CH$	-0.12			86	18
5.14	H_2O	$H_3O^+ + C_2N$	minor?	0.035	2.2	?	?
		$H_2O^+.HC_2N$	major			?	?

Table 5.3 continued.

5.15	N_2	-	-	<0.00001	0.77

(a) These reaction enthalpies are upper limits only as ΔH_f° (C_2NO^+) is an upper estimate (section 5.3, p.169).

The ion HC_2N^+ was generated by electron impact on CH_3CN, CH_3NC and HC_3N, and also by reaction between CH^+ and HCN (5.16).

$$\begin{aligned} CH^+ + HCN &\rightarrow H_2CN^+ + C \quad (0.75)^{85} \\ &\rightarrow C_2N^+ + H_2 \quad (0.15) \\ &\rightarrow HC_2N^+ + H \quad (0.10) \end{aligned} \qquad (5.16)$$

From the observations of Harland and McIntosh[94] electron impact on both CH_3CN and HC_3N should produce solely the $HCCN^+$ isomer, while both the addition of HCN to CH^+ and electron impact on CH_3NC should give only $HCNC^+$.

After electron impact on either CH_3CN or CH_3NC, and the injection of HC_2N^+ ions from either of these neutrals into the flow tube, the optimal percentage of ions at 39 amu was only 28% of the total ion swarm (impurity ions at 38 amu were 18%, 40 amu (44%) and 41 amu (10%)). After electron impact on HC_3N the best attainable ratio of the 39 amu ion peak to that at 38 amu was 2.5/1, while for the reaction of CH^+ with HCN (reaction (5.16)) HC_2N^+ was only a minor (~10%[85]) product ion channel. Table 5.2 summarizes the percentages of ion impurities for each method of HC_2N^+ ion formation.

The inability to create a swarm consisting predominantly of HC_2N^+ ions in the flow tube resulted in serious complications in both the analysis of the HC_2N^+ ion decay curves and the determination of product distributions for the reactions detailed in this section. When a significant

proportion of ions at m/e= 38 (C_2N^+) were present in the swarm along with HC_2N^+ in the flow tube, the natural percentages of ^{13}C (1.11%) and ^{15}N (0.37%) also resulted in significant contributions due to isotopes of C_2N^+ ions at 39 amu (typically ~5%). Therefore, because of the C_2N^+ isotope contribution to the 39 amu peak, only neutrals that reacted slowly with C_2N^+ were chosen for reaction with HC_2N^+. Limits to the rate coefficients for reaction of C_2N^+ with these neutrals (O_2, H_2, H_2O, and N_2) are shown in table 5.1.

The rate coefficients measured for the following reactions (5.12-5.15) were obtained by subtracting the unreactive background of C_2N^+ isotopes at m/e= 39 before data analysis.

Reaction (5.12) $HC_2N^+ + O_2$

For this reaction HC_2N^+ was formed from electron impact on CH_3CN and through the reaction of CH^+ with HCN. A single exponential decay was observed for the reaction of the H_2CN^+ ion with added O_2, for both sources of the primary ion. The average rate coefficient was measured to be 2.6×10^{-10} cm^3 s^{-1}. The background from isotopes of C_2N^+ did not react at all with O_2, as can be seen in figure 5.1b (an upper limit of 1×10^{-14} cm^3 s^{-1} was able to be set for the reaction of C_2N^+ with O_2 (shown in table 5.1)). The major observed product for reaction (5.12) was HCO^+, along with a smaller C_2NO^+ ion contribution and a possible minor product ion, O_2^+ (the enthalpy change for the charge transfer product channel of reaction (5.12) was unable to be determined as ΔH_f° (HC_2N)

is unknown).

When HC_2N^+ ions were formed through the addition of HCN at portal 1 to a swarm of CH^+ ions, only a small decay of the 39 amu peak was observed upon the addition of O_2 at portal 2. The CH^+ ions were generated by electron impact on CH_4 and consequently a small amount (~10%) of C^+ ions were also present. As C_2N^+ is a major product ion formed in the reaction of CH^+ with HCN (reaction (5.16)) and the reaction of C^+ with HCN (reaction (5.00)) produces only C_2N^+, a major part of the 39 amu peak results from isotopes of C_2N^+. Figure 5.1a shows a plot of the 39 amu ion signal, generated in the reaction of a CH^+ ion swarm with HCN (reaction (5.16)), against neutral O_2 flow. If reaction (5.12) has a significant product channel leading to the formation of the HC_2N^+ ion (10% as suggested by Anicich et al[85]) this ion will react with O_2 leaving only unreactive $^{13}C_2N^+$ ions.

Available thermodynamic data (table 3.3, section 3.4) indicates that the formation of HC_2N^+ from the reaction of CH^+ with HCN is endothermic (by ~18 kJ mol^{-1} for $HCNC^+$ and ~86 kJ mol^{-1} for $HCCN^+$). However as the extent of endothermicity for the formation of the $HCNC^+$ ion is small it is still possible that a small amount of this isomer may be formed in the reaction of CH^+ and HCN.

Metastable $(C^+)^*$ ions may also react with HCN to form HC_2N^+ ions. However electron impact on CH_4 at low energies should form mostly ground state C^+ ions (table 5.2) and therefore it is unlikely that more than a small percentage of the reactive component of the 39 amu peak results from $(C^+)^*$.

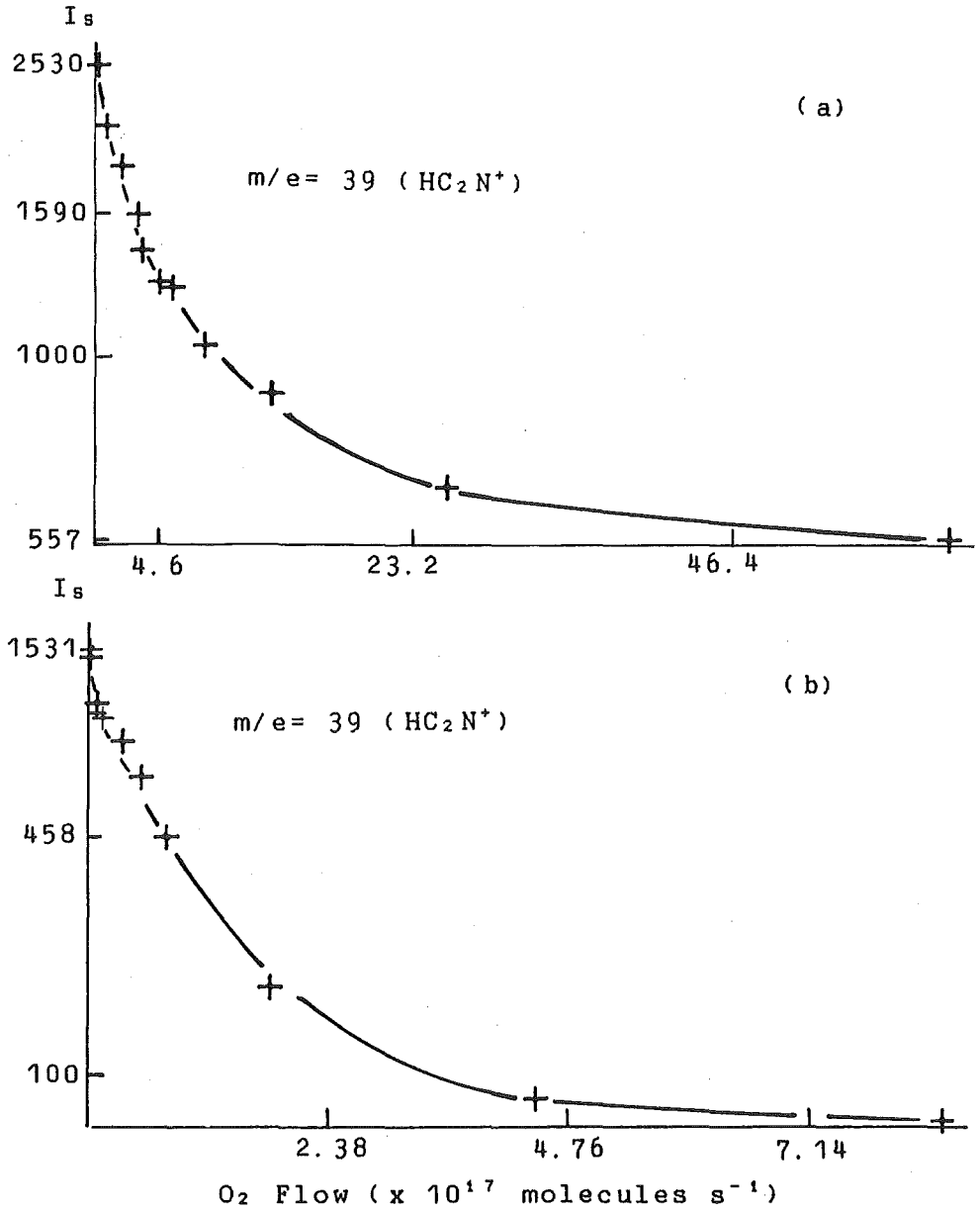

Fig. 5.1: Semilogarithmic plots of I_s, the ion signal at m/e= 39 against the flow of O_2, where the mass peak at 39 amu is formed through (a) $CH^+ + HCN \rightarrow HC_2N^+ + H$
(b) $CH_3CN + e \rightarrow HC_2N^+ + H_2 + 2e$

Reaction (5.13) $HC_2N^+ + H_2$

In the reaction of HC_2N^+ with H_2, as for reaction (5.12), a single exponential decay was observed when HC_2N^+ was generated either from reaction between CH^+ and HCN (reaction (5.16)) or from electron impact on CH_3CN and CH_3NC. For all three forms of generation a large background of unreactive ions, due to the presence of ^{13}C and ^{15}N isotopes of C_2N^+, was again noted upon the addition of H_2 to the 39 amu ion swarm (C_2N^+ ions react only very slowly with H_2, k being $<1 \times 10^{-13}$ cm^3 s^{-1} (table 5.1)).

When HC_2N^+ was formed from CH_3CN, two product channels were observed, leading to the two ions CH_3^+ (88%) (formation of the other possibility at this mass peak, NH^+, is endothermic for both isomers) and H_2CN^+ (12%) with an overall reaction rate coefficient of 5.0×10^{-10} cm^3 s^{-1}. However it is also feasible thermodynamically for CH_3CN^+, the only other ion present in the flow tube to also have reacted with H_2 ($k \sim 1 \times 10^{-12}$ cm^3 s^{-1}), to have produced the H_2CN^+ ion ($-\Delta H^\circ \sim$ 200 kJ mol^{-1} for the reaction of CH_3CN^+ with H_2 to produce H_2CN^+ where $\Delta H_f^\circ(CH_3CN^+) = 1282$ kJ mol^{-1} [94]). For this reason the observed product distribution for reaction (5.13) is at best only approximate (the estimated error for each product ion is ±20%).

Reaction (5.14) $HC_2N^+ + H_2O$

When HC_2N^+ was formed through electron impact on HC_3N a single exponential decay with a rate coefficient of 3.5 x

10^{-11} cm^3 s^{-1} at 0.29 Torr was noted upon the addition of H_2O. The major product appeared to be the association adduct $HC_2N^+.H_2O$.

Reaction (5.15) $H_2CN^+ + N_2$

No reaction was detected between H_2CN^+ and N_2 up to the highest sustainable neutral flows from portal 2 allowing an upper limit of $<1 \times 10^{-14}$ cm^3 s^{-1} to be set for reaction (5.15).

Summary

In summary, from the reactions studied it appears that the two isomers $HCCN^+$ and $HCNC^+$ are indistinguishable on the basis of their reactivities in the gas phase. This statement needs to be qualified however, as swarms of the ion HC_2N^+ were not able to be formed sufficiently free of impurity ions to allow for straightforward interpretation of any of the data obtained for the reactions discussed. Two alternative conclusions may be drawn from the data presented; either the barrier to isomerisation between the two ions $HCCN^+$ and $HCNC^+$ is insufficient to prevent interconversion in the gas phase within the timescale of the SIFT experiment; or the reactivities of the separately formed isomers (ie. $HCCN^+$ from CH_3CN and HC_3N and $HCNC^+$ from CH_3NC) are similar in all of the reactions investigated.

Harland and MacIntosh[94] in their electron impact study of the fragment ions of CH_3CN and CH_3NC concluded that the

observation of single separate appearance potentials (corresponding to $HCCN^+$ and $HCNC^+$ respectively) for each neutral meant that the isomerisation barrier between the HC_2N^+ isomers was too high to be crossed at the energies involved. If this is the case then the results obtained for the reactions of the HC_2N^+ ion in this chapter indicate that the two isomers $HCNC^+$ and $HCCN^+$ are of similar reactivity.

CHAPTER SIX

PROTON AFFINITY MEASUREMENTS OF C_4H_2 AND REACTIONS OF SELECTED HYDROCARBON IONS WITH C_2H_2, HCN, C_6H_6 AND H_2

6.1 INTRODUCTION.

Detection of acetylenic hydrocarbons, methylcyanopoly-ynes, cyanopoly-ynes and HCN in interstellar clouds[88,89,90,91] has led to increased interest in the ion-molecule chemistry of these compounds. Studies of a number of reactions of unsaturated hydrocarbon ions with HCN have been reported in the literature recently[85,142]. Acetylenic type ions have also been identified in hydrocarbon flames[143,144]. Various ion-molecule reaction schemes have been proposed[145,146] to explain the presence of these ions in flames, while many experimental studies have been performed in attempts to elucidate information on the reactions involved[85,145,147].

The results of reaction studies that were undertaken to determine the proton affinity of diacetylene (C_4H_2, IUPAC name butadiyne) are discussed in this chapter (section 6.2). Only one value for the PA of C_4H_2 (753 ± 4 kJ mol^{-1}), obtained through "bracketing" the C_4H_2 molecule with the ions $CH_3OH_2^+$ and $CH_3NO_2H^+$, has been reported in the literature[148].

Reactions of ions derived from unsaturated hydrocarbons, viz., $C_2H_n^+$(n= 0, 1, 2), $C_4H_n^+$(n= 0-8), and $C_6H_n^+$(n= 1-7) with HCN and C_2H_2 were studied to compare with previous ICR spectroscopy measurements of the rate coefficients and product

distributions for these reactions. Selected unsaturated hydrocarbon ions were also generated from different sources and their reactions investigated in an attempt to observe evidence for the existence of stable structural isomers of the ions concerned. For example the ion $C_4H_3^+$ was generated through chemical reaction,

$$C_2H_2^+ + C_2H_2 \rightarrow C_4H_3^+ + H$$

and also by electron impact on C_4H_2, C_4H_4 (vinyl acetylene, IUPAC name 1-buten-3-yne) and C_4H_6 (IUPAC name 1,3-butadiene). The reactions of the $C_4H_3^+$ ion at m/e= 51, when formed from each of the above sources, are discussed in section 6.3 for the reaction with C_2H_2 and in section 6.4 for the reaction with HCN.

6.2 THE PROTON AFFINITY OF C_4H_2.

Table 6.0 lists the rate coefficients and product ratios used to determine the PA of C_4H_2. The proton transfer reactions between $C_4H_3^+$ and the two protonated species $CH_3OH_2^+$ and H_2CN^+ were studied initially to indicate an approximate value for the PA of C_4H_2, (ie. whether this value is higher or lower than the respective PA values[92] for CH_3OH (761 kJ mol^{-1}) and HCN (717 kJ mol^{-1})).

Table 6.0: Ion-molecule reactions used to establish the proton affinity of C_4H_2. Rate coefficients, k, have units of 10^{-9} cm^3 s^{-1}. $\Delta H°$ values are in units of kJ mol^{-1}. The abbreviation "no." stands for reaction number whilst "B.R." represents the reaction product distribution.

no.	ion	neutral	products	B.R.	k	k(lit.)[a]	k_L or k_{App}	$-\Delta H°$ [b]
6.00	$CH_3OH_2^+$	C_4H_2	$CH_3OH_2^+ . C_4H_2$	1.0	0.26	<0.02	1.2	?
6.01	H_2CN^+	"	$C_4H_3^+ + HCN$	1.0	1.85		1.2	7
6.02	$CH_3NO_2H^+$	"	$C_2H_4N^+ + C_2H_2 + CO_2$	1.0	1.1	0.38	0.98	478[c]
6.03	$C_4H_3^+$	CH_3NO_2	$CH_3NO_2H^+ + C_4H_2$	0.78	2.45		2.9	18
			$C_4H_4O^+ + NH_2CO$	0.22				?
		or	$C_3H_2NO^+ + CH_4 + CO$					?
6.04	$HCOOH_2^+$	C_4H_2	$C_4H_3^+ + HCOOH$	major	0.97	0.62	1.0	-16
			$HCOOH_2^+ . C_4H_2$	minor				?
6.05	$HBrCN^+$	"	$HBrCN^+ . C_4H_2$	0.98	0.53		0.89	?
			$C_4H_3^+ + BrCN$	0.02				-10[e]
6.06	$C_4H_3^+$	BrCN	$HBrCN^+ + C_4H_2$	0.66	1.3		2.1	10
			$C_4H_3^+ . BrCN$	0.34				?
6.07	$C_2H_5IH^+$	C_4H_2	$C_4H_3^+ + C_2H_5I$	~0.58[d]	0.084		0.84	2[e]
			$C_6H_7^+ + HI$	~0.33				390
			$C_2H_6I^+ . C_4H_2$	~0.09				?
6.08	$C_4H_3^+$	C_2H_5I	$C_4H_3^+ . C_2H_5I$	~0.37[d]	1.5		1.8	?
			$C_4H_5I^+ + C_2H_3$	~0.35				?
			$C_6H_6^+ + I$	~0.26				251
			$C_2H_5IH^+ + C_4H_2$	~0.02				4

(a) Values from reference 148.
(b) A positive $\Delta H°$ value represents an exothermic reaction channel.
(c) Production of both CH_3CNH^+ and CH_3NCH^+ is exothermic by 521 and 478 kJ mol^{-1} respectively.
(d) The estimated error involved in the determination of these product distributions is ±20%.
(e) Value determined in this study.

Reaction (6.00) $CH_3OH_2^+ + C_4H_2$

The ion $CH_3OH_2^+$ was generated by electron impact on a mixture of H_2 (500 Torr) and CH_3OH (saturated vapour pressure= 100 Torr at 21°C). After injection into the flow tube the major impurity ion present was CH_3^+ at 20% of the primary ion concentration (other impurity peaks occurred at m/e values of 31, 32, and 34 and were <1% of the $CH_3OH_2^+$ peak). However as CH_3^+ reacted with C_4H_2 to give as the only product $C_3H_3^+$ (with a rate coefficient of 2.4×10^{-9} cm^3 s^{-1}), product analysis for reaction (6.00) was uncomplicated. Association with C_4H_2 to give the adduct $CH_3OH_2^+.C_4H_2$ was the only product channel observed for $CH_3OH_2^+$. Thus no proton transfer occurred from $CH_3OH_2^+$.

Reaction (6.01) $H_2CN^+ + C_4H_2$

The reaction of C_4H_2 with H_2CN^+ resulted in the proton transfer product, $C_4H_3^+$, as the only channel with a rate coefficient of 1.85×10^{-9} cm^3 s^{-1}. The primary ion, H_2CN^+, was formed through electron impact on a 20/1 mixture of H_2 and HCN. The two adjacent ion peaks at m/e values of 27 and 29 were also present at concentrations of less than 4% of the primary ion.

The observation of single association and proton transfer channels for reactions (6.00) and (6.01) respectively bracketed the PA of C_4H_2 between 761 and 717 kJ mol^{-1}, the proton affinites of CH_3OH and HCN respectively. The reactions

of C_4H_2 with the protonated compounds $CH_3NO_2H^+$ (PA (CH_3NO_2) = 751 kJ mol^{-1} [92]) and $HCOOH_2^+$ (PA (HCOOH) = 748 kJ mol^{-1} [92]) were then studied.

Reaction (6.02) $CH_3NO_2H^+ + C_4H_2$

The reaction of $CH_3NO_2H^+$ with C_4H_2 produced only a single product channel at m/e= 42. This product ion, $C_2H_4N^+$ (representing both of the isomers CH_3CNH^+ and CH_3NCH^+), was produced with a rate coefficient of 1.1×10^{-9} cm^3 s^{-1}. An alternative ion product at m/e=42 is CNO^+ but this second channel is endothermic by 208 kJ mol^{-1}. $CH_3NO_2H^+$ was formed from electron impact on H_2 (500 Torr) and CH_3NO_2 (saturated vapour pressure= 40 Torr at 27.5°C) with the only impurity being a 2% NO^+ peak in the resulting ion swarm. No evidence for a proton transfer channel was observed.

The reverse of reaction (6.02) was also studied to observe if proton transfer occurred from $C_4H_3^+$ to nitromethane.

Reaction (6.03) $C_4H_3^+ + CH_3NO_2$

$C_4H_3^+$ was generated by electron impact on a 20/1 mixture of H_2 and C_4H_2, and also by proton transfer from HCO^+ to C_4H_2 (added at portal 1). When $C_4H_3^+$ (m/e= 51) ions were formed through electron impact and injected into the flow tube, the adjacent impurity ion peaks at m/e= 50 and m/e= 52 were also present at 7% of the $C_4H_3^+$ signal ($C_4H_3^+$ impurities are detailed in table 6.1).

Table 6.1: Methods of generation for specific ions.

ion	neutral	%impurities[a,b]		
C_4^+	C_4H_2 + e	49 (150%)	50 (60%)	
	C_4H_4 + e	49 (180%)	50 (80%)	
C_4H^+	C_4H_2 + e	48 (50%)	50 (30%)	
	C_4H_4 + e	48 (35%)	50 (58%)	
	C_2H_2 + e → C_2^+ [c]			
	$C_2^+ + C_2H_2$	50 (5%)		
$C_4H_2^+$	C_4H_2 + e	49 (1%)	51 (2%)	
	C_4H_4 + e	48 (3%)	49 (16%)	51 (12%)
	C_2H_2 + e → C_2H^+ [c]			
	$C_2H^+ + C_2H_2$	49 (25%)	51 (20%)	52 (2%)
$C_4H_3^+$	C_4H_2/H_2 + e	50 (7%)	52 (7%)	
	C_4H_4 + e	50 (50%)	52 (25%)	
	C_4H_6	50 (26%)	52 (30%)	
	C_2H_2 + e → $C_2H_2^+$ [c]			
	$C_2H_2^+ + C_2H_2$	50 (8%)	52 (1%)	
	$HCO^+ + C_4H_2$	101 (440%)	151 (133%)	201 (64%)
$C_4H_4^+$	C_4H_4 + e	51 (<10%)	53 (<10%)	
	C_4H_6 + e	51 (30%)	53 (30%)	54 (5%)
	C_2H_2 + e → $C_2H_2^+$ [c]			
	$C_2H_2^+ + C_2H_2$	50 (~500%)	51 (~350%)	
$C_4H_5^+$	C_4H_6 + e	52 (19%)	54 (15%)	
	C_4H_4 + e [d]	52 (15%)		
$C_4H_6^+$	C_4H_6 + e	53 (8%)	55 (5%)	
$C_4H_7^+$	C_4H_6 + e [d]	-		
$C_4H_8^+$	C_4H_6 + e [d]	-		
C_6H^+	C_6H_6 + e	74 (100%)		
	$C_4^+ + C_2H_2$ [e]	48 (5%)	49 (5%)	74 (90%)
$C_6H_2^+$	C_6H_6 + e	73 (40%)	75 (9%)	
	$C_4H^+ + C_2H_2$ [e]	49 (10%)		
$C_6H_3^+$	C_6H_6 + e	74 (20%)	76 (30%)	77 (5%)
$C_6H_4^+$	C_6H_6 + e	75 (17%)	77 (5%)	
	$C_4H_2^+ + C_2H_2$ [e]	50 (7%)	74 (2%)	77 (8%)
$C_6H_5^+$	C_6H_6 + e	76 (30%)	78 (40%)	
	$C_4H_3^+ + C_2H_2$ [e]	50 (3%)	51 (5%	76 (4%)
$C_6H_6^+$	C_6H_6 + e	77 (11%)	79 (4%)	
$C_6H_7^+$	C_6H_6 + e [d]	-		
H_2CN^+	H_2/HCN + e	27 (0.8%)	29 (2.7%)	

(a) Represents the optimum ratio of the required ion to the other ions.
(b) The m/e values shown represent impurity ions present in the relevant primary ion swarm, while the numbers in parenthesis represent the magnitudes of these impurity ions. eg. 49 (150%) indicates a m/e peak at 49 1.5 times that of the primary ion peak.
(c) The relevant primary ion has been formed by the indicated reaction at portal 1 after electron impact on C_2H_2.
(d) Formed at ion source pressures >1 x 10^{-4} Torr.
(e) The relevant primary ion has been formed by the indicated reaction at portal 1 after electron impact on either C_4H_2, C_4H_4 or C_4H_6.

When $C_4H_3^+$ ions were formed by the addition of sufficient C_4H_2 to reduce an injected HCO^+ ion concentration to zero in the flow tube, the higher clusters $(C_4H_2)_nH^+$ (n= 2, 3, 4) were also produced in greater concentrations than the $C_4H_3^+$ ion. For product analysis in this reaction therefore, electron impact on a C_4H_2/H_2 mixture was used as the source of $C_4H_3^+$ ions.

Upon the addition of CH_3NO_2 two product channels were observed; the first resulting in the ion $CH_3NO_2H^+$ (78%) through proton transfer and the second giving a peak at m/e= 68 (22%), with a combined rate coefficient of 2.45×10^{-9} cm^3 s^{-1}. Two possible mass configurations, $C_4H_4O^+$ and $C_3H_2NO^+$, can be written for the minor product peak observed at m/e= 68. As no measurements have been reported in the literature for the heat of formation of either of these ions however, it is not known whether one or both of them are formed in reaction (6.03).

Reaction (6.04) $HCOOH_2^+ + C_4H_2$

The $HCOOH_2^+$ ion swarm formed for reaction (6.04) was created by electron impact in the ion source on a mixture of H_2 (500 Torr) and HCOOH (saturated vapour pressure= 40 Torr at 24°C). Unfortunately collisional dissociation of these $HCOOH_2^+$ ions occurred upon injection into the flow tube. Even at very low injection energies the breakup ions, H_3O^+ and HCO^+, were still present in the $HCOOH_2^+$ ion swarm, at 6% and 15% respectively of the parent ion concentration. As both these ions underwent proton transfer to C_4H_2 an accurate product analysis for reaction (6.04) was precluded. Under

these conditions it was possible to only roughly estimate that association to form the adduct $HCOOH_2^+.C_4H_2$ was a minor channel, while proton transfer to produce $C_4H_3^+$ was the larger channel. The overall rate coefficient for reaction (6.04) was measured to be 9.7×10^{-10} cm^3 s^{-1}.

The results for reactions (6.02) and (6.03), viz., formation of the $C_2H_4N^+$ ion in the absence of a proton transfer channel for the former reaction and proton transfer from $C_4H_3^+$ to CH_3NO_2 as the major channel for the latter, indicate that the PA of C_4H_2 is presumably at least 5 kJ mol^{-1} below the PA of CH_3NO_2 (750 kJ mol^{-1} [92]). A limit of <745 kJ mol^{-1} is justified by the absence of a proton transfer channel for reaction (6.02), for reasons which are discussed in the HC_3N PA determination (section 3.4).

These results, together with the inability to determine the extent of proton transfer in reaction (6.04), meant that it was necessary to choose additional compounds with which to measure an equilibrium constant for proton transfer to C_4H_2. Thus cyanogen bromide, BrCN, (PA= 748 kJ mol^{-1}, table 3.2, Chapter 3) and ethyl iodide, C_2H_5I, (PA~736 kJ mol^{-1} [92]), were chosen as these two were the only compounds both readily available and with documented PA's in the range of 742±6 kJ mol^{-1}.

The PA of C_4H_2 was able to be "bracketed" through the use of these two compounds, but as both were of high mass they were potentially subject to larger than usual mass discrimination errors in product analysis. The rate coefficients and product distributions for reaction between

the two compounds and C_4H_2 are shown in table 6.0, whilst the individual reactions are detailed in the following paragraphs.

Reaction (6.05) $HBrCN^+ + C_4H_2$

After electron impact on a mixture of H_2 and BrCN, a swarm containing only $H^{81}BrCN^+$ ions (m/e= 108) was able to be formed in the flow tube (the adjacent mass ion at 109 amu, at ~1% of the primary ion concentration, resulted from $H^{81}Br^{13}CN^+$ only). Upon the addition of C_4H_2 two product channels were noted; an association channel to produce the adduct $HBrCN^+.C_4H_2$ (98%) and a small proton transfer channel to give the ion $C_4H_3^+$ (2%), with an overall rate coefficient of 5.3×10^{-10} cm^3 s^{-1}.

Reaction (6.06) $C_4H_3^+ + BrCN$

The $C_4H_3^+$ ions studied in this reaction were generated by electron impact in the same manner as for reaction (6.03). The products for reaction (6.06), $HBrCN^+$ (66%) and $C_4H_3^+.BrCN$ (34%), were produced with a combined rate coefficient of 1.3×10^{-9} cm^3 s^{-1}.

Ions at m/e= 50, $C_4H_2^+$, and m/e= 52, $C_4H_4^+$, each present in concentrations of less than 5% of the primary ion after electron impact (as the natural abundance of the ^{13}C isotope in a swarm of $^{12}C_4H_3^+$ ions is 4.4%, ions containing this isotope will represent a significant proportion of the ion peak at 52 amu), were observed to react only slowly with BrCN; the former, C_4H^+, producing the charge transfer ion $BrCN^+$ and the latter, $C_4H_4^+$, a product at m/e= 75 (HC_5N^+).

Reaction (6.07) $C_2H_5IH^+ + C_4H_2$

$C_2H_5IH^+$ was formed by subjecting a mixture of H_2 (500 Torr) and C_2H_5I (SVP= 100 Torr at 18°C) to electron impact in the ion source. Upon injection of $C_2H_5IH^+$ into the flow tube a small amount (2%) of impurity ions at a mass of 29 amu ($C_2H_5^+$) were also present in the resulting ion swarm. When the ion at m/e= 29 was injected separately, it produced products on reaction with C_4H_2 at m/e= 51 ($C_4H_3^+$ ~33%) and m/e= 77 ($C_6H_5^+$ ~67%).

Upon addition of C_4H_2 to the $C_2H_5IH^+$ ion swarm, product ion peaks at m/e= 51 (~58%), 79 (~33%) and 207 (~9%) were produced with an overall rate coefficient of 8.4×10^{-11} cm^3 s^{-1}. A small ion peak (<1%) at m/e= 86 (structure unknown) was also produced by the reaction.

A larger experimental error (±20% rather than ±10% as detailed in section 2.10) was involved in the determination of the product distribution for this reaction and also for that of reaction (6.08). The magnitude of this error was due to the larger mass discrimination factor present in the determination of these product distributions (a compilation of measured mass discrimination factors is shown in table 2.1, Chapter Two).

Reaction (6.08) $C_4H_3^+ + C_2H_5I$

The $C_4H_3^+$ ions studied in this reaction were formed as in reactions (6.03) and (6.06). The overall rate coefficient for this reaction was measured to be 1.5×10^{-9} cm^3 s^{-1}. The

observed distribution of the products was as follows: ~37% of the association adduct $C_4H_3^+.C_2H_5I$; ~35% of m/e= 180 (probably the ion $C_4H_5I^+$), ~26% of $C_6H_8^+$, and ~2% of the ion $C_2H_5IH^+$ resulting from proton transfer.

From the measurements described above the equilibrium constant values, K_1 and K_2, for the equilibrium systems (6.09) and (6.10)

$$HBrCN^+ + C_4H_2 \rightleftharpoons C_4H_3^+ + BrCN \qquad (6.09)$$

$$C_2H_5IH^+ + C_4H_2 \rightleftharpoons C_4H_3^+ + C_2H_5I \qquad (6.10)$$

may be determined as 0.012 and 1.620 respectively.

The relative gas phase basicities (GB) for the two equilibrium systems, determined from the equilibrium constants, K_1 and K_2, as for the GB of HC_3N in section 3.4, are shown in table 6.2. The GB for C_4H_2 is assigned a value of zero for comparison purposes. Table 6.2 also lists the relative PA's for the three compounds BrCN, C_4H_2 and C_2H_5I calculated from the relative GBs obtained in this study. If a relative value for the PA (BrCN) of 748 kJ mol^{-1} (determined indirectly in Chapter Three) is used as a reference point, the PA (C_4H_2) is 738±3 kJ mol^{-1}.

Table 6.2: Relative gas phase basicities (GB) and proton affinities (PA) of BrCN, C_4H_2 and C_2H_5I (in kJ mol^{-1}).

compound	ΔGB^a	PA^a	PA(lit.)
BrCN	11	748	746[b]
C_4H_2	0	738	753±4[c]
C_2H_5I	-2	736	~736[b]

(a) The estimated uncertainty is ±3 kJ mol^{-1}.
(b) Reference 92
(c) Reference 148.

The rather large experimental error limits for the C_4H_2 PA measurement (±3 kJ mol^{-1}) are due to two factors. The first was the small value of the equilibrium constant (K_1 = 0.012) for proton transfer between the species BrCN and C_4H_2, while the second was the large mass discrimination factor involved in determining the proton transfer equilibrium constant between C_2H_5I and C_4H_2. The summation of the uncertainties due to these two factors resulted in an error of ±3 kJ mol^{-1} in the GB of C_4H_2.

In a recent ICR study Meot-Ner et al[148] obtained a value of 753±4 kJ mol^{-1} by "bracketing" the PA of C_4H_2 between the compounds CH_3OH and CH_3NO_2. Meot-Ner et al were unable to measure accurately the rate of proton transfer to and from compounds of similar PA because of the effect of secondary reactions between $C_4H_3^+$ and C_4H_2 in their ICR cell (not a problem with the SIFT technique). For the reactions of the ions $CH_3NO_2^+$ and $HCOOH_2^+$ with C_4H_2 (reactions (6.02) and (6.04)) the measured rate coefficients were significantly lower than the values measured in this study (table 6.0). They also assumed that the only possible product channel for

the reactions studied in bracketing the value of PA(C_4H_2) was proton transfer. The considerable difference between the PA value obtained in this study and the ICR result is therefore probably due to the relatively larger errors involved in determining the PA of the C_4H_2 neutral through the use of "bracketing techniques" in an ICR cell[92].

The proton affinity of 738 kJ mol^{-1} determined in this study for C_4H_2 (table 6.2) leads to ΔH_f° [$C_4H_3^+$] = 1271±10 kJ mol^{-1} (ΔH_f° (C_4H_2) = 473 kJ mol^{-1} [167]).

$C_4H_3^+$ was also generated through electron impact on 1,3-butadiene (C_4H_6) and vinyl acetylene (C_4H_4) in an attempt to observe evidence for the presence of more than one $C_4H_3^+$ isomer at flow tube pressures (>0.1 Torr). When C_4H_6 was the source of $C_4H_3^+$ ions, the measured rate coefficient for reaction with cyanogen bromide (2.0 x 10^{-9} cm^3 s^{-1}) was the same (within experimental error) as the rate coefficient measured for $C_4H_3^+$ generated from a mixture of C_4H_2 and hydrogen (1.3 x 10^{-9} cm^3 s^{-1}). When produced from C_4H_4 the $C_4H_3^+$ ion, upon reaction with CH_3NO_2, also gave a rate coefficient that was the same as that observed for $C_4H_3^+$ when formed from C_4H_2. Unfortunately, accurate product analyses for both these reactions were precluded because of high impurity ion levels when the $C_4H_3^+$ ion was generated by electron impact on C_4H_6 and C_4H_4 (table 6.1). No significant differences were observed, however, for the product distributions of reactions (6.03) and (6.06) with these source gases when compared to the product distributions observed after formation of $C_4H_3^+$ through electron impact on a C_4H_2/H_2 mixture.

If it is possible for two or more structural isomers of the $C_4H_3^+$ ion to have separate stable identities at flow tube pressures of 0.3 Torr, then differences in their reactivity are more likely to become apparent in slow ion-molecule reactions as was observed in the reactions of the CCN^+ and CNC^+ isomers (section 5.3). Reactions involving the $C_4H_3^+$ ion in this study (those detailed in the PA (C_4H_2) determination (table 6.0) as well as the reaction with C_2H_2 (reaction (6.17), section 6.3)) were all observed to occur close to the relevant reaction collision limit, with the single exception of the reaction between $C_4H_3^+$ and HCN (reaction (6.34), section 6.4). For all these reactions a single exponential decay of the $C_4H_3^+$ ion was observed upon the addition of the relevant neutral. A single exponential decay suggests that if more than one $C_4H_3^+$ isomer is present in the ion swarm, then the reactivities of these potential isomers are similar in all of the reactions studied.

Anicich et al[147] observed no difference in reactivity for the $C_4H_3^+$ ion with the compounds C_4H_2 and C_4H_4, or in a separate study of $C_4H_3^+$ with C_2H_2 and HCN[85]. Meot-Ner et al[148] in their ICR determination of the PA of C_4H_2 also reported no evidence for two $C_4H_3^+$ isomers. It is therefore probable that under typical SIFT conditions (pressures >0.1 Torr) there exists only a single stable $C_4H_3^+$ ion, with a possible ionic structure as shown in structure (1).

$$HC{\equiv}C\text{-}C^+{=}CH_2 \qquad (1)$$

6.3 REACTIONS WITH ACETYLENE.

The rate coefficients and product distributions for the reactions detailed in the following discussion are shown in table 6.3. Collision limit rate coefficients calculated from the ADO theory[58], and data from previous studies[85,145,149,150,151,152] on some of these reactions are also included for comparison, along with the overall enthalpy change for each reaction channel (where known). Tables 2.0 (section 2.5) and 6.1 (section 6.2) show both the method of ion generation and associated impurity ions at other m/e values for all of the reactant ions discussed in this section.

Reactions (6.11, 6.12, 6.13) $C_2H_n^+$ (n= 0-2) with acetylene

A swarm consisting of C_2^+ ions only was achieved in the flow tube using electron impact on C_2Cl_4 (tetrachloroethylene) followed by injection of ions of 24 amu. As noted in a recent ICR study by Anicich et al[85], the ion C_4H^+ was the only product observed upon the addition of the neutral C_2H_2. Using the SIFT technique the measured rate coefficient for reaction (6.11) was 1.2 x 10^{-9} cm^3 s^{-1}, the same (within experimental error) as the ICR result of 1.7 x 10^{-9} cm^3 s^{-1}.

The ions C_2H^+ and $C_2H_2^+$ were both generated by electron impact on acetylene in the ion source. Upon the addition of C_2H_2, C_2H^+ produced $C_4H_2^+$ with a rate coefficient of 1.2 x 10^{-9} cm^3 s^{-1}, while $C_2H_2^+$ reacted with an overall rate coefficient of 1.2 x 10^{-9} cm^3 s^{-1} to produce three products; $C_4H_2^+$ (43%), $C_4H_3^+$ (48%) and an association adduct

Table 6.3: Reactions of selected ions with C_2H_2. The rate coefficients k listed are in units of 10^{-9} cm^3 s^{-1}, while the units for the ΔH° values are kJ mol^{-1}. Unless otherwise noted all the measurements presented in this table were performed at 0.30 Torr and 302±2 K.

no.	ion	products	B.R.	k	k(lit.)	k_L	$-\Delta H^\circ$
6.11	C_2^+	$C_4H^+ + H$	1.0	1.2	1.7[a], 2.6[b]	1.2	381
6.12	C_2H^+	$C_4H_2^+ + H$	1.0	1.2	1.7[a], 1.5[c] 2.5[b]	1.2	186
6.13	$C_2H_2^+$	$C_4H_2^+ + H_2$	0.43	1.2	1.4[a,b,d]	1.2	100
		$C_4H_3^+ + H$	0.48		1.2[e]		65
		$C_2H_2^+ . C_2H_2$	0.07				326[g]
6.14	C_4^+	$C_6H^+ + H$	1.0	~1.4	1.5[a]	1.1	~319
6.15	C_4H^+	$C_6H_2^+ + H$	1.0	1.4	1.5[a]	1.1	~219
6.16	$C_4H_2^+$	$C_4H_2^+ . C_2H_2$	>0.98	1.3	0.14[a], 0.33[f]	1.1	~374
		$C_6H_3^+ + H$	<0.02		0.23[c], 0.1[b]		~279[g]
6.17	$C_4H_3^+$	$C_4H_3^+ . C_2H_2$	1.0	0.95	0.24[a], 0.21[f] ~0.04[c]	1.1	~322[g]
6.18	$C_4H_4^+$	$C_4H_4^+ . C_2H_2$	>0.98	0.48[h]	0.12[a]	1.1	~444[j]
		$C_6H_5^+ + H$	<0.02	<0.1[i]			
6.19	C_6H^+	$C_6H^+ . C_2H_2$	major	~0.9		1.0	~219
		$C_8H_2^+ + H$	minor				~757
6.20	$C_6H_2^+$	$C_6H_2^+ . C_2H_2$	major	0.9		1.0	~329
		$C_8H_3^+ + H$	minor				~502
6.21	$C_6H_3^+$	$C_6H_3^+ . C_2H_2$	>0.98	~0.25		1.0	~362
		$C_8H_4^+ + H$	<0.02				~36[k]
6.22	$C_6H_4^+$	$C_6H_4^+ . C_2H_2$	>0.98	~0.07	cyclic	1.0	~365[j]
		$C_8H_5^+ + H$	<0.02	~0.01	acyclic		~360[j]
6.23	$C_6H_5^+$	$C_6H_5^+ C_2H_2$	>0.98	~0.4	cyclic	1.0	~533[j]
		$C_8H_6^+ + H$	<0.02	~0.01	acyclic		~183[j,k]
6.24	$C_6H_6^+$	-	1.0	<0.0001		1.0	~240
6.25	$C_6H_7^+$	-	1.0	<0.0001		1.0	~224
6.26	H_2CN^+	$H_2CN^+ . C_2H_2$	1.0	0.0038		1.2	?
				0.0052[l]			

(a) Reference 85.
(b) " 150.
(c) " 149.
(d) Reference 151.
(e) " 152.
(f) " 145.

(g) These values represent the overall ΔH° for formation of the highest energy isomer involved.
(h) The rate coefficient of the linear $C_4H_4^+$ ion.
(i) The rate coefficient of the cyclic methylene cyclopropene ion.
(j) These values represent the overall ΔH° after reaction of the lowest energy isomer involved.
(k) The error limits of these ΔH° values are such that labelled channels may be exothermic.
(l) Measured at a pressure of 0.40 Torr.

$C_2H_2^+.C_2H_2$ (7%). The measured rate coefficient for reaction (6.13) was invariant over the pressure range 0.30-0.38 Torr. Figure 6.0 shows typical data observed for the reaction of $C_2H_2^+$ with C_2H_2. The rate coefficient and product distribution measured for reaction (6.13), shown in table 6.3, also agree with previous ICR studies of the reaction[85,149,150] with the exception of the association product channel which would not be observed in a low pressure ICR experiment. The rate coefficient measured in this study for the reaction of the ion C_2H^+ with C_2H_2 (6.12) is in agreement with recent ICR determinations[150,85] of 1.5 x 10^{-9} cm^3 s^{-1} and 1.7 x 10^{-9} cm^3 s^{-1}.

Reactions (6.14-6.18) $C_4H_n^+$ (n= 0 to 4) with acetylene

The ions C_4^+ and C_4H^+ were both observed to react with C_2H_2 through hydrogen atom elimination from the respective collision complexes to produce the ions C_6H^+ and $C_6H_2^+$. The measured rate coefficients, ~1.4 x 10^{-9} cm^3 s^{-1} for C_4^+ and 1.4 x 10^{-9} cm^3 s^{-1} for C_4H^+, and the observed product distributions are in good agreement with the results of Anicich et al[85] (shown in table 6.3). C_4^+ was generated by electron impact on vinyl acetylene (C_4H_4), while C_4H^+ was generated by electron impact on C_4H_4 and C_4H_2 and also by chemical reaction between C_2^+ and C_2H_2 in the ion source (table 6.1). No difference in the measured rate coefficient was observed for the reaction between C_4H^+ and C_2H_2 when C_4H^+ was produced from the different sources listed above.

$C_4H_2^+$ was also formed in the ion source using several

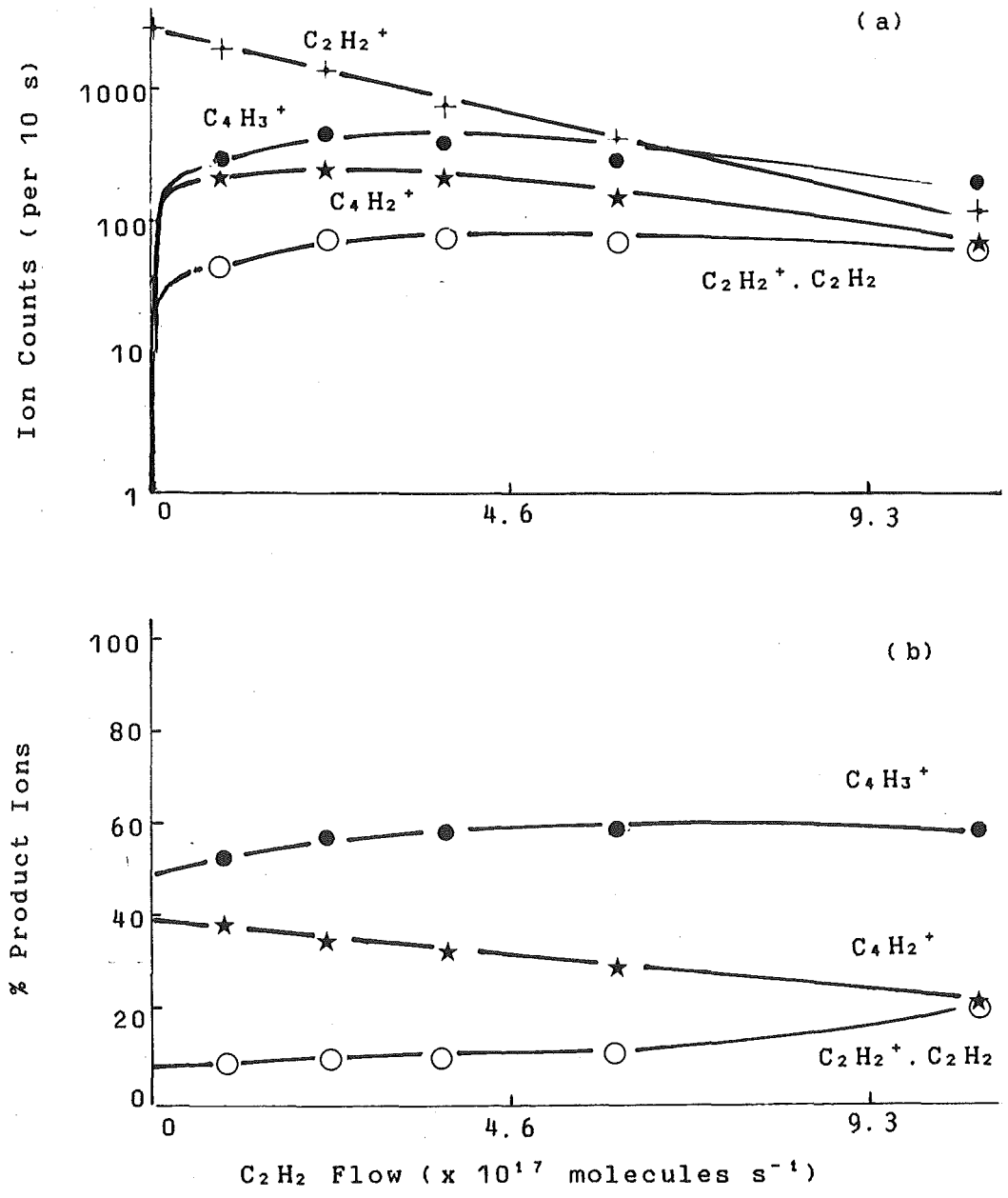

Fig. 6.0: Data obtained for the reaction of $C_2H_2^+$ with C_2H_2.
(a) Ion count versus C_2H_2 flow for this reaction.
(b) Product ion percentage versus C_2H_2 flow.

methods similar to those used to produce C_4H^+; viz., by reaction of C_2H^+ and $C_2H_2^+$ with C_2H_2 in the ion source and by electron impact on the neutrals C_4H_2 and C_4H_4. After addition of C_2H_2, the dominant product channel observed for reaction (6.16), with all three methods of production of the primary ion, was association to form the adduct $C_4H_2^+.C_2H_2$. When generating $C_4H_2^+$ from C_4H_2, the adjacent ions at m/e= 49 and m/e= 51 were present at less than 4% in total of the parent $C_4H_2^+$ ion signal. The presence of these impurity ions meant that an upper limit only (<2%) could be determined for a possible product at m/e= 75, $C_6H_3^+$, along with the dominant product ion, the adduct $C_4H_2^+.C_2H_2$ (>98%). The upper limit of 2% was set after subtraction of the C_4H^+ impurity ion contribution ($C_4H^+.C_2H_2$) to the peak at 75 amu from reaction (6.15).

The adduct ion was reported by Anicich et al[85], but not by Brill and Eyler[145] in separate low pressure ICR studies of reaction (6.16). The rate coefficient for the reaction of $C_4H_2^+$ (reaction 6.16) was measured to be 1.3×10^{-9} cm^3 s^{-1} over the pressure range 0.29-0.38 Torr, in contrast to the recent low pressure ICR results[85,145] of 1.4×10^{-10} cm^3 s^{-1} and 3.3×10^{-10} cm^3 s^{-1} where collisional stabilisation of reaction intermediates would have been very slow.

The ion $C_4H_3^+$ was produced in a similar way to the ions C_4H^+ and $C_4H_2^+$; viz., by electron impact on C_4H_2 and C_4H_4, and also by chemical reaction between $C_2H_2^+$ and C_2H_2. The reaction with acetylene produced the association adduct $C_4H_3^+.C_2H_2$ with a pseudo second order rate coefficient of 9.5×10^{-10} cm^3 s^{-1} over the pressure range 0.22-0.40 Torr. The

association adduct was also the only product observed in the previous investigations of this reaction, even at very low pressures[85,145,149].

$C_4H_4^+$ was formed by electron impact on vinyl acetylene. Upon the addition of C_2H_2 two separate exponential decay regimes were observed for the $C_4H_4^+$ ion (see figure 6.1). The rate coefficient of the faster decay was measured to be 4.8×10^{-10} cm^3 s^{-1}, while that of the slower one was $<1 \times 10^{-10}$ cm^3 s^{-1}. Wagner-Redeker et al[153], who also observed two decays for this reaction, interpreted their results in terms of two structural isomers of $C_4H_4^+$, one reactive and one non-reactive with C_2H_2. These isomers are discussed further in section 6.4.

A single reaction channel to produce the association adduct $C_4H_4^+.C_2H_2$ was observed in this study for the reaction of $C_4H_4^+$ (reaction (6.18)). In the low pressure ICR study of Anicich et al[85] three reaction products were reported; $C_6H_4^+$ (10%), $C_6H_5^+$ (75%) and the association adduct $C_4H_4^+.C_2H_2$ at 15%. These products were also observed in an earlier high pressure and tandem mass spectrometer study[154] at pressures between 0.1 and 0.3 Torr, but no branching ratios were reported. In this SIFT study two foreign ions, the adjacent mass peaks at m/e= 51 (<10%) and m/e= 53 (<10%), were present in the $C_4H_4^+$ ion swarm created for reaction (6.18). As both these adjacent ions were observed to cluster only with C_2H_2, a limit of <2% could be placed on the formation of the ion $C_6H_5^+$ as a product ion from the reaction of $C_4H_4^+$ with C_2H_2 in this study.

Possibly the discrepancy between the observed products of

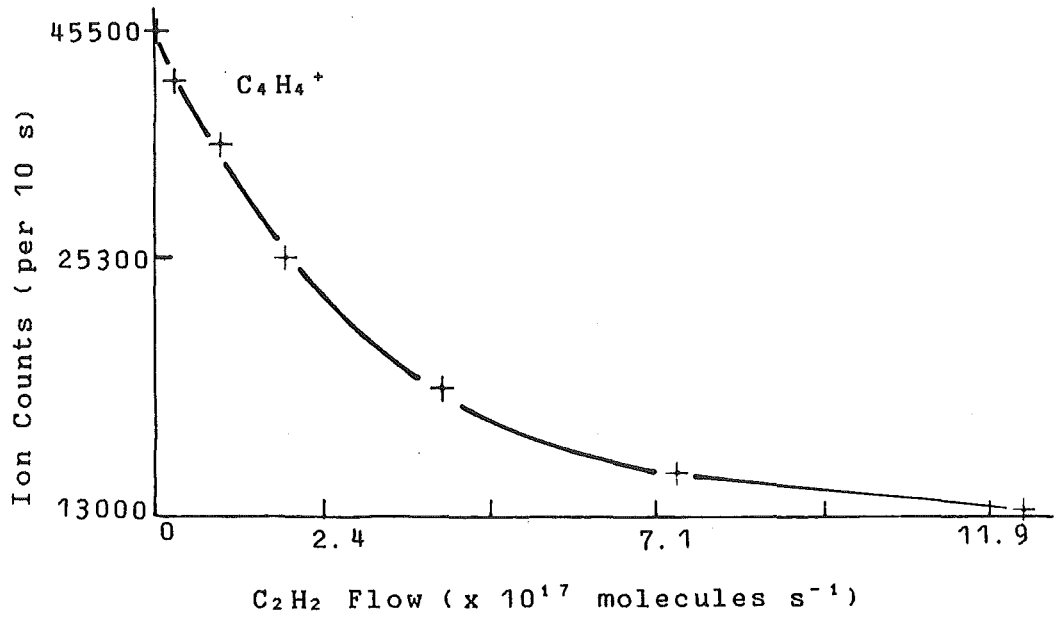

Fig. 6.1: Semilogarithmic plot of the $C_4H_4^+$ (m/e= 52) ion count versus the flow of C_2H_2.

reaction (6.18) for this SIFT study and those of the earlier studies[85,154] arises from the inability in both the ICR cell work[85] and the high pressure mass spectrometer work[154] to generate the $C_4H_4^+$ ion in isolation. Also, in our SIFT measurements performed at pressures of 0.3 Torr, the lifetime of the $(C_4H_4^+.C_2H_2)^*$ complex towards product formation apart from the adduct $C_4H_4^+.C_2H_2$ may be shortened, especially with respect to the ICR results.

As noted above, previous low pressure studies[85,154,145,149] of the reactions of C_2H_2 with $C_4H_2^+$ (6.16), $C_4H_3^+$ (6.17) and $C_4H_4^+$ (6.18) have observed the formation of association products in each case. Brill and Eyler[145] suggested that the adduct intermediates formed from reactions (6.16) and (6.17), $(C_4H_2^+.C_2H_2)^*$ and $(C_4H_3^+.C_2H_2)^*$, were collisionally stablised even at pressures as low as 2×10^{-6} Torr. If this were so then, at a pressure of 2×10^{-6} Torr, reaction (6.16) would have a termolecular rate coefficient of $\sim 5 \times 10^{-21}$ cm^6 s^{-1}. Because such a value for collisional stabilisation is unacceptably large, Anicich et al[85] have concluded that the observed association intermediates are more likely to be stablised by radiation rather than collision at low pressures.

Reactions (6.19-6.25) $C_6H_n^+$ (n= 1, 2, 3, 4, 5, 6, 7) with acetylene

The ions $C_6H_n^+$ (n= 1-7) were formed by electron impact on benzene, while the ions $C_6H_n^+$ (n= 1, 2, 4, 5) were also produced by chemical reaction between C_4^+, C_4H^+, $C_4H_2^+$, and $C_4H_3^+$ with C_2H_2 at portal 1 (table 6.1). In the latter method the

$C_4H_n^+$ ions with n= 0, 1, 2 and 3 were formed in the ion source by electron impact on C_4H_2.

C_6H^+ and $C_6H_2^+$ were both observed to react with C_2H_2 through two channels, in each case a major association channel and a minor channel in which an H atom was lost from the reaction intermediate complex before collisional stabilisation. It was not possible to measure accurately the product distributions for either C_6H^+ or $C_6H_2^+$ because neither of these ions were able to formed free of impurity ions (Table 6.1). For $C_6H_2^+$ (reaction (6.20)) the product ions $C_6H_2^+.C_2H_2$ and $C_8H_3^+$ were produced with an overall rate coefficient of 9.0×10^{-10} cm^3 s^{-1}, while C_6H^+ formed $C_6H^+.C_2H_2$ and $C_8H_2^+$. The rate coefficient for the reaction of C_6H^+ (6.19), whilst not accurately measured, was observed to be approximately the same as that for $C_6H_2^+$ (ie ~9×10^{-10} cm^3 s^{-1}).

The ions $C_6H_3^+$ (6.21), $C_6H_4^+$ (6.22), $C_6H_5^+$ (6.23), $C_6H_6^+$ (6.24) and $C_6H_7^+$ (6.25) were all observed to form association adducts upon the addition of C_2H_2. However of these ions, only $C_6H_6^+$ and $C_6H_7^+$ were able to be injected into the flow tube in the absence of significant impurity ion peaks. Therefore for the ions $C_6H_3^+$, $C_6H_4^+$ and $C_6H_5^+$, in addition to association, competition from H atom elimination from the reaction intermediate complex leading to $C_8H_4^+$ (reaction (6.21)), $C_8H_5^+$ (reaction (6.22)) and $C_8H_6^+$ (reaction (6.23)) may also have occurred with product distributions of up to 2%. For the reactions of the $C_6H_3^+$ and $C_6H_5^+$ ions this alternative reaction channel is endothermic by ~36 and ~18 kJ mol^{-1} respectively (table 6.3). It is therefore unlikely that

hydrogen atom elimination is a viable process for reactions (6.21) and (6.23). Brill and Eyler[145] observed the association product ion $C_8H_6^+$ for the reaction of $C_6H_4^+$ with C_2H_2 and both the ions $C_8H_6^+$ and $C_8H_7^+$ for the reaction of the $C_6H_5^+$ ion with C_2H_2. These authors did not report either rate coefficients or product distributions in their ICR study of these reactions.

In this study a rate coefficient of 2.5×10^{-10} cm^3 s^{-1} was measured for the reaction of $C_6H_3^+$ with C_2H_2.

$C_6H_4^+$, when formed **from benzene**, associated with C_2H_2 at a rate coefficient of 7.0×10^{-11} cm^3 s^{-1} (at 0.30 Torr). However, when $C_6H_4^+$ was generated **from the reaction between $C_4H_2^+$ and C_2H_2** the rate coefficient for reaction (6.22) dropped to 1.2×10^{-11} cm^3 s^{-1} at a pressure of 0.30 Torr. These two different decay rates for reaction (6.22), when the $C_6H_4^+$ ion was produced from the two methods, are shown in figure 6.2. Both semilogarithmic decays for the ion signal were linear indicating that a single, but different, $C_6H_4^+$ isomer was formed from the respective methods of ion generation. The most likely isomer formed through chemical reaction between $C_4H_2^+$ and C_2H_2 is the acyclic ion shown in structure (2).

$$HC{\equiv}C\text{-}C^{+}{=}C^{\cdot}\text{-}CH{=}CH_2 \qquad (2)$$

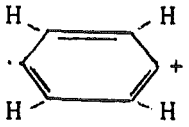

(3)

The cyclic ion (structure (3)) is the probable result of electron impact on benzene. The observation of single exponential decays in reaction (6.22) for both types of the

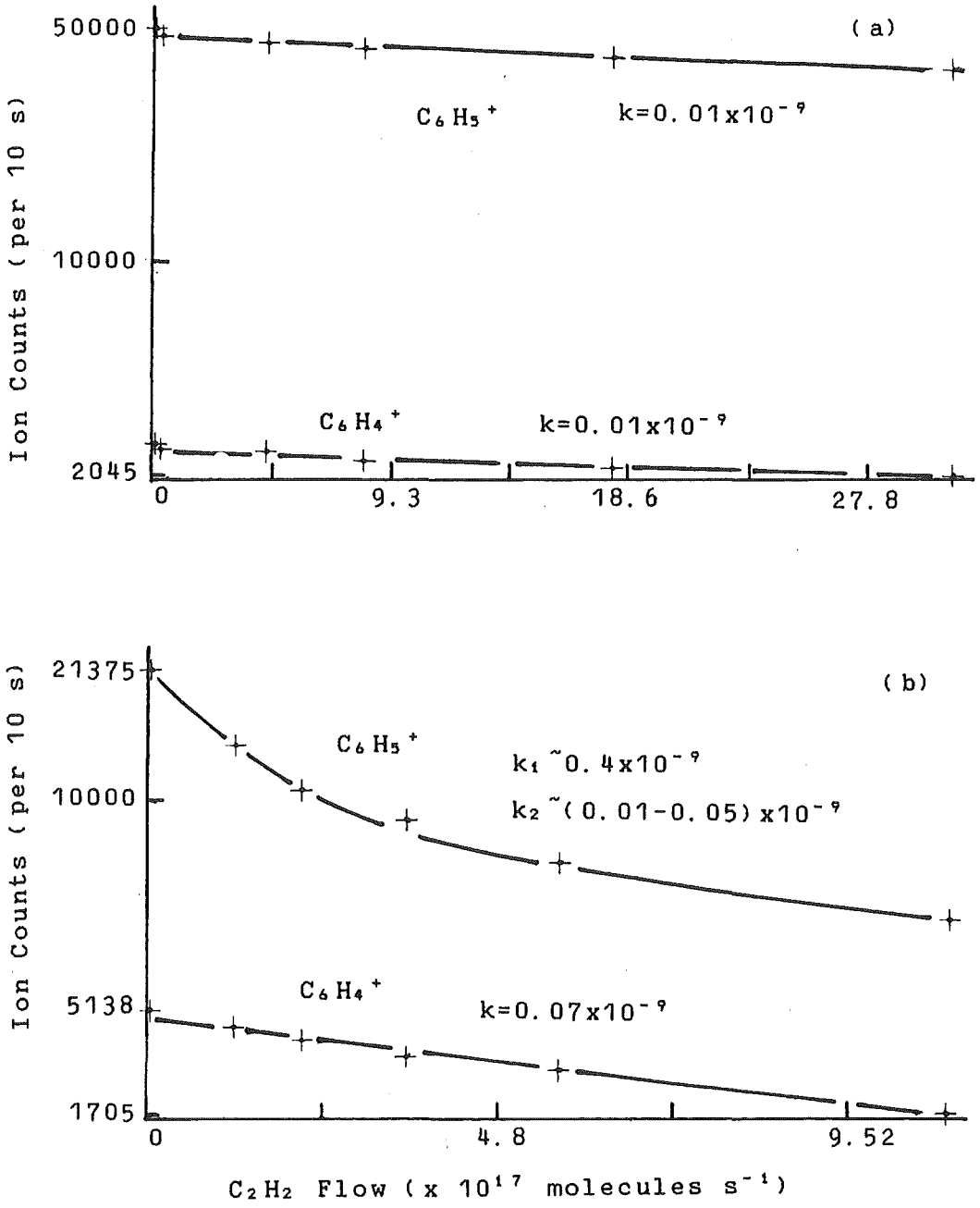

Fig. 6.2: Semilogarithmic plots of the $C_6H_4^+$ (m/e= 76) and $C_6H_5^+$ (m/e= 77) ion counts versus the flow of C_2H_2 where the primary ions were generated by
(a) The reactions between C_2H_2 and $C_4H_2^+$ and $C_4H_3^+$ respectively.
(b) Electron impact on C_6H_6.

$C_6H_4^+$ ion indicates that the barrier to isomerisation between the acyclic and cyclic isomers is large. Ausloos[155] has also observed evidence for two isomers of $C_6H_4^+$ in the reactions of this ion with benzene after generation by 30 eV electron impact on benzene in an ICR cell.

Evidence for two separate isomers was also noted for the ion $C_6H_5^+$ upon reaction with C_2H_2 (reaction (6.23)). When $C_6H_5^+$ was generated from the reaction of $C_4H_3^+$ with C_2H_2 (reaction (6.17)) at portal 1, a single (pseudo second order) decay with a rate coefficient of 1.0×10^{-11} cm^3 s^{-1} (at 0.30 Torr) for $C_6H_5^+$ was observed upon the addition of C_2H_2 at portal 2 (see fig. 6.2a). When the $C_6H_5^+$ ion was generated by electron impact on benzene however, two separate exponential components were observed for the decay of the ion upon reaction with C_2H_2 (see figure 6.2b). The rate coefficient for the slower exponential decay approximately equalled the value above (between 1 and 5×10^{-11} cm^3 s^{-1} at 0.30 Torr), while that for the more rapid decay was measured to be 4.0×10^{-10} cm^3 s^{-1}. In each case the only product ion observed for reaction (6.23) was the association adduct $C_6H_5^+.C_2H_2$.

Eyler and Campana[146] have recently conducted an extensive pulsed ICR mass spectrometer study of the behaviour of a number of $C_6H_5^+$ ion species upon the addition of C_2H_2. They concluded that the cyclic $C_6H_5^+$ phenylium ion (structure (4)), produced by chemical ionisation of a number of halobenzenes, was unreactive to C_2H_2, while the acyclic $C_6H_5^+$ isomer (5), which they produced through the reaction of $C_2H_2^+$ and C_2H_2 to give $C_4H_3^+$ followed by further addition of C_2H_2, reacted further to produce both cyclic and acyclic ions.

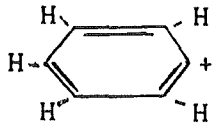

(4)

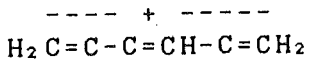

(5)

In the present study the cyclic isomer of $C_6H_5^+$ was generated by electron impact on benzene, rather than through the halogenation reactions (such as reaction (6.27)) ultilised by Eyler and Campana[146].

$$CH_5^+ + C_6H_5F \rightarrow C_6H_5^+ + HF + CH_4 \qquad (6.27)$$

The observation of two separate exponential decay regimes in this study for the reaction of the $C_6H_5^+$ ion, when formed by electron impact on benzene, suggests that some interconversion to the acyclic structure has occurred in the ion source. In contrast, Eyler and Campana observed only a single decay for the reaction of $C_6H_5^+$ ions with C_2H_2 in their ICR study after generating the cyclic $C_6H_5^+$ isomers through dehalogenation reactions . In accord with the conclusions of these authors, the slower decay observed in this study will result from the cyclic $C_6H_5^+$ ion while the faster will be due to the acyclic ion. This result suggests that the single slow rate coefficient observed for the reaction of the $C_6H_5^+$ ion with C_2H_2, when generated from $C_4H_3^+$ and C_2H_2, is also due to a cyclic isomer being formed.

The observation in the ICR work of two separate decays for reaction (6.23) when $C_6H_5^+$ was formed through the reaction of $C_4H_3^+$ and C_2H_2, in contradiction to the single decay seen in this study, has two possible explanations:

1. Internally excited $C_6H_5^+$ ions of a single isomeric

structure (either vibrationally or electronically excited or both) formed in the ICR cell at low pressures (~10^{-6} Torr), may have reacted at different rates.

2. The initial presence of internally excited $C_4H_3^+$ ions (formed through the reaction of $C_2H_2^+$ with C_2H_2) in reaction (6.23), may have resulted in the production of both the cyclic and acyclic $C_6H_5^+$ isomers.

MINDO/3 calculations performed by Tasaka et al[156] have indicated that interconversion from either of two possible acyclic $C_6H_5^+$ structures to the cyclic phenylium ion can occur with as little as 197 kJ mol^{-1} of excess internal energy (the activation energy required for the reverse process was estimated to be at least 65 kJ mol^{-1}). The reaction of $C_2H_2^+$ with C_2H_2 (reaction (6.13)) occurs to form $C_4H_3^+$ with an overall exothermicity of ~65 kJ mol^{-1}, while the cyclic and acyclic $C_6H_5^+$ isomers are produced in the reaction of $C_4H_3^+$ and C_2H_2 (reaction (6.17)) with ~347 kJ mol^{-1} and ~322 kJ mol^{-1} of excess energy respectively. In the ICR cell internally excited $C_4H_3^+$ may therefore have resulted in the formation of both excited acyclic and cyclic isomers for reaction (6.23), as has been observed[146]. With the SIFT technique however, the excess internal energy produced in forming $C_6H_5^+$ through reactions (6.13) and (6.17) will be rapidly removed by third body collision.

When C_2H_2 is added to collisionally stabilised $C_4H_3^+$ in the flow tube, both isomers of $C_6H_5^+$ will be produced initially. This is because the internal energies of both the acyclic and cyclic ions are likely to be greater than the top of the isomerisation barrier between the two ions. Therefore

the isomeric structures will be continously interconverting in the flow tube until their internal energies are reduced through third body collision to less than that required to surmount this barrier. The observation of a single decay for reaction (6.23) when the $C_6H_5^+$ ion was formed from acetylene precursor ions in the SIFT has two possible explanations.

1. The excited $(C_6H_5^+)^*$ intermediate initially formed has relaxed to a single isomeric structure because this structure has by far the higher density of accessible vibration-rotation states. If it is assumed that the faster decay observed in the reaction of $C_6H_5^+$ (when generated from C_6H_6) with C_2H_2 resulted from acyclic $C_6H_5^+$ then this isomer will have a cyclic structure.

2. Either the overall energies of formation for the acyclic and cyclic ions from the reaction of $C_4H_3^+$ with C_2H_2 at 322 and 347 kJ mol^{-1} respectively are incorrect, or the activation energy required to surmount the barrier to isomerisation has been underestimated by Tasaka et al[156].

The former explanation for the behaviour of the $C_6H_5^+$ ion (when formed from reaction of $C_4H_3^+$ with C_2H_2) observed in this study is unlikely. This is because two separate exponential decays were observed for reaction (6.23) when $C_6H_5^+$ was formed by electron impact on C_6H_6. The cyclic and acyclic $C_6H_5^+$ structures therefore once formed are both collisionally stabilised because each has available a sufficient number of internal states for energy storage. Therefore, if the $(C_6H_5^+)^*$ intermediate initially formed in the reaction of $C_4H_3^+$ with C_2H_2 (reaction (6.17)) has sufficient energy available to interconvert between the acyclic and cyclic

structural isomers, both forms will result from the reaction.

If the collisionally stablised $C_4H_3^+$ ions react with C_2H_2 to form only internally excited cyclic $(C_6H_5^+)^*$ ions (ie. formation of the acyclic $C_6H_5^+$ isomer is endothermic) and if the top of the barrier to isomerisation to an acyclic structure is above the initial internal energy of the complex then only collisionally stablised cyclic $C_6H_5^+$ ions will be formed in the flow tube. If the reaction of cyclic $C_6H_5^+$ ions with C_2H_2 is slower than the equivalent acyclic reaction, as observed in the ICR study of Eyler and Campana[146], the single decay observed in this SIFT study for the reaction of $C_6H_5^+$ (when formed from acetylene precursor ions) with C_2H_2 will therefore result from cyclic $C_6H_5^+$ ions only.

The question of identification of the isomeric forms of the $C_6H_5^+$ ions involved in this study is addressed futher in Chapter Seven.

The ions $C_6H_6^+$ and $C_6H_7^+$ were observed to react only very slowly with C_2H_2, the overall decay rate coefficients for both ions being less than 1×10^{-13} cm^3 s^{-1}. No reaction products were noted for either ion, even at high flows (10^{18} molecules s^{-1}) of C_2H_2.

Reaction (6.26) H_2CN^+ with acetylene

To investigate the reaction of H_2CN^+ with C_2H_2, a swarm of H_2CN^+ ions was produced by electron impact on a 20:1 mixture of H_2 and HCN. The adjacent impurity peaks at m/e= 27

and m/e= 29 were present in the flow tube at less than 0.8% and 2.7% of the primary ion concentration respectively. The proton affinity of HCN (718 kJ mol^{-1} [92]) is 77 kJ mol^{-1} higher than the PA (C_2H_2) (641 kJ mol^{-1} [92]). Therefore, as expected, upon the addition of C_2H_2 no proton transfer channel was observed, as was evidenced by a very slow decay of the H_2CN^+ ion. Instead the association adduct $H_2CN^+.C_2H_2$ was the dominant ion formed. A product ion at m/e= 60, of unknown configuration, was also noted. This ion is presumably the result of a reaction between a very small impurity (probably acetone) in the acetylene neutral reagent and the primary ion H_2CN^+. After correction of the H_2CN^+ decay for this impurity, an upper limit of $<4 \times 10^{-28}$ cm^6 s^{-1} was measured for the rate coefficient of the ternary reaction (6.26) over a pressure range of 0.30-0.40 Torr.

6.4 REACTIONS WITH HYDROGEN CYANIDE.

The rate coefficients and product distributions for the reactions discussed in the following section are listed in table 6.4, along with the relevant collision limit rate coefficient, previous literature results and where known the overall reaction exothermicity. Tables 2.0 (section 2.5) and 6.1 (section 6.2) detail the methods of generation used for each ion discussed in the next section, along with the relevant impurity ions.

Table 6.4: Reactions of selected ions with HCN. Rate coefficients, k, are in units of 10^{-9} cm^3 s^{-1} and the units of the overall reaction enthalpy changes, ΔH°, are kJ mol^{-1}. All the measurments presented in this table were performed at 0.3 Torr.

no.	ion	products	B.R.	k	k(lit.)	k_{ADO}	$-\Delta H^\circ$
6.28	C_2^+	$C_2H^+ + CN$	0.04	1.9	2.6[a], 2.8[b]	3.1	60
		$C_3H^+ + N$	0.26				34
		$C_3N^+ + H$	0.46				59[c]
		$C_2^+.HCN$	0.24				657
6.29	C_2H^+	$C_2H_2^+ + CN$	0.22	2.7	2.7[a], 2.8[b]	3.1	4
		$H_2CN^+ + C_2$	0.33				-11
		$HC_3N^+ + H$	0.45				79
6.30	$C_2H_2^+$	$H_2CN^+ + C_2H$	0.05	0.35	0.36[a], 0.39[b]	3.1	46
		$H_2C_3N^+ + H$	0.15				106
		$C_2H_2^+.HCN$	0.80				?
6.31	C_4^+	$C_4H^+ + CN$	<0.02	2.7	2.8[a]	2.7	10
		$C_3N^+ + H$	>0.06				<-213[d]
		$C_4^+.HCN$	>0.92				?
6.32	C_4H^+	$C_4H^+.HCN$	>0.97	2.6	1.7[a]	2.7	?
		$HC_3N^+ + H$	<0.03				<-228[d]
6.33	$C_4H_2^+$	$C_4H_2^+.HCN$	1.0	0.28	<0.02[a]	2.6	?
6.34	$C_4H_3^+$	$C_4H_3^+.HCN$	1.0	0.34	<0.05[a]	2.6	?
6.35	$C_4H_4^+$	$C_4H_4^+.HCN$	>0.97	0.043	<0.03[a]	2.6	?
		$H_4C_3N^+ + H$	<0.03				?
6.36	$C_4H_5^+$	$C_4H_5^+.HCN$	1.0	~0.05		2.6	?
6.37	$C_4H_6^+$	$C_4H_6^+.HCN$	1.0	~0.0002		2.6	?
6.38	$C_4H_7^+$	-	1.0	<0.0001		2.6	?
6.39	$C_4H_8^+$	-	1.0	<0.0001		2.6	?
6.40	$C_6H_2^+$	$C_6H_2^+.HCN$	1.0	~0.3		2.5	?
6.41	$C_6H_4^+$	$C_6H_4^+.HCN$	1.0	0.013		2.5	151[e]
6.42	$C_6H_5^+$	$C_6H_5^+.HCN$	1.0	~0.001		2.5	?

(a) Reference 85.
(b) " 72.
(c) Formation of the higher energy C_3N^+ isomer is endothermic by 26 kJ mol^{-1}.
(d) Upper limits only as the ΔH_f° values of C_3N^+ and HC_3N^+ (Table 3.3) are upper limits.
(e) Assumes formation of a cyclic ion from the cyclic benzyne ion.

Reactions (6.28-6.30) $C_2H_n^+$ (n= 0-2) with hydrogen cyanide

C_2^+ was formed by electron impact on either of the two neutrals C_2Cl_4 or trichloroethylene (C_2HCl_3). When formed from C_2Cl_4, a swarm of pure C_2^+ ions could be produced in the flow tube. Upon the addition of HCN four product peaks, corresponding to the ions C_3N^+ (46%), C_3H^+ (26%), C_2^+.HCN (24%) and C_2H^+ (4%), were produced with an overall rate coefficient of 1.9×10^{-9} cm^3 s^{-1} (figure 6.3 gives a graphical presentation of this data). No difference was observed in either the product distribution or the rate coefficient in reaction (6.28) for both sources of C_2^+. In each case a single exponential decay only was observed for the reaction of C_2^+ with HCN.

In an earlier SIFT study MacKay et al[72] observed a single product, the ion C_3N^+, while in a recent low pressure ICR study Anicich et al[85] observed the products C_2H^+, C_3H^+ and C_3N^+ for reaction (6.28). In the ICR study C_2^+ was formed through electron impact on C_2H_2. The product distribution observed in the ICR investigation of reaction (6.28) was in agreement with this study, with the exception of the collision-stabilised adduct C_2^+.HCN which is produced only slowly under the low pressure conditions of an ICR cell. MacKay et al[72] in their SIFT study formed C_2^+ ions through chemi-ionisation of C_2H_2 by helium ions in a flowing afterglow ion source. They possibly encountered complications in the analysis of product ions for reaction (6.28) from the reaction products of the adjacent ions C_2H^+ and $C_2H_2^+$.

For the reactions of the ions C_2H^+ and $C_2H_2^+$ with HCN no

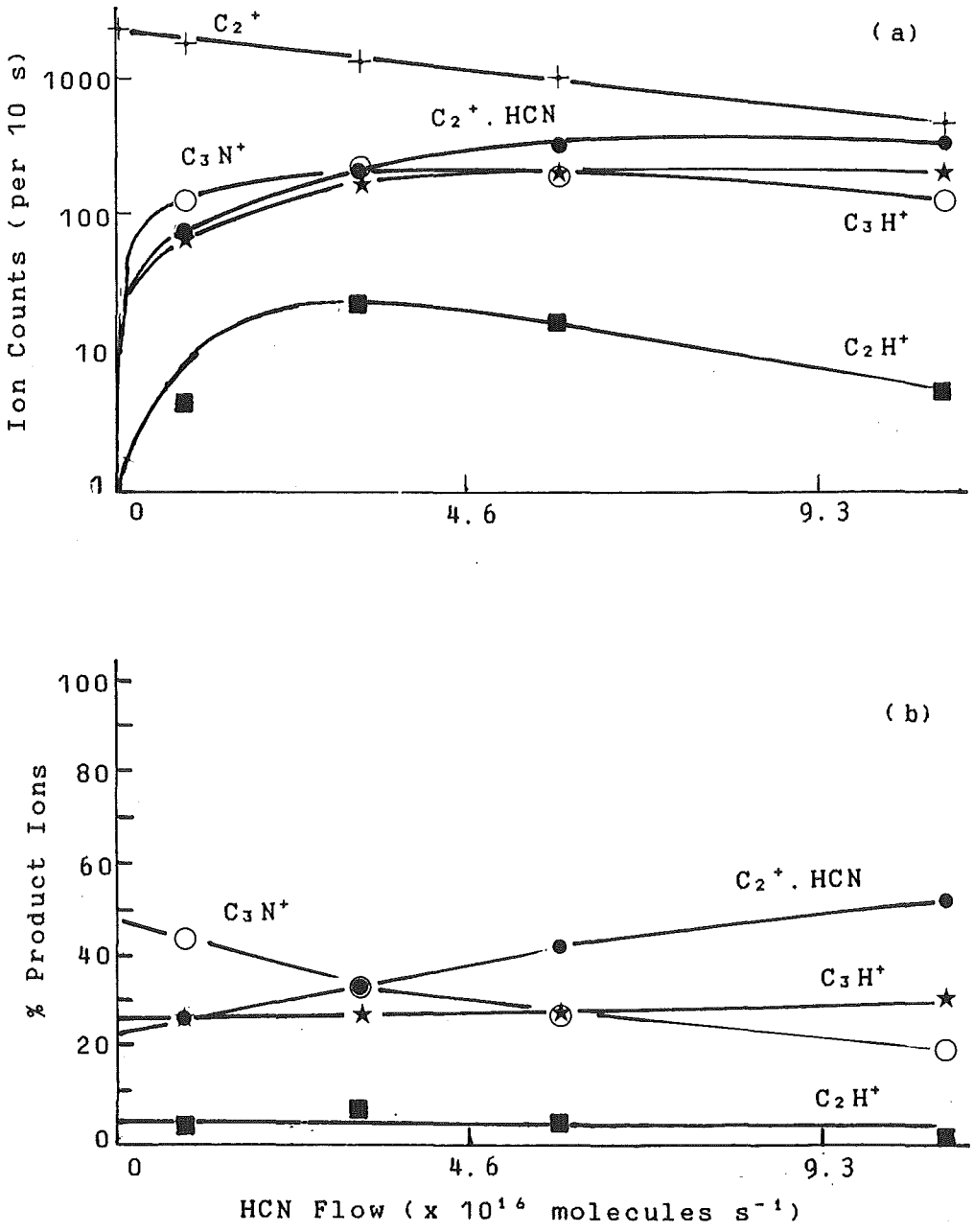

Fig. 6.3: Data obtained for the reaction of C_2^+ with HCN.
(a). Ion count versus flow for this reaction.
(b). Product ion percentage versus HCN flow.

evidence was observed for the presence of internally excited or metastable ions in the flow tube. No differences in rate coefficients or product distributions were noted for either reaction when differing sources were used for either primary ion.

C_2H^+ was formed by electron impact upon either C_2H_2 or C_2HCl_3. For the latter neutral the adjacent ions C_2^+ and $C_2H_2^+$ (formed by ion-molecule reactions in the ion source at pressures >1 x 10^{-4} torr) and H_3O^+ were present at 12%, 7% and 10% respectively of the primary ion concentration. The products HC_3N^+ (45%), H_2CN^+ (33%) and $C_2H_2^+$ (22%) were formed upon addition of HCN with an overall rate coefficient of 2.7 x 10^{-9} cm^3 s^{-1}. Figure 6.4 shows a typical set of data for the reaction of C_2H^+ with HCN (6.29). An alternative to the product ion assignment of $C_2H_2^+$ at m/e= 26 is the ion CN^+, but as its production is endothermic by 254 kJ mol^{-1} it has been disregarded. MacKay et al did not report the hydrogen abstraction product ion, $C_2H_2^+$, for reaction (6.29) in their SIFT study[72].

$C_2H_2^+$ was generated by electron impact on C_2H_2 and also dibromoethylene ($C_2H_2Br_2$). Impurity ion peaks in the $C_2H_2^+$ swarm created with the latter neutral were observed at m/e= 19 (H_3O^+, 2%), 25 (C_2H^+, 1.4%), 27 ($C_2H_3^+$, 1.4%), and 28 (N_2^+, 4.2%). The observed product distribution for this reaction was as follows; 80% of the association adduct $C_2H_2^+.HCN$; 15% of the ion $H_2C_3N^+$; and 5% of the H_2CN^+ ion. The results of the two previous studies[72,85] shown in table 6.4 are in agreement with the data reported for this study.

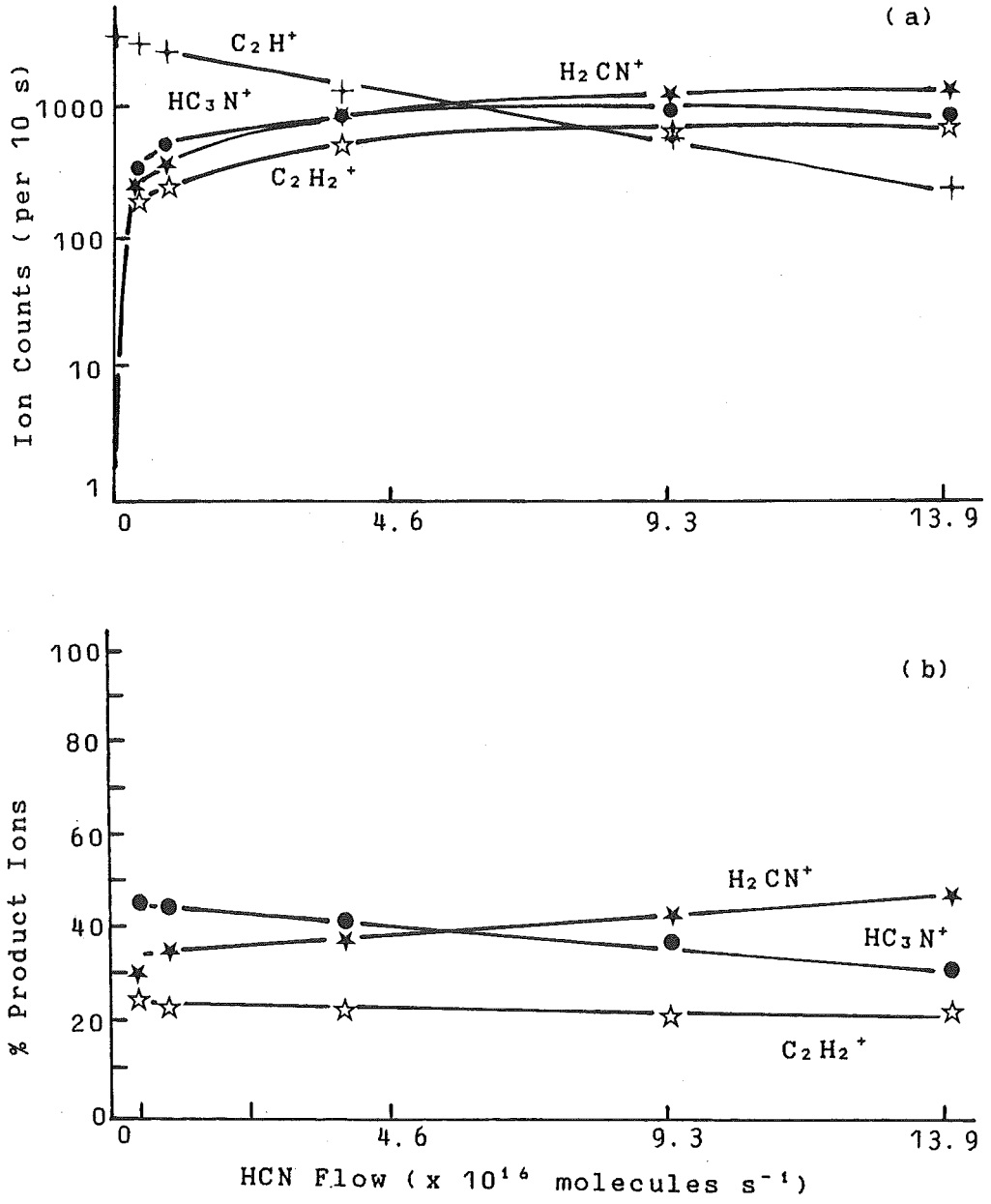

Fig. 6.4: Data obtained for the reaction of C_2H^+ with HCN.
(a). Ion count versus flow for this reaction.
(b). Product ion percentage versus HCN flow.

Reactions (6.31-6.39) $C_4H_n^+$ (n= 0-8) with hydrogen cyanide

The ions $C_4H_n^+$ (n= 0-3) were produced by electron impact on diacetylene (C_4H_2). The ions $C_4H_n^+$ (n= 0-5) were produced by electron impact on vinyl acetylene (C_4H_4) and the ions $C_4H_n^+$ (n= 2-8) were produced by electron impact on 1,3-butadiene (C_4H_6). $C_4H_7^+$ and $C_4H_8^+$ were formed using high pressures (>1 x 10^{-4} Torr) of C_4H_6 in the ion source. It is probable that a significant proportion of the ion peaks at m/e= 55 and 56 resulted from ^{13}C containing isotopes of $C_4H_6^+$ and $C_4H_7^+$ respectively. Association was observed to be the dominant product channel for the reactions of all the ions $C_4H_n^+$ (n= 0-6) with C_2H_2. No significant differences in rate coefficients or product distributions were noted for all ions of type $C_4H_n^+$ where it was possible to form the ion from more than one neutral.

The reaction of C_4^+ with HCN gave association to form the adduct $C_4^+.HCN$ (94%) as the dominant channel, along with a minor channel to give C_3N^+ (6%). The overall rate coefficient for this reaction was measured to be 2.7 x 10^{-9} cm^3 s^{-1}, in good agreement with the low pressure ICR result of Anicich et al[85]. However, these authors also observed the ion C_4H^+ (30%) as a product for reaction (6.31). It was not possible in this study to produce C_4^+ in the flow tube free from approximately equal amounts of the impurity ion C_4H^+ with any of the neutral source gases used. No change in the simultaneous decay of the C_4H^+ ion was observed at high flows of HCN however, when C_4^+ was the primary ion of interest. This observation allowed a limit of <2% to be placed on the production of C_4H^+ from the

reaction of C_4^+ with HCN. If C_4H^+ had been a significant product channel for reaction (6.31), as suggested in the ICR study of Anicich et al[85], then production of C_4H^+ via reaction (6.31) would have resulted in a non-exponential decay of the C_4H^+ ion signal at high flows of HCN under flow tube conditions.

For the reaction of C_4H^+ with HCN (6.32) the major product ion produced was the adduct $C_4H^+.HCN$ and a rate coefficient of 2.6×10^{-9} cm^3 s^{-1} was measured at 0.30 Torr. Anicich et al[85] observed HC_3N^+ as the major product (95%) in their ICR study of the reaction of C_4H^+ with HCN, along with a small association channel (5%) which they assumed to be the result of radiative stabilisation at the low pressures of their study. When C_4H^+ was generated from electron impact on C_4H_2, the adjacent impurity ions at m/e= 48 and m/e= 50 were also present in the flow tube at 50% and 30% respectively of the primary ion concentration. An upper limit of <3% was able to be set for the potential occurrence of the product ion HC_3N^+ via reaction (6.32) upon the addition of HCN. The possibility remains however, that HC_3N^+ may be a very small product of reaction (6.32) as a significant error is involved in making the necessary correction for the large C_4^+ impurity ion contribution to the HC_3N^+ product ion peak.

For the reactions of $C_4H_2^+$ (6.33), $C_4H_3^+$ (6.34) and $C_4H_5^+$ (6.36) with HCN, association was confirmed as the only product channel in each case. Swarms of each of the ions $C_4H_2^+$, $C_4H_3^+$ and $C_4H_5^+$ were able to be created in the flow tube with a minimum number of impurity ions present (table 6.1), thus allowing unambiguous product assignment for each

reaction. The measured pseudo second order rate coefficients were 2.8 ($C_4H_2^+$), 3.4 ($C_4H_3^+$) and 0.5 ($C_4H_5^+$) x 10^{-10} cm^3 s^{-1} at a flow tube pressure of 0.30 Torr.

Two product channels were observed for the reaction of $C_4H_4^+$ with HCN (6.35); a major association channel to form the adduct $C_4H_4^+$.HCN and possibly a very small channel to form the ion $H_4C_5N^+$. Again the ion $C_4H_4^+$ could not be injected cleanly into the flow tube after electron impact on any of the hydrocarbons C_4H_2 (at high source pressures), C_4H_4 or C_4H_6. The cleanest source of $C_4H_4^+$ ions resulted from electron impact on C_4H_4, after which impurity ions at the adjacent mass peaks of m/e= 51 and 53 were 20% and 9% respectively of the m/e= 52 peak magnitude. As a result it was not possible to eliminate the occurrence of a channel leading to the production of $H_4C_5N^+$ in reaction (6.35). An upper limit of 3% for the possible production of the $H_4C_5N^+$ ion at 78 amu in reaction (6.35) was set after making appropriate correction for the production of $C_4H_3^+$.HCN at m/e= 78 by reaction of the impurity ion, $C_4H_3^+$, through reaction (6.34).

For the ion $C_4H_6^+$ (reaction 6.37) an association product channel resulting in the adduct ion $C_4H_6^+$.HCN was observed only at high flows of HCN (>7 x 10^{17} molecules s^{-1}), corresponding to a pseudo second order rate coefficient of ~2 x 10^{-13} cm^3 s^{-1}.

At neutral flow rates of HCN of ~8 x 10^{17} molecules s^{-1} no decay of either the $C_4H_7^+$ or $C_4H_8^+$ ion signals was detected, allowing an upper limit of <1 x 10^{-13} cm^3 s^{-1} to be placed upon the rate coefficients for the reactions of these two ions, $C_4H_7^+$ (6.38) and $C_4H_8^+$ (6.39) with HCN.

Reactions (6.40-6.42) $C_6H_n^+$ (n= 2,4,5) with hydrogen cyanide

The three ions $C_6H_2^+$, $C_6H_4^+$ and $C_6H_5^+$ were produced through chemical reaction between C_2H_2, introduced at inlet portal 1, and the injected ions C_4H^+ (reaction (6.15)), $C_4H_2^+$ (6.16) and $C_4H_3^+$ (6.17) respectively. These initial reactant ions were produced by electron impact on C_4H_2 in the ion source.

When the ions $C_6H_2^+$ and $C_6H_5^+$ were formed in this manner in the flow tube, impurity ion peaks were small; C_4H^+ was ~10% of the $C_6H_2^+$ ion signal while $C_4H_2^+$, $C_4H_3^+$ and $C_6H_4^+$ were ~3%, ~5% and ~4% respectively of the $C_6H_5^+$ ion signal. The only product channel observed for both the ions $C_6H_2^+$ and $C_6H_5^+$ upon the addition of HCN was association (table 6.4). Impurity peaks present after the formation of the $C_6H_4^+$ ion through reaction (6.16) were at m/e= 50 ($C_4H_2^+$, 7%), m/e= 74 ($C_6H_2^+$, 2.4%) and m/e= 77 ($C_6H_5^+$, 8%). As the two ions at m/e= 74 and m/e= 77 associated with HCN, association to give the adduct $C_6H_4^+$.HCN was confirmed as the only product channel for reaction (6.41).

The rate coefficients measured for reactions (6.40) ($C_6H_2^+$ with HCN) and (6.41) ($C_6H_4^+$ with HCN) were ~3 and 0.13 x 10^{-10} cm^3 s^{-1} respectively. An accurate rate coefficient for the reaction between $C_6H_5^+$ (m/e= 77) and HCN (reaction 6.42) was unable to be obtained. Unfortunately the decay of the primary ion signal ($C_6H_5^+$) with added HCN was masked by the growth of the product ion signal ($C_4H_2^+$.HCN, m/e= 77) from the relatively fast reaction (2.8 x 10^{-10} cm^3 s^{-1}) of the impurity $C_4H_2^+$ with HCN. Using data obtained at low neutral flows however, the rate coefficient for reaction (6.42) was

estimated to be ~1 x 10^{-12} cm^3 s^{-1}.

6.5 REACTIONS OF THE $C_4H_4^+$ ION WITH BENZENE.

The structure and reactivity of the $C_4H_4^+$ ion in the gas phase has been extensively studied in the past and a number of isomeric structures for the ion have been proposed. $C_4H_4^+$ isomers derived from electron impact on benzene and pyridine were shown in appearance potential experiments by Rosenstock et al[157] to be 29-75 kJ mol^{-1} lower in energy than the linear isomer derived from vinyl acetylene (C_4H_4). Baer et al[158] suggested that the two predominant isomeric structures of $C_4H_4^+$ are the cyclic methylene cyclopropene ion (6) and the linear ion shown in structure (7).

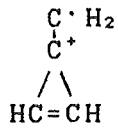

(6)

$$H_2C{=}C^{\cdot}{-}C^{+}{=}CH_2 \qquad (7)$$

In a recent trapped ion ICR cell study of the $C_4H_4^+$ ion produced by unimolecular decomposition of excited $C_6H_6^+$, Ausloos[155] was able to distinguish between two isomeric forms of $C_4H_4^+$ from a difference in their reactivity with benzene. Ausloos showed that the higher energy acyclic $C_4H_4^+$ isomer reacted rapidly with benzene, whilst the more stable cyclic structure did not. When $C_4H_4^+$ was formed with as little excess internal energy as possible, in this case by charge transfer from CO^+ to C_4H_4, only 5% of the reactive isomer was observed. It was also demonstrated that as the internal energy of the $C_4H_4^+$ ion was increased the percentage of the reactive isomer (acyclic $C_4H_4^+$) noted in the reaction of $C_4H_4^+$

with benzene increased.

As discussed in section 6.3, Wagner-Redecker et al[153] observed the same behaviour for $C_4H_4^+$ (one reactive and one unreactive isomer) upon the addition of C_2H_2 in a tandem ICR experiment. In their study, when $C_4H_4^+$ was generated by electron impact on C_4H_4, the percentage of the reactive isomer was found to be approximately 40%. The observation of two separate exponential components in the decay of the $C_4H_4^+$ signal upon reaction with C_2H_2 was confirmed in the present SIFT study (section 6.3).

For this study of the reactions of $C_4H_4^+$ with C_6H_6 the ion was formed in two ways; by electron impact on vinyl acetylene (C_4H_4) and by the reaction of $C_2H_2^+$ (generated from electron impact on C_2H_2) with C_2H_2 (reaction (6.13)) introduced at portal 1. The overall exothermicities of reaction (6.13) for formation of the two isomeric forms of $C_4H_4^+$, the acyclic and cyclic isomers, are 326 and 363 kJ mol^{-1} respectively.

Table 6.5 shows the rate coefficients and product distributions measured in this study for the reaction of $C_4H_4^+$ with benzene along with previous literature data for this reaction.

Table 6.5: Reactions of the $C_4H_4^+$ ion with benzene. The rate coefficients, k, have units of 10^{-9} cm^3 s^{-1}, while the listed ΔH° values are in units of kJ mol^{-1}.

source	isomer	product	B.R.	k	k(lit.)	k_L	$-\Delta H^\circ$
C_4H_4	acyclic	$C_6H_6^+ + C_4H_4$	small	~0.7	0.6[a]	1.4	-5
		$C_6H_7^+ + C_4H_3$	v. small				~42
		$C_4H_4^+.C_6H_6$	major				~415
C_4H_4	cyclic	-	-	~0.001	<0.0005[a]		
C_2H_2[b]	acyclic	-	-	~0.7		1.4	
C_2H_2[b]	cyclic	-	-	~0.001			

(a) Reference 155.
(b) $C_4H_4^+$ was formed from the reaction of $C_2H_2^+$ with C_2H_2 in the ion source.

The major product ion observed for the reaction of $C_4H_4^+$ (formed from electron impact on C_4H_4 (vinyl acetylene)) with benzene (C_6H_6) was the association adduct, $C_4H_4^+.C_6H_6$, along with a minor charge transfer product, $C_6H_6^+$, and a very small peak corresponding to the proton transfer product $C_6H_7^+$. As $C_4H_4^+$ is a minor product only (7%) of the reaction between $C_2H_2^+$ and C_2H_2 (reaction (6.13), table 6.3), product analysis for the reaction of benzene with $C_4H_4^+$ from this source was not attempted. Previous ICR studies of this reaction[155,159] have noted the charge transfer product $C_6H_6^+$ as the major product ion along with the minor product ions $C_{10}H_9^+$, $C_{10}H_8^+$ and $C_9H_9^+$. No association channel was observed as expected in these low pressure ICR studies.

Upon the addition of benzene to the ion $C_4H_4^+$ two separate exponential components for the ion decay were observed for both methods of $C_4H_4^+$ ion formation utilised; electron impact and chemical reaction. The average rate coefficient for the faster decay was measured to be 7.0×10^{-10} cm^3 s^{-1}, while

that for the slower decay was ~1 x 10^{-12} cm^3 s^{-1} in both cases (figure 6.5 shows a semilogarithmic plot of the $C_4H_4^+$ ion signal versus benzene flow for each method of $C_4H_4^+$ ion generation). The observation of two separate exponential components of the ion decay can be interpreted in terms of two isomers of $C_4H_4^+$, probably a reactive linear structure and a less reactive cyclic structure, being formed both from electron impact on C_4H_4 and from reaction between $C_2H_2^+$ and C_2H_2. In each case the ratio of reactive to unreactive isomer (determined as described in section 4.4) was measured to be approximately three to one in favour of the reactive (acyclic) isomer.

More work needs to be performed on the reaction of $C_4H_4^+$ with C_2H_2 to establish firstly whether it is possible that internally excited or metastable $C_4H_4^+$ ions could be present in the flow tube, and secondly to identify the two components of the $C_4H_4^+$ decay with added benzene under SIFT physical conditions of 0.3 Torr.

Admittedly it is unlikely that an ion as large as $C_4H_4^+$ would have an easily accessed metastable electronic state that could be populated during formation of this ion in the reaction of $C_2H_2^+$ with C_2H_2 at inlet portal 1. Once formed the $C_4H_4^+$ ion would also be unlikely to remain internally excited for a significant time at flow tube pressures of 0.3 Torr. Therefore, the observation of two decay components for the reaction of $C_4H_4^+$ with C_6H_6 in this study is almost certainly due to the presence of two isomeric forms of the $C_4H_4^+$ ion.

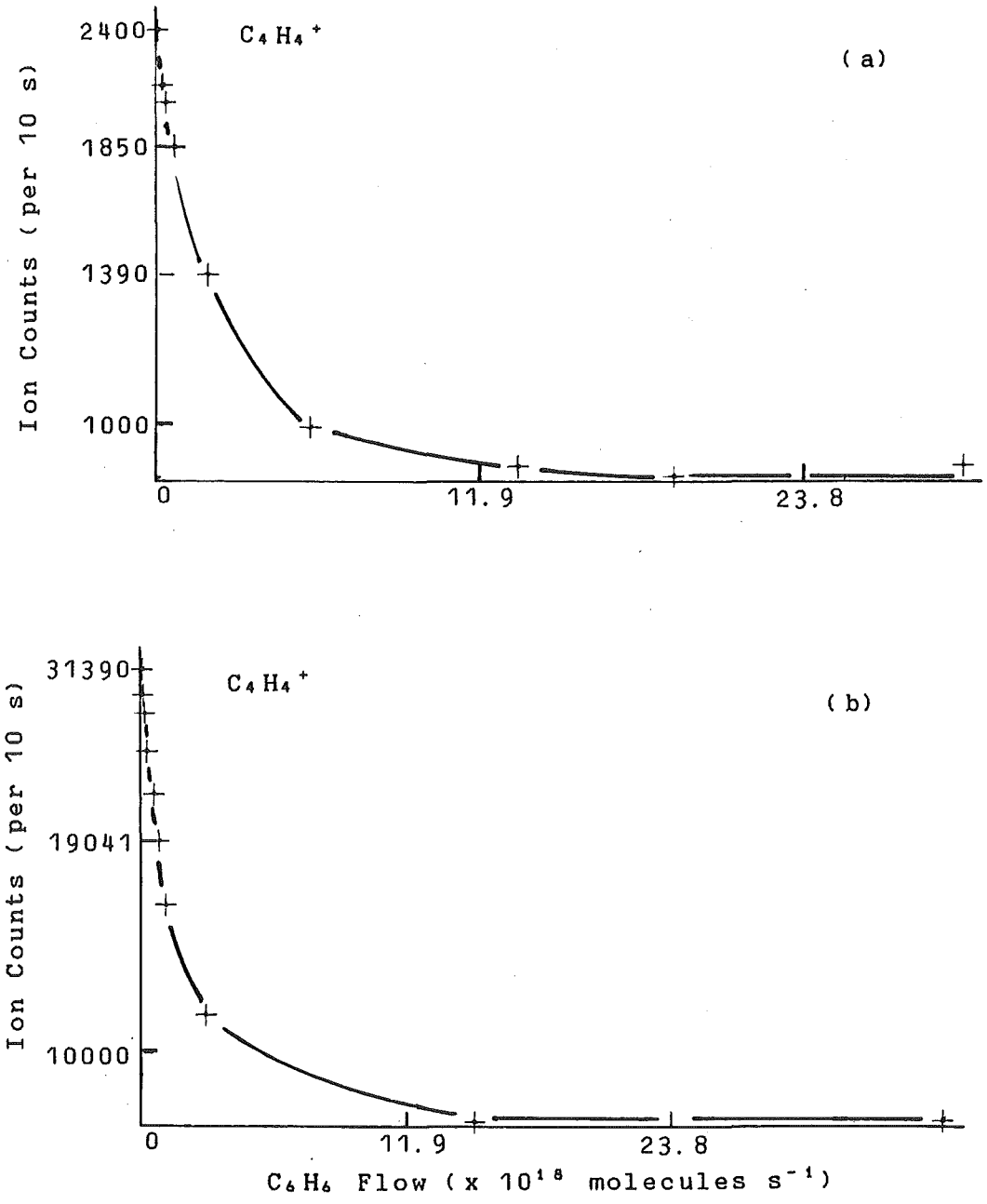

Fig. 6.5: Semilogarithmic plots of the $C_4H_4^+$ (m/e= 52) ion count versus the flow of C_6H_6 where the primary ions were generated by
(a). The reaction between $C_2H_2^+$ and C_2H_2.
(b). Electron impact on C_4H_4.

The reactions of the $C_4H_4^+$ ion with C_2H_2 and C_6H_6 are discussed further in Chapter Seven.

6.6 REACTIONS OF THE C_2H^+ AND $C_2H_2^+$ IONS WITH HYDROGEN.

The ions C_2H^+ and $C_2H_2^+$ were each generated by electron impact on C_2H_2. Upon the addition of H_2, C_2H^+ underwent hydrogen atom abstraction only to produce $C_2H_2^+$ at a rate of 1.2×10^{-9} cm^3 s^{-1}. $C_2H_2^+$ was observed to associate with H_2 to form the adduct $C_2H_2^+.H_2$ (80%) as well as undergoing hydrogen atom abstraction to form $C_2H_3^+$ (20%). At 0.30 Torr the pseudo second order rate coefficient for the reaction was 2.2×10^{-11} cm^3 s^{-1} increasing to 2.7×10^{-11} cm^3 s^{-1} at 0.34 Torr.

Table 6.6 shows the rate coefficients and product distributions measured in this study for the reactions of C_2H^+ and $C_2H_2^+$ with H_2 as well as a number of literature values for comparison.

Table 6.6: Reactions of the ions C_2H^+ and $C_2H_2^+$ with H_2. Rate coefficients have units of 10^{-9} cm^3 s^{-1}. Units of $\Delta H°$ are kJ mol^{-1}, while the tube pressure has units of Torr.

ion	products	B.R.[a]	k	pressure	k(lit.)	k_L	$-\Delta H°$
C_2H^+	$C_2H_2^+ + H$	1	1.2	0.30	1.7[b], 0.78[c]	1.5	86
$C_2H_2^+$	$C_2H_3^+ + H$	0.20 (1[c])	0.022	0.30[d]	0.01[c]	1.5	-3
	$C_2H_2^+.H_2$	0.80	(0.027	0.33)			35

(a) Product distributions were determined at 0.3 Torr.
(b) Reference 160.
(c) Reference 161.
(d) The upper limit to the ternary rate coefficient for this reaction is ~2×10^{-27} cm^6 s^{-1} at 0.33 Torr.

6.7 CONCLUSION.

In this chapter the proton affinity of diacetylene, C_4H_2, has been established to be 738±3 kJ mol^{-1}. The reactions of a number of different hydrocarbon ions with the neutrals C_2H_2, HCN, C_6H_6 and H_2 have also been investigated. For ions of the type $C_xH_y^+$ (where x= 2, 4, 6) the predominant reaction channel at SIFT pressures with the neutrals C_2H_2 and HCN was observed to be association. Usually the reactivity increased as the value of y decreased.

Evidence was also observed for isomeric forms of several of the hydrocarbon ions investigated, notably for the ion $C_4H_4^+$ from its reactions with C_2H_2 and C_6H_6, and for the ions $C_6H_4^+$ and $C_6H_5^+$ reacting with C_2H_2. More work on these reactions needs to be performed to confirm both the identities and reactivities of the relevant isomeric structures for each of these collisionally stabilised ions.

CHAPTER SEVEN

SUGGESTIONS FOR FURTHER WORK.

This chapter details a number of areas of work described in this thesis that were unable to be fully investigated due to the constraints of time. Each area is introduced briefly along with suggestions, where appropriate, for further study. The topics discussed are introduced approximately in order of their original appearance in this thesis.

(1) The differing product distributions observed for the reaction of $CH_3NO_2H^+$ with HC_3N (reaction (3.20)) when studied in a hydrogen carrier (3.20a), as opposed to a helium one (3.20b), have been tentatively explained (p.88, section 3.2) as being due to the involvement of hydrogen in the reaction in some other way than as an inert third body.

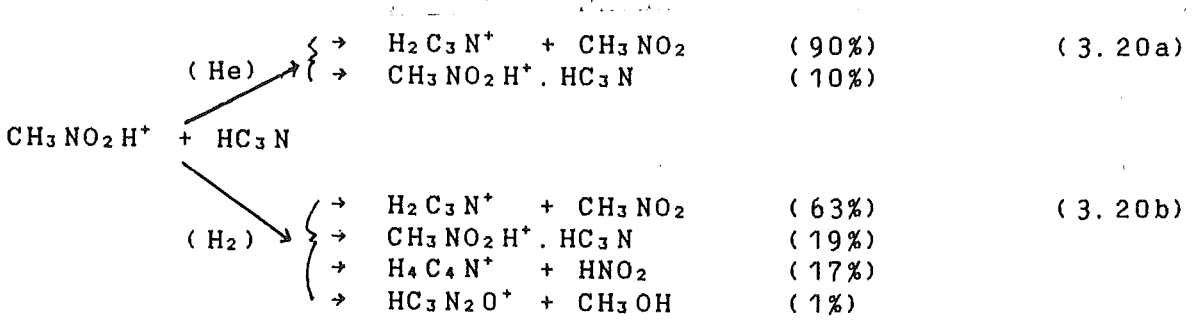

The reaction needs to be investigated further in a hydrogen carrier over as wide as possible a range of pressures to study in detail the effect of hydrogen as a third body. The effect of an increase in the centre of mass energy on the reaction in a helium carrier would also be of interest. Such a study

would involve the selected ion flow drift tube technique. This would enable the extent of endothermicity of the two extra product channels observed in a hydrogen carrier to be characterised.

(2) The reaction of HC_3N^+ with H_2 (reaction (3.29)) has been considered as a possible source reaction for the ultimate production of HC_3N in interstellar clouds (p.107, section 3.5). The measurement of an overall rate coefficient of 7 x 10^{-12} cm^3 s^{-1} at 300 K in this study appears to have eliminated the reaction as a significant precursor for HC_3N.

$$\begin{array}{lll} HC_3N^+ + H_2 \rightarrow & H_2C_3N^+ + H & (76\%) \\ & C_2H_2^+ + HCN & (24\%) \end{array} \qquad (3.29)$$

It is possible however, that while the reaction is very slow at room temperature it may be considerably faster at interstellar cloud temperatures (below 50 K). Therefore the temperature dependence of the rate coefficient for this reaction needs to be investigated.

(3) The investigation of the reaction of the ion C_3N^+ with H_2 (reaction (3.30) p.94, section 3.3) showed two exponential components in the decay of the ion, C_3N^+, upon the addition of H_2. Further studies of the reactions of this ion with other neutrals over a range of carrier pressures are needed to determine the reason for the two separate exponential decays. These may be due to either two stable isomers of C_3N^+ or to metastable excited states of a single stable ion structure (or to a combination of both).

The C_3N^+ ion has been confirmed as the major product from the reaction of C_2^+ with HCN (reaction (6.28), section 6.4).

$$C_2^+ + HCN \rightarrow C_3N^+ + H \quad (46\%) \qquad (6.28)$$

If it is assumed that the C_3N^+ ion is formed in two isomers (see structures (21) and (22), p.95) then production of the higher energy C_3N^+ isomer in this reaction is endothermic by ~26 kJ mol^{-1}, while the other C_3N^+ isomer is formed with ~59 kJ mol^{-1} of internal energy (table 6.4, section 6.4). If C_3N^+ can be formed at portal 1 through reaction (6.28), then the addition of H_2 at portal 2 to a swarm of collisionally stablised C_3N^+ ions should result in the observation of a single exponential decay for reaction (3.30). The identities and reactivities of the two isomers could then be confirmed.

(4) In Chapter Six evidence was presented for the existence of discrete stable isomers of the ions $C_4H_4^+$ (p.221, section 6.5) and $C_6H_5^+$ (p.206, section 6.3) at SIFT pressures. To confirm the structural identity of the two $C_4H_4^+$ isomers observed in this study a source is needed which gives $C_4H_4^+$ ions of a single structure only (ie. acyclic or cyclic). It may be possible to form essentially 100% cyclic $C_4H_4^+$ ions through ion-molecule reactions where the production of only the lower energy cyclic isomer is exothermic.

If the subsequent addition of C_6H_6 to a swarm of cyclic $C_4H_4^+$ ions gives a single exponential decay in the ion signal (presumably corresponding to the lower energy cyclic isomer), the reactivity of the isomer formed could be characterised.

Alternatively, the observation of two separate exponential decay components for the reaction of $C_4H_4^+$ with C_6H_6 would allow an upper limit to the isomerisation barrier between the two stable isomeric forms of $C_4H_4^+$ to be set (assuming that the faster decay is not due to metastable $C_4H_4^+$). To set such a limit the following assumption would need to be made: that the isomerisation barrier between the two isomers at flow tube pressures is sufficient to allow for the separate stable existence of each isomer in the flow tube.

Determination of the isomer ratio and the product distribution in the reaction of collisionally stabilised $C_4H_4^+$ with benzene in the SIFT should also indicate whether the primary ion contained significant internal excitation in the previous ICR studies of the $C_4H_4^+$ ion with benzene[155,159] and acetylene[153].

(5) To investigate further the magnitude of the reactivities of the cyclic and acyclic $C_6H_5^+$ isomers observed in this study a swarm containing only the cyclic $C_6H_5^+$ isomer needs to be created in the flow tube. This could be achieved, for example, using dehalogenation reactions at portal 1 (similar to reaction (6.27), p.207) to generate $C_6H_5^+$ and then

$$CH_5^+ + C_6H_5F \rightarrow C_6H_5^+ + HF + CH_4 \qquad (6.27),$$

adding C_2H_2 downstream to establish a rate coefficient for the cyclic isomer at high pressures. A comparison with the rate coefficient observed for the $C_6H_5^+$ ion formed from the reaction of $C_4H_3^+$ and C_2H_2 (reaction (6.17)) at high pressures

(p.207, section 6.3) could then confirm the identity of the isomer formed in reaction (6.17).

(6) Many of the reactions investigated in this thesis were observed to form association products. The rate coefficients of a number of these reactions having association channels were noted to vary appreciably as the pressure changed, signifying that these ternary reactions were occurring in the "falloff" regime (as opposed to the "pressure-saturated" regime where the rate coefficient for a ternary reaction is independent of pressure). These reactions include the following:

CH_3^+	+	HCN	(4.12, table 4.6)
CH_3^+	+	CH_3CN	(4.13, ")
CH_3NCH^+	+	HCO_2CH_3	(4.23, table 4.7)
H_2CN^+	+	C_2H_2	(6.26, table 6.3)

The rate coefficients of a number of other reactions leading to association adducts were observed to have values significantly below the calculated collision limit theory values. These reactions, which were studied at a single flow tube pressure, include the following:

$C_4H_2^+$	+	HC_3N	(3.11, table 3.0)
CH_3CNH^+	+	HC_3N	(3.16, ")
$H_2C_3N^+$	+	HC_3N	(3.23, ")
$H_2C_3N^+$	+	BrCN	(3.28, table 3.1)
CH_3CNH^+	+	CH_3CHO	(table 4.0)

C_2N^+	+ HCN	(5.10,	table 5.1)
HC_2N^+	+ H_2O	(5.14,	table 5.3)
$C_4H_4^+$(a,c)	+ C_2H_2	(6.18,	table 6.3)
$C_6H_3^+$	+ C_2H_2	(6.21,	")
$C_6H_4^+$(a,c)	+ C_2H_2	(6.22,	")
$C_6H_5^+$(a,c)	+ C_2H_2	(6.23,	")
$C_2H_2^+$	+ HCN	(6.30,	table 6.4)
$C_4H_2^+$	+ HCN	(6.33,	")
$C_4H_3^+$	+ HCN	(6.34,	")
$C_4H_4^+$(a,c)	+ HCN	(6.35,	")
$C_4H_5^+$	+ HCN	(6.36,	")
$C_6H_2^+$	+ HCN	(6.40,	")
$C_6H_4^+$	+ HCN	(6.41,	")

Data obtained from studies of the temperature and pressure dependences of ternary ion-molecule reactions such as those listed above are important in developing models of interstellar cloud chemistry (section 3.5) and also in the development of theories predicting the pressure dependence of unimolecular reactions[128]. Further investigation is needed on the reactions listed above to establish whether the apparent pseudo second order rate coefficient for the relevant reaction varies in the pressure range accessible to the SIFT technique. Investigation of the temperature dependence of the ternary reactions listed above, where the participating ions and neutrals are of importance to interstellar cloud chemistry, is also needed.

REFERENCES.

1. F.C. Fehsenfeld, E.E Ferguson and A.L. Schmeltekopf, J. Chem. Phys., 44, 3022 (1966).

2. E.E Ferguson, F.C. Fehsenfeld and A.L. Schmeltekopf, Adv. At. Mol. Phys. 5, 1 (1969).

3. P.H.G. Dickinson and J. Sayers, Proc. Phys. Soc., London, 76, 137 (1960).

4. J. Sayers and D. Smith, Proc. Int. Conf. Phys. Electron. At. Collisions, 3rd, p.871 (1964).

5. W.R. Gentry, in "Gas Phase Ion Chemistry" (M.T. Bowers ed.), Vol.2, p.221 (Academic Press, New York, 1979).

6. W.R. Gentry, in "Kinetics of Ion Molecule Reactions" (P. Ausloos ed.), p.81 (Plenum, New York, 1979).

7. R.T. McIver, Jr., in "Kinetics of Ion Molecule Reactions" (P. Ausloos ed.), p.255 (Plenum, New York, 1979).

8. H. Hartmann and K.P. Wanczek (eds.), "Lecture Notes in Chemistry", Vol.7 (Springer-Verlag, Berlin, 1978).

9. H. Hartmann and K.P. Wanczek (eds.), "Lecture Notes in Chemistry", Vol.31 (Springer-Verlag, Berlin, 1982).

10. E.W. McDaniel, V. Cermak, A. Dalgarno, E.E. Ferguson and L. Friedman, "Ion-molecule Reactions" (Wiley, New York, 1970).

11. N.D. Twiddy, Contemp. Phys., 15, 427 (1974).

12. F.C. Fehsenfeld, C.J. Howard, W.J. Harrop and E.E Ferguson, J. Geophy. Res., 80, 2229 (1975).

13. G.G. Meisels, in "Interactions Between Ions and Molecules" (P. Ausloos ed.), p.604 (Plenum, New York, 1975).

14. D. Smith and N.G. Adams, in "Gas Phase Ion Chemistry" (M.T. Bowers ed.), Vol.1, p.1 (Academic Press, New York, (1979).

15. M. MacFarland, D.L. Albritton, F.C. Fehsenfeld, E.E. Ferguson and A.L. Schmeltekopf, J. Chem. Phys., 59, 6610 (1973).

16. M. MacFarland, D.L. Albritton, F.C. Fehsenfeld, E.E. Ferguson and A.L. Schmeltekopf, J. Chem. Phys., 59, 6620 (1973).

17. M. MacFarland, D. L. Albritton, F. C. Fehsenfeld, E. E. Ferguson and A. L. Schmeltekopf, J. Chem. Phys., 59, 6629 (1973).

18. D. L. Albritton, I. Dotan, W. Lindinger, M. MacFarland, J. Tellinghuisen and F. C. Fehsenfeld, J. Chem. Phys., 66, 410 (1977).

19. W. Lindinger and D. Smith, in "Reactions of Small Transient Species", (A. Fontijn and M. A. A Clyne, eds.), p. 387 (Academic Press, London, 1984).

20. J. K. Kim and W. T. Huntress, Jr., Int. J. Mass Spectrom. Ion Phys., 16, 451 (1975).

21. D. Smith and N. G. Adams, in "Kinetics of Ion-molecule reactions", (P. Ausloos, ed.), p. 345 (Plenum, New York, 1979).

22. D. Smith and N. G. Adams, in "Topics in Current Chemistry, 89", (S. Veprek and M. Venugopalan, eds.), p. 1 (Springer-Verlag, Berlin, 1980).

23. D. Smith and N. G. Adams, Int. Rev. Phys. Chem., 1, 271 (1981).

24. J. F. Paulson and F. Dale, J. Chem. Phys., 77, 4006 (1982).

25. C. H. DePuy and V. M. Bierbaum, Acc. Chem. Res., 14, 146 (1981).

26. C. H. DePuy, in "Chemistry of Ions in the Gas Phase", (Reidel, Vimeiro, Portugal, 1983).

27. F. C. Fehsenfeld, D. L. Albritton, Y. A. Bush, P. G. Fournier, T. R. Govers and J. Fournier, J. Chem. Phys., 61, 2150 (1974).

28. F. C. Fehsenfeld, in "Interactions Between Ions and Molecules" (P. Ausloos ed.), p. 387 (Plenum, New York, 1975).

29. M. Meot-Ner, in "Gas Phase Ion Chemistry" (M. T. Bowers, ed.), Vol. 1, p. 198 (Academic Press, New York, 1979).

30. N. G. Adams and D. Smith, in "Reactions of Small Transient Species" (A. Fontijn and M. A. A. Clyne, eds.), p. 311 (Academic Press, London, 1983).

31. N. G. Adams and D. Smith, in "Swarms of Ions and Electrons in Gases" (W. Lindinger, T. D. Mark and F. Howorka, eds.), p. 194 (Springer-Verlag, Wien, 1984).

32. D. Smith and N.G. Adams, in NATO Advanced Workshop on "Molecular Astrophysics - State of the Art and Future Directions", (Bad Windsheim, Germany, 1984).

33. D. Smith and N.G. Adams, in "Ionic Processes in the Gas Phase" (M.A.A Almoster-Ferreira, ed.), p.41 (Reidal, New York, 1984).

34. C.H. Depuy, in "Ionic Processes in the Gas Phase" (ed. M.A.A Almoster-Ferreira), p.227 (Reidal, New York, 1984).

35. A.A. Viggiano and J.F. Paulson, in "Swarms of Ions and Electrons in Gases" (W. Lindinger, T.D. Mark and F. Howorka, eds.), p.218 (Springer-Verlag, Wien, 1984).

36. E. Herbst, in "Interstellar Molecules" (B.H. Andrews ed.), p.317 (Reidel, Dordrecht, Holland 1980).

37. N.G. Adams and D. Smith, Chem. Phys. Lett., 79, 563 (1981).

38. S.E. Barlow, G.H. Dunn and M. Schauer, Phys. Rev. Letters, 52, 902 (1984).

39. E.E. Ferguson, F.C. Fehsenfeld and D.L. Albritton, in "Gas Phase Ion Chemistry" (M.T. Bowers, ed.), Vol.1, p.45 (Academic Press, New York, 1979).

40. C.M. Leung, E. Herbst, and W.F. Huebnes, Astrophys. J. Suppl. Ser., 56, 231 (1984).

41. T.J. Millar and A. Freeman, Mon. Not. R. Astr. Soc., 207, 405 (1984).

42. E. Herbst, N.G. Adams and D. Smith, Astrophys. J., 285, 618, (1984).

43. J. Luine and G.H. Dunn, Phys. Rev. Lett, to be published (1985).

44. B.R. Rowe, G. Dupeyrat J.B. Marquette, D. Smith, N.G. Adams and E.E. Ferguson, J. Chem. Phys., 80, 241 (1984).

45. B.R. Rowe, G. Dupeyrat J.B. Marquette and P. Gaucherel, J. Chem. Phys. 80, 4915 (1984).

46. G. Dupeyrat J.B. Marquette and B.R. Rowe, Phys. Fluids, 28, 1279 (1985).

47. B.R. Rowe, J.B. Marquette, G. Dupeyrat and E.E. Ferguson, Chem. Phys. Lett., 113, 403 (1985).

48. F. Howorka, I. Dotan, F.C. Fehsenfeld and D.L. Albritton, J. Chem. Phys., 73, 758 (1980).

49. N.G. Adams and D. Smith, J. Phys. B., 9, 1439 (1976).

50. J.L. McCrumb and P. Warneck, J. Chem. Phys., 66, 5416 (1977).

51. D. Smith, N.G. Adams and T.M. Miller, J. Chem. Phys., 69, 308 (1978).

52. M. Tichy, A.B. Raksit, D.G. Lister, N.D. Twiddy, N.G. Adams and D. Smith., Int. J. Mass Spectrom. Ion Phys., 29, 231 (1979).

53. B.R. Rowe, D.W. Fahey, F.C. Fehsenfeld and D.L. Albritton, J. Chem. Phys., 73, 194 (1980).

54. D. Smith and N.G. Adams, Pure and Appl. Chem., 56, 175 (1984).

55. I. Dotan, F.C. Fehsenfeld and D.L. Albritton, J. Chem. Phys., 68, 5665 (1978).

56. M. Durup-Ferguson, H. Böhringer, D.W. Fahey, F.C. Fehsenfeld and E.E. Ferguson, J. Chem. Phys., 81, 2657 (1984).

57. N.G. Adams, D. Smith and E.E Ferguson, Int. J. Mass Spectrom. Ion Phys., 67, 67 (1985).

58. T. Su and M.T. Bowers, in "Gas Phase Ion Molecule Chemistry" (M.T. Bowers, ed.) Vol.1, p.83 (Academic Press, New York, 1979).

59. G. Gioumousis and D.P. Stevenson, J. Chem. Phys., 29, 294 (1958).

60. see for example reference 30 p.318.

61. T. Su and M.T. Bowers, Int. J. Mass Spectrom. Ion Phys., 17, 309 (1975).

62. T. Su and M.T. Bowers, Int. J. Mass Spectrom. Ion Phys., 12, 347 (1973).

63. T. Su and M.T. Bowers, Int. J. Mass Spectrom. Ion Phys., 17, 211 (1975).

64. L.P. Theard and W.H. Hamill, J. Am. Chem. Soc., 84, 1134 (1962).

65. T. Su, E.C.F. Su and M.T. Bowers, J. Chem. Phys., 69, 2243 (1978).

66. E.T. Hsieh and A.W. Castlemann, Jr., Int. J. Mass Spectrom. Ion Phys., 40, 295 (1981).

67. D.C. Clary, Mol. Phys., 54, 605 (1985).

68. D.C. Clary, D. Smith and N.G. Adams, Chem. Phys. Lett., 119, 320 (1985).

69. N.G. Adams, D. Smith and D.C. Clary, Astrophys. J. (Lett.), submitted (1985).

70. B.R. Rowe, private communication to the authors of reference 68.

71. G. Dupreyrat, B.R. Rowe, D.W. Fahey and D.L. Albritton, Int. J. Mass Spectrom. Ion Phys., 44, 1 (1982).

72. G.I. MacKay, G.D. Vlachos, D.K. Bohme and H.I. Schiff, Int. J. Mass Spectrom. Ion Phys., 36, 259 (1980).

73. See, for example, G. Lawson and J.F.J. Todd, Chem. Brit., 8, 373 (1972).

74. C. Moreu and J.C. Bongrand Ann. Chemie, 14, 47 (1920).

75. J.B. Armitage, E.R.H. Jons and M.C. Whiting, J. Chem. Soc., 154, 44 (1951).

76. P.D. Landor, S.R. Landor and P. Leighton, J. Chem. Soc., Perkin Trans. 1, 1628 (1975).

77. J. Casanova, Jr., R.E. Schuster and N.D. Werner, J. Chem. Soc. (L), 4280 (1963).

78. N.G. Adams, M.J. Church and D. Smith, J. Phys. D 8, 1409 (1975).

79. R.C. Bolden, R.S. Hemsworth, M.J. Shaw and N.D. Twiddy, J. Phys. B, 3, 45 (1970).

80. D. Smith, N.G. Adams, A.G. Dean and M.J. Church, J. Phys. D, 8, 141 (1975).

81. W. Lindinger and D.L. Albritton, J. Chem. Phys., 62, 3517 (1975).

82. H.W. Ellis, E.W. McDaniel, D.L. Albritton, L.A. Viehland, S.L. Lin and E.A. Mason, At. Data Nucl. Data Tables, 22, 179 1978); 17, 177 (1976).

83. P.W. Harland and B.J. McIntosh, Int. J. Mass Spectrom. Ion Phys., 57, 283 (1984).

84. J. Glosik, A.B. Raksit, N.D. Twiddy, N.G. Adams and D. Smith, J. Phys. B., 11, 3365 (1978).

85. V.G. Anicich, W.T. Huntress, Jnr., and M.J. McEwan, J. Phys. Chem., in press, (1986).

86. D.K. Bohme, R.S. Hemsworth, H.W. Rundle and H.I. Schiff, J. Chem. Phys., 58, 3504 (1973).

87. C.G. Freeman, P.W. Harland and M.J. McEwan, Mon. Not. R. Astron. Soc., 187, 441 (1979).

88. H.W. Kroto, C. Kirby, D.R.M. Walton, L.W. Avery, N.W. Broten, J.M. MacLeod, and T. Oka, Astrophys. J., 219, L133 (1978).

89. J.M. Broten, T. Oka, L.W. Avery, J.M. MacLeod, H.W. Kroto, Astrophys. J., 223, L105 (1978).

90. P.J. Benson and P.C. Myers, Astrophys. J., 270, 589 (1983).

91. R.L. Snell, F.P. Schloerb, J.S. Young, A. Hjalmarson and P. Friberg, Astrophys. J., 244, 45 (1981).

92. S.G. Lias, J.F. Liebman and R.D. Levin, J. Phys. Chem. Ref. Data, 13, 695 (1984).

93. H.M. Rosenstock, K. Draxl, B.W. Steiner and J.T. Herron, J. Phys. Chem. Ref. Data, 6, Suppl. 1 (1977).

94. P.W. Harland and B.J. McIntosh, Int. J. Mass Spectrom. Ion Proc., 67 29, (1985).

95. P.W. Harland, Int. J. Mass Spectrom. Ion Proc., to be submitted (1986).

96. A.B. Raksit and D.K. Bohme, Int. J. Mass Spectrom. Ion Phys. 57, 211 (1984).

97. A.B. Raksit and D.K. Bohme, Can. J. Chem., 63, 854 (1985).

98. D.K. Bohme and A.B. Raksit, Mon. Not. R. Astro. Soc., 213, 717 (1985).

99. C. Petrongolo, P.J. Bruna, S.D. Peyerimhoff and R.J. Buenker, J. Chem. Phys. 74, 4594 (1981).

100. D. Smith, N.G. Adams and E. Alge, J. Chem. Phys., 77, 1261 (1982).

101. S.G. Lias in "Lecture Notes in Chemistry", (H. Hartmann and K. Wanczek eds.), Vol. 7, p. 159 (Springer-Verlag, Berlin, 1978).

102. T. McAllister and P. Pitman, Int. J. Mass Spectrom. Ion Phys. 19, 241 (1976).

103. G.I. McKay and D.K. Bohme, Int. J. Mass Spectrom. Ion Phys. 26, 327 (1978).

104. S.G. Lias, D.M. Shold and P. Ausloos, J. Am. Chem. Soc., 102, 2540 (1980).

105. V. H. Dibeler, R. M. Reese, and J. L. Franklin J. Amer. Chem. Soc., 83, 1813 (1961).

106. E. Herbst, D. Smith and N. G. Adams, Astrophys. J., in press (1985).

107. E. Herbst, Astrophys. J. Supp. Ser., 53, 41 (1983).

108. E. Churchwell, G. Winnewisser and C. M. Walmsley, Astron. Astrophys., 67, 139 (1978).

109. W. M. Irvine, B. Hoglund, P. Friberg, J. Askne and J. Ellder, Astrophys. J., 248, L113 (1981).

110. J. M. MacLeod, L. W. Avery, N. W. Broten, Astrophys. J., 282, L89 (1984).

111. N. W. Broten, J. M. MacLeod, L. W. Avery, W. M. Irvine, B. Hoglund, P. Friberg and A. Hjalmasson, Astrophys. J., 276, L25 (1984).

112. N. G. Adams and D. Smith, Int. J. Mass Spectrom. Ion Proc., 61, 133 (1984).

113. G. H. Dunn and S. E. Barlow, private communication to the authors of reference 112.

114. J. A. Luine and G. H. Dunn, 12th Int. Conf. Phys. Electron. At. Collisions, Gatlinburg, Tennessee, (July 1981).

115. D. R. Bates, Astrophys. J., 267, L121 (1983).

116. W. Lindinger, private communication to D. Smith (1985).

117. M. J. McEwan, V. G. Anicich, W. T. Huntress, P. R. Kemper, and M. T. Bowers, Chem. Phys. lett., 75, 278 (1980).

118. G. I. MacKay, L. D. Betowski, J. D. Payzant, H. I. Schiff, D. K. Bohme, J. Phys. Chem. 80, 2919 (1976).

119. J. F. Wolf, R. H. Staley, I. Koppel, M. Taagepera, R. T. McIver, J. L. Beauchamp, and R. W. Taft, J. Am. Chem. Soc., 99, 5417 (1977).

120. S. G. Lias, D. M. Shold, and P. Ausloos, J. Am. Chem. Soc., 102, 2540 (1980).

121. A. J. Illies, S. Liu and M. T. Bowers, J. Am. Chem. Soc., 103, 5674 (1981).

122. D. Aue, M. Pedley and M. T. Bowers, private communication to authors of 121.

123. M. H. Bagal-Vayjooee, J. L. Collister and H. O. Pritchard, Can. J. Chem., 55, 2634 (1977).

124. D.H. Aue and M.T. Bowers in "Gas Phase Chemistry" (M.T. Bowers ed.), Vol. 2, p. 1 (Academic Press, New York, 1979).

125. W.R. Davidson, M.T. Bowers, T. Su, and D.H. Aue, Int. J. Mass Spectrom. Ion Phys., 24, 83 (1977).

126. M.T. Bowers, private communication.

127. H.I. Schiff, and D.K. Bohme, Astrophys. J. 232, 740 (1979).

128. R.G. Gilbert, and M.J. McEwan, Aust. J. Chem., 38, 231 (1980).

129. D.J. DeFrees, A.D. McLean and E. Herbst, Astrophys. J., 293, 236 (1985).

130. T.W. Harquist and A. Dalgarno in "Giant Molecular Clouds in the Galaxy" (P.M. Solomon and M.G. Edmunds eds.), p.315 (Pergamon Press, London, 1980).

131. G.F. Mitchell, J.L. Ginsberg, and P.J. Kuntz, Ap. J. Suppl., 38, 39 (1978).

132. N.N. Haese and R.C. Woods, Astrophys. J. (letters), 246, L51 (1981).

133. M. Yoshimime and W.P. Kraemer, Chem. Phys. Lett., 90, 145 (1982).

134. L.E. Synder, J.M. Hollis and D. Buhl, Astrophys. J. (letters), 215, L87 (1977).

135. M.J. McEwan, V.G. Anicich and W.T. Huntress, Jnr., Int. J. Mass Spectrom. Ion Phys., 50, 179 (1983).

136. J.P. Liddy, C.G. Freeman and M.J. McEwan, Mon. Not. R. Astron. Soc., 180, 683 (1977).

137. V.G. Anicich, W.T. Huntress and J.H. Futrell, Chem. Phys. Lett., 40, 233 (1976).

138. M.N. Paddon-Row, C.Santiago and K.N. Houk, J. Am. Chem. Soc., 102, 6561 (1980).

139. C.G. Freeman, P.W. Harland, J.P. Liddy and M.J. McEwan, Aust. J. Chem., 31, 963 (1978).

140. R.L. Huang, S.H. Goh and S.H. Ong, "The Chemistry of Free Radicals" (Arnold, London, 1974).

141. C. Lifshitz, P. Gotchiguian and R. Roller, Chem. Phys. Lett., 95, 106 (1983).

142. Reference 72 and references 5 and 6 therein.

143. A.N. Hayhurst and D.B. Kittelson, Combust. Flame, 31, 37 (1978).

144. Von H.J. Spangenberg, I. Borger, H. Hoffman and G. Mogel, Z. Phys. Chem. (Leipzig), 259, (1978).

145. F.W. Brill and J.R. Eyler, J. Phys. Chem., 85, 1091 (1981). and references 3 and 4 therein.

146. J.R. Eyler and J.E. Campana, Int. J. Mass Spectrom. Ion Phys., 55, 171 (1983/1984).

147. V.G. Anicich, G.A. Blake, J.K. Kim, M.J. McEwan and W.T. Huntress, Jr., J. Phys. Chem., 88, 4608 (1984).

148. M. Meot-Ner, T.A. Buckley, R. Metz and C.A. Deakyne, J. Chem. Phys., in press (1986).

149. P.G. Miasek and J.L. Beauchamp, Int. J. Mass Spectrom. Ion Phys., 15, 49 (1979).

150. A.A. Herod and A.G. Harrison, Int. J. Mass Spectrom. Ion Phys., 4, 415 (1970).

151. W.T. Huntress, Jr., Astrophys. J. Suppl. Ser., 33, 495 (1977).

152. S.E. Buttrill, Jr., J. Chem. Phys., 50, 4125 (1969).

153. W. Wagner-Redeker, A.J. Illies, P.R. Kemper and M.T. Bowers, J. Am. Chem. Soc., 105, 5719 (1983).

154. J.H. Futrell and T.O. Tiernan, J. Phys. Chem., 72, 158 (1968).

155. P Ausloos, J. Am. Chem. Soc., 103, 3931 (1981).

156. M. Tasaka, M. Ogata and H. Ichikawa, J. Am. Chem. Soc., 103, 1885 (1981).

157. H.M. Rosenstock, R. Stockbauer and A.C. Parr, Int. J. Mass Spectrom. Ion Phys., 38, 323 (1981).

158. T. Baer, G.D. Willet, D. Smith and J.S. Phillips, J. Chem Phys., 70, 4076 (1979).

159. R.D. Smith, J.J. DeCorpo and J.H. Futrell, Int. J. Mass Spectrom. Ion Phys., 26, 279 (1978).

160. N.G. Adams and D. Smith, Chem. Phys. Lett., 47, 383 (1977).

161. J.K. Kim, L.P. Thread and W.T. Huntress Jr., J. Chem. Phys., 62, 45 (1975).

162. J. Applequist, J.R. Carl and K.K. Kung, J. Am. Chem. Soc., 94, 2952 (1972).

163. E.R. Lippincott, G. Nagarajan and J.M. Stutman, J. Phys. Chem., 70, 78 (1966)

164. J.O. Hirschfelder, C.F. Curtiss and R.B. Bird, "Molecular Theory of Gases and Liquids", p.947 (Wiley, New York, 1964).

165. A.L. McClellan, "Tables of Experimental Dipole Moments", (Freeman, San Francisco, 1963).

166. R.D. Nelson, Jnr., D.R. Lide, Jr. and A.A. Maryott, NSRDS-NBS 10 (1967).

167. D.R. Stull and H. Prophet, "JANAF Thermochemical Tables", NSRDS-NBS 37 (1971).

168. M.W. Chase, J.L. Curnutt, H. Prophet, R.A. McDonald and A.N. Syverud, "JANAF Thermochemical Tables, 1975 supplement", J. Phys. Chem. Ref. Data, 4, 1 (1975).

169. M.W. Chase, Jr., J.L. Curnutt, J.R. Downey, Jr., R.A. McDonald and A.N. Syverud, J. Phys. Chem. Ref. Data, 11, 695 (1982).

170. D. Smith and N.G. Adams, private communication, 1985.

APPENDIX 1.

1.1 SIFT Data Sampling.

(a) Requirements- The voltage output of the pressure transducers monitoring the change in pressure in the neutral volumes supporting the neutral reactant inlet portals 1 and 2 needs to be sampled. Because the voltage output of a transducer will vary widely during the course of a reaction the magnitude of the voltage sample range must be able to be varied quickly while maintaining the required standard of accuracy. The rate of voltage samples per unit time must also be able to be varied during the course of a reaction experiment. For example, a very slow ion-molecule reaction will require a large range of neutral flow rates for analysis. At very high neutral flow rates the sampling rate of the transducer voltage output must be fast, whereas at low flows the sample rate must be slow to accurately monitor the neutral flow volume. The raw voltage output per unit time of the transducer must be converted to a pressure change per second value. This value must be sorted and stored. After input of the ion count over the unit time the selected flow rate must be displayed on a real-time plot of the log of the ion count versus the neutral flow per second.

(b) Hardware- "Ada-lab" (tm) data acquistion/control interface.

- integrating A/D converter.
- D/A converter.

- digital (parallel) input and output.
- real-time clock and counter/timer.
- hardware switch voltage input/output range.
- software variable voltage range.

"Ada-amp" (tm) instrumentation amplifier.

- 16 channel input.
- programmable attenuation by factors of 2^n (n= 1-10).
- instrumentation amp. with gains of 0.1, 1, 10, 100.
- operational amp. with a variable gain of 1-10.
- low pass filter.
- differential input.

Apple 2e microcomputer.

(c) Solution- 3 input channels of the "Ada-amp" were utilised as follows- 1. portal 1 transducer signal input.

2. portal 2 transducer signal input.
3. DC voltage supply test signal (for calibration purposes).

The instrumentation amplifier was set to a gain of 1 while the "Ada-lab" voltage switch was set to a 1V limit.

Four assembly language (AL) subroutinues were then written to control and communicate with the ADALAB hardware. These subroutines are listed on pages 247-250. The TEMP1 subroutine

initiates the ADALAB unit. TEMP2 handles interrupt calls generated by ADALAB while MADMAIN contains the main timing routine and the interrupt vector locations. The CONVERT and APPEND (not listed) routines convert the data sampled by ADALAB into a form recognisable to the TEMPWAND basic routine (detailed below).

An initial test programme written to call these AL subroutines is "TEMPWAND" (Basic language, Applesoft 3.3). The TEMPWAND programme can be set up to sample the ADALAB continously during the course of a experimental run with each sampled pressure change being printed out in units of Torr s^{-1} for later analysis. The time interval between data samples, the ADALAB voltage input and operational amplifier gain ranges can also be varied through simple software commands during the course of an experiment.

The MR BIG programme (listed in appendix 1.2) includes an option labelled "real-time" sampling. This routine functions in the same manner as for the TEMPWAND programme except that the addresses of the assembly language routines have been changed to allow the MR BIG programme to run on an Apple 2e microcomputer. The routine allows the selection of one particular neutral flow from a number of values measured using ADALAB during the course of a neutral flow determination. The ion count at this flow can then be input into the programme with both values being stored for later analysis using MR BIG.

The real-time routine has been tested and can be excuted successfully independently of the MR BIG programme. Unfortunately however, when changing the locations for storage

of the assembly language routines an error was introduced. The real-time option of MR BIG, whilst desirable for use in this study, was not essential as the TEMPWAND routine was satisfactory for data sampling. After initial unsuccessful attempts to correct the error in the real-time routine the TEMPWAND routine was utilised for the collection of data presented in this thesis.

Assembled source code for the TEMPWAND and MR BIG programmes.

MADMAIN 1 of 1

```
 1 DADHI    =    $C400
 2 DTOLO    =    $C404
 3 DTOHI    =    $C405
 4 DTOLL    =    $C406
 5 DTOHL    =    $C407
 6 T2LOW    =    $C434
 7 T2HIG    =    $C435
 8 T2LOL    =    $C436
 9 T2HIL    =    $C437
10 T3LOL    =    $C438
11 T3HIG    =    $C439
12 NUM      =    $06
13 INIT     =    $6100
14          ORG  $6000
15          SEI
16          JSR  INIT
17          LDA  #$05
18          STA  NUM
19          LDA  #$BE
20          STA  DTOLO
21          STA  T2LOW
22          LDA  #$C7
23          STA  DTOHI
24          STA  T2HIG
25          LDA  #$FF
26          STA  T3LOL
27          STA  T3HIG
28          STA  DADHI
29          CLI
30 TEST     LDA  #$02
31          CMP  NUM
32          BNE  TEST
33          SEI
34          RTS
```

TEMP1 1 of 1

```
 1 DADHI     =     $C400
 2 DDALO     =     $C401
 3 DDIBR     =     $C402
 4 DDIAR     =     $C403
 5 DTOLO     =     $C404
 6 DTOHI     =     $C405
 7 DTOLL     =     $C406
 8 DTOHL     =     $C407
 9 DT1LO     =     $C408
10 DT1HI     =     $C409
11 DAUXR     =     $C40B
12 DPERR     =     $C40C
13 DINFR     =     $C40D
14 DINER     =     $C40E
15 DATLO     =     $C410
16 DATHI     =     $C420
17 PORTB     =     $C430
18 PORTA     =     $C431
19 BDATR     =     $C432
20 ADATR     =     $C433
21 AUXCR     =     $C43B
22 INTER     =     $C43E
23 SAMPLE    =     $61D0
24 DELAY     =     $61D2
25 POINTR    =     $02
26 XAXIS     =     $61D4
27 ADVALUE   =     $61DA
28 CHAATT    =     $61E4
29 TDELAY    =     $03
30 MEMPT     =     $04
31 HIRES     =     $C057
32 MIX       =     $C053
33 NOTMIX    =     $C052
34 PRIM      =     $C054
35 SEC       =     $C055
36 GRAPH     =     $C050
37 TEXT      =     $C051
38 CLEAR     =     $6370
39           ORG   $6100
40           LDA   #$05
41           STA   XAXIS
42           LDA   #$00
43           STA   MEMPT
44           LDA   #$8F
45           STA   DDIBR
46           LDA   #$FF
47           STA   DDIAR
48           LDA   #$FF
49           STA   ADATR
50           LDA   #$00
51           STA   BDATR
52           LDA   #$E0
53           STA   DAUXR
54           LDA   #%01100000
55           STA   AUXCR
56           LDA   #$8A
57           STA   DPERR
58           LDA   CHAATT
59           STA   PORTA
60           LDA   DELAY
61           STA   TDELAY
62           STA   POINTR
63           LDA   #%11000000
64           STA   DINER
65           LDA   #%11100000
66           STA   INTER
67           LDA   #$00
68           STA   $3FE
69           LDA   #$64
70           STA   $3FF
71           RTS
```

TEMP2 1 of 1

```
 1 DADHI    =    $C400
 2 DTOLO    =    $C404
 3 DTOHI    =    $C405
 4 DTOHL    =    $C407
 5 DATLO    =    $C410
 6 DATHI    =    $C420
 7 T2LOW    =    $C434
 8 T2HIG    =    $C435
 9 T2LOL    =    $C436
10 T2HIL    =    $C437
11 T3LOL    =    $C438
12 T3HIG    =    $C439
13 INTFR    =    $C43D
14 INTER    =    $C43E
15 DINFR    =    $C40D
16 DINER    =    $C40E
17 SAMPLE   =    $61D0
18 ADVALUE  =    $61DA
19 CONVERT  =    $6270
20 PLOT     =    $63A0
21 CHAATT   =    $61E4
22 MEME     =    $61CE
23 NUM      =    $06
24 COUNT    =    $01
25 POINTR   =    $02
26 DELAY    =    $61D2
27 TDELAY   =    $03
28          ORG  $6400
29          STA  $45
30          LDY  POINTR
31          LDA  #%10000000
32          BIT  INTFR
33          BEQ  AD
34          LDA  #$BE
35          STA  T2LOL
36          LDA  #$C7
37          STA  T2HIL
38          DEY
39          STY  POINTR
40          CPY  #$00
41          BNE  END
42          LDA  DELAY
43          STA  POINTR
44          LDA  T3LOL
45          EOR  #$FF
46          STA  MEME
47          LDA  T3HIG
48          EOR  #$FF
49          STA  MEME+1
50          LDA  #$00
51          STA  INTER
52 END      LDA  $45
53          RTI
54          BRK
55 AD       LDX  TDELAY
56          DEX
57          LDA  #$C7
58          STA  DTOHL
59          STX  TDELAY
60          CPX  #$00
61          BNE  ADEND
62          LDA  DATLO
63          STA  ADVALUE
64          LDA  DATHI
65          STA  ADVALUE+1
66          JSR  CONVERT
67          LDA  DELAY
68          STA  TDELAY
69          DEC  SAMPLE
70          LDA  #$00
71          CMP  SAMPLE
72          BEQ  FIN
73          LDA  #$BE
74          STA  DTOLO
75          LDA  #$C7
76          STA  DTOHI
77          STA  DADHI
78 ADEND    LDA  $45
79          RTI
80          BRK
81 FIN      LDA  #$00
82          STA  DINER
83          LDA  #$02
84          STA  NUM
85          LDA  $45
86          RTI
87          BRK
```

CONVERT 1 of 1

```
 1 ADVALUE  =    $61DA
 2 MEME     =    $7A00
 3 MEMPT    =    $04
 4          ORG  $6270
 5          LDY  MEMPT
 6 CONVERT  LDA  ADVALUE+1
 7          AND  #$20
 8          BNE  PLUS
 9 MINUS    LDA  ADVALUE
10          EOR  #$FF
11          STA  MEME,Y
12          INY
13          STA  ADVALUE
14          LDA  ADVALUE+$01
15          EOR  #$FF
16          ORA  #$E0
17          STA  MEME,Y
18          STA  ADVALUE+$01
19          INY
20          STY  MEMPT
21          JMP  FIN
22 PLUS     LDA  ADVALUE+1
23          AND  #$1F
24          STA  MEME,Y
25          STA  ADVALUE+1
26          INY
27          LDA  ADVALUE
28          STA  MEME,Y
29          INY
30          STY  MEMPT
31 FIN      RTS
32          BRK
```

TEMPWAND 1 of 3

```
10  PRINT  CHR$ (4)"PR#3"
20  LOMEM: 32768
30  DIM IN$(20)
40  DIM SEL(20,2)
50  DIM SL(100,2)
60 LS = 120
70 LA = 25
80 CD$ =  CHR$ (13) +  CHR$ (4)
120  PRINT CD$"BLOADATTENT"
130  PRINT CD$"BLOADTEMP1"
140  PRINT CD$"BLOADCONVERT"
150  PRINT CD$"BLOADMADMAIN"
170  PRINT CD$"BLOADTEMP2"
180  TEXT : HOME : PRINT  TAB( 7)"** MENU **"
190  PRINT : PRINT "0 = QUIT"
230  PRINT "1= SCROLLER"
240  PRINT : PRINT "ENTER OPTION (0-1)? ";: GET C$: PRINT C$: OP =  ASC (C$
     ) - 48: IF OP = 0 THEN  END
250  IF OP <  > 1 THEN  GOTO 240
260  ON OP GOSUB 280
280  HOME
290 Z = 0: D = 0:  REM : TO ALLOW SETTING UP STEP
295 DZ = 0
300  PRINT : PRINT "INPUT FILENAME ELSE DEFAULT RETURN"
310 DTET = 0: VT = 1
320 S = 0:  PRINT : PRINT : S$ = "LOAD WHICH FORMAT FILE": RG$ = "": IN$(S) =
     "NONE":  GOSUB 760:  IF A$ = "" GOTO 340
330  PRINT CD$;"OPEN";IN$(S):  GOSUB 1000:  PRINT CD$;"READ";B$:  INPUT NS:  FOR
     I = 1 TO NS:  INPUT IN$(I):  NEXT :  PRINT CD$;"CLOSE"
340  HOME : PRINT "INPUT VALUES":  PRINT :  PRINT : IN$(1) = "3"
350 S = 2: S$ = "AD SAMPLE": RG$ = "1:256":  GOSUB 760: AD = VO
360 S = 3: S$ = "DELAY(20=1SEC)": RG$ = "1:256":  GOSUB 760: DD = VO
370  PRINT
380  POKE 25040, AD:  POKE 25042, DD
390 S = 9: S$ = "CHANNEL NO": RG$ = "0:7":  GOSUB 760: CH = VO
400 S = 10: S$ = "ATTENUATION": RG$ = "0:9":  GOSUB 760: TT = VO
410  PRINT
420 CH = CH + (TT * 16)
430  POKE 25060, CH
440 S = 4: S$ = "ADALAB VOLTAGE RANGE": RG$ = "0.5,1,2,4":  GOSUB 760: AGAIN =
     VO
450  PRINT
460 S = 5: S$ = "AMP HARDWARE GAIN RANGE": RG$ = "0.1,1,10,100":  GOSUB 760: H
    GAIN = VO
470  PRINT
474  POKE 31232,0
475  POKE 31233,0
476  POKE 31235,0
477  POKE 31234,0
480  CALL 24576:  REM  AD SAMPLE
505 XH =  PEEK (31232)
507 XL =  PEEK (31233)
510 XH = (XH * 256) + XL
520 SH =  PEEK (31234)
530 SL =  PEEK (31235)
540 SH = (SH * 256) + SL
550 BH =  PEEK (29408 + TT * 2)
560 BL =  PEEK (29408 + TT * 2 + 1)
565 V1H =  PEEK (25051)
567 V2L =  PEEK (25050)
570 BH = BH * 256 + BL
580 P1T = (XH * BH) / (HGAIN * AGAIN)
582 P2T = (SH * BH) / (HGAIN * AGAIN)
584 P1T = P1T / 8141
586 P2T = P2T / 8141
590 SLOPE = (P2T - P1T) / (DD * .05)
610 CH =  PEEK (25039)
620 CL =  PEEK (25038)
630 CT = CL + (CH * 256)
635 SLOPE = SLOPE * 10
640  TEXT : HOME : PRINT  CHR$ (4)"PR#1"
650  PRINT "SLOPE(torr/s) = "; SLOPE
```

TEMPWAND 2 of 3

```
652  PRINT P1T
653  PRINT P2T
660  PRINT  CHR$ (4)"PR#3"
690 S = 7: S$ = "CONTINUE SCROLL": RG$ = "Y/N": GOSUB 760
700  IF IN$(S) = "N" THEN  GOTO 1220
750  GOTO 340
760  PRINT S$;"(";RG$;")?<";IN$(S);">";: GOSUB 1020: OK = 0: IF A > 0 THEN
     IN$(S) = A$: GOTO 800
770 A =  LEN (IN$(S)): IF A = 0 GOTO 980
780  FOR I = 1 TO A: IF  MID$ (IN$(S),I,1) = "," THEN B = I + 1: I = A
790  NEXT
800  IF S = 4 OR 5 GOTO 990
810 L =  LEN (RG$): IF L = 0 GOTO 990
820  PRINT A$
830  PRINT L
840 R$ = "": R = 0: FOR J = 1 TO L
850  IF  MID$ (RG$,J,1) <  > ":" THEN R$ = R$ +  MID$ (RG$,J,1): IF J < L GOTO
     970
860  IF  VAL (R$) = 0 AND  ASC (R$) <  > 48 GOTO 930
870  IF R = 0 THEN V0 =  VAL (IN$(S)): IF V0 <  VAL (R$) GOTO 950
880  PRINT V0
890  IF R = 1 THEN  IF V0 >  VAL (R$) GOTO 950
900  IF R = 2 THEN V1 =  VAL ( MID$ (IN$(S),B)): IF V1 <  VAL (R$) GOTO 95
     0
910  IF R = 3 THEN  IF V1 >  VAL (R$) GOTO 950
920 R = R + 1: OK = 1: R$ = "": GOTO 970
930  IF IN$(S) <  > R$ THEN R$ = "": GOTO 970
940 OK = 1: GOTO 960
950 OK = 0
960 J = L
970  PRINT R$: NEXT
980  IF OK = 0 THEN  PRINT  CHR$ (7);"INVALID ENTRY;CHECK (RANGE)": AUT = 0
     : GOTO 760
990 V0 =  VAL (IN$(S)): RETURN
1000  IF B THEN B$ =  LEFT$ (IN$(S),B - 2): RETURN
1010 B$ = IN$(S): RETURN
1020 A = 0: B = 0: A$ = "": IF AUT = 1 AND S < LS AND  PEEK ( - 16384) < 128
      THEN  PRINT : RETURN
1030 AUT = 0
1050  GET C$: C =  ASC (C$): IF C > 31 GOTO 1200
1060  IF C <  > 8 GOTO 1120
1070  IF A = 0 GOTO 1020
1080  PRINT C$;" ";C$;: A = A - 1
1090  IF A > 0 THEN A$ =  LEFT$ (A$,A)
1100  IF A < 1 GOTO 1020
1110  GOTO 1050
1120  IF C = 13 THEN  PRINT : RETURN
1130  IF C = 27 AND ES THEN  GOSUB 11000: AUT = 1:  POP :  POP :  GOTO 110
1140  IF C = 1 THEN AUT = 1: LS = 50: DTET = 1:  GOTO 1020
1150  IF C = 4 THEN  PRINT : PRINT CD$;A$:  POP :  GOTO 760
1160  IF C = 7 THEN  GOSUB 730 GOTO 1050
1170  IF C = 20 THEN  GOSUB 840 GOTO 1050
1180  IF C = 19 THEN  GOSUB 840
1190  IF C = 24 THEN  PRINT  CHR$ (92): GOTO 1020
1200  IF C = 44 AND B = 0 THEN B = A + 2
1210  PRINT C$;: A = A + 1: A$ = A$ + C$: GOTO 1050
1220  PRINT "SAVE FILES": AUT = 0
1230 E = 11
1240 S = 11: S$ = "WRITE DATA FILENAME"
1250 RG$ = "": IN$(S) = "NONE"
1260  GOSUB 760: IF A$ = "" GOTO 1290
1270  PRINT CD$;"OPEN";IN$(S): GOSUB 1000: PRINT CD$;"WRITE";B$
1275 Z = VT
1280  FOR A = 1 TO Z: PRINT SEL(A,1): PRINT SEL(A,2): NEXT : PRINT CD$;"CL
     OSE"
1290 S = E + 1: S$ = "WRITE FORMAT FILENAME": RG$ = "": IN$(S) = "NONE": GOSUB
     760: IF A$ = "" THEN  GOTO 180
1300  PRINT CD$;"OPEN";IN$(S): GOSUB 1000: PRINT CD$;"WRITE";B$: PRINT S
1310  FOR I = 1 TO S: PRINT  CHR$ (34);IN$(I); CHR$ (34): NEXT : PRINT CD$
     ;"CLOSE"
1320  GOTO 180
```

TEMPWAND 3 of 3

```
1330  PRINT "NO. OF PTS NOW EQUALS 100"
1340 DTET = 0
1355 QQ = .2
1360 TALLY = 0: TIT = 0: A = 0: B = 0: C = D:
1365 C = C - DZ
1380  FOR I = 1 TO C: TALLY = SL(I,1) + TALLY
1390  NEXT
1400 TVE = TALLY / C
1410 TMI = QQ * TVE
1420  FOR I = 1 TO C: TCAL = TVE - SL(I,1)
1430  IF  ABS (TCAL) > TMI THEN SL(I,1) = 0: A = A + 1
1440  NEXT
1450 VENT = 0
1460  FOR I = 1 TO C: VENT = SL(I,1) + VENT: NEXT
1470 C = C - A
1475  IF C = 0 THEN C = 1: PRINT "ALL PTS ARE OUTSIDE ";TMI;" FROM AVE "
1480 TVE = VENT / C
1485 SEL(VT,1) = TVE
1530  FOR I = 1 TO Z: TIT = SL(I,2) + TIT
1540  NEXT
1550  FOR I = 1 TO Z: PRINT "Z= ";I
1552  PRINT "CT= ";SL(I,2)
1555  NEXT
1560 TET = TIT / Z
1565 : PRINT "TET= ";TET
1570 TFT = QQ * TET
1580  FOR I = 1 TO Z: TGT = TET - SL(I,2)
1590  IF  ABS (TGT) > TFT THEN SL(I,2) = 0: B = B + 1
1600  NEXT
1605  PRINT "B= ";B
1610 TH = 0
1620  FOR I = 1 TO Z: TH = SL(I,2) + TH
1630  NEXT
1640 Z = Z - B
1645  IF Z = 0 THEN Z = 1: PRINT "ALL PTS ARE OUTSIDE ";TFT;" FROM AVE"
1650 TJ = TH / Z
1655 SEL(VT,2) = TJ
1656  PRINT  CHR$ (4)"PR#1"
1657  PRINT "FOR PT ";VT
1658  PRINT "AVE SLOPE = ";TVE
1660  PRINT "AVE COUNT = ";TJ
1665  PRINT  CHR$ (4)"PR#3"
1670  INPUT "PRESS CR TO CONTINUE";A$
1675 Z = 1: D = 1: DZ = 0: VT = VT + 1
1680  GOTO 340
```

1.2 Data Analysis Programmes.

(a) MR BIG.

The MR BIG programme (APPLESOFT 3.3) is divided into two separate sections. The first allows for input, manipulation and storage of data files obtained for ion-molecule reactions. The second section allows for analysis of these files.

The rate of decay for any particular ion-molecule reaction can be calculated from a least-squares fit of the log of the ion count versus the neutral flow. The rate coefficient is then obtained from a routine utilising equation (2.8), as detailed in section 2.10. A plot of the ion count versus neutral flow for an ion-molecule reaction can also be made. Analysis of the products of an ion-molecule reaction is another option. The routine calculates the percentage of each product ion as a function of neutral flow. These results can also be plotted.

The following page shows the output from MR BIG after data analysis of a typical ion-molecule reaction run (C^+ + HC_3N (reaction (3.01))).

Data output from MR BIG for the reaction of C^+ with HC_3N.

2-2-85 No1 C+/HC3N .3 torr 302.2k port2 HEcarrier mobility 20
filename C+/HC3N/1 tylan 292

	X	Y1	Y2	Y3	Y4	Y5
1	0	29354	1	0	2	1
2	.03439	2738	100	1218	56	467
3	.0246	4408	148	1829	77	614
4	.0138	9567	178	1960	74	678
5	6.88E-03	15833	148	1908	71	635
6	1.47E-03	24739	69	936	22	317
7	5E-04	28449	49	706	33	237
8	0	30184	1	1	0	3

Kcorr= 4.79+/-.10 E-9 Intercept= 4.447 +/-.5336

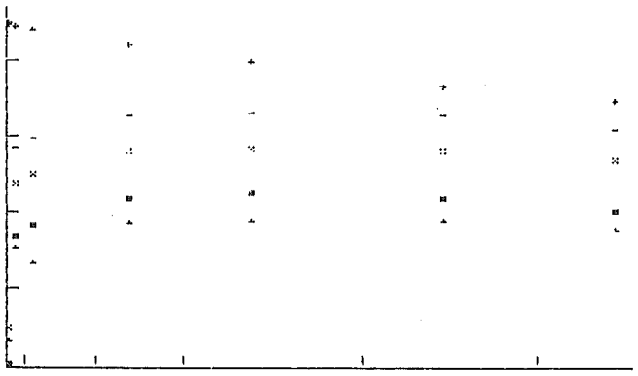

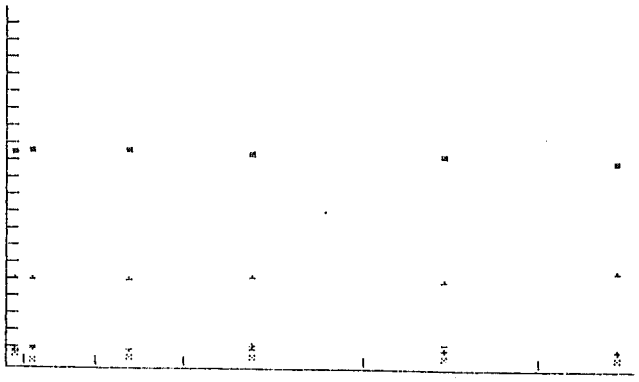

MR BIG 1 of 13

```
5  ONERR  GOTO 140
10  PRINT  CHR$ (4)"PR#3"
20  PRINT  CHR$ (4)"BRUN LOMEM:": &  LOMEM: 16384
30 CD$ =  CHR$ (13) +  CHR$ (4)
40 CC$ =  CHR$ (9)
50  POKE 7,0: POKE 8,0
60  DIM IN$(27)
70 N = 7: I = 17: MAX = 1
80 TRAD = 3.66: PI = 3.14159
90  DIM Y(I,N), X(I), YP(I,N), XP(I)
100  DIM PERC(I,N), TT(I), DF(N)
110 Z1 = 0: I = 0: N = 1
120 PTS = 0
122  HGR : HCOLOR= 1: X = 0: Y = 0:  ROT= 0:  SCALE= 1
123  TEXT : XAXIS = 270: YAXIS = 180: BASE = 2
130  GOTO 160
140  PRINT "error !! NO SUCH FILE "
150  INPUT "PRESS <CR>"; A$
160  TEXT :  HOME :  PRINT  TAB( 7)"** MENU **"
170  PRINT :  PRINT "0 = runtime data entry "
180  PRINT "1 = add one or more pts "
190  PRINT "2 = load data file "
200  PRINT "3 = edit any pt no. "
210  PRINT "4 = delete any pt no. "
220  PRINT "5 = save data file "
230  PRINT "6 = list data file "
240  PRINT "7 = calculations menu "
250  PRINT :  PRINT "ENTER OPTION (0-7)? ";:  GET C$:  PRINT C$: OP =  ASC (C$
     ) - 48
260  IF OP <  > 7 THEN  GOTO 330
270  FOR I = 1 TO PTS
280  FOR N = 1 TO MAX
290 XP(I) = X(I): YP(I,N) = Y(I,N)
300  NEXT
310  NEXT
320  GOTO 1270
330  IF OP = 0 THEN  GOTO 3460
340  IF OP = 1 THEN  GOTO 460
350  IF OP = 2 THEN  GOTO 720
360  IF OP = 3 THEN  GOTO 890
370  IF OP = 4 THEN  GOTO 1020
380  IF OP = 5 THEN  GOTO 1140
390  IF OP = 6 THEN  GOTO 410
400  IF OP < 0 OR OP > 7 THEN  GOTO 160
410  HOME :  PRINT  TAB( 7)"** data file listing **":  PRINT
420  IF PTS = 0 THEN  GOTO 160
430  GOSUB 600
440  INPUT A$
450  GOTO 160
460  HOME :  PRINT  TAB( 7)"** pts addition **":  PRINT
470  INPUT "NO OF IONS? "; MAX
480  HOME :  PRINT  TAB( 7)"** pts addition **":  PRINT
490 I = I + 1
500  IF PTS = 0 THEN  GOTO 520
510  GOSUB 600
520  PRINT :  INPUT "  X?"; X(I)
530  FOR N = 1 TO MAX
540  PRINT N;:  INPUT " Y?"; Y(I,N)
550  NEXT
560  INPUT "~N~ TO QUIT "; A$
570  PRINT : PTS = I
580  IF A$ = "N" THEN  GOTO 160
590  GOTO 480
600  VTAB 3:  POKE 1403,2:  PRINT "X"
610  FOR N = 1 TO MAX
620  VTAB 3:  POKE 1403,(7 * (N + 1)):  PRINT "Y";:  PRINT N
630  NEXT
640  FOR I = 1 TO PTS
650  VTAB (I + 4):  PRINT I
660  VTAB (I + 4):  HTAB 3:  PRINT X(I)
670  FOR N = 1 TO MAX
```

MR BIG 2 of 13

```
680  VTAB (I + 4): POKE 1403,(7 * (N + 1)): PRINT Y(I,N)
690  NEXT
700  NEXT
710  RETURN
720  HOME : PRINT  TAB( 7)"** data file input **": PRINT
730 Z = 0
740 S = 17: PRINT : PRINT :S$ = "LOAD WHICH DATA FILE":RG$ = "":IN$(S) = "
     NONE": GOSUB 1750: IF A$ = "" GOTO 160
750  PRINT CD$;"OPEN";IN$(S):
760  GOSUB 1990: PRINT CD$;"READ";B$:
770  INPUT PTS
780  INPUT MAX
790  FOR I = 1 TO PTS
800  FOR N = 1 TO MAX
810  INPUT Y(I,N): INPUT X(I)
820  NEXT
830  NEXT
840  PRINT CD$;"CLOSE"
850  HOME : PRINT  TAB( 7)"** data file input **": PRINT
860  GOSUB 600
870  INPUT A$
880  GOTO 160
890  HOME : PRINT  TAB( 7)"** edit file **": PRINT
900  IF PTS <  > 0 THEN  GOTO 930
910  PRINT "no pts to edit"
920  INPUT "PRESS A KEY FOR MENU";A$: GOTO 160
930  GOSUB 600
940  PRINT : INPUT "WHICH PT? ";I
950  INPUT "  X?";X(I)
960  FOR N = 1 TO MAX
970  INPUT " Y?";Y(I,N)
980  NEXT
990  PRINT : INPUT "ANOTHER? ";A$
1000  IF A$ = "Y" THEN  GOTO 890
1010  GOTO 160
1020  HOME : PRINT  TAB( 7)"** delete pts **": PRINT
1030  IF PTS <  > 0 THEN  GOTO 1050
1040  PRINT "no pts to edit": INPUT "PRESS A KEY FOR MENU";A$: GOTO 160
1050  GOSUB 600
1060  PRINT : INPUT "WHICH PT? ";I
1070  FOR A = I TO PTS
1080  FOR N = 1 TO MAX
1090 Y(A,N) = Y(A + 1,N):X(A) = X(A + 1): NEXT
1100  NEXT
1101 A = 0:I = 0:N = 1
1110 PTS = PTS - 1
1120  INPUT "ANOTHER? ";A$: IF A$ = "Y" THEN  GOTO 1020
1130  GOTO 160
1140  HOME : PRINT  TAB( 7)"** save file **": PRINT
1150 S = 19:S$ = "WRITE DATA FILENAME ":RG$ = "":IN$(S) = "NONE"
1160  GOSUB 1750: IF A$ = "" GOTO 160
1170  PRINT CD$;"OPEN";IN$(S): GOSUB 1990: PRINT CD$;"WRITE";B$
1180 N = 1
1190  PRINT PTS
1200  PRINT MAX: FOR I = 1 TO PTS
1210  FOR N = 1 TO MAX
1220  PRINT Y(I,N): PRINT X(I)
1230  NEXT : NEXT
1240  PRINT CD$;"CLOSE"
1250  IF P1 = 2 THEN  RETURN
1260  GOTO 160
1270  TEXT : HOME : PRINT  TAB( 7)"** MENU **"
1280  PRINT : PRINT "0 = load rate variables "
1290  PRINT "1 = reset rate variables "
1300  PRINT "2 = save rate variables "
1310  PRINT "3 = calculate rate constant "
1320  PRINT "4 = calculate product ratio "
1330  PRINT "5 = hires screen 1 plot (new or old) "
1340  PRINT "6= data menu "
1350  PRINT "7 = quit "
1360  PRINT : PRINT "ENTER OPTION (0-7)? ";: GET C$: PRINT C$:OP =  ASC (C
```

MR BIG 3 of 13

```
     $) - 48
1370  IF OP = 7 THEN  END
1380  IF OP < 0 OR OP > 7 THEN  GOTO 1270
1390  IF OP = 0 THEN  GOTO 1530
1400  IF OP = 1 THEN  GOTO 1570
1410  IF OP = 2 THEN  GOTO 2220
1420  IF OP = 3 THEN  GOTO 2390
1430  IF OP = 4 THEN  GOTO 4910
1440  IF OP = 5 THEN  GOTO 6930
1450  IF OP = 6 THEN  GOTO 1460
1460  FOR I = 1 TO PTS
1470  FOR N = 1 TO MAX
1480 X(I) = XP(I)
1490 Y(I,N) = YP(I,N)
1500  NEXT
1510  NEXT
1520  GOTO 160
1530  HOME : PRINT  TAB( 7)"** load file **": PRINT
1540 S = 0: PRINT : PRINT :S$ = "LOAD WHICH FILE":RG$ = "":IN$(S) = "NONE"
     : GOSUB 1750: IF A$ = "" GOTO 1270
1550  PRINT CD$;"OPEN";IN$(S): GOSUB 1990: PRINT CD$;"READ";B$: INPUT NS: FOR
     I = 1 TO NS: INPUT IN$(I): NEXT : PRINT CD$;"CLOSE"
1560  GOTO 1270
1570  HOME : PRINT "INPUT VALUES": PRINT : PRINT :IN$(1) = "3"
1572 Z1 = 1
1580 S = 5:S$ = " RUN NO. ":RG$ = "1:30": GOSUB 1750:RU = VO
1590 S = 6:S$ = " DATE ":RG$ = "": GOSUB 1750:DA$ = IN$(S)
1600 S = 7:S$ = " PORTAL NO. ":RG$ = "1:2": GOSUB 1750:PO = VO
1610 S = 8:S$ = " NEUTRAL VOL.":RG$ = "100:7000": GOSUB 1750:NVOL = VO
1620 S = 2:S$ = "ROOM TEMP ('C) ":RG$ = "15:40": GOSUB 1750:TE = VO
1630 TE = TE + 273.2
1640 S = 13:S$ = "TUBE PRESS. ":RG$ = "0.1:1.0": GOSUB 1750:PRESS = VO
1650 S = 3:S$ = " TYLAN FLOW VALUE ":RG$ = "50:500": GOSUB 1750:T8Y = VO
1660 S = 4:S$ = " REACTION TITLE ":RG$ = "": GOSUB 1750:TI$ = IN$(S)
1670 S = 9:S$ = " ION MOBILITY ":RG$ = "1:500": GOSUB 1750:IN = VO
1680 S = 10:S$ = " CARRIER TYPE ":RG$ = "HE:H2:AR:N2": GOSUB 1750:CARR$ =
     IN$(S)
1690 S = 11:S$ = " COMMENTS ":RG$ = "": GOSUB 1750:COMM$ = IN$(S)
1700 S = 12:S$ = " CONTINUE SCROLL ":RG$ = "Y/N": GOSUB 1750
1710  IF IN$(S) = "N" THEN  GOTO 1270
1720 Z = Z + 1: IF Z <  = 25 GOTO 1570
1730 Z = Z - 1
1740  GOTO 1970
1750  PRINT S$;"(";RG$;")?<";IN$(S);">";: GOSUB 2010:OK = 0: IF A > 0 THEN
     IN$(S) = A$: GOTO 1790
1760 A =  LEN (IN$(S)): IF A = 0 GOTO 1970
1770  FOR I = 1 TO A: IF  MID$ (IN$(S),I,1) = "," THEN B = I + 1:I = A
1780  NEXT
1790  IF S = 4 OR 5 GOTO 1980
1800 L =  LEN (RG$): IF L = 0 GOTO 1980
1810  PRINT A$
1820  PRINT L
1830 R$ = "":R = 0: FOR J = 1 TO L
1840  IF  MID$ (RG$,J,1) <  > ":" THEN R$ = R$ +  MID$ (RG$,J,1): IF J < L
      GOTO 1960
1850  IF  VAL (R$) = 0 AND  ASC (R$) <  > 48 GOTO 1920
1860  IF R = 0 THEN VO =  VAL (IN$(S)): IF VO <  VAL (R$) GOTO 1940
1870  PRINT VO
1880  IF R = 1 THEN  IF VO >  VAL (R$) GOTO 1940
1890  IF R = 2 THEN V1 =  VAL ( MID$ (IN$(S),B)): IF V1 <  VAL (R$) GOTO 1
     940
1900  IF R = 3 THEN  IF V1 >  VAL (R$) GOTO 1940
1910 R = R + 1:OK = 1:R$ = "": GOTO 1960
1920  IF IN$(S) <  > R$ THEN R$ = "": GOTO 1960
1930 OK = 1: GOTO 1950
1940 OK = 0
1950 J = L
1960  PRINT R$: NEXT
1970  IF OK = 0 THEN  PRINT  CHR$ (7);"INVALID ENTRY;CHECK (RANGE)":AUT =
     0: GOTO 1750
1980 VO =  VAL (IN$(S)): RETURN
```

MR BIG 4 of 13

```
1990  IF B THEN B$ =  LEFT$ (IN$(S),B - 2): RETURN
2000 B$ = IN$(S): RETURN
2010 A = 0: B = 0: A$ = "": IF AUT = 1 AND S < LS AND  PEEK ( - 16384) < 128
     THEN  PRINT : RETURN
2020 AUT = 0
2030  GET C$: C =  ASC (C$): IF C > 31 GOTO 2180
2040  IF C <  > 8 GOTO 2100
2050  IF A = 0 GOTO 2010
2060  PRINT C$;" ";C$;: A = A - 1
2070  IF A > 0 THEN A$ =  LEFT$ (A$,A)
2080  IF A < 1 GOTO 2010
2090  GOTO 2030
2100  IF C = 13 THEN  PRINT : RETURN
2110  IF C = 27 AND ES THEN  GOSUB 11000: AUT = 1: POP : POP : GOTO 1650
2120  IF C = 1 THEN AUT = 1: LS = 50: GOTO 2010
2130  IF C = 4 THEN  PRINT : PRINT CD$;A$: POP : GOTO 1750
2140  IF C = 7 THEN  GOSUB 2560 GOTO 2030
2150  IF C = 20 THEN  GOSUB 3010 GOTO 2030
2160  IF C = 19 THEN  GOSUB 3010
2170  IF C = 24 THEN  PRINT  CHR$ (92): GOTO 2010
2180  IF C = 44 AND B = 0 THEN B = A + 2
2190  PRINT C$;: A = A + 1: A$ = A$ + C$: GOTO 2030
2200  INPUT "CALC. RATE? (Y/N)";A$: IF A$ = "Y" THEN  GOSUB 2560
2210  GOSUB 2280
2220  HOME : PRINT  TAB( 7)"** save rate variables **"
2230  PRINT : PRINT : E = 19
2240 S = E + 1: S$ = "WRITE FORMAT FILENAME": RG$ = "": IN$(S) = "NONE": GOSUB
     1750: IF A$ = "" THEN  GOTO 1270
2250  PRINT CD$;"OPEN";IN$(S): GOSUB 1990: PRINT CD$;"WRITE";B$: PRINT S
2260  FOR I = 1 TO S: PRINT  CHR$ (34);IN$(I); CHR$ (34): NEXT : PRINT CD$
     ;"CLOSE"
2270  GOTO 1270
2279 N = 1: AA = 13
2280  HOME : VTAB N: POKE 1403,1: PRINT DA$;: POKE 1403,9: PRINT "No";RU
2282  VTAB N: POKE 1403,AA: PRINT TI$
2283 L =  LEN (TI$): L = L + AA + 1
2284  VTAB N: POKE 1403,L: PRINT PR
2285 AA = 4
2286  VTAB N: POKE 1403,L + AA: PRINT "torr ";: PRINT TE
2287 AA = L + AA + 10
2288  VTAB N: POKE 1403,AA: PRINT "k ";: PRINT "port";PO;: PRINT " ";CA$;:
      PRINT "carrier"
2289 AA = AA + 18
2290  VTAB N: POKE 1403,AA: PRINT " mobility ";IN
2292  VTAB N + 1: POKE 1403,AA: PRINT " tylan
";T8Y
2293  IF IN$(19) = "" THEN IN$(19) = "NONE"
2294 L9 =  LEN (IN$(19)): L9 = L9 + 10
2296  VTAB N + 1: POKE 1403,AA - L9: PRINT "filename ";IN$(19)
2298  GOSUB 600
2300 KC = 1.42
2302 N = PTS + 6
2303  VTAB N: POKE 1403,0: PRINT "K=      ";R2;: PRINT " E";E
2304 R2 = R2 * KC: R2 = R2 * 1000: R2 =  INT (R2): R2 = R2 / 1000
2305 S1 = S1 * R2 * 100
2306 S1 =  INT (S1): S1 = S1 / 10000
2308 AA = 13
2309 N = N + 1
2314  VTAB N: POKE 1403,0: PRINT "Kcorr= ";R2;: POKE 1403,AA: PRINT "+/-";
     S1
2315 AA = AA + 7
2316  VTAB N: POKE 1403,AA: PRINT " E";E
2318 I1 = I1 * 1000: I1 =  INT (I1): I1 = I1 / 1000
2319 I2 = I1 * 12 * 100: I2 =  INT (I2): I2 = I2 / 10000
2321 AA = 26: BB = 17
2326  VTAB N: POKE 1403,AA: PRINT "Intercept= ";I1;: POKE 1403,AA + BB: PRINT
     "+/-";I2
2329  VTAB N + 2: POKE 1403,0: PRINT "rate 1 corr.  = ";ET;: POKE 1403,25: PRINT
     "orginal slope = ";SL
2335  VTAB N + 3: POKE 1403,0: PRINT "slope corr.  = ";ZT
2360  VTAB N + 5: POKE 1403,0: INPUT "HARDCOPY ? (Y/N)";A$
```

MR BIG 5 of 13

```
2362  IF A$ <  > "Y" THEN  GOTO 2376
2363  VTAB N + 6: POKE 1403,0: INPUT "dump GRAPH as well ? (Y/N)";AA$
2364  PRINT  CHR$ (4)"PR#1"
2365  PRINT CC$"8S"
2368  PRINT  CHR$ (4)"PR#3"
2369  IF AA$ <  > "Y" THEN  GOTO 2376
2370  REM  :need a protect. here if 'no' graph
2371  GOSUB 6140
2376 N = 1
2380  RETURN
2390  HOME : PRINT  TAB( 7)"** rate calculation **": PRINT
2392  IF Z1 = 1 THEN  GOTO 2400
2393  HOME : PRINT  TAB( 7)"**   INITIATE RATE VARIABLES !!   **"
2394  INPUT A$: GOTO 1270
2400  FOR I = 1 TO PTS
2410  FOR N = 1 TO MAX
2420 XP(I) = X(I)
2430 YP(I,N) = Y(I,N)
2440  NEXT
2450  NEXT
2460  GOSUB 600
2470 WSLIP = 0:BSLIP = 0:AI = 0:BI = 0
2480 CI = 0:DEN = 0:DLTA = 0:GAM = 0:SLOPE = 0
2490 AXK = 0:R2 = 0
2500 AZE = 0:FLOW = 0:W1 = 0:W2 = 0:W3 = 0:MIC = 0:ZAP = 0
2510 I1A = 0
2512  IF MAX = 1 THEN N = 1: GOTO 2522
2520  PRINT : INPUT "FOR WHICH ION? ";N
2522  VTAB PTS + 7: POKE 1403,0: PRINT "CALCULATING"
2560  GOSUB 3200 REM  neutral flow cac
2570  GOSUB 3020 REM  carrier flow calc
2580  GOSUB 3270 REM  leastsq. analysis
2590  FOR I = 1 TO PTS
2600 Y(I,N) = X(I) * SLOA + I1A
2610  NEXT
2612 S1 =  - Z1 * 100 / SL:I2 = Z2 * 100 / I1
2620  GOSUB 3270
2650 WSLIP = 2 / (1 + (5.52 * YMFP / (PRESS * TRAD)))
2660 BSLIP = 1 + (2.76 * YMFP) * (PRESS * TRAD)
2680 AI = (.25 - BSLIP) * (.1 - .6 * BSLIP) - ((.15 - .75 * BSLIP) * (.15 -
     .75 * BSLIP))
2690 BI = (1.6 * BSLIP) - .4
2700 CI = .025 - (.075 * BSLIP)
2710 DEN =  SQR (BI * BI - 32.0 * AI)
2720 A = 2 * AI:B = BI - DEN
2730 DLTA = (1 / A) * B
2740 GAM =  - (.5 / AI) * (CI - (2 * BI * CI + 6.4 * AI) * .5 / DEN)
2750 DLTA = DLTA / WSLIP
2760 GAMMA = GAM / WSLIP
2780 SLOPE =  - SLOPE * 1E - 14 * 2.302585
2800 A = PI * TRAD * TRAD * FLOW * FLOW
2810 R1 = SLOPE * A / (GAMMA * RLNGTH)
2812 ET = A / (GAMMA * RLNGTH)
2830 NEUTFLOW = NEUTFLOW * 1E14
2840 BC = NEUTFLOW / (PI * TRAD * TRAD * FLOW)
2850 AXK = ((DLTA / (TRAD * TRAD) + (GAMMA * R1 * BC / DI)) / FLOW)
2860 AXK = (AXK / FLOW) * (DI * DI)
2870 R2 = R1 / (1 - AXK)
2872 E = 0
2873 R2 = R2 * 10:E = E - 1
2874  IF R2 < 1000 THEN  GOTO 2873
2876 E = E + 3:R2 =  INT (R2):R2 = R2 / 1000
2878 EPS = (1 / (1 - AXK) - 1) * 100
2879 SLIP = (.629 / GA - 1) * 100
2880  GOTO 2940
2900 N = 5:AA = 20:BB = 20
2902  HOME : PRINT  TAB( 7)"**  MORE rate data  **"
2916  VTAB N: POKE 1403,0: PRINT "slope= ";SL;: POKE 1403,AA: PRINT "diff=
     ";DI;: POKE 1403,AA + BB: PRINT "ymfp= ";YM
2917 AA = 0:N = N + 2
2918  VTAB N: POKE 1403,AA: PRINT "gas= ";GA;: POKE 1403,AA + BB: PRINT "v
```

MR BIG 6 of 13

```
     is= ";VIS
2920 AA = 20:N = N + 2
2922  VTAB N: POKE 1403,0: PRINT "axk= ";AX;: POKE 1403,AA: PRINT "delta=
     ";DL;: POKE 1403,AA + BB: PRINT "bslip= ";BS
2923 AA = 30
2924  VTAB N + 2: POKE 1403,0: PRINT "ave neut flow= ";NE;: POKE 1403,AA: PRINT
     "gamma= ";GA;: POKE 1403,AA + BB: PRINT "carrier flow= ";FL
2930  VTAB N + 4: POKE 1403,0: PRINT "eps= ";EP;: POKE 1403,AA: PRINT "sli
     p= ";SL
2932  INPUT A$
2934  RETURN
2940  FOR I = 1 TO PTS
2950  FOR N = 1 TO MAX
2960 X(I) = XP(I)
2970 Y(I,N) = YP(I,N)
2980  NEXT
2990  NEXT
2992  GOSUB 2279
3000  HOME : INPUT "LIST EXTRA RATE DATA ?";A$
3004  IF A$ = "Y" THEN  GOSUB 2900
3010  GOTO 1270
3020 TY = T8Y
3030  IF CARR$ = "H2" THEN GAS = 8.75E - 5:M1SS = 2:TY = (TY + 10.29) / 2.
     898
3040  IF CARR$ = "HE" THEN GAS = 1.94E - 4:M1SS = 4:TY = (TY + 10.29) / 2.
     898 * 1.402
3050  IF CARR$ = "N2" THEN GAS = 1.76E - 4:M1SS = 14:TY = (TY + 9.703) / 1
     .754
3060  IF CARR$ = "AR" THEN GAS = 2.217E - 4:MASS = 40:TY = (TY + 9.703) /
     1.754 * 1.44
3070 VIS = GAS *  SQR (TE / 273.2)
3100 YMFP = 8.59 * VIS *  SQR (TE / M1SS)
3120 DI = (760 / PRESS * (TE / 273.15) * .02354)
3130 DI = DI * IN
3150 P1RESS = PRESS
3160  GOSUB 3400
3170 P1RESS = PRESS * FLOW / CARRIERV
3180  GOSUB 3400
3190  RETURN
3200  IF PO = 1 THEN RLNGTH = 84.7
3210  IF PO = 2 THEN RLNGTH = 44.7
3220  FOR I = 1 TO PTS
3230 Y(I,N) = ( LOG (Y(I,N)) / 2.302585)
3240 X(I) = X(I) * NVOL / TEMP * 9.656E4
3250  NEXT
3252 ZT = NVOL / TEMP * 9.656E + 18
3260  RETURN
3268  PRINT CC$"e"
3270 A = 0:B = 0:C = 0:D = 0:E = 0
3272 W1 = 0:W2 = 0:W3 = 0
3274 SLOA = 0:I1A = 0:ZAP = 0:MIC = 0
3280  FOR I = 1 TO PTS
3290 A = A + X(I):B = B + Y(I,N):C = C + X(I) * X(I):D = D + Y(I,N) * Y(I,
     N):E = E + X(I) * Y(I,N)
3300  NEXT
3310 W1 = PTS * C - A * A:W2 = PTS * D - B * B:W3 = PTS * E - A * B
3320 NEUT = A / PTS
3330 SLOA = W3 / W1
3340 I1A = (B * C - A * E) / W1
3350 ZAP = PTS * D - B * B - W3 * W3 / W1
3360 ZAP =  SQR (ZAP * ZAP):SIG =  SQR (ZAP):COMP = 2 * SIG / PTS
3370 MIC = (PTS - 2.0) * W1
3380 Z1 = SIG /  SQR (MIC):Z2 = SIG *  SQR (C) /  SQR (PTS * MIC)
3390  RETURN
3400 CARRIERV = (TY * 760 * TE) / (PRESS * 273.2 * TRAD * TRAD * PI)
3410 AZE = (1 - 5.52 * YMFP / (P1RESS * TRAD))
3420 ADE = 160 * VIS / (TRAD * TRAD * CARRIERV * P1RESS * 1.328E4)
3430 FLOW = 1 /  SQR (1 / (CARRIER * CARRIER) - (ADE * AZE * ( - RLNGTH /
     2)))
3450  RETURN
3460  TEXT : HOME : PRINT  TAB( 7)"** runtime data entry **": PRINT
```

MR BIG 7 of 13

```
3470  INPUT "NO OF IONS? ";MAX
3480 P = 0
3490  INPUT "TESTING? ";EZ$
3500  IF EZ$ = "Y" THEN  GOTO 3600
3510 LA = 0
3520 TE =  PEEK (8)
3530  IF TE = 1 THEN  GOTO 3600
3540  PRINT CD$"BLOADATTENT"
3550  PRINT CD$"BLOADTEMP1"
3560  PRINT CD$"BLOADCONVERT"
3570  PRINT CD$"BLOADMADMAIN"
3580  PRINT CD$"BLOADTEMP2"
3590  POKE 8,1
3600  TEXT : HOME : PRINT  TAB( 7)"** runtime data entry **": PRINT
3610 I = 20:V = 0
3620 DZ = 0
3630  PRINT : PRINT "INPUT FILENAME ELSE DEFAULT RETURN"
3640 DTET = 0:VT = 1
3650 S = 21: PRINT : PRINT :S$ = "LOAD WHICH FORMAT FILE":RG$ = "":IN$(S) =
     "NONE": GOSUB 1750: IF A$ = "" GOTO 3670
3660  PRINT CD$;"OPEN";IN$(S): GOSUB 1990: PRINT CD$;"READ";B$: INPUT NS: FOR
     I = 1 TO NS: INPUT IN$(I): NEXT : PRINT CD$;"CLOSE"
3670  PRINT
3680 S = 22:S$ = "CHANNEL NO":RG$ = "0:7": GOSUB 1750:CH = VO
3690 S = 23:S$ = "ATTENTUATION":RG$ = "0:9": GOSUB 1750:TT = VO
3700  PRINT
3710 CH = CH + (TT * 16)
3720  POKE 8168,CH
3730 A =  PEEK (8168): PRINT "CH= ";CH: INPUT AA$
3740 S = 24:S$ = "ADALAB VOLTAGE RANGE":RG$ = "0.5,1,2,4": GOSUB 1750:AGAI
     N = VO
3750  PRINT
3760 S = 25:S$ = "AMP HARDWARE GAIN RANGE":RG$ = "0.1,1,10,100": GOSUB 175
     0:HGAIN = VO
3770  PRINT
3780 LA = LA + 1:V = 0
3790  HOME : POKE 1403,7: PRINT "** neutral flow sampling **": PRINT
3800  PRINT
3810 S = 20:S$ = "DELAY(20 = 1SEC)":RG$ = "1:256": GOSUB 1750:DD = VO
3820 V = V + 1
3830  PRINT
3840  IF EZ$ = "Y" THEN  GOTO 4180
3850 AD = 2
3860  POKE 8160,AD: POKE 8162,DD
3870 A =  PEEK (8160): PRINT "AD= ";A: INPUT AA$
3880 A =  PEEK (8162): PRINT "DD= ";A: INPUT AA$
3890  POKE 4160,0
3900  POKE 4161,0
3910  POKE 4162,0
3920  POKE 4163,0
3930  CALL 2048: REM  ad sample
3940 XH =  PEEK (4160)
3950 XH =  PEEK (4161)
3960 XH = (XH * 256) + XL
3970 SH =  PEEK (4162)
3980 SL =  PEEK (4163)
3990 SH = (SH * 256) + SL
4000 BH =  PEEK (4096 + TT * 2)
4010 BL =  PEEK (4096 + TT * 2 + 1)
4020 V1H =  PEEK (8167)
4030 V2L =  PEEK (8166)
4040 BH = BH * 256 + BL
4050 P1T = (XH * BH) / (HGAIN * AGAIN)
4060 P2T = (SH * BH) / (HGAIN * AGAIN)
4070 P1T = P1T / 8141
4080 P2T = P2T / 8141
4090 SLOPE = (P2T - P1T) / (DD * .05)
4100 CH =  PEEK (8173)
4110 CL =  PEEK (8172)
4120 CT = CL + (CH * 256)
4130 SLOPE = SLOPE * 10
4140 X(V) = SLOPE
```

MR BIG 8 of 13

```
4150  TEXT : HOME : PRINT  CHR$ (4)"PR#1"
4160  PRINT "SLOPE(torr/s) = ";SLOPE
4170  PRINT  CHR$ (4)"PR#3"
4180  HOME
4190  IF EZ$ = "Y" THEN  INPUT "SLOPE? ";X(V)
4200 TT = V
4210 S = 26:S$ = "CONTINUE SAMPLING":RG$ = "Y/N": GOSUB 1750
4220  IF IN$(S) = "N" THEN  GOTO 4240
4230  GOTO 3790
4240  HOME : PRINT  TAB( 7)"** flow values **": PRINT
4250 VV = 1:NN = 0:ET = 11
4260  FOR V = 1 TO TT
4270  VTAB (VV + 2): POKE 1403,(ET * NN): PRINT V
4280  VTAB (VV + 2): POKE 1403,(3 + (ET * NN)): PRINT X(V)
4290 VV = VV + 1
4300  IF VV = 6 THEN VV = 1:NN = NN + 1
4310  NEXT
4320 FE = 11
4330  VTAB (FE - 1): PRINT "WHICH FLOW? ";: GET B$: PRINT B$:V =  ASC (B$)
      - 48
4340  IF V < 1 OR V > TT THEN  GOTO 4330
4350  VTAB (FE + 1): HTAB 2: PRINT V
4360  VTAB (FE + 1): HTAB 5: PRINT X(V)
4370  VTAB (FE + 1): HTAB 14: PRINT "CORRECT? ";: GET B$: PRINT B$:DD =  ASC
     (B$) - 48
4380  IF B$ = "N" THEN  GOTO 4240
4390  IF DD =  - 35 THEN  GOTO 4420
4400  IF B$ = "Y" THEN  GOTO 4420
4410  GOTO 4240
4420 XP(LA) = X(V)
4430  HOME : PRINT  TAB( 7)"** ion counts **": PRINT
4440 T = 1
4450  FOR N = 1 TO MAX
4460  VTAB (2 * N + 1): POKE 1403,0: PRINT "CT ";N;: PRINT " ? "
4470 TT = 7
4480  VTAB (2 * N + 1): POKE 1403,(TT): GOSUB 5290
4490  NEXT
4500 T = 0
4510  HOME : PRINT  TAB( 7)"** ion counts **": PRINT
4520 NN = 0
4530  FOR N = 1 TO MAX
4540  VTAB 4: POKE 1403,(9 * NN): PRINT Y(LA,N)
4550 NN = NN + 1
4560  NEXT
4570  VTAB 6: PRINT "CORRECT? ";: GET B$: PRINT B$:DD =  ASC (B$) - 48
4580  IF B$ = "Y" THEN  GOTO 4630
4590  IF B$ = "N" THEN  GOTO 4430
4600  GOTO 4570
4610  PRINT : INPUT "CORRECT? ";C$
4620  IF C$ = "N" THEN  GOTO 4430
4630 PTS = LA
4640  FOR N = 1 TO MAX
4650 YP(LA,N) = Y(LA,N)
4660  NEXT
4670 X(LA) = XP(LA)
4680 Q = LA
4690 B = 0: IF X(Q) = 0 THEN  GOTO 4720
4700 X(Q) = X(Q) * 10:B = B - 1
4710  IF B <  >  - 4 THEN  GOTO 4700
4720  IF P = 2 THEN  RETURN : REM  to graph plot
4730  IF P = 1 THEN  RETURN : REM  to product ratio routine
4740  IF LA < 2 THEN  GOTO 4780
4750 XAXIS = 270:YAXIS = 180
4760 BASE = 2
4770  GOSUB 5380
4780 S = 27:S$ = "runtime end":RG$ = "Y/N": GOSUB 1750
4790  IF IN$(S) = "N" THEN  GOTO 3780
4800  FOR LA = 1 TO PTS
4810  FOR N = 1 TO MAX
4820 Y(LA,N) = YP(LA,N)
4830  NEXT
4840  NEXT
```

MR BIG 9 of 13

```
4850  FOR LA = 1 TO PTS
4860 X(LA) = XP(LA)
4870  NEXT
4880  HOME : GOSUB 600
4890  INPUT A$
4900  GOTO 160
4910 Q = 0: TA = 0
4940  HOME : PRINT  TAB( 7)"** product ratios **": PRINT
4942  IF MAX = 1 THEN  GOTO 1270
4962  FOR I = 1 TO PTS
4963  FOR N = 1 TO MAX
4964 YP(I, N) = Y(I, N)
4965  NEXT : NEXT
4966  FOR I = 1 TO PTS
4967 XP(I) = X(I)
4968  NEXT
4980  FOR CC = 1 TO MAX
4990 DF(CC) = 1
5000  NEXT
5010 D$ = "": E = 0: A = 0
5020  VTAB 4: INPUT "PT 1 zero factor? (Y/N) "; AA$: IF AA$ <  > "Y" THEN  GOTO
     5150
5030 BB = 1
5040  FOR TA = 2 TO PTS
5050  FOR NT = 1 TO MAX
5060 Y(TA, NT) = Y(TA, NT) - Y(BB, NT)
5070  IF Y(TA, NT) < 0 THEN Y(TA, NT) = 0
5080  NEXT
5090  NEXT
5100 BB = 0
5150  HOME : GOSUB 600
5151 AA = 8: M = 15
5152  FOR A1 = 1 TO MAX
5160  VTAB PTS + AA: POKE 1403, 0: PRINT "this ion? ";: PRINT A1
5161  VTAB PTS + AA: POKE 1403, M: INPUT A$
5170  IF A$ <  > "Y" THEN  GOTO 5222
5172  VTAB PTS + AA: POKE 1403, M: PRINT "      "
5180  VTAB PTS + (AA + 2): PRINT "Mass discrimination factor? (default=1)"
     ;: GOSUB 5290
5190 E = E + 1
5200  FOR I = 1 TO PTS
5210 Y(I, E) = Y(I, A1) * DF(A1)
5220  NEXT
5222  NEXT
5240 TP = E
5270  GOSUB 6490
5280  GOTO 1270
5290  GET C$: C =  ASC (C$): IF C > 31 THEN  GOTO 5320
5300  IF C = 13 THEN  GOTO 5330
5301 BB = 8
5302  IF C = BB THEN  GOTO 5321
5310  GOTO 5290
5320  PRINT C$;: A = A + 1: D$ = D$ + C$: GOTO 5290
5321 A = A - 1
5322  IF A <  = 0 THEN A = 0: GOTO 5290
5323 D$ =  LEFT$ (D$, A)
5324 CC = 39
5327  VTAB PTS + (AA + 2): POKE 1403,(CC + A - 1): PRINT "   ";: POKE 1403
     ,(CC + A - 1)
5328  GOTO 5290
5330  IF A = 0 THEN  GOTO 5360
5350 DF(A1) =  VAL (D$)
5355  PRINT "DF="; DF(A1)
5360 A = 0: D$ = ""
5361  GOTO 5370
5362  VTAB PTS + (AA + 2): POKE 1403, CC: PRINT "
5370  RETURN
5380  IF Q > 2 THEN  GOTO 5400
5390  FOR Q = 1 TO 2
5400  FOR N = 1 TO MAX
5410  IF Y(Q, N) <  > 0 THEN Y(Q, N) =  LOG (Y(Q, N))
```

MR BIG 10 of 13

```
5420  NEXT
5430  IF Q > 2 THEN  GOTO 5590
5440  NEXT
5460 LYGE = Y(1,1):LXGE = X(2)
5470  IF X(1) > X(2) THEN LXGE = X(1)
5480  IF Y(2,1) > Y(1,1) THEN LY = Y(2,1)
5490  IF MAX = 1 THEN  GOTO 5550
5500  FOR T4P = 1 TO 2
5510  FOR N = 2 TO MAX
5520  IF Y(T4P,N) - LY > 0 THEN LY = Y(T4P,N)
5530  NEXT
5540  NEXT
5550  GOSUB 5730: REM  scale
5570  INPUT A$
5580  TEXT : HOME : RETURN : REM  from scale
5590  FOR N = 1 TO MAX
5600 TYE = Y(Q,N) - LY:TXE = X(Q) - LX
5610  IF TYE > 0 AND TXE > 0 THEN LY = Y(Q,N):LX = X(Q): GOSUB 5730: REM
    scale
5620  IF Y(Q,N) > LY THEN LYGE = Y(Q,N):RE = 1: GOSUB 5730: REM  scale
5630  NEXT
5640  IF X(Q) > LX THEN LXGE = X(Q):RE = 1: GOSUB 5730: REM  scale
5650  IF RE = 1 THEN RE = 0: GOTO 5700
5660  FOR N = 1 TO MAX
5670 Y = Y(Q,N):X = X(Q): GOSUB 6240: REM  plot
5680  NEXT
5700  INPUT S$
5710  TEXT : HOME
5720  RETURN : REM  to display
5730 YSPAN = (LYGE - 0) / YAXIS
5740 A = 0: REM  temporary
5750 XSPAN = (LXGE - 0) / XAXIS
5760 I =  PEEK (7): IF I = 1 THEN  GOTO 5790
5770  PRINT CD$"BLOAD GRAPH,A$1050": POKE 232,80: POKE 233,16
5780  POKE 7,1
5790  HGR : HCOLOR= 3: HPLOT 1,191 TO 279,191
5800  HPLOT 1,1 TO 1,191: TEXT
5810  IF P = 1 THEN  GOTO 5870
5820  FOR I = 1 TO PTS
5830  FOR N = 1 TO MAX
5840 Y = Y(I,N):X = X(I): GOSUB 6240
5850  NEXT
5860  NEXT
5870 E = 1
5880 EZ = LXGE
5890 LXGE = LXGE / 10
5900 E = E * 10
5910 X = E:Y = 0:A = 1: GOSUB 6240
5920  IF LXGE >  = 10 THEN  GOTO 5890
5930 LXGE = EZ
5940 WW = 2
5950  IF LXGE <  = E * WW THEN  GOTO 5990
5960 X = E * WW:Y = 0:A = 1: GOSUB 6240
5970 WW = WW + 1
5980  GOTO 5950
5990 E = E / 10
6000 X = E * 5:Y = 0:A = 1: GOSUB 6240
6010  IF P = 1 GOTO 6720
6020 CC =  LOG (10)
6030 E = 0
6040 TENT = LYGE
6050  IF P1 = 1 THEN TENT = L1Y
6060 TENT = TENT - CC
6070 E = E + 1
6080  IF TENT >  = CC THEN  GOTO 6060
6090 Y = E * CC:X = 0:A = 2: GOSUB 6240
6100 E = E - 1
6110  IF E <  > 0 THEN  GOTO 6090
6120  RETURN : REM  from scale
6130  TEXT : HOME
6140 AA$ = ""
```

MR BIG 11 of 13

```
6150  VTAB 15: INPUT "DUMP GRAPHICS SCREEN?(Y/N)";A$
6160  IF A$ = "Y" THEN  GOTO 6190
6170  IF A$ = "N" THEN  GOTO 6220
6180  GOTO 6150
6190  PRINT CD$"PR#1"
6200  PRINT CC$"G";AA$
6210  PRINT CD$"PR#3"
6220  RETURN
6240  POKE 49236,1
6250  POKE 49232,1
6260  POKE 49234,1
6270  POKE 49239,1
6280  IF A = 1 THEN  GOTO 6350
6290  IF P1 <  > 1 THEN  GOTO 6350
6300 Y = Y / Y1SPAN
6310  IF Y < WEE THEN A = 0: RETURN
6320 Y = Y - WEE
6330 Y = Y * S1C
6340  GOTO 6360
6350 Y = Y / YSPAN
6360 Y =  INT (Y)
6370 Y =  - Y + 191
6380 X = X / XSPAN
6390 X =  INT (X)
6400 X = X + BASE
6410 Y = Y - BASE
6420  HCOLOR= 3
6430  PRINT "Q= ";Q
6440  PRINT "X=";X:  PRINT "Y=";Y:  PRINT "N=";N
6450  IF A = 1 THEN  DRAW 8 AT X,Y: A = 0:  RETURN
6460  IF A = 2 THEN  DRAW 9 AT X,Y: A = 0:  RETURN
6470  DRAW N AT X,Y
6480  RETURN
6490  FOR Q = 1 TO PTS
6500 TT(Q) = 0.0
6510  NEXT
6520  FOR Q = 1 TO PTS
6530  FOR N = 1 TO TP
6540 TT(Q) = TT(Q) + Y(Q,N)
6550  NEXT
6560  NEXT
6562  FOR Q = 1 TO PTS
6564  IF TT(Q) = 0 THEN TT(Q) = 1
6565  NEXT
6570  FOR Q = 1 TO PTS
6580  FOR N = 1 TO TP
6590 PERC(Q,N) = (Y(Q,N) / TT(Q)) * 100
6600  NEXT
6610  NEXT
6620 P = 1
6630  FOR Q = 1 TO PTS
6640  GOSUB 4690
6650  NEXT
6660 LYGE = 100: LXGE = X(2)
6670  FOR Q = 1 TO PTS
6680  IF X(Q) - LX > 0 THEN LX = X(Q)
6690  NEXT
6710  GOTO 5730
6720  FOR I = 1 TO 20
6730 Y = 5 * I: X = 0: A = 2:  GOSUB 6240
6740  NEXT
6750  FOR Q = 1 TO PTS
6760  FOR N = 1 TO TP
6770 Y = PERC(Q,N): X = X(Q):  GOSUB 6240
6780  NEXT
6790  NEXT
6820  FOR I = 1 TO PTS
6830 X(I) = XP(I)
6840  NEXT
6842  FOR I = 1 TO PTS
6843  FOR N = 1 TO MAX
```

MR BIG 12 of 13

```
6844 Y(I,N) = YP(I,N)
6845  NEXT : NEXT
6850  RETURN
6930  HOME : PRINT  TAB( 7)"** hires screen 1 plot **"
6940  VTAB 6: PRINT "OPTIONS 1: OLD SCREEN"
6950  VTAB 7: PRINT "         2: NEW PLOT"
6960  VTAB 8: PRINT "                          ?";: GET B$: PRINT B$
6970  IF B$ = "1" THEN  GOTO 7000
6980  IF B$ = "2" THEN  GOTO 7050
6990  GOTO 6930
7000  POKE 49236,1: POKE 49232,1: POKE 49234,1: POKE 49239,1
7010 P = 2
7020  INPUT A$
7030  TEXT : GOSUB 6140
7040  GOTO 1270
7050  HOME : PRINT  TAB( 7)"** NEW PLOT ** "
7070 RE = 0: P = 2: TA = 0
7080  GOSUB 600
7090  FOR I = 1 TO PTS
7100  FOR N = 1 TO MAX
7110 YP(I,N) = Y(I,N)
7120 XP(I) = X(I)
7130  NEXT
7140  NEXT
7220 SMALL = Y(1,1)
7230  FOR I = 1 TO PTS
7240  FOR N = 1 TO MAX
7250  IF SMALL - Y(I,N) > 0 THEN SMALL = Y(I,N)
7260  NEXT : NEXT
7270 LYGE = Y(1,1)
7280  FOR I = 1 TO PTS
7290  FOR N = 1 TO MAX
7300  IF Y(I,N) > LY THEN LY = Y(I,N)
7310  NEXT : NEXT
7313 LY =  LOG (LY)
7315  IF SMALL > 0 THEN SMALL =  LOG (SMALL)
7320  PRINT : A$ = ""
7330  VTAB PTS + 7: INPUT "BASE: smallest pt (Y) OR zero (N) "; A$
7340  IF A$ = "N" THEN P1 = 2: GOTO 7470
7350  IF A$ = "Y" THEN P1 = 1: GOTO 7400
7360  IF A$ = "" THEN P1 = 2: GOTO 7470
7370  GOTO 7330
7400 Y1SPAN = LY / YAXIS
7410 BIG = LY / Y1SPAN: WEE = SMALL / Y1SPAN
7420 B2G = BIG - WEE
7430 S1C = BIG / B2G
7450 L1Y = LY
7460  IF P1 = 1 THEN  GOTO 7580
7470 A$ = ""
7471 N = PTS + 9
7472  VTAB N: POKE 1403,0: PRINT "YSCALE FACTOR? (Y/N) ";: INPUT A$
7474  IF A$ = "" THEN  GOTO 7580
7475  IF A$ = "N" THEN  GOTO 7580
7476  IF A$ = "Y" THEN  VTAB N: POKE 1403,26: INPUT "VALUE? "; SMALL: GOTO
     7480
7478  GOTO 7472
7480  FOR I = 1 TO PTS
7490  FOR N = 1 TO MAX
7500 Y(I,N) = Y(I,N) - SMALL
7510  IF Y(I,N) < 0 THEN Y(I,N) = 0
7520  NEXT : NEXT
7530  HOME
7540  GOSUB 600
7560  VTAB PTS + 9: INPUT "SAVE DATA? "; A$
7570  IF A$ = "Y" THEN  GOSUB 1140
7580  FOR I = 1 TO PTS
7590  FOR N = 1 TO MAX
7600  IF Y(I,N) <  > 0 THEN Y(I,N) =  LOG (Y(I,N))
7610  NEXT : NEXT
7611  FOR Q = 1 TO PTS
7612  GOSUB 4690
7613  NEXT
```

MR BIG 13 of 13

```
7614 LX = X(1)
7615  FOR I = 2 TO PTS
7616  IF X(I) > LX THEN LX = X(I)
7617  NEXT
7620  GOSUB 5730
7630  FOR I = 1 TO PTS
7640  FOR N = 1 TO MAX
7650 Y(I,N) = YP(I,N)
7660 X(I) = XP(I)
7670  NEXT : NEXT
7680  INPUT A$: GOTO 1270
```

(b) EXPON.

The EXPON programme is used to fit initial data obtained from an ion-molecule reaction if, after data analysis from MR BIG, two distinct exponential decay regions are noted suggesting that two isomers of the primary ion may be present. Initial concentrations of each isomer, C1 and C2, and initial decay constants, k_1 and k_2, are fitted by EXPON to a double exponential decay curve of the form shown in equation (4.0), section 4.4.

This programme is a modification of a programme written by H.S. Stock (Physics Div., CSIRO, Sydney, Australia) and P.W. Harland (Chemistry Dept., University of Canterbury, Christchurch, New Zealand). It has been altered slightly to allow data files from MR BIG to be loaded into the programme.

EXPON 1 of 5

```
4 CD$ =  CHR$ (13) +  CHR$ (4)
10  REM  PROGRAM HSFITTEM(SIMPLEX)
11  REM  WILL FIT 2 EXPONENTIALS TO
12  REM  DECAY
15  DIM B(150),C(150),D(150),T(150)
16  DIM A(20),S(20),V(20),X(20),Y(21),P(21,20)
20  REM   INPUT OF DATA
21  GOSUB 1000
24  PRINT "HI"
25  REM  CALCULATION OF WEIGHTS
26  GOSUB 1200
30  REM  INPUT OF TRIAL VALUES
31  GOSUB 1400
35  REM  LOADING OF INITIAL SIMPLEX POINTS
36  GOSUB 1600
40  REM  CALCULATION OF INITIAL SIMPLEX VALUES
41  GOSUB 1800
45  REM  SET EXPANSION AND CONTRACTION PARAMETERS
46  GOSUB 2000
50  REM  FIND HIGHEST & LOWEST POINTS, & SIMPLEX CENTROID
51  GOSUB 2200
55  REM  ITERATION TO IMPROVE SIMPLEX
56  GOSUB 2400
60  REM  CHECK IF MINIMUM REACHED
61  GOSUB 2800
65  REM  IF MINIMUM REACHED THEN OUTPUT,
66  REM  ELSE REPEAT ITERATION
67  IF C3 = 0 GOTO 50
68  GOSUB 3000
70  REM  DETERMINE WHETHER COUNTDATA TO      BE REUSED
71  GOSUB 3400
72  IF I <  > 1 GOTO 75
73  GOTO 30
75  END
1000  REM  INPUT OF DATA
1002 DA$ = ""
1004  INPUT "DATA FILENAME? ";DA$
1005  IF DA$ = "" THEN  GOTO 1028
1007  PRINT CD$;"OPEN";DA$
1009  PRINT CD$;"READ";DA$
1010  INPUT L
1011  INPUT M
1012  FOR A = 1 TO L
1014  INPUT T(A): INPUT C(A)
1015  NEXT
1016  PRINT CD$;"CLOSE"
1017  HOME
1018  PRINT "PTS TOT =";L
1019  FOR A = 1 TO L
1020 D(A) =  SQR (T(A))
1021  VTAB (A + 1): POKE 1403,0: PRINT T(A)
1022  VTAB (A + 1): POKE 1403,6: PRINT C(A)
1023  VTAB (A + 1): POKE 1403,15: PRINT D(A)
1025  NEXT
1027  GOTO 1065
1028 I = 0
1029 I = I + 1
1030  INPUT T(I)
1035  IF T(I) < 0 THEN  GOTO 1046
1040  INPUT C(I),D(I)
1042  PRINT
1044  GOTO 1029
1045  PRINT
1046 L = I - 1
1048 DA$ = ""
1050  INPUT "SAVE DATA? (NAME?) ";DA$
1052  IF DA$ = "" THEN  GOTO 1065
1053  PRINT CD$;"OPEN";DA$: PRINT CD$;"WRITE";DA$
1055  PRINT L
1057  FOR A = 1 TO L
```

EXPON 2 of 5

```
1059  PRINT T(A): PRINT C(A): PRINT D(A)
1060  NEXT
1061  PRINT CD$;"CLOSE"
1065  RETURN
1200  REM  CALCULATION OF WEIGHTS
1205  FOR I = 1 TO L
1210 B(I) = .5 / (D(I) * D(I))
1215  NEXT I
1220  RETURN
1400  REM  INPUT OF TRIAL VALUES
1405  GOSUB 5000
1410  PRINT " ENTER A, AK, STEPA, STEPAK"
1415  GOSUB 5000
1420 I =  - 1
1425 I = I + 2
1430  INPUT A(I)
1435  IF A(I) = 0 GOTO 1455
1440  INPUT A(I + 1), S(I), S(I + 1)
1445  PRINT
1450  GOTO 1425
1455 M = I
1460 N = I - 1
1465 L1 = L - N
1470  GOSUB 5000
1475  IF L1 > 0 GOTO 1490
1480  PRINT "INSUFFICIENT DATA POINTS!!"
1485  PRINT
1490  RETURN
1600  REM  LOADING OF INITIAL SIMPLEX POINTS
1605  GOSUB 5000
1610  PRINT "TYPE 1 FOR RANDOMLY LOADED SIMPLEX"
1615  INPUT I
1620  GOSUB 5000
1625  IF I = 1 GOTO 1640
1630  GOSUB 6200
1635  GOTO 1645
1640  GOSUB 6400
1645  RETURN
1800  REM  CALCULATION OF INITIAL SIMPLEX VALUES
1805  FOR I = 1 TO M
1810  FOR J = 1 TO N
1815 A(J) = P(I, J)
1820  NEXT J
1825  GOSUB 5200
1830 Y(I) = X1
1835  NEXT I
1838  PRINT "INITIAL SIMPLEX ": INPUT A$
1840  RETURN
2000  REM  SET EXPANSION & CONTRACTION PARAMETERS
2005 A1 = 1
2010 B1 = .5
2015 G1 = 2
2020 C1 = 0
2025 C9 = .0001
2030  RETURN
2200  REM  FIND HIGHEST & LOWEST POINTS, & SIMPLEX CENTROID
2205 C1 = C1 + 1
2210 J1 = 1
2215 K1 = 1
2220  FOR I = 2 TO M
2225  IF Y(I) < Y(J1) GOTO 2235
2230 J1 = I
2235  IF Y(I) > Y(K1) GOTO 2245
2240 K1 = I
2245  NEXT I
2250  FOR J = 1 TO N
2255 X(J) = 0
2260  FOR I = 1 TO M
2265  IF I = J1 GOTO 2275
2270 X(J) = X(J) + P(I, J)
```

EXPON 3 of 5

```
2275  NEXT I
2280 X(J) = X(J) / N
2285  NEXT J
2290  RETURN
2400  REM  ITERATION TO IMPROVE SIMPLEX
2402  PRINT "1:ITER"
2405  FOR I = 1 TO N
2410 V(I) = ((1 + A1) * X(I)) - (A1 * P(J1,I))
2415  NEXT I
2420  GOSUB 5600
2425  GOSUB 5200
2430 Y1 = X1
2435  IF Y1 > Y(K1) GOTO 2485
2440  FOR I = 1 TO N
2445 A(I) = ((G1 + 1) * V(I)) - (G1 * X(I))
2450  NEXT I
2455  GOSUB 5200
2460 Y2 = X1
2462  PRINT "2:ITER"
2465  IF Y2 > Y(K1) GOTO 2520
2470  GOSUB 5800
2475 Y(J1) = Y2
2480  GOTO 2650
2485 J2 = 0
2490  FOR I = 1 TO M
2495  IF I = J1 GOTO 2510
2500  IF Y1 > Y(I) GOTO 2510
2505 J2 = J2 + 1
2510  NEXT I
2515  IF J2 = 0 GOTO 2540
2520  GOSUB 5600
2525  GOSUB 5800
2530 Y(J1) = Y1
2535  GOTO 2650
2540  IF Y1 > Y(J1) GOTO 2560
2545  GOSUB 5600
2550  GOSUB 5800
2555 Y(J1) = Y1
2560  FOR I = 1 TO N
2565 A(I) = (B1 * P(J1,I)) + ((1 - B1) * X(I))
2570  NEXT I
2575  GOSUB 5200
2580 Y1 = X1
2585  IF Y1 > Y(J1) GOTO 2605
2588  PRINT "Y1= ";Y1
2590  GOSUB 5800
2595 Y(J1) = Y1
2598  PRINT "3:ITER"
2600  GOTO 2650
2605  FOR I = 1 TO N
2610 A(I) = P(K1,I)
2615  NEXT I
2620  FOR I = 1 TO M
2625  FOR J = 1 TO N
2630 P(I,J) = (P(I,J) + A(J)) / 2
2635  NEXT J
2640  NEXT I
2645  GOSUB 1800
2648  PRINT "C1= ";C1:  INPUT A$
2650  RETURN
2800  REM  CHECK IF MINIMUM REACHED
2802  PRINT "C1= ";C1
2805 Y1 = 0
2810 Y2 = 0
2815  FOR I = 1 TO M
2820 Y1 = Y1 + Y(I)
2825  NEXT I
2830 Y1 = Y1 / M
2835  FOR I = 1 TO M
2840 Y2 = Y2 + (Y1 - Y(I)) * (Y1 - Y(I))
2845  NEXT I
```

EXPON 4 of 5

```
2850 Y2 =  SQR ( Y2 / M)
2855  IF C1 > 1 GOTO 2885
2860 Y3 = Y2
2865 Y4 = Y2  .
2870 K9 = 0
2875 C3 = 0
2880  GOTO 2950
2885  IF Y2 > C9 GOTO 2900
2890 C3 = 1
2895  GOTO 2950
2900  IF C1 < 100 GOTO 2915
2905 C3 = 2
2910  GOTO 2950
2915  IF Y2 < .98 * Y3 GOTO 2940
2920 K9 = K9 + 1
2925  IF K9 < 6 GOTO 2945
2930 C3 = 3
2935  GOTO 2950
2940 K9 = 0
2945 Y3 = Y2
2950  RETURN
3000  REM  OUTPUT OF RESULTS
3005  GOSUB 5000
3010  GOSUB 2200
3013  INPUT "PRINTOUT? "; A$
3014  IF A$ = "Y" THEN  PRINT  CHR$ (4)"PR#1"
3015  IF C3 <  > 1 GOTO 3030
3020  PRINT "ITERATION SUCCESSFUL."
3025  GOTO 3075
3030  PRINT " ITERATION UNSUCCESSFUL"
3035  GOSUB 5000
3040  IF C3 <  > 2 GOTO 3055
3045  PRINT " TOO MANY ITERATIONS REQUIRED."
3050  GOTO 3075
3055  IF C3 <  > 3 GOTO 3070
3060  PRINT "CHANGE DURING LAST ITERATION TOO SMALL."
3065  GOTO 3075
3070  PRINT " REASON FOR FAILURE UNKNOWN."
3075  GOSUB 5000
3079 AS = C1 - 1
3080  PRINT "NO. OF ITERATIONS ="; AS
3085  PRINT
3090  PRINT "DEGREE OF FIT ="; Y2
3095  PRINT "IMPROVED FROM INITIAL FIT OF "; Y4
3100  GOSUB 5000
3105  PRINT " A          AK"
3110  GOSUB 5000
3115  FOR I = 1 TO N STEP 2
3120 A(I) = P(K1, I)
3125 A(I + 1) = P(K1, I + 1)
3130  PRINT A(I), A(I + 1)
3135  NEXT I
3140  GOSUB 5000
3145  PRINT "THESE VALUES GIVE A FIT OF "; Y(K1)
3150  GOSUB 5000
3155  PRINT " TYPE 1 FOR OUTPUT OF TABLE"
3160  INPUT I
3165  IF I <  > 1 GOTO 3220
3168  HOME
3170  GOSUB 5000
3175  PRINT " T      Z      Y      DY"
3180  GOSUB 5000
3185  FOR J = 1 TO L
3190  GOSUB 5400
3191 A = 3
3194  VTAB (A + J): POKE 1403, 0: PRINT T(J)
3195  VTAB (A + J): POKE 1403, 6: PRINT Z
3196  VTAB (A + J): POKE 1403, 10: PRINT "  ";: PRINT C(J)
3197  VTAB (A + J): POKE 1403, 20: PRINT D(J)
3198  VTAB (A + J): POKE 1403, 25: PRINT "        "
3200  NEXT J
3205  GOSUB 5000
3210  PRINT "  ......................."
```

EXPON 5 of 5

```
3215  GOSUB 5000
3217  IF A$ = "Y" THEN  PRINT  CHR$ (4)"PR#3"
3220  RETURN
3400  REM  DETERMINE WHETHER COUNTDATA TO BE REUSED
3405  GOSUB 5000
3410  PRINT " TYPE 1 TO ENTER NEW A, AK, B, BK"
3415  INPUT I
3420  RETURN
5000  REM  LINEFEEDS
5005  PRINT
5010  PRINT
5015  RETURN
5200  REM   CALCULATION OF SIMPLEX VALUE
5205 X1 = 0
5210  FOR J = 1 TO L
5215  GOSUB 5400
5220 X1 = X1 + ( B( J) * ( Z - C( J)) * ( Z - C( J)))
5225  NEXT J
5230 X1 = X1 / L1
5235  RETURN
5400  REM  CALCULATION OF FUNCTION
5405 Z = 0
5410  FOR K = 1 TO N STEP 2
5415 Z = Z + ( A( K) *  EXP ( A( K + 1) * T( J)))
5420  NEXT K
5425  RETURN
5600  REM  REARRANGEMENT OF CURVE FITTINGPARAMETERS
5605  FOR I = 1 TO N
5610 A( I) = V( I)
5615  NEXT I
5620  RETURN
5800  REM  INSERTION INTO SIMPLEX OF NEW VALUES
5805  FOR I = 1 TO N
5810 P( J1, I) = A( I)
5815  NEXT I
5820  RETURN
6000  REM  RANDOM NUMBER GENERATOR FOR SIMPLEX LOADING
6005 J1 = 0
6010  IF I = 1 GOTO 6030
6015 J1 =  INT ( 10 *  RND ( I + J))
6020  IF J1 - 5 < 0 GOTO 6030
6025 J1 = 5 - J1
6030  RETURN
6200  REM  LOADING OF ORDERED INITIAL SIMPLEX
6205  FOR I = 1 TO M
6210  FOR J = 1 TO N
6215 P( I, J) = A( J)
6220  IF I = 1 GOTO 6235
6225  IF I <  > J + 1 GOTO 6235
6230 P( I, J) = P( I, J) + S( J)
6235  NEXT J
6240  NEXT I
6245  RETURN
6400  REM  LOADING OF RANDOM INITIAL SIMPLEX
6405  FOR I = 1 TO M
6410  FOR J = 1 TO N
6415  GOSUB 6000
6420 P( I, J) = A( J) + ( J1 * S( J))
6425  NEXT J
6430  NEXT I
6435  RETURN
6600  REM  DIAGNOSTIC FOR VALUES OF SIMPLEX POINTS
6605  GOSUB 5000
6610  FOR I = 1 TO M
6615  FOR J = 1 TO N STEP 4
6620  PRINT P( I, J), P( I, J + 1), P( I, J + 2), P( I, J + 3), Y( I)
6625  NEXT J
6630  NEXT I
6635  GOSUB 5000
6640  RETURN
6650  STOP
```

Appendix 2.

Collision Limit Rate Coefficient Programme.

The theoretical collision limit rate coefficients k_L (Langevin theory), k_{ADO} (reference 58) and k_{AADO} (reference 65) have been calculated using the programme KCOLLISION. This programme utilises the parameterised version of the AADO theory of Su and Bowers[65] shown in equation (1.2), section 1.2. The molecular constants used for the calculation of collision limit rate coefficients in this study are shown in table 1.

The collision limit rate coefficients, k_{AC}, shown in table 3.0, section 3.2, have been calculated using the activated complex theory of Clary[67]. These values have been supplied by D. Smith and N.G. Adams[170].

KCOLLISION 1 of 1

```
2  PRINT  CHR$ (4)"PR#3": PRINT
5  PRINT "PROGRAM TO CALCULATE ANGULAR MOMENTUM CONSERVED ADO RATE CONSTAN
     TS FOR REACTIONS BETWEEN IONS AND NEUTRALS"
7  PRINT : PRINT
10  DIM A(10)
11 A$ = ""
12  IF A$ = "Y" THEN  HOME : PRINT : PRINT
15  PRINT "C, THE DIPOLE LOCKING CONST, FOR YOUR REACTION CAN BE OBTAINED FR
     OM  SU J.C.P. VOL 69 P 2249"
20  INPUT "DIPOLE MOMENT ? (DEBYES) "; A(1)
22 A(1) = A(1) * 1E - 18
24  INPUT " DIPOLE LOCKING CONST. C ? "; A(2)
40 A(4) = 300
50 P = 3.14159
55 X = 1.3806 * (10 ^  - 16)
56  REM  BOLTZMANNS CONST (ERG K-1)
60 ADO1 =  SQR (2 / (P * X * A(4)))
70 ADO1 = A(1) * A(2) * ADO1
80  INPUT "MOMENT OF INERTIA I ? (g cm3) scale by E +37"; A(6)
82  INPUT " ION MASS ? (atomic wt) "; AS
84  INPUT "NEUTRAL MASS ? (atomic wt) "; A1
85 AV = 1.6606E - 24
86 A(7) = AV * ((AS * A1) / (AS + A1))
110 A(7) =  SQR (A(7))
130 A(8) = 4.8029 * 10 ^  - 10: REM  ION CHARGE Q (ESU)
132  INPUT "NEUTRAL POLARIZABILITY ? (cm3) "; A(9)
134 B = A(9)
138 B = ((1.39) / (B * 1E24 + 2.74)) + .375
142 B = 1.06 + B
143 C = ((A(6) * 1.4) + .79)
144 A(9) =  SQR (A(9)): A2 =  SQR (A(9))
145 AA = ( SQR (C / B)) * (A(1) / A2)
150 ABO2 = (2 * P * A(8)) / (A(7))
180 KA = AB * (A(9) + AD)
182 K1 = AB * (A(9) + AD + AA)
183  HOME : A = 2
185  VTAB A: PRINT "Kado = "; KA" cm3 s-1"
187  VTAB A + 2: PRINT "kaado = "; K1" cm3 s-1"
190  VTAB A + 6: INPUT "CONTINUE ? (Y/N) "; A$
191  IF A$ = "N" THEN  END
192  IF A$ = "Y" THEN  GOTO 12
200  GOTO 190
```

Table 1: Molecular constants used in the calculations of rate coefficients from the Langevin, ADO and AADO theories. Polarisabilities (α) are in units of 10^{-24} cm^3, dipole moments (u_D) in Debyes, molecular weights (u) in amu and moments of inertia values in g cm^2.

molecule	α[a]	u_D[b]	u	C[c]	I[d]
HC_3N	6.24	3.60	51	0.258	
HCO_2CH_3	5.04	1.77	60	0.231	
CH_3OH	3.23	1.70	32	0.241	
CH_3CHO	4.59	2.69	44	0.254	
CH_3NO_2	8.91	3.50	61	0.251	
$^{79}BrCN$	4.99	2.94	105	0.255	
H_2	0.79	0.0	2	0.0	
CH_3CN	4.48	3.92	41	0.265	1.05^{-38}
CH_3NC	4.48[e]	3.80	41	0.265	" [e]
THP	11.7	1.63	86	0.198	
THF	9.77	1.63	72	0.204	
NH_3	2.145	1.47	17	0.245	2.82^{-40}
EtOEt	10.42	4.15	74	0.2545	
HCN	2.56	2.98	27	0.265	1.92^{-39}
C_2N_2	4.30	0.0	52	0.0	
CH_4	2.60	0.0	16	0.0	
C_2H_2	3.33	0.0	26	0.0	
N_2O	2.92	0.167	44	0.07	
H_2O	1.45	1.84	18	0.260	
O_2	1.57	0.0	32	0.0	
N_2	1.76	0.0	28	0.0	
C_4H_2	4.80	0.0	50	0.0	
C_2H_5I	10.32	1.85	146	0.212	
C_6H_6	10.32	0.0	78	0.0	

(a) Values obtained either from references 68, 162 and 163 or by adding the individual bond polarisabilities as detailed in reference 164.
(b) Values obtained from references 165 and 166.
(c) Calculated from data tabulated in reference 65 (at 300K).
(d) Values obtained from reference 65.
(e) CH_3NC values have been assumed to equal the equivalent CH_3CN value.

Appendix 3.

Definitions of Non-SI Units.

Quantity	Non-SI unit	Definition
rate coefficient (2nd order)	CM^3 $molec^{-1}$ s^{-1}	1.66×10^{-18} m^3 mol^{-1} s^{-1}
rate coefficient (3rd order)	CM^6 $molec^{-2}$ s^{-1}	2.76×10^{-36} m^6 mol^{-2} s^{-1}
pressure	Torr	133.3 Pa
volume flow rate	STP cm^3 s^{-1}	STP 10^{-6} m^3 s^{-1}
diffusion coefficient	cm^2 s^{-1}	10^{-4} m^2 s^{-1}
mass	amu	1.6605×10^{-27} Kg
energy	eV	96.49 kJ mol^{-1}
dipole moment	Debye (D)	3.33564^{-30} C.m
moment of inertia	gm cm^2	10^{-7} Kg m^2
polarisability	cm^3	1.112×10^{-16} C.m^2V^{-1}

List of Illustrations.

List of Tables.

ACKNOWLEDGEMENTS.

I would like to express my gratitude to my supervisors, Dr M. J. McEwan and Dr C. G. Freeman, for their advice and interest throughout this work. I am also indebted to many members of the technical staff of the Chemistry Department for their assistance in the construction of some of the apparatus used in this thesis. I also wish to thank Professor D. Smith and Dr N. G. Adams for many helpful discussions during their opportune visit to this department and to thank Miss Pat Bates for her help in the printing of this thesis.